

TECHNICAL UNIVERSITY OF LIBEREC

FACULTY OF MECHANICAL ENGINEERING



Doctoral Dissertation

Liberec 2010

9. Publications of Author

- Tuong N.V., Tuan H.S., Pokorny P.: *Matlab-based programming for free-form surfaces*. International Conference 2009 Manufacturing systems today and tomorrow. TUL, Liberec, November 19-20, 2009, Czech, pp. 17, ISBN 978-80-7372-541-9.
- H. S. Tuan, B. Marvalová: *Magnetoelastic anisotropic elastomers in a static magnetic field: Constitutive equations and FEM solutions*. Proceedings of the sixth European Conference on Constitutive Models for Rubber, Ed.: Taylor & Francis Group. Dresden, September 7-10, 2009, Germany, pp. 453-458, ISBN 978-0-415-56327-7.
- Jarmil Vlach, Hoang Sy Tuan, Bohdana Marvalová: *Experimental and numerical research of Magneto-sensitive elastomers*. 47th International Conference of Experimental Stress Analysis. Syrchov, June 8-11, 2009, Czech Republic, pp.283-290, ISBN 978-80-7372-483-2.
- Hoang Sy Tuan, Marvalová Bohdana: *Simulation of Viscoelastic Fiber-Reinforced Composites at Finite Strains in Comsol Multiphysics*. Applied Mechanics 2009, 11th International Scientific Conference. Smolenice, April 6-8, 2009, Slovak Republic, pp. 45-46, ISBN 978-80-89313-32-7.
- Hoang Sy Tuan, B. Marvalová: *Relaxation of Fiber-reinforced Composites: FEM Simulations*. Conference Mechanical Composite Material and Structure. Pilsen, March 12-13, 2009, Czech Republic, pp. 70-77, ISBN 978-80-7043-782-7.
- Sy Tuan Hoang, Bohdana Marvalová: *Coupling of magnetoelastic material and magnetic field in Comsol Multiphysics*. Výpočty Konstrukcí Metodou Konečných Prvků. Pilsen, November 20, 2008, Czech Republic, pp. 8-18, ISBN 978-80-7043-735-3.
- Hoang S. T., Marvalová B.: *Numerical Differentiation of Experimentally Measured Displacements*. 16th Annual Conference Proceedings. Prague, November 11, 2008, Czech Republic, pp. 40, ISBN 978-80-7080-692-0.
- Hoang S.T., Marvalová B.: *Magneto-hyperelastic material in a uniform magnetic field: FEM Calculation of Stress and Strain*. Engineering Mechanics 2008, National Conference with International Participation. Svratka, May 12-15, 2008, Czech Republic, pp. 86-87, ISBN 978-80-87012-11-6.
- Jan Růžicka, Hoang Sy Tuan, Bohdana Marvalová: *Dynamic measuring methods of viscoelastic properties of materials*. 14th International Conference, Structure and Structural Mechanics of Textiles. TU of Liberec, November 26-28, 2007, Czech Republic, pp. 97-104. ISBN 978-80-7372-271-5.
- Hoang Sy Tuan, Bohdana Marvalová: *FE analysis of cord-reinforced rubber composites at finite strains*. Výpočty Konstrukcí Metodou Konečných Prvků. Prague, November 22, 2007, Czech Republic, pp. 9-20, ISBN 978-80-01-03942-7.
- Hoang S.T., Marvalová B.: *Constitutive Material Model of Fiberreinforced Composites in Comsol Multiphysics*. Technical Computing Prague 2007, 15th Annual Conference Proceedings. Prague, November 14, 2007, Czech Republic, pp. 53, ISBN 978-80-7080658-6.
- Tuan Hoang Sy, Marvalová B.: *Relaxation of the Rubber Plate with Central Hole – FEM Simulation in Comsol Multiphysics*. Applied Mechanics 2007, 9th International Scientific Conference. Malenovice, April 16-19, 2007, Czech Republic, pp. 214-215, ISBN 978-80-248-1389-9.

TECHNICAL UNIVERSITY OF LIBEREC
FACULTY OF MECHANICAL ENGINEERING

Ing. Hoang Sy Tuan

ELASTIC AND VISCOELASTIC BEHAVIOUR OF COMPOSITES
WITH ELASTOMERIC MATRIX

ELASTICKÉ A VISKOELASTICKÉ CHOVÁNÍ KOMPOZITŮ
S ELASTOMERICKOU MATRICÍ

Doctoral Dissertation

Supervisor:

Doc. Ing. Bohdana Marvalová, CSc
Technical University of Liberec

Liberec - 2010

ABSTRACT

The viscous behavior of the fiber-reinforced composite materials with rubber-like matrix is modeled in the continuum mechanics framework by the Helmholtz free energy function and the evolution equations of the internal variables. The decomposition of the free energy function and the chosen viscoelastic model are bases for formulation and description of the viscous characteristics of these anisotropic materials. Numerical simulations to predict the response of these materials in finite strains are performed.

The dissertation focused on experimental evaluating the purely elastic and viscoelastic material parameters of proposed models via some standard experiments on relaxation, such as simple tension, pure shear and biaxial tensile tests. Both the isotropic and anisotropic materials were tested.

Several numerical examples were implemented in FEM software COMSOL Multiphysics and compared with the experimental results. The applications of the model were enlarged to predict other viscoelastic phenomena i.e. creep and influence of loading velocities on stresses. The influence of the directions of reinforcing fibers was also examined. The viscoelastic model was applied to a practical example that is an air-spring with two fiber reinforcements undergoing an internal pressure.

An extension of nonlinear theory for rubber-like anisotropic composites was applied to magneto-sensitive (MS) elastomers under an external magnetic field. The constitutive equations of both magnetic and mechanical fields were presented. Some numerical computations of a coupling of magnetic and mechanical problems were illustrated in order to describe a nonlinear characteristic of MS elastomer.

ABSTRAKT

Viskózní chování kompozitních materiálů s pryžovou maticí vyztuženou kordy je modelováno v rámci mechaniky kontinua pomocí Helmholtzovy funkce volné energie a vývojových rovnic pro vnitřní proměnné. Rozklad funkce volné energie a zvolený viskoelastický model jsou základem pro formulaci a popis viskózní vlastnosti těchto anizotropních materiálů. Jsou uvedeny numerické simulace pro přepověď odezvy těchto materiálů na konečné deformace.

Disertační práce se zaměřuje na experimentální určení elastických a viskoelastických materiálových parametrů navrhovaných modelů pomocí některých standardních testů jako je tahová zkouška, čistý smyk a dvouosé tahové zkoušky kvazistatické i relaxační. Byly testovány izotropní a anizotropní (kompozitní) materiály. Několik numerických případů je implementováno do MKP prostředí COMSOL Multiphysics a srovnáno s experimentálními výsledky. Aplikace modelu byly rozšířeny o numerickou předpověď dalších viskoelastických jevů jako je tečení a vliv rychlosti zatížení na napětí. Vliv směru vlákně vyztuže byl rovněž zkoumán. Viskoelastický model byl aplikován na numerickou simulaci vnitřním přetlakem zatížené vzduchové válcové pružiny, jejíž pryžový plášť je vyztužen dvěma skupinami kordů.

Nelineární materiálový anizotropní model byl rozšířen na případ magneto-senzitivních elastomerů mechanicky zatížených ve vnějším magnetickém poli. Numerické simulace odezvy tělesa s magneto-mechanickou vazbou jsou uvedeny s cílem popsat nelineární vlastnosti magneto-senzitivních elastomerů.

8. Literatures

- Brigadnov, I. A. & Dorfmann, A. (2003). Mathematical modelling of magneto-sensitive elastomers. *Int. J. of Solids Struct.*, Vol. 40, pp. 4659–4674.
- Dorfmann, A., & Ogden, R. W. (2003). Magnetoelastic modelling of elastomers. *Eur. J. Mech. A/ Solids*, Vol. 22, pp. 497–507.
- Dorfmann, A., & Ogden, R. W. (2004). Nonlinear magnetoelastic deformations of elastomers. *Acta Mechanica*, Vol. 167, No. 1-2, pp. 13-28.
- Dorfmann, A., & Ogden, R. W. (2005). Some problems in nonlinear magnetoelasticity. *Z. angew. Math. Phys. (ZAMP)*, Vol. 56, pp. 718-745.
- Holzappel, G. A. (2000). *Nonlinear Solid Mechanics, A Continuum Approach for Engineering*. John Wiley, & Son Ltd, Chichester, England.
- Holzappel, G. A., & Gasser, T. C. (2001). A viscoelastic model for fiber-reinforced composites at finite strains: Continuum basic, computational aspects and applications. *Comput. Methods Appl. Mech. Engrg.*, Vol. 190, pp. 4379-4403.
- Kuwabara, T., Ikeda, S., & Kuroda, K. (1998). Measurement and analysis of differential work hardening in cold-rolled steel sheet under biaxial tension. *Journal of Materials Processing Technology*, Vol. 80–81, pp. 517–523.
- Nguyen, T. D., Jones, R. E., & Boyce, B. L. (2007). Modeling the anisotropic finite-deformation viscoelastic behavior of soft fiber-reinforced composites. *International Journal of Solids and Structures*, Vol. 44, pp. 8366–8389.
- Truesdell, C., & Noll, W. (1992). *The Non-Linear Field Theories of Mechanics*. Springer-Verlag, Berlin, Germany.

7. Conclusions, discussions and future perspectives

In this dissertation, the viscoelastic behavior of the fiber-reinforced elastomer has been studied. The viscous characteristics of the anisotropic composites were identified by the suitable free energy function and the chosen viscoelastic models. Herein, the generalized Maxwell element model was used in two approaches with either inelastic strains or overstresses playing a role of internal variables.

Some standard experiments such as simple tensile, pure shear and biaxial tensile tests for isotropic rubber-like materials and composite elastomers reinforced by two families of fibers under many relaxation stages were carried out. The non-contact optical stereo-correlation technique was used to determine precisely for experimental measurements of large deformations and evaluation of strains. The evaluation results were in good agreement with experimental data.

The implementation of the set of constitutive equations and evolution equations into a finite element program, Comsol Multiphysics, was established for modeling viscoelastic behaviour of both hyperelastic isotropic and anisotropic composites. The ability of the model to predict nonlinear viscoelastic behavior of isotropic and anisotropic materials was examined by comparing the theory to experimental results. Several examples relevant to viscoelastic responses, for instance the influence of the loading velocities, one- or multi- step relaxations and a creep were presented. More simulations of complicated boundary value problems of an air-spring tube with two fiber reinforcement were performed using the finite element method. The comparison between two approaches in overstress and inelastic strain variables was considered, this is just the initial step towards the nonlinear approach in inelastic strain variables.

The remaining task of the study was to develop a formulation of constitutive equations for anisotropic MS elastomers. We implemented several numerical solutions of simple boundary problems of nonlinear magneto-mechanical response of a body made of isotropic or anisotropic magnetosensitive elastomer subjected to a static magnetic field. The finite element software used proved a flexibility and ability of an easy implementation of fairly complicated coupled problem. The FE simulations involved not only the edge effects due to the finite geometry of the body but also the influence of the large displacement of the boundaries. The free energy functions that we have used are very simple forms and represent only a first approach towards a valuable constitutive model. Appropriate experiments which are in preparation will allow the elaboration of the constitutive relations. The constitutive model should involve also the complex dissipative (viscoelastic) behaviour of the material.

Contents

1. Introduction	4
2. Overview of literature	6
3. The decomposition of free energy function	6
4. Experiments and material parameter identification	7
4.1. <i>Isotropic composite materials</i>	7
4.2. <i>Fiber-reinforced composite materials</i>	10
5. Numerical simulations of viscoelastic composites	12
5.1. <i>Isotropic (hyperelastic) rubber-like materials</i>	12
5.2. <i>Fiber-reinforced composites</i>	14
5.3. <i>Viscous responses of internal stress-like and strain-like variables</i>	16
6. Magneto-sensitive elastomer materials	17
6.1. <i>FEM solutions of MS isotropic materials</i>	17
6.2. <i>FEM solutions of MS anisotropic materials</i>	19
7. Conclusions, discussions and future perspectives	22
8. Literatures	23
9. Publications of Author	24

1. Introduction

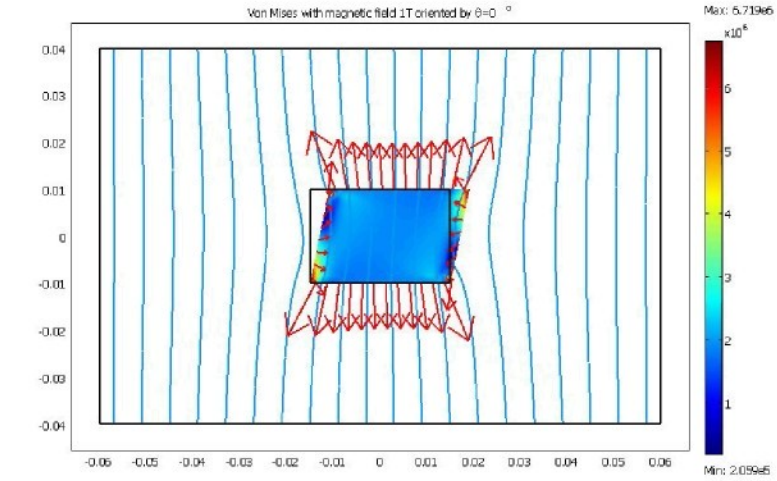
Fiber-reinforced elastomers (FREs) also well-known as anisotropic hyperelastic composites are widely used in practice, including industrial engineering, automobile, aircraft, biomechanics and medicine, for example gas pipes, automotive tyres, absorbers, belts, man-made (elastomeric) composites, etc...

These composites have many potential advantages due to high specific stiffness and strength, good corrosion resistance and thermal insulation. The typical anisotropic behavior is often formed by a number of fiber cords (usually one or two fibers coincide at each point) which are systematically arranged in a rubber-like matrix material. However, these materials not only have a highly non-linear behavior and possess anisotropic mechanical properties but also exhibit viscoelastic material behavior. Furthermore particularly important to this behavior is the heating of the structure because of internal dissipation and the temperature dependence of the material parameters. Therefore the ability to accurately predict the mechanical behavior of these materials is an important technological problem that is still far from being completely understood.

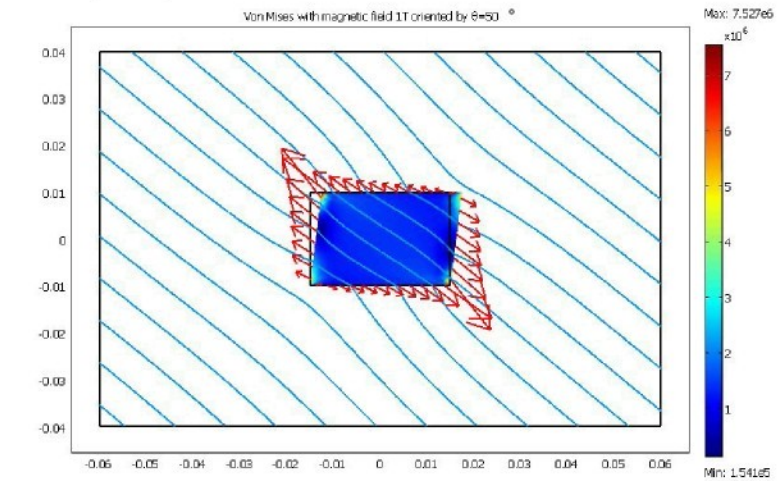
The main objective of the thesis is to identify and simulate the viscous characteristics of the fiber-reinforced composite materials with rubber-like matrix. The identification of the material parameters and the implementation of the numerical simulations that base on the chosen viscoelastic model are presented.

In this work both a mechanical experiment and a numerical simulation have been used in an effort to gain better insight into the mechanics causing the observed behavior and to facilitate ability performance of a viscoelastic model. There are many proposed viscoelastic models to deal viscoelastic problems of isotropic rubber-like materials as well as anisotropic hyperelastic composites with rubber-like matrix. However we focus on an approach in the continuum mechanical point of view.

In particular, to describe a viscoelastic behavior of anisotropic hyperelastic materials the existence of the Helmholtz free-energy functions is postulated. The free energy function is splitted into equilibrium (hyperelastic) and non-equilibrium (viscoelastic) responses, respectively. The non-equilibrium contribution of the free energy function depends not only on external variables, which are measurable and controllable quantities, but also on internal variables (hidden to the external observers). We use two approaches for the viscous response:

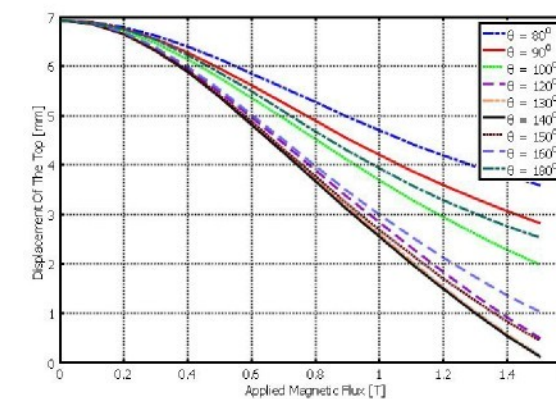


a) Magnetic field oriented in a vertical direction

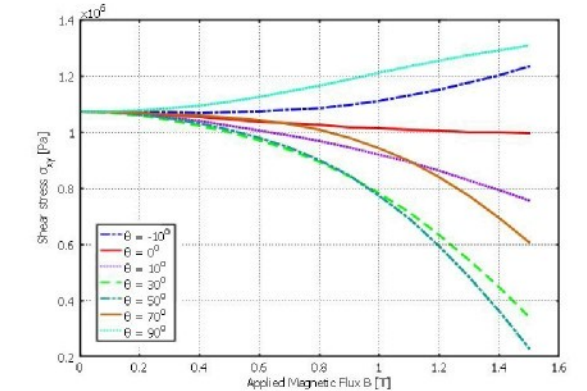


b) Magnetic orientation compared to a vertical direction $\theta=50^\circ$

Figure 26 – Simple shear state of the plate with different magnetic directions



a) Displacement of the top surface versus different directions of the applied magnetic field



b) Shear stress at the center of the body versus different directions of the applied magnetic field

Figure 27 – Dependencies of displacement and shear stress on the magnetic field

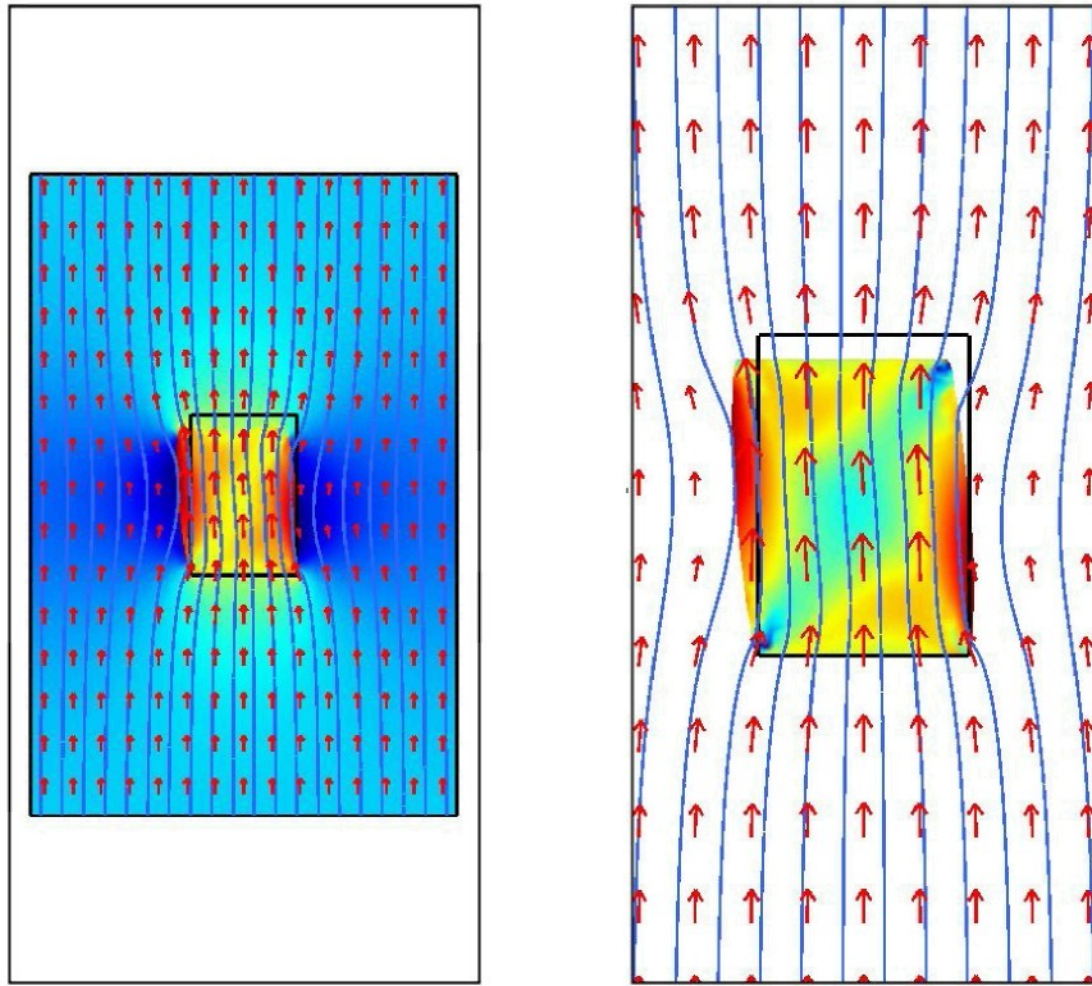
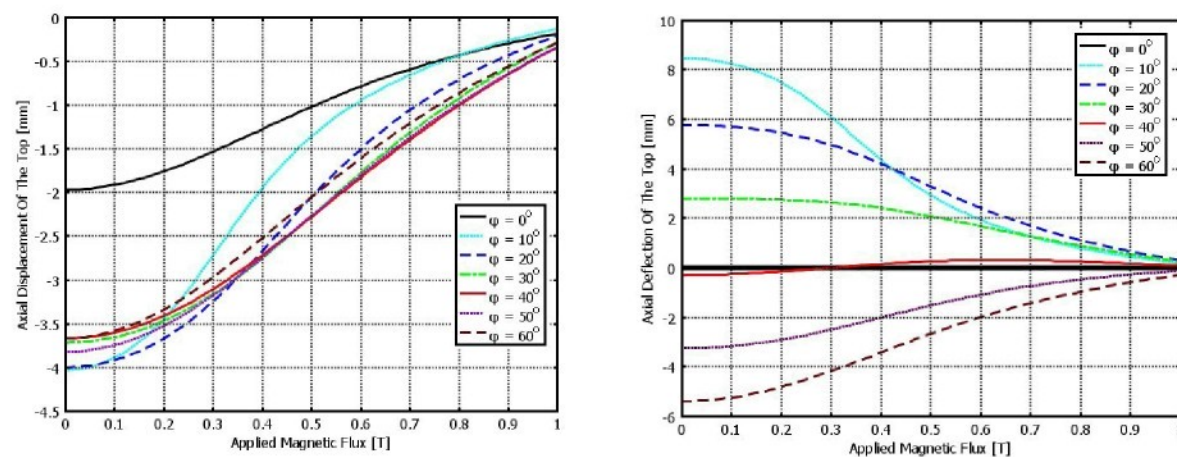


Figure 24 – Distribution of the magnetic field and the magnetization of the MS anisotropic material



a) Vertical displacement

b) Horizontal displacement

Figure 25 – Displacements of the top surface of the block versus the magnetic flux density

- The first approach is formulated for internal stress-like variables (so called over stresses) and the formulation of the evolution equations is linear for loading close to thermodynamic equilibrium.
- The second approach with nonlinear evolution equations is formulated for internal strain-like variables (so called inelastic strains) by assuming parallel multiplicative decompositions of the deformation gradient into elastic and viscous parts.

We use rheological models such as Kelvin-Voigt or Maxwell models to establish evolution equations for internal variables.

Finally, we expand attention to develop constitutive formulations of anisotropic magneto-sensitive (MS) elastomer materials. Owing to the magnetic field is considered as a preferred direction in the reference configuration, hence the MS elastomers are subjected simultaneously to the action of the mechanical loading and magnetic field as similar to composites reinforced by fiber families. The theory of nonlinear magnetoelasticity for MS elastomers is applied to a number of simple boundary-value problems.

In order to achieve the above objectives, many tasks related to experimental and numerical FEM calculations should be implemented, namely some main tasks as follows:

- Propose the free energy functions used in the research.
- Formulate explicit expressions of equilibrium stress in deformation plane.
- Perform experiments in relaxation to measure the forces and the strains.
- Develop a Matlab program for evaluating the material parameters.
- Establish the viscoelastic model in FEM to calculate numerical simulations of viscoelastic materials.
- Extend constitutive equations of the anisotropic MS elastomers.
- Compute numerically some examples of MS elastomers in FEM.

2. Overview of literature

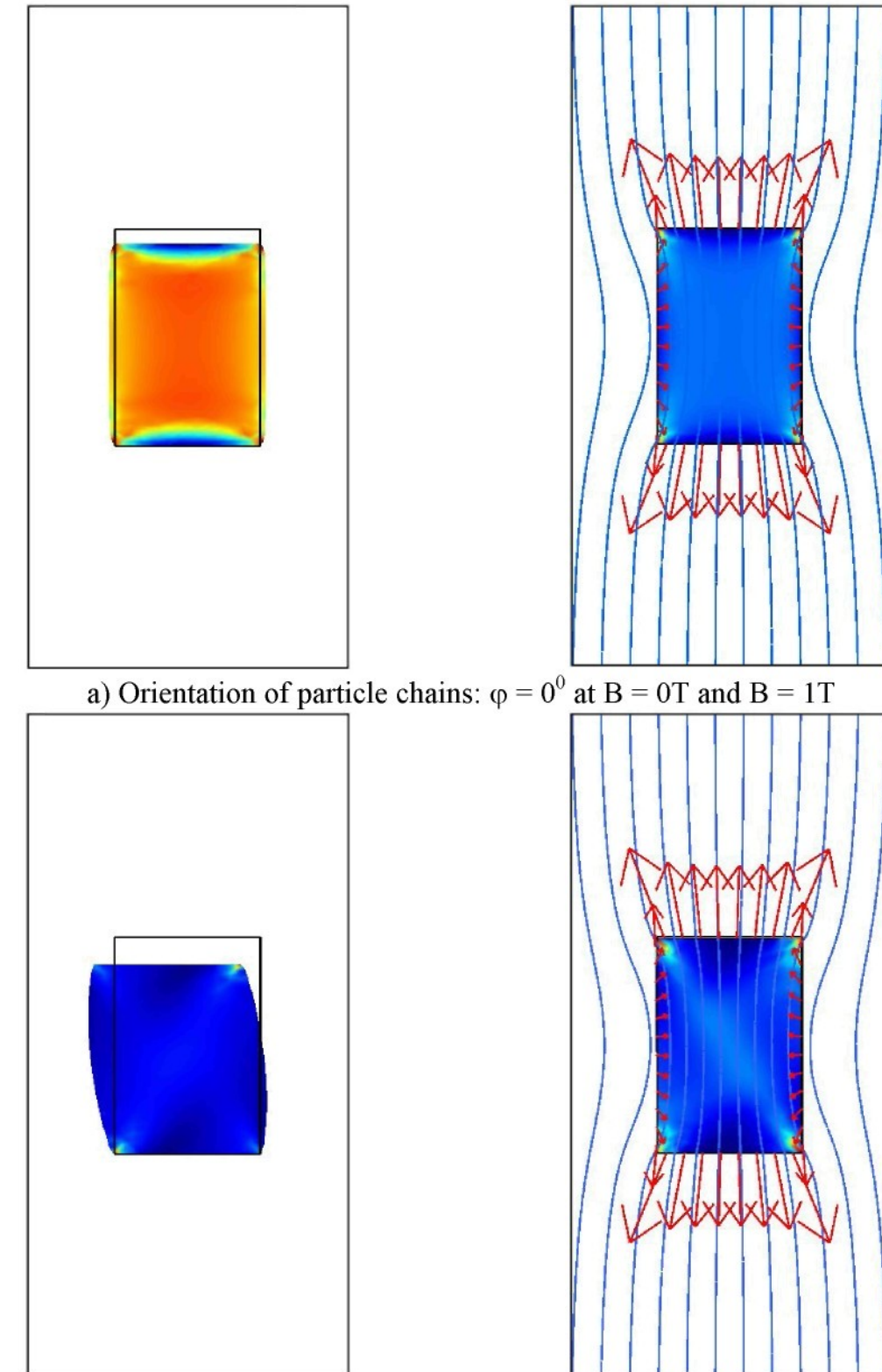
In this thesis, the viscoelastic behavior of the isotropic as well as anisotropic rubber-like materials is studied in the continuum mechanical theory by means of the free energy functions. The constitutive equation which interrelate the stress components and the strain components within a nonlinear regime can be found out, for example, Holzapfel (2000) or Truesdell & Noll (1992). The viscoelastic model of the anisotropic materials depends on the choice of internal variables and evolution equations. Evolution equations of over stresses proposed by Holzapfel & Gasser (2001) in the theory of linear viscoelasticity is quite simple to utilize for evaluating material parameters by experimental performances and implementing numerical simulations in FEM. However this model is believed in not credible the general problem of large deformations and large perturbations away from thermodynamic equilibrium, such as full thermo-mechanical coupling or high strain rates. Therefore, for this reason, the nonlinear viscoelastic model proposed by Nguyen et al (2007) is also given.

The constitutive formulation of magnetic and mechanical equations for MS elastomers is provided in series of recent studies by Brigadnov & Dorfmann (2003) and Dorfmann & Ogden (2003-2005). Specially, the influence of the magnetic field on the mechanical stress in the deforming body is incorporated through a magnetic stress tensor instead of through magnetic body forces included to the mechanical equilibrium equation, because the resulting total Cauchy stress tensor has the advantage of being symmetric, it can be referred to Dorfmann & Ogden (2004). The magnetic induction vector \mathbf{B} and the magnetic field vector \mathbf{H} are regarded as fundamental field variables and defined by the total free energy function.

3. The decomposition of free energy function

The decomposition of the equilibrium part Ψ_{EQ} of free energy function within the isothermal regime is postulated to describe each contribution (volumetric, isotropic and anisotropic isochoric) which allows modeling an isotropic rubber-like material and a composite in which a rubber-like matrix material is reinforced by families of fibers. In all cases incompressible composite materials are assumed. The isotropic (isochoric) part of the free energy function is usually used classical models such as neo-Hookean, Mooney-Rivlin and Ogden models. To represent the anisotropic behaviour of the composite the anisotropic contribution of the free energy function can be chosen by either polynomial or exponential functions.

6.2. FEM solutions of MS anisotropic materials



a) Orientation of particle chains: $\varphi = 0^\circ$ at $B = 0T$ and $B = 1T$
b) Orientation of particle chains: $\varphi = 30^\circ$ at $B = 0T$ and $B = 1T$
Figure 23 – Deformation of the MS anisotropic block without and with a uniform magnetic field

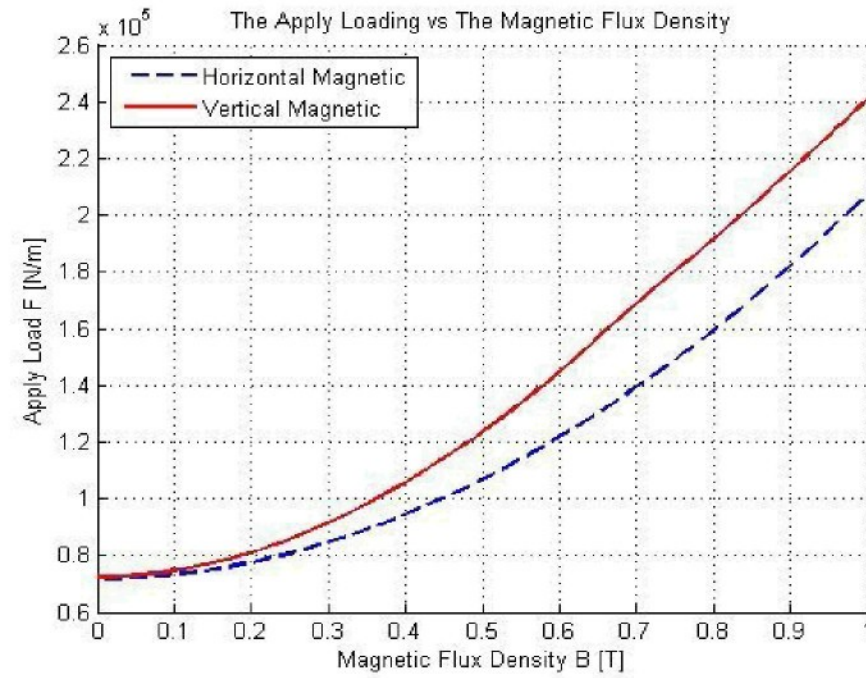


Figure 20 – Loading depends on direction and magnitude of magnetic field

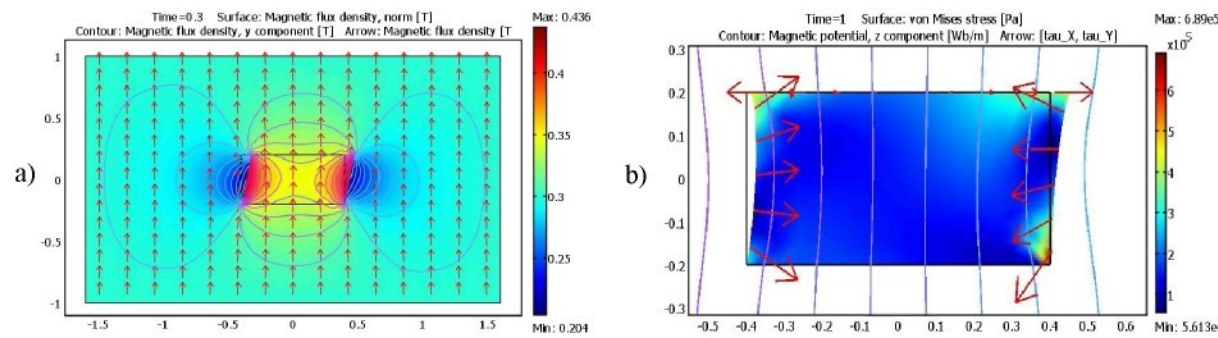


Figure 21 – MS Block in simple shear: a) Distribution of magnetic field, b) Magnetic traction and Von Mises stress

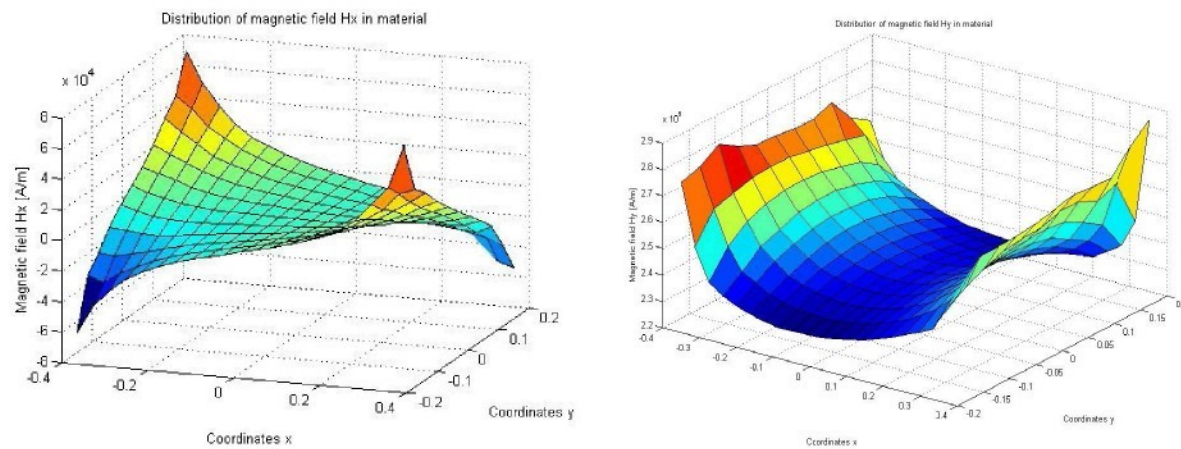


Figure 22 – Variation of magnetic fields H_x , H_y in the deformation body

4. Experiments and material parameter identification

For simplifying numerical estimations three assumptions are issued as follows

- Load is applied suddenly.
- Time in a relaxation process is long enough.
- Strain is unchanged throughout a relaxation process.

The elastic and viscoelastic parameters are evaluated by fitting experimental data by means of using linear and nonlinear least-square methods in Matlab software.

4.1. Isotropic composite materials

Evaluation of material parameters of the viscoelastic isotropic rubber-like materials is performed via basic experiments, namely simple tension, pure shear and biaxial tensile tests.

Simple tension

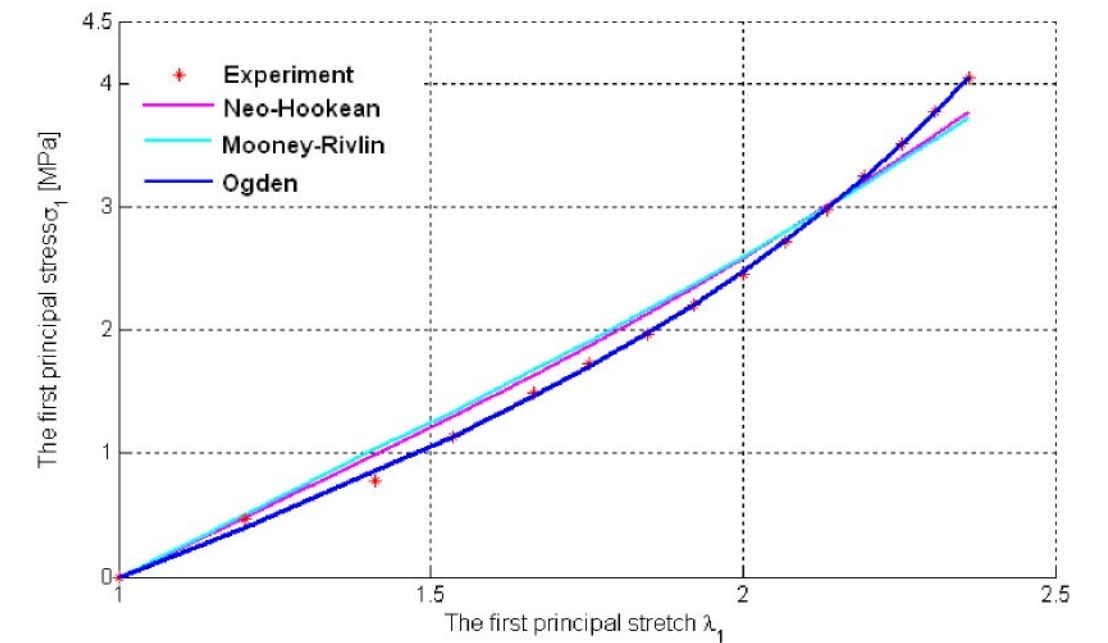


Figure 1 – Estimation of elastic coefficients of the isotropic material by a simple tensile test with different models

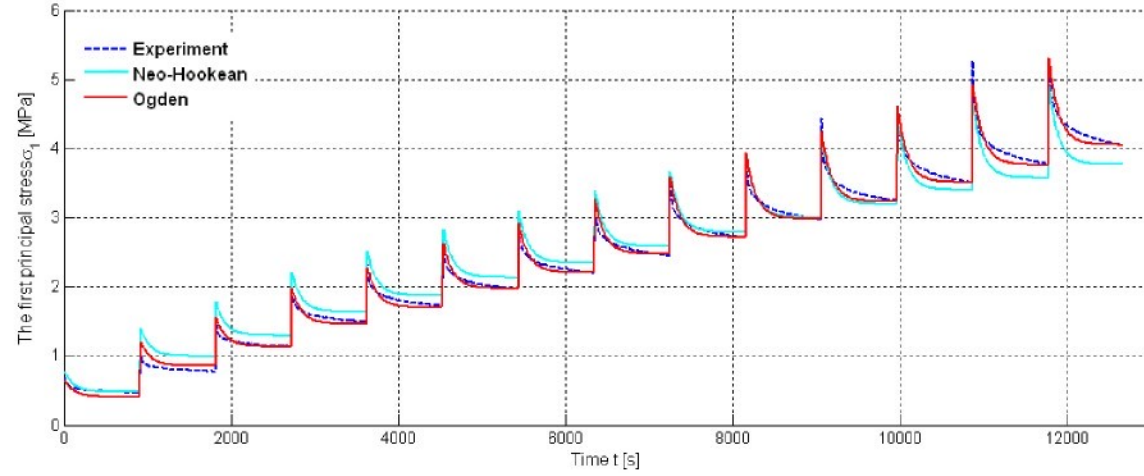


Figure 2 – Estimation of viscoelastic coefficients of the isotropic material by a simple tensile test with neo-Hookean and Ogden models

Table 1 – Elastic coefficients of the isotropic material by the simple tensile test

Model	Neo-Hookean	Mooney-Rivlin	Ogden
Material coefficients	$c = 0,3678$ MPa	$c_1 = 0,3441$ MPa $c_2 = 0,0492$ MPa	$\mu_1 = 0,5428$ MPa; $\alpha_1 = 2,25$ $\mu_2 = 0,00056$ MPa; $\alpha_2 = 7,99$
Shear modulus	$\mu = 0,7356$ MPa	$\mu = 0,6883$ MPa	$\mu = 0,6115$ MPa

Table 2 – Viscoelastic coefficients of the isotropic material by the simple tensile test

Model	Neo-Hookean	Ogden
Relaxation time	$\tau = 114,2$ [s]	$\tau = 118,9$ [s]
Scale coefficients	$\beta = 0,278$	$\beta = 0,293$

Pure shear test

Table 3 – Elastic coefficients of the isotropic material by the pure shear test

Model	Neo-Hookean	Ogden's 2 parameters	Ogden's 4 parameters
Material coefficients	$c = 0,2537$ MPa	$\mu_1 = 0,3161$ MPa $\alpha_1 = 2,84$	$\mu_1 = -0,0001$ MPa; $\alpha_1 = -15,41$ $\mu_2 = 64,776$ MPa; $\alpha_2 = 0,016$
Shear modulus	$\mu = 0,5074$ MPa	$\mu = 0,4483$ MPa	$\mu = 0,5054$ MPa

Table 4 – Viscoelastic coefficients of the isotropic material by the pure shear test

Model	Neo-Hookean	Ogden
Relaxation time	$\tau = 135,4$ [s]	$\tau = 153,9$ [s]
Scale coefficients	$\beta = 0,16$	$\beta = 0,003$

6. Magneto-sensitive elastomer materials

We adopt the formulation of Dorfmann & Ogden (2003-2005) as the starting point. The general formulation of constitutive equations for anisotropic magnetoelastic interactions are based on Dorfmann & Ogden (2005) for both compressible and incompressible magnetoelastic materials.

The influence of the magnetic field on the mechanical stress in the deforming body may be incorporated through a magnetic stress tensor (see Dorfmann & Ogden, 2005).

For incompressible MS elastomers the volumetric component of the free energy function is chosen in the form

$$\Psi_{vol} = -p(J-1) \quad (1)$$

where p is the hydrostatic pressure.

In order to simulate behaviors of the incompressible magnetoelastic elastomer, we refer and inherit a simple form of the free energy function as proposed in Dorfmann's paper (2005). The isotropic and anisotropic contributions of the free energy function are used as follows

$$\Psi_{iso} = \frac{G}{4} \left[(1+\gamma)(\bar{I}_1 - 3) + (1-\gamma)(\bar{I}_2 - 3) \right] \quad (2)$$

$$\Psi_{ani} = \frac{1}{\mu_0} (\alpha I_4 + \beta \bar{I}_5) \quad (3)$$

or

$$\Psi_{ani} = \frac{1}{\mu_0} (\alpha I_4 + \beta \bar{I}_5) + \frac{k}{2} (\bar{I}_7 - 1)^2 \quad (4)$$

here $\bar{I}_1, \bar{I}_2, I_4, \bar{I}_5, \bar{I}_7$ are invariants of the right Cauchy-Green \mathbf{C} and the magnetic field \mathbf{B} , $G = G_0(1 + \eta_G I_4)$, G_0 is the field independent shear modulus and $k = k_0(1 + \eta_k I_4)$ represents the anisotropic characteristic of MS elastomers.

6.1. FEM solutions of MS isotropic materials

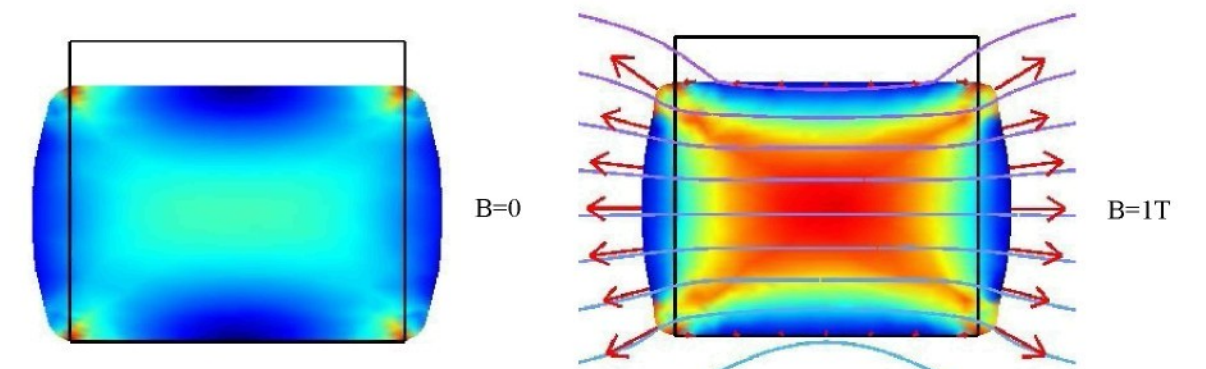
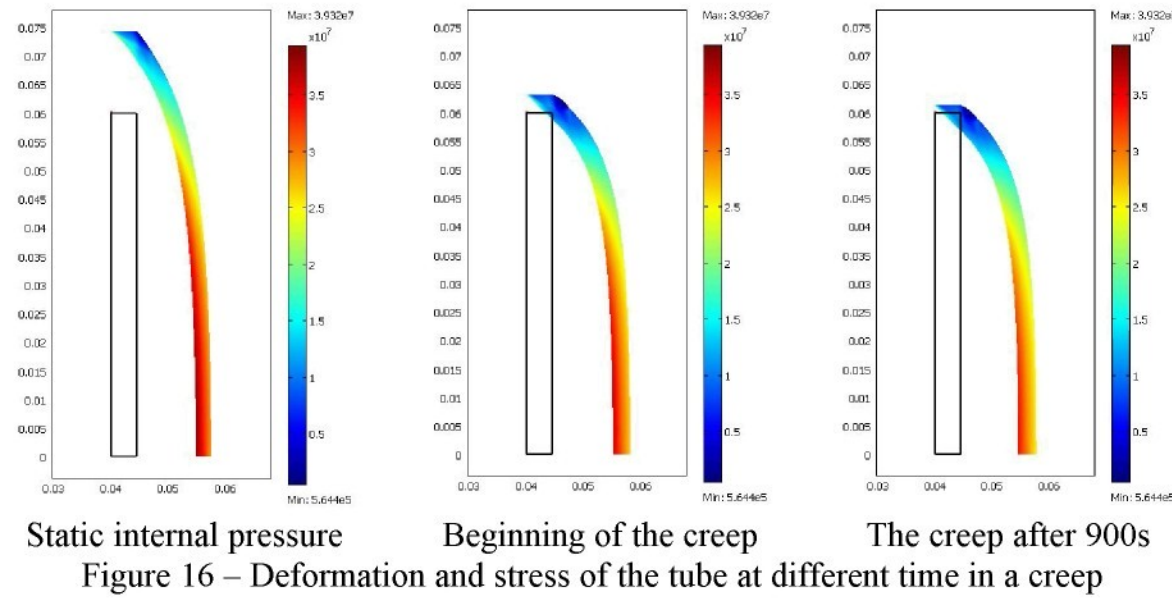
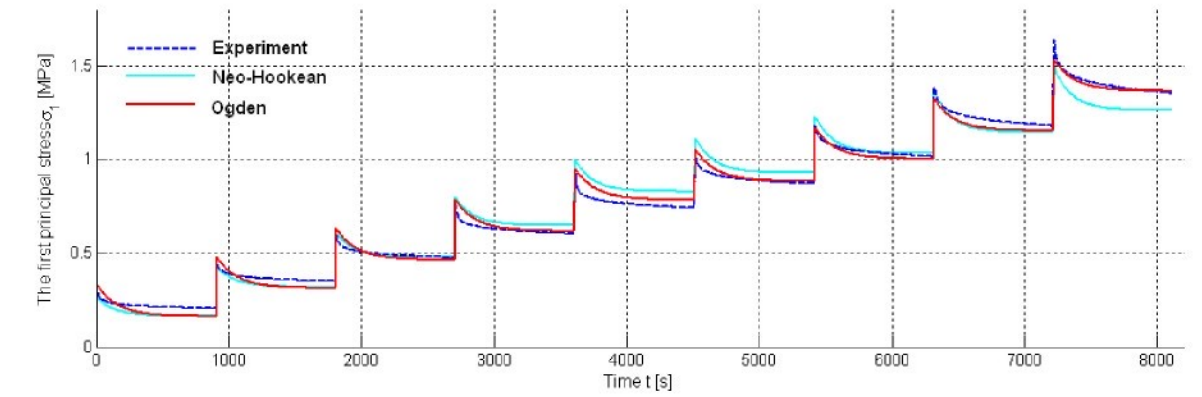
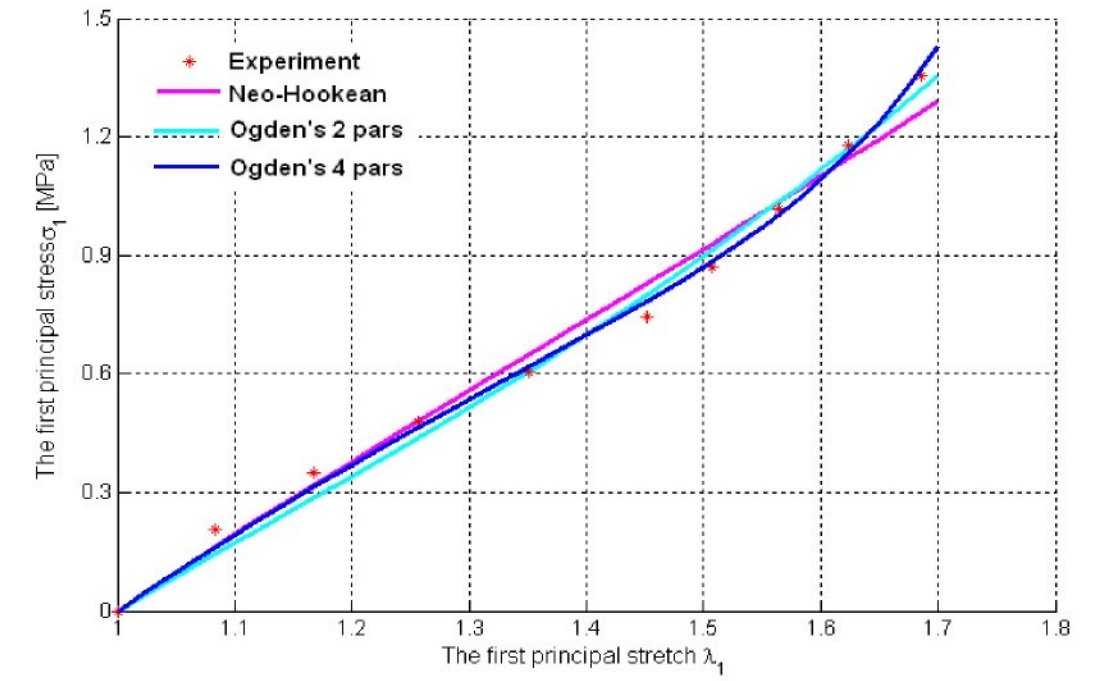
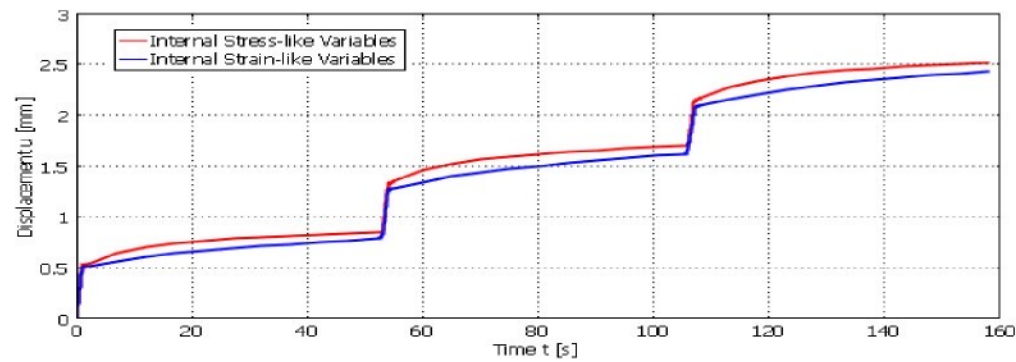
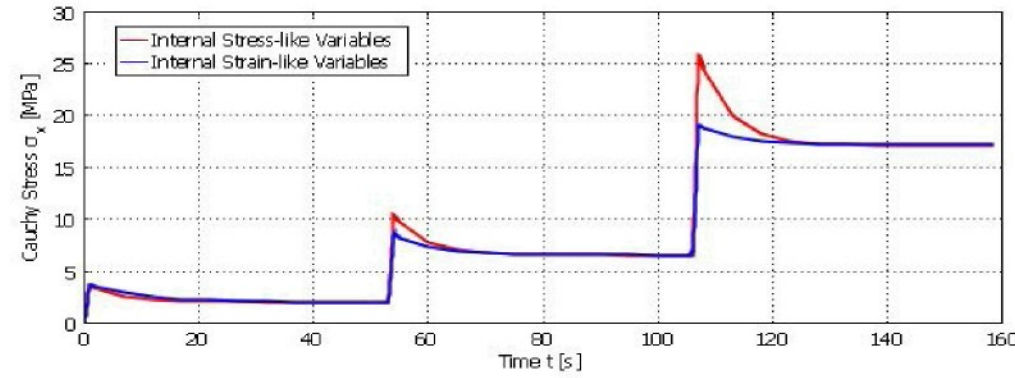


Figure 19 – Deformation of the block in horizontal magnetic field

Viscoelastic behavior of an air-spring



5.3. Viscous responses of internal stress-like and strain-like variables



Biaxial tensile test

The evaluating results by biaxial tensile test are incredible due to the imperfect form of the specimen, specifically the effective cross-sectional area of the specimen arms. This effect can be eliminated by slits made in each of arms as recommended in Kuwabara et al (1998).

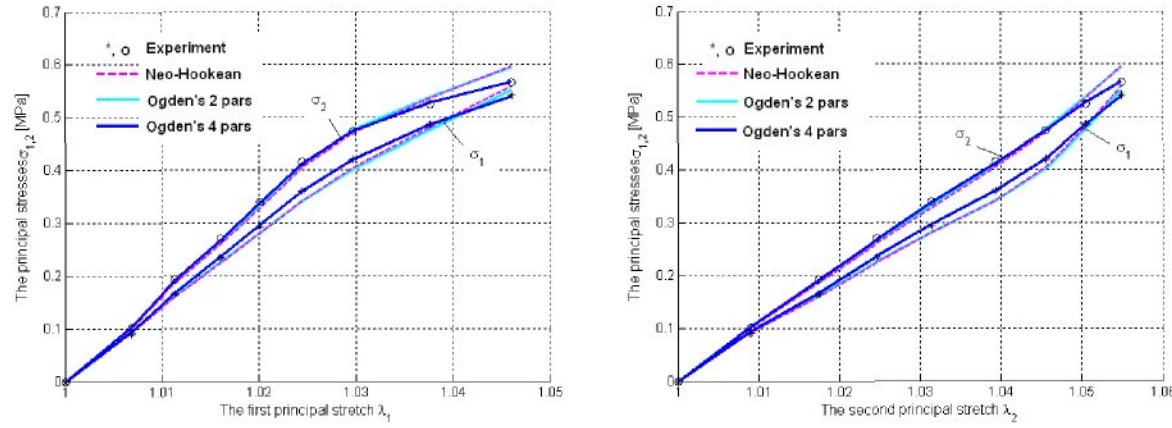


Figure 5 – Estimation of elastic coefficients of the isotropic material by a biaxial tensile test with different models

4.2. Fiber-reinforced composite materials

We implement experiments for composites reinforced with different fiber angles as 30° , 40° , 50° and 60° in multi-step relaxations, in which rectangular sheets with 30mm high and $4,5 \times 220$ mm cross section.

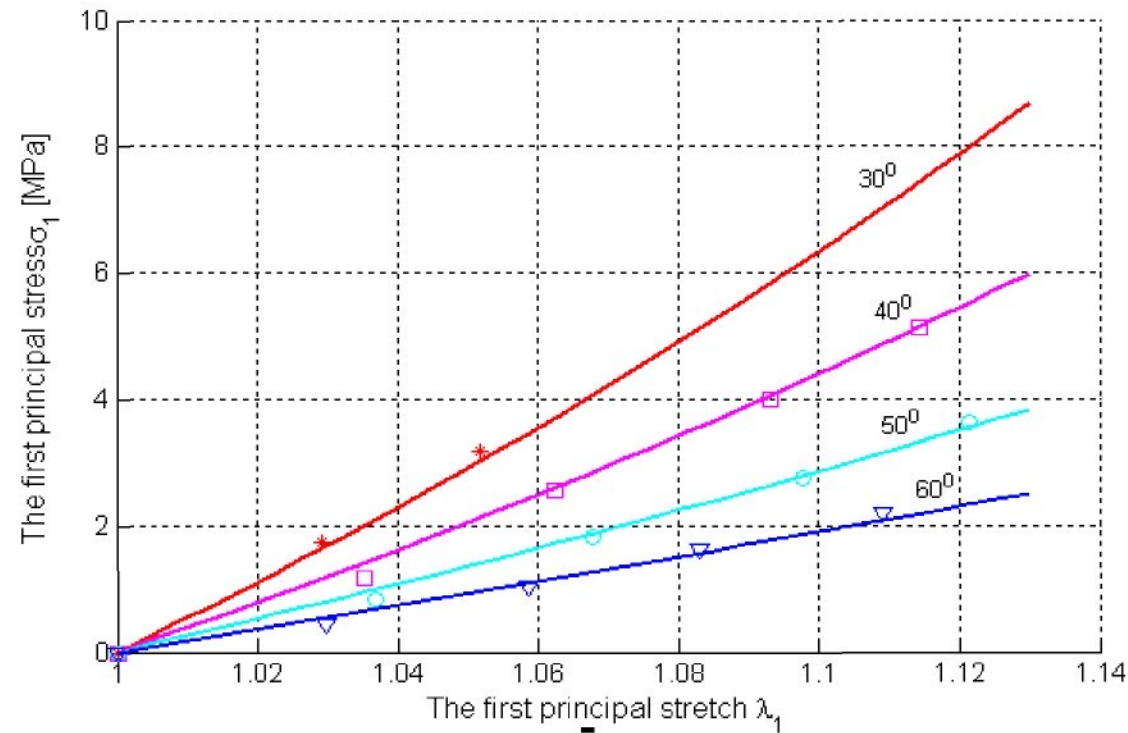


Figure 6 – Estimation of elastic coefficients of the composite reinforced with different fiber orientations by a pure shear test

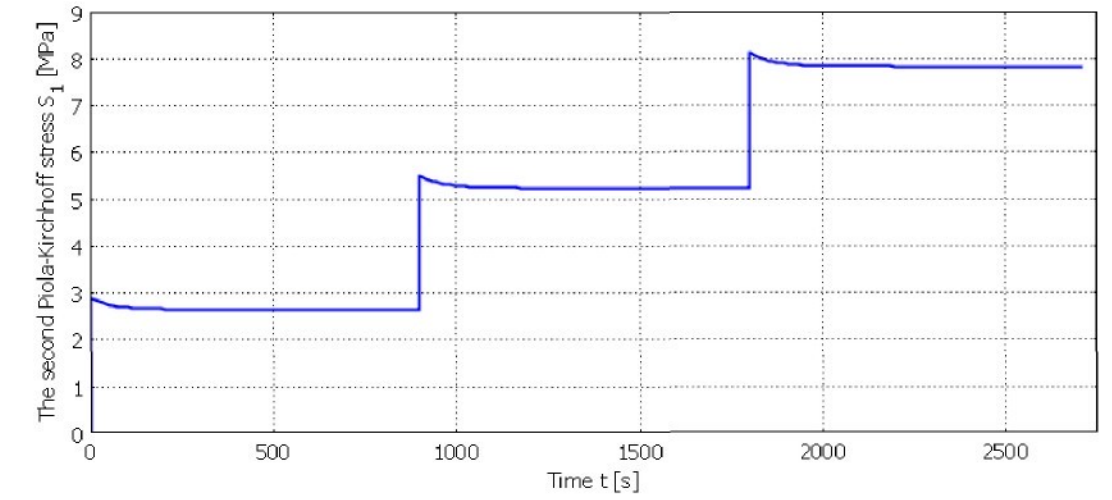
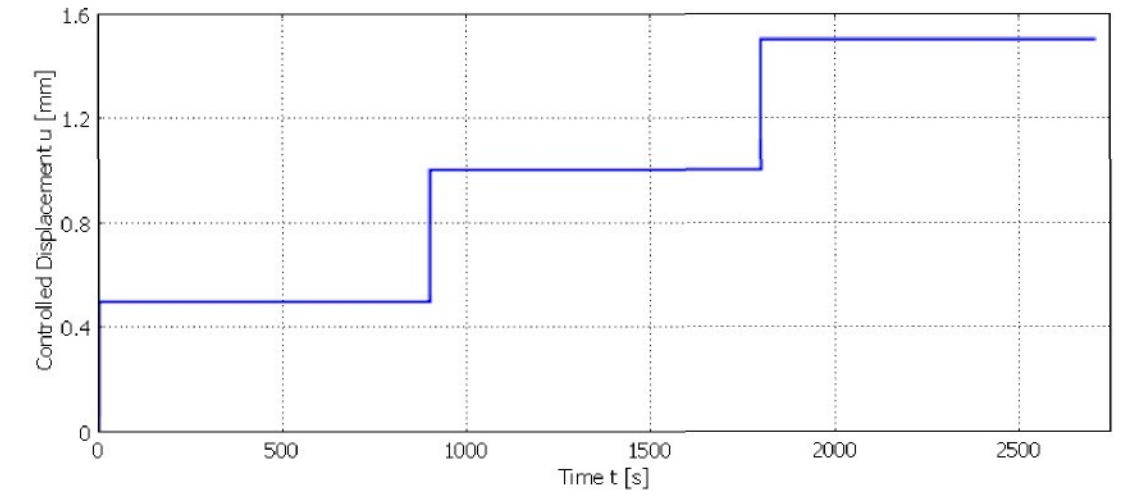


Figure 14 – Displacement and Piola-Kirchhoff stress of the anisotropic composite with fiber angles by 30° in relaxations

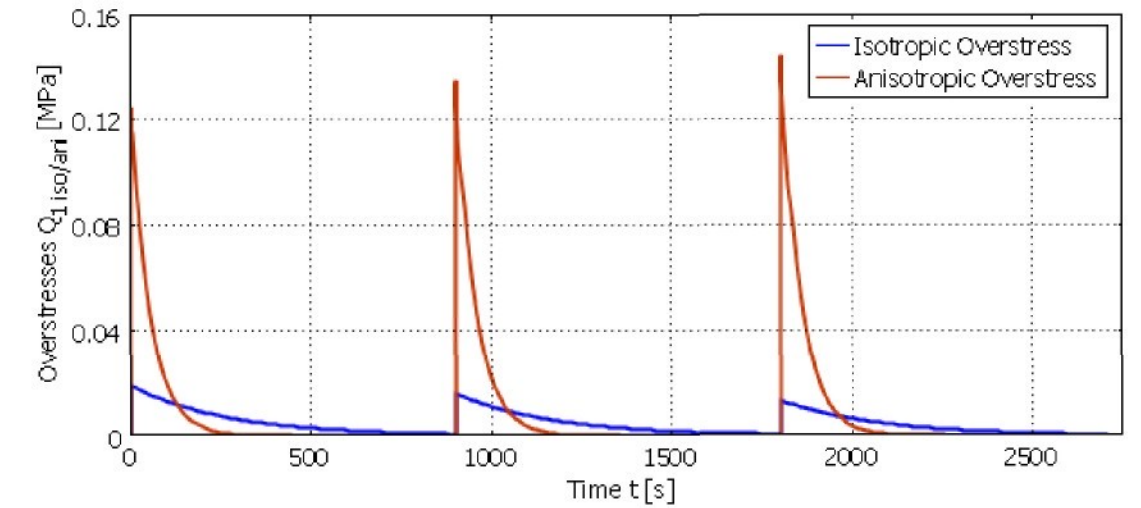


Figure 15 – The components of overstresses in the pure shear deformation

Prediction of creep process

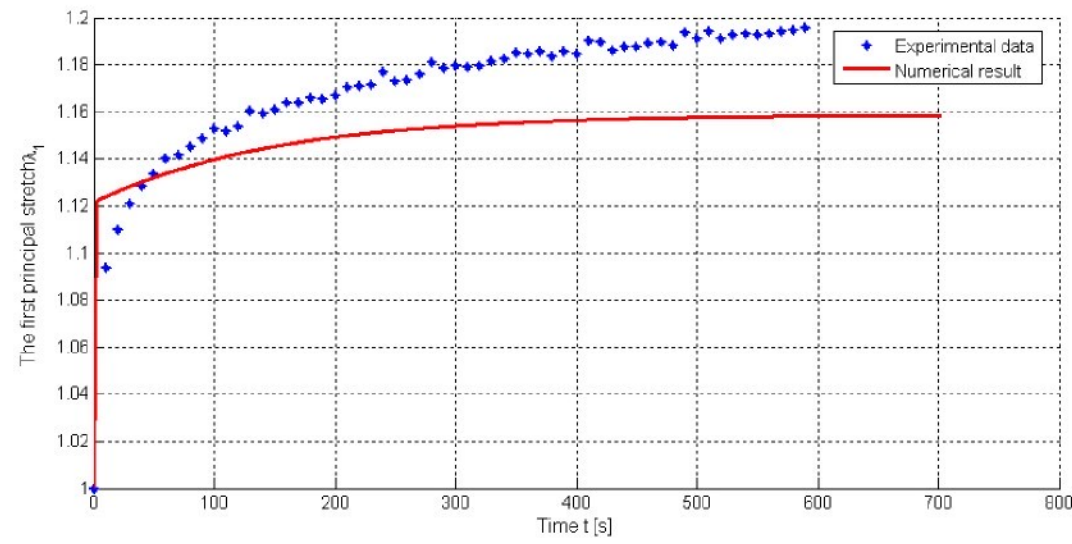


Figure 12 – Controlled force and displacement of simple tension in a creep

5.2. Fiber-reinforced composites

Equilibrium response of fiber-reinforced composite in pure shear

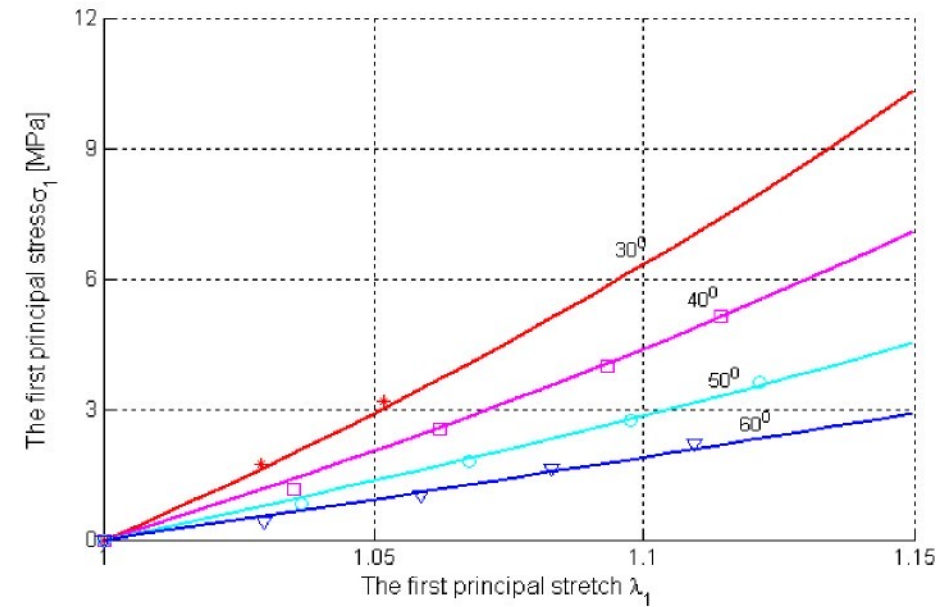
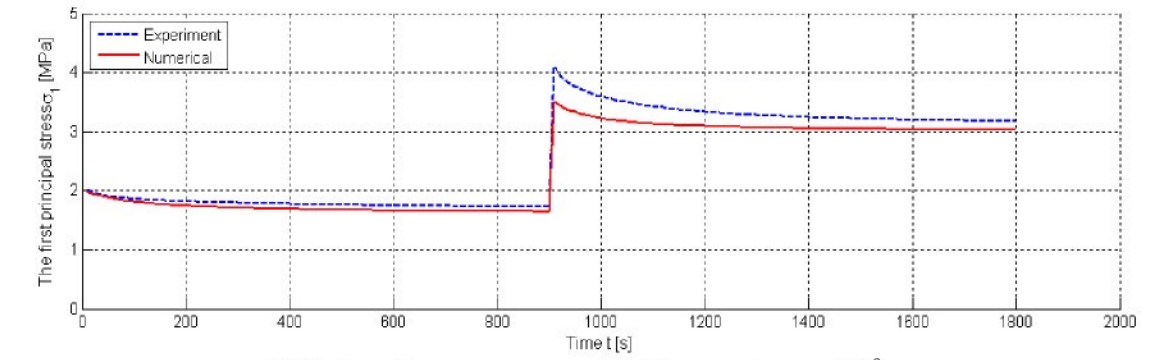
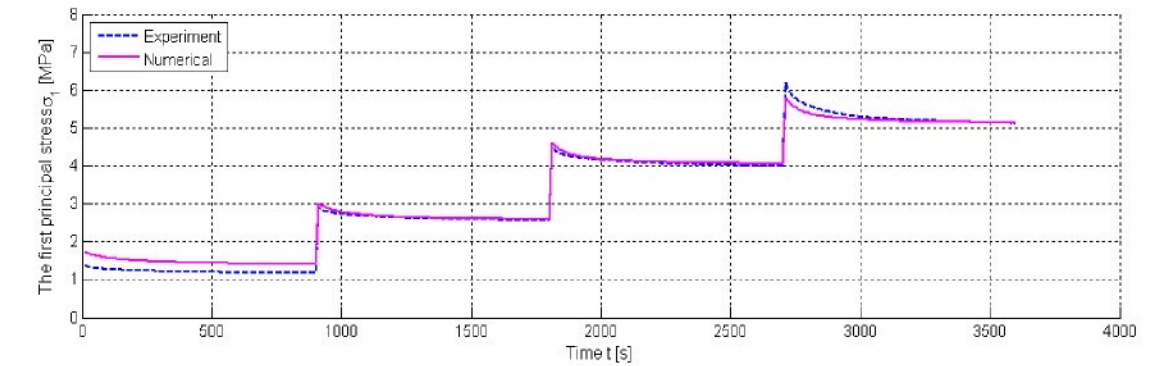


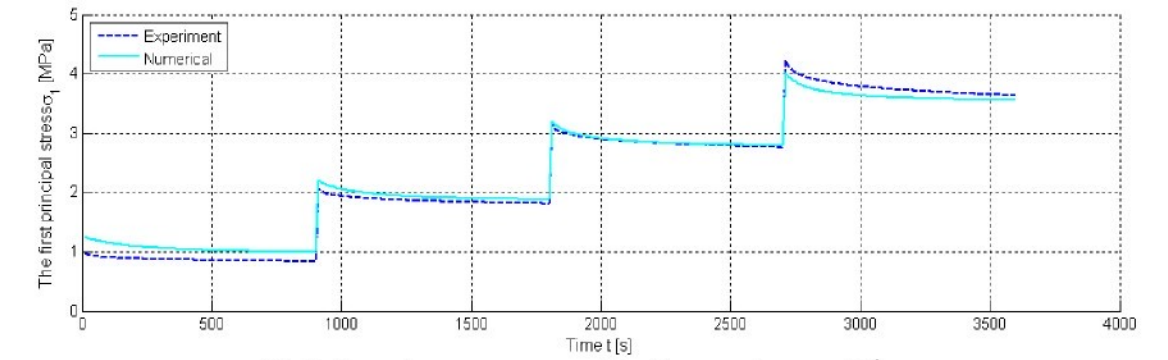
Figure 13 – Equilibrium Cauchy stress with different fiber directions in pure shear deformation (points denote experimental data, solid lines denote numerical results)



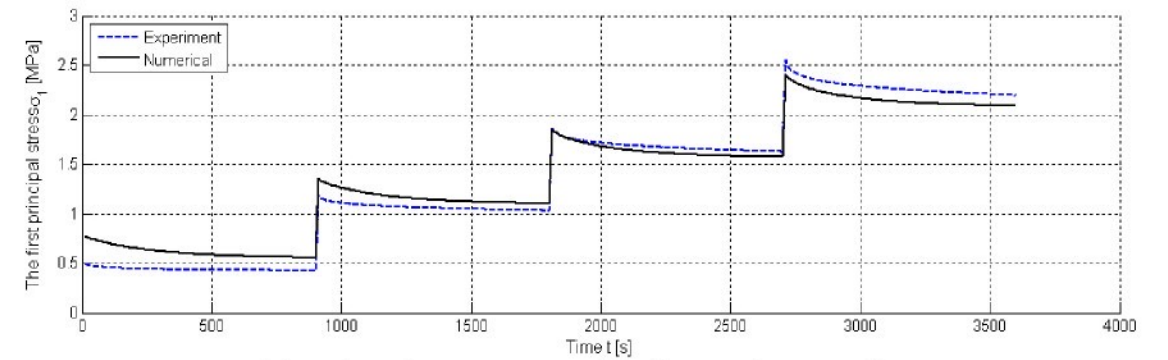
(a) Relaxation processes with fiber angle $\varphi = 30^\circ$



(b) Relaxation processes with fiber angle $\varphi = 40^\circ$



(c) Relaxation processes with fiber angle $\varphi = 50^\circ$



(d) Relaxation processes with fiber angle $\varphi = 60^\circ$

Figure 7 – Estimation of viscoelastic coefficients of the composite reinforced with different fiber orientations by a pure shear test

5. Numerical simulations of viscoelastic composites

In this section we will represent some numeric simulations of hyperelastic as well as viscoelastic behavior of composite materials. The main goal is to verify the performance of constitutive viscoelastic models presented associating with the material parameters determined from the evaluation of experiments.

5.1. Isotropic (hyperelastic) rubber-like materials

Equilibrium stress-strain responses

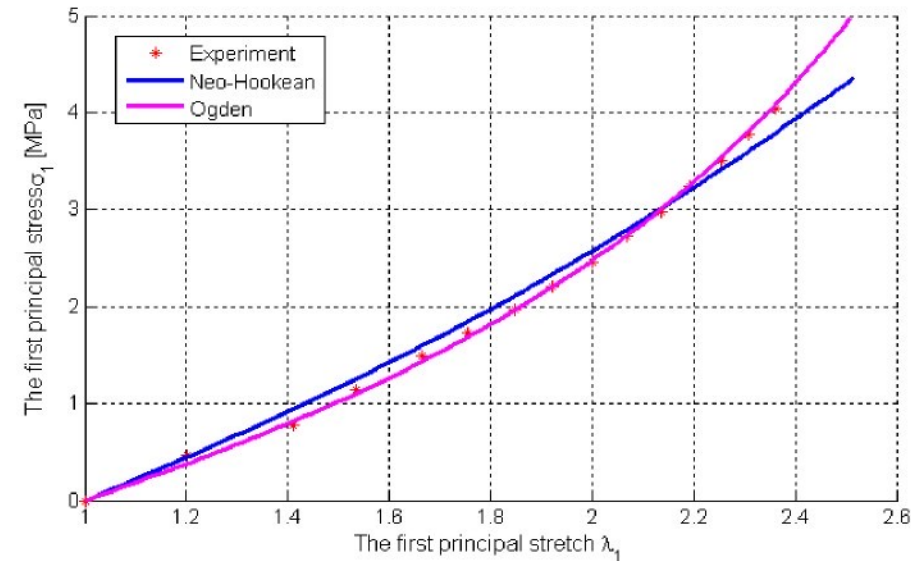


Figure 8 – First principal stress versus stretch of simple tension deformation

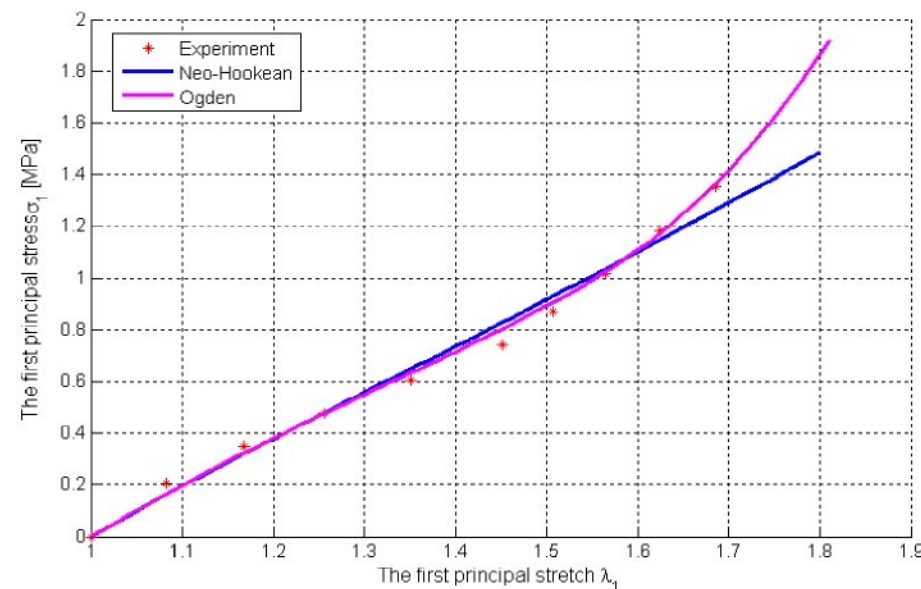


Figure 9 – First principal stress versus stretch of pure shear deformation

Viscoelastic behavior of isotropic materials

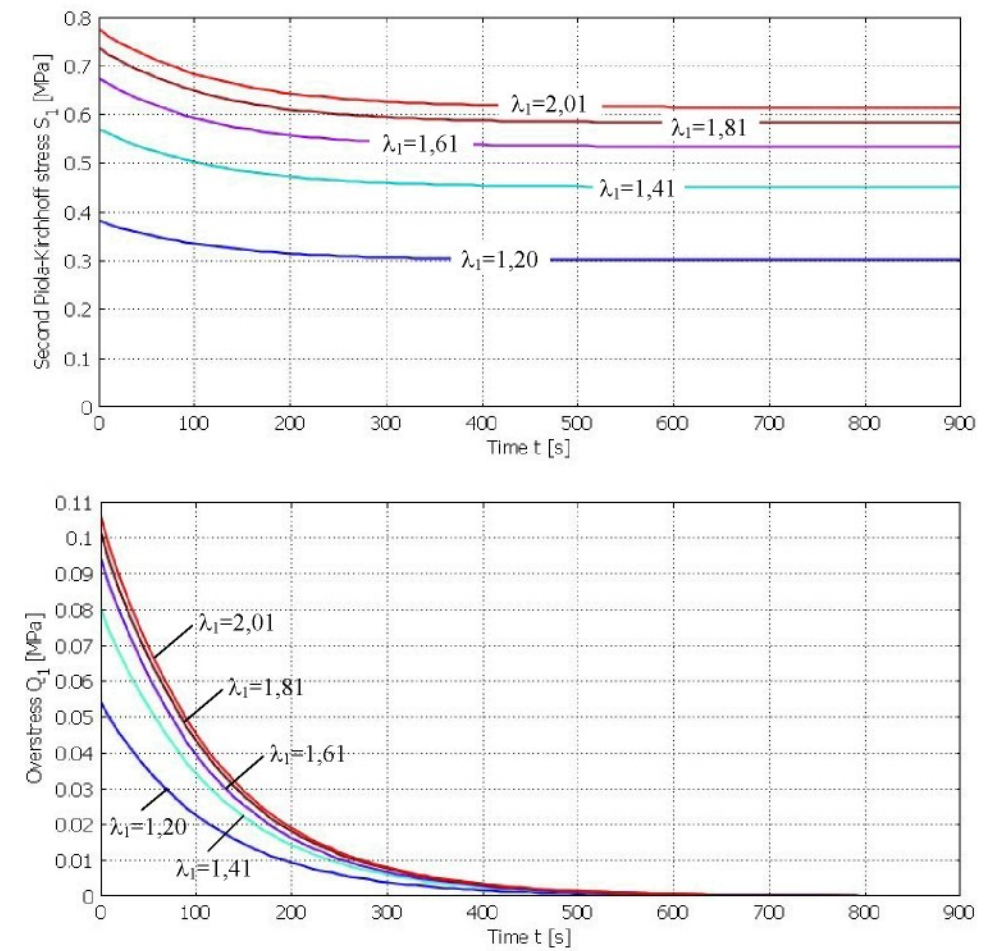


Figure 10 – The second Piola-Kirchhoff stresses and overstresses versus time at different stretches

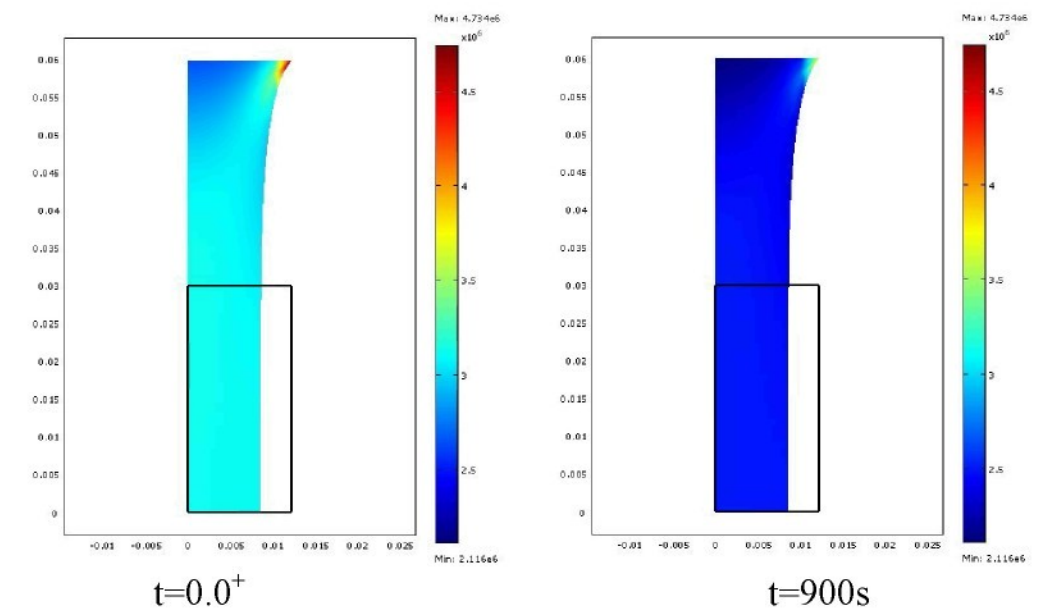


Figure 11 – Stress and deformation of simple tension in relaxation

Prof. Ing. Petr Louda, CSc.
Děkan strojní fakulty
TUL v Liberci

Věc: Žádost o obhajobu disertační práce

Vážený pane děkane, vzhledem k tomu, že mám splněny všechny studijní povinnosti a napsanu svou disertační práci, žádám o obhajobu mé disertační práce na téma
Elastické a viskoelastické chování kompozitů s elastomerickou maticí.

V Liberci 25.1.2010

Ing. Hoang Sy Tuan
doktorand KMP

CURRICULUM VITAE

Surname: **Hoang**

First name: **Sy Tuan**

PERSONAL DATA

Current occupation: PhD student

Date of birth: 26 Dec. 1978.

Place of birth: Thanhhoa, Vietnam.

Nationality: Vietnamese.

Phone: +420 773459758

E-mail: Hoang.Sy.Tuan@tul.cz

EDUCATION

Master of science Faculty of Mechanical Engineering, Hanoi University of Technology, Vietnam, Oct 2005.

Thesis: *Study behavior and computation of textile composite materials.*

Advisor: Dr. Nhu Phuong Mai

Bachelor of science Faculty of Mechanical Engineering, Hanoi University of Technology, Vietnam, Jun 2002.

Thesis: *Study and FEM calculation of instability of a rectangular plate under bending loads.*

Advisor: Dr. Nhu Phuong Mai

WORK EXPERIENCES

Ph.D. student Faculty of Mechanical Engineering, Technical University of Liberec, Czech Republic
From Aug 2006 to present.

Lecturer Faculty of Mechanical Engineering, Hanoi University of Technology.

From 2002 to 2006

Courses taught:

- *Strength of materials.*
- *Fundamental theory of applied elasticity.*
- *Applied mechanics.*
- *FEM.*

TECHNICAL SKILLS

<i>Software</i>	Microsoft office, Matlab and Maple.
<i>Modelling 3-D</i>	Solidworks.
<i>Programming</i>	Visual C ⁺⁺ , Visual Basic.
<i>FEM</i>	ANSYS, Comsol Multiphysics.

LANGUAGES KNOWN

<i>English</i>	- Good fluency.
<i>Vietnamese</i>	- Native fluency.
<i>Czech</i>	- Normal.

RESEARCH INTERESTS

- ✓ Viscoelastic analysis of composites.
- ✓ Mechanics of nonlinear continuum solids.
- ✓ Mechanics of composite materials, Finite Element Method.
- ✓ Analysis of magnetoelastic elastomer.

PUBLICATIONS

1. **H. S. Tuan**, B. Marvalová: Magnetoelastic anisotropic elastomers in a static magnetic field: Constitutive equations and FEM solutions. Proceedings of the sixth European Conference on Constitutive Models for Rubber. Dresden, 7-10 September 2009, Germany, pp. 453-458, ISBN 978-0-415-56327-7.
2. Jarmil Vlach, **Hoang Sy Tuan**, Bohdana Marvalová: Experimental and numerical research of Magneto-sensitive elastomers. 47th International Conference of Experimental Stress Analysis. Syrchov, June 8-11, 2009, Czech Republic, pp. 283-290, ISBN 978-80-7372-483-2.
3. **Hoang Sy Tuan**, Marvalová Bohdana: Simulation of Viscoelastic Fiber-Reinforced Composites at Finite Strains in Comsol Multiphysics. Applied Mechanics 2009, 11th International Scientific Conference. Smolenice, April 6-8, 2009, Slovak Republic, pp. 45-46, ISBN 978-80-89313-32-7.
4. **Hoang Sy Tuan**, B. Marvalová: Relaxation of Fiber-reinforced Composites: FEM Simulations. Conference Mechanical Composite Material and Structure. Pilsen, March 12-13, 2009, Czech Republic, pp. 70-77, ISBN 978-80-7043-782-7.
5. **Hoang S. T.**, Marvalová B.: Numerical Differentiation of Experimentally Measured Displacements. 16th Annual Conference Proceedings. Prague, November 11, 2008, Czech Republic, pp. 40, ISBN 978-80-7080-692-0.

6. **Sy Tuan Hoang**, Bohdana Marvalová: Coupling of magnetoelastic material and magnetic field in Comsol Multiphysics. Výpočty Konstrukcí Metodou Konečných Prvků. Pilsen, November 20, 2008, Czech Republic, pp. 8-18, ISBN 978-80-7043-735-3.
7. **Hoang S.T.**, Marvalová B.: Magneto-hyperelastic material in a uniform magnetic field: FEM Calculation of Stress and Strain. Engineering Mechanics 2008, National Conference with International Participation. Svratka, May 12-15, 2008, Czech Republic, pp. 86-87, ISBN 978-80-87012-11-6.
8. **Hoang Sy Tuan**, Bohdana Marvanová: FE analysis of cord-reinforced rubber composites at finite strains. Výpočty Konstrukcí Metodou Konečných Prvků. Prague, November 22, 2007, Czech Republic, pp. 9-20, ISBN 978-80-01-03942-7.
9. **Hoang. S.T.**, Marvalová B.: Constitutive Material Model of Fiberreinforced Composites in Comsol Multiphysics. Technical Computing Prague 2007, 15th Annual Conference Proceedings. Prague, November 14, 2007, Czech Republic, pp. 53, ISBN 978-80-7080658-6.
10. **Tuan Hoang Sy**, Marvalová B.: Relaxation of the Rubber Plate with Central Hole – FEM Simulation in Comsol Multiphysics. Applied Mechanics 2007, 9th International Scientific Conference. Malenovice, April 16-19, 2007, Czech Republic, pp. 214-215, ISBN 978-80-248-1389-9.
11. Nhu Phuong Mai - **Hoang Sy Tuan**. "Research on behaviour and calculation of Textile Composite Materials and layered plates". Proceedings of The National Conference on Mechanics. April-2004.
12. Nhu Phuong Mai - **Hoang Sy Tuan**. "Elasto-Plastic stability of the Triangular Layered Plate". Proceedings of The National Conference on Mechanics. Hanoi. December 18-20th, 2002 pp. 135-141.

HONORS AND AWARDS

Sep 2006: Selected for receiving scholarship of Czech government for Ph.D study.

May 2001: Encouragement prize in the Vietnam national annual mechanics competition for university students.

May 2000: Third prize in the Vietnam national annual mechanics competition for university students.

OTHER ACTIVITIES & HOBBIES

Football, jogging, movie and travel.

TECHNICAL UNIVERSITY OF LIBEREC

FACULTY OF MECHANICAL ENGINEERING



Doctoral Dissertation

2010

Ing. Hoang Sy TUAN

TECHNICAL UNIVERSITY OF LIBEREC
FACULTY OF MECHANICAL ENGINEERING

Ing. Hoang Sy Tuan

**ELASTIC AND VISCOELASTIC BEHAVIOUR OF COMPOSITES
WITH ELASTOMERIC MATRIX**

**ELASTICKÉ A VISKOELASTICKÉ CHOVÁNÍ KOMPOZITŮ
S ELASTOMERICKOU MATRICÍ**

Doctoral Dissertation

submitted to Department of Engineering Mechanics,
in partial fulfillment of the requirements
for the degree of doctor
of Philosophy in Mechanical Engineering

Supervisor:

doc. Ing. Bohdana Marvalová, CSc.

Liberec – 2010

Acknowledgments

The work presented in this dissertation has been possible thanks to several individuals whose contributions I would like to acknowledge. I first wish to express my deep gratitude and many thanks to my supervisor and her family, Associate Professor Bohdana Marvalová for all her guidance, support, advice and encouragement throughout my study in more than three years. The support which I have received from her is immeasurable. For this, I will never forget her.

I would like to thank Dr. Plešek, Prof. Holeček, Dr. Šimůnková and Prof. Holý for their useful lectures.

Specially, I am very grateful to Dr. Petriková for the financial support to perform experiments during my work.

I wish to acknowledge the important role of my family in my life, especially my parents. They always encourage and remind me to work hard to achieve my goals. They also teach me to realize the value of education and knowledge.

I also thank all my friends who have shared difficulties in real life. Their warm friendship is the reason I do not feel lonely.

Finally, I would like to thank all the members of Department of Engineering Mechanics for their kindness, friendliness and essential support during my work. I wish to thank Faculty of Mechanical Engineering of Technical University of Liberec and the Czech government for their provided fellowship.

This work was supported by the subvention from Ministry of Education of the Czech Republic through the Contract Code MSM 4674788501.

Prohlášení

Byl jsem seznámen s tím, že na mou doktorskou práci se plně vztahuje zákon č. 121/2000 o právu autorském, zejména §60 (školní dílo) a §35 (o nevýdělečném užití díla k vnitřní potřebě školy).

Beru na vědomí, že Technická univerzita v Liberci má právo na uzavření licenční smlouvy o užití mé práce a prohlašuji, že souhlasím s případným využitím mé práce (prodej, zapůjčení apod.).

Jsem si vědom toho, že užít své doktorské práce či poskytnout licenci k jejímu využití mohu jen se souhlasem Technické univerzity v Liberci, která má právo ode mne požadovat přiměřený příspěvek na úhradu nákladů, vynaložených univerzitou na vytvoření díla (až do jejich skutečné výše).

V Liberci

.....

vlastnoruční podpis

Místopřísežné prohlášení

Místopřísežně prohlašuji, že jsem doktorskou práci vypracoval samostatně s použitím uvedené literatury, pod vedením školitelkou.

V Liberci

.....

ABSTRACT

The viscous behavior of the fiber-reinforced composite materials with rubber-like matrix is modeled in the continuum mechanics framework by the Helmholtz free energy function and the evolution equations of the internal variables. The decomposition of the free energy function and the chosen viscoelastic model are bases for formulation and description of the viscous characteristics of these anisotropic materials. Numerical simulations to predict the response of these materials in finite strains are performed.

The dissertation focused on experimental evaluating the purely elastic and viscoelastic material parameters of proposed models via some standard experiments on relaxation, such as simple tension, pure shear and biaxial tensile tests. Both the isotropic and anisotropic materials were tested.

Several numerical examples were implemented in FEM software COMSOL Multiphysics and compared with the experimental results. The applications of the model were enlarged to predict other viscoelastic phenomena i.e. creep and influence of loading velocities on stresses. The influence of the directions of reinforcing fibers was also examined. The viscoelastic model was applied to a practical example that is an air-spring with two fiber reinforcements undergoing an internal pressure.

An extension of nonlinear theory for rubber-like anisotropic composites was applied to magneto-sensitive (MS) elastomers under an external magnetic field. The constitutive equations of both magnetic and mechanical fields were presented. Some numerical computations of a coupling of magnetic and mechanical problems were illustrated in order to describe a nonlinear characteristic of MS elastomer.

Key words:

Composites, rubber-like matrix, fiber-reinforced, viscoelasticity, magneto-sensitive elastomers, experimental, FEM.

ABSTRAKT

Viskózní chování kompozitních materiálů s pryžovou maticí vyztuženou kordy je modelováno v rámci mechaniky kontinua pomocí Helmholtzovy funkce volné energie a vývojových rovnic pro vnitřní proměnné. Rozklad funkce volné energie a zvolený viskoelastický model jsou základem pro formulaci a popis viskózní vlastnosti těchto anizotropních materiálů. Jsou uvedeny numerické simulace pro přepověď odezvy těchto materiálů na konečné deformace.

Disertační práce se zaměřuje na experimentální určení elastických a viskoelastických materiálových parametrů navrhovaných modelů pomocí některých standardních testů jako je tahová zkouška, čistý smyk a dvouosé tahové zkoušky kvazistatické i relaxační. Byly testovány izotropní a anizotropní (kompozitní) materiály.

Několik numerických případů je implementováno do MKP prostředí COMSOL Multiphysics a srovnáno s experimentálními výsledky. Aplikace modelu byly rozšířeny o numerickou předpověď dalších viskoelastických jevů jako je tečení a vliv rychlosti zatížení na napětí. Vliv směru vlákněné výztuže byl rovněž zkoumán. Viskoelastický model byl aplikován na numerickou simulaci vnitřním přetlakem zatížené vzduchové válcové pružiny, jejíž pryžový plášť je vyztužen dvěma skupinami kordů.

Nelineární materiálový anizotropní model byl rozšířen na případ magneto-senzitivních elastomerů mechanicky zatížených ve vnějším magnetickém poli. Numerické simulace odezvy tělesa s magneto-mechanickou vazbou jsou uvedeny s cílem popsat nelineární vlastnosti magneto-senzitivních elastomerů.

Klíčová slova:

Kompozity, pryžová matrice, kordová výztuž, viscoelasticita, magneto-senzitivní elastomery, experiment, MKP.

Table of Contents

List of figures	xiii
List of tables	xvii
Notation and symbols	xviii
Chapter 1. Introduction	1
Outline of the dissertation	3
Chapter 2. Overview of literature	5
Chapter 3. Free energy functions and constitutive relations for equilibrium and viscoelastic response of rubber-like composite	11
3.1. Free energy functions	11
3.1.1. Volumetric free energy function	11
3.1.2. Isotropic (isochoric) free energy functions	12
3.1.3. Anisotropic (isochoric) free energy functions	13
3.2. Equilibrium stress responses in plane-stress deformations	14
3.2.1. Isotropic rubber-like materials	14
3.2.2. Composites reinforced by two families of fibers	15
3.3. Non-equilibrium stress responses	16
3.3.1. Solution of evolution equations for overstresses	16
3.3.2. Solution of evolution equations for inelastic strains	17
Chapter 4. Experiments and material parameter identification	19
4.1. Experimental equipments and specimens	19
4.1.1. Universal testing machine TIRAtest 2810	19
4.1.2. Biaxial testing equipment	19
4.1.3. System Q-400 digital cameras Dantec Dynamics	20
4.1.4. Specimen preparation	21
4.2. Experiments and identification methods	21

4.2.1. Experimental descriptions	21
4.2.2. Identification methods	23
4.3. Isotropic composite materials	24
4.3.1. Simple tension	25
4.3.2. Pure shear test	27
4.3.3. Biaxial tensile test	29
4.4. Fiber-reinforced composite materials	30
Chapter 5. Numerical simulations of viscoelastic composites	35
5.1. FEM implementation in COMSOL Multiphysics	35
5.2. Isotropic (hyperelastic) rubber-like materials	36
5.2.1. Equilibrium stress-strain responses	36
5.2.2. Viscoelastic behavior of isotropic materials	39
5.2.2.1. <i>Effect of loading velocities</i>	39
5.2.2.2. <i>One-step and multi-step relaxations</i>	40
5.2.2.3. <i>Prediction of creep process</i>	42
5.3. Fiber-reinforced composites	43
5.3.1. Equilibrium response of fiber-reinforced composite in pure shear	43
5.3.2. Elastic response of a rectangular fiber-reinforced composite plate with a hole	45
5.3.3. Viscoelastic response of fiber-reinforced composite	46
5.4. Viscoelastic behavior of an air-spring	48
5.4.1. Equilibrium responses of an air-spring tube	48
5.4.2. Viscous responses of an air-spring tube	50
5.5. Viscous responses of internal stress-like and strain-like variables	52
Chapter 6. Magneto-sensitive elastomer materials	55
6.1. Governing equations	56
6.1.1. Magnetic equations	56
6.1.2. Mechanical equations	57
6.1.3. Constitutive equations	57
6.1.4. The free energy function in terms of invariants	58
6.2. Numerical simulations of MS elastomers	60

6.2.1. FEM solutions of MS isotropic materials	60
6.2.1.1. <i>A plane strain compression of isotropic material block</i>	61
6.2.1.2. <i>A simple shear strain of isotropic material plate</i>	63
6.2.1.3. <i>A pure shear deformation of isotropic material tube</i>	65
6.2.2. FEM solutions of MS anisotropic materials	67
6.2.2.1. <i>Compression of anisotropic material block</i>	68
6.2.2.2. <i>Simple shear of anisotropic materials</i>	71
6.3. Conclusion	73
Chapter 7. Conclusions, discussions and future perspectives	75
Literatures	77
Publications	83
Appendix A. Overview of continuum mechanics	A-1
A.1. Finite strain kinematics	A-1
A.1.1. Motions of continuum bodies	A-2
A.1.2. Deformation gradient	A-4
A.1.3. Strain tensors	A-5
A.1.4. Structural tensor	A-7
A.2. Stress tensors	A-7
A.2.1. Cauchy stress tensor and equilibrium equation	A-7
A.2.2. Alternative stress tensors	A-8
A.2.3. Conjugate pairs of stress and strain tensors	A-9
A.3. Balance principles	A-10
A.3.1. Conservation of mass	A-10
A.3.2. Momentum balance principles	A-10
A.3.3. Balance of mechanical energy	A-11
A.3.4. Balance of energy in continuum thermodynamics	A-12
Appendix B. Anisotropic viscoelastic models	A-13
B.1. Constitutive equations	A-13
B.1.1. The decomposition of the free energy function	A-13
B.1.2. Constitutive equations of stress responses	A-14

B.1.2.1. <i>Transversely isotropic materials</i>	A-15
B.1.2.2. <i>Two fiber-reinforced composite materials</i>	A-16
B.2. Evolution equations with internal variables	A-18
B.2.1. Internal stress-like variables	A-18
B.2.2. Internal strain-like variables	A-19
Appendix C. Implementation of user material models in Comsol Multiphysics	A-23
C.1. Definition of modules for viscoelastic problems	A-23
C.2. Definition of constitutive equations	A-23
C.3. Redefine free energy functions	A-24
C.4. Formulation of evolution equations	A-25
C.5. Define a function in Comsol	A-25
C.6. Integration of volume	A-26
Appendix D. Some m-function and script files in Matlab®	A-27
D.1. Some functions of analyzing data	A-27
D.1.1. “ConnectDataSteps” function	A-27
D.1.2. Main program of analyzing data	A-28
D.2. Estimation of purely elastic coefficients	A-28
D.2.1. “VolStress” function	A-28
D.2.2. “IsoStress” function	A-29
D.2.3. “AniStress” function	A-29
D.2.4. “FitElasticParameter” function	A-29
D.2.5. The main program of evaluation of purely elastic parameters	A-30
D.3. Estimation of viscoelastic coefficients	A-30
D.3.1. “OverStress” function	A-30
D.3.2. “FitLinearViscousCoeff” function	A-31
D.3.3. “FitViscousParamerter” function	A-31
D.3.4. Main program of evaluation of viscoelastic material parameters	A-31

List of Figures

Figure 1.1	Some applications of FREs	1
Figure 4.1	Universal testing machine TIRAtest 2810	19
Figure 4.2	The main window application of TIRAtest software	19
Figure 4.3	Biaxial testing equipment	19
Figure 4.4	Digital cameras	20
Figure 4.5	Main window of Istra 4D software	20
Figure 4.6	Shapes of specimens for simple tensile, pure shear and biaxial tests	21
Figure 4.7	Mullins effect in cyclic tests	22
Figure 4.8	Strain evaluation by the image correlation	22
Figure 4.9	A standard Maxwell element	24
Figure 4.10	Controlled displacement in the simple tensile test	25
Figure 4.11	Applied force in the simple tensile test	25
Figure 4.12	Estimation of elastic coefficients of the isotropic material by a simple tensile test with different models	26
Figure 4.13	Estimation of viscoelastic coefficients of the isotropic material by a simple tensile test with neo-Hookean and Ogden models	27
Figure 4.14	Controlled displacement in the pure shear test	27
Figure 4.15	Applied force in the pure shear test	28
Figure 4.16	Principal stretches in the pure shear test	28
Figure 4.17	Estimation of elastic coefficients of the isotropic material by a pure shear test with different models	28
Figure 4.18	Estimation of viscoelastic coefficients of the isotropic material by a pure shear test with neo-Hookean and Ogden models	29
Figure 4.19	Estimation of elastic coefficients of the isotropic material by a biaxial tensile test with different models	30
Figure 4.20	Estimation of elastic coefficients of the composite reinforced with different fiber orientations by a pure shear test	31

Figure 4.21	Estimation of viscoelastic coefficients of the composite reinforced with different fiber orientations by a pure shear test	32
Figure 5.1	Geometries and FE models in simple tension and pure shear deformations	37
Figure 5.2	First principal stress versus stretch of simple tension deformation	37
Figure 5.3	First principal stress versus stretch of pure shear deformation	38
Figure 5.4	Stress distribution of simple tension and pure shear	38
Figure 5.5	Stress-strain response at different loading velocities	40
Figure 5.6	Deformation of isotropic materials in a simple tension at different extensions	40
Figure 5.7	The second Piola-Kirchhoff stresses and overstresses versus time at different stretches	41
Figure 5.8	Stress and deformation of simple tension in relaxation	41
Figure 5.9	Displacement and Cauchy stress of simple tension in multistep relaxations	42
Figure 5.10	Controlled force and displacement of simple tension in a creep	43
Figure 5.11	Geometry and FE model of fiber-reinforced composite in pure shear deformation	43
Figure 5.12	Deformation and stress distribution of composite with different fiber angles	44
Figure 5.13	Equilibrium Cauchy stress with different fiber directions in pure shear deformation	44
Figure 5.14	Deformation and stress distribution of a composite plate with a hole	45
Figure 5.15	Cauchy stress versus the first principal stretch of a composite with a hole	46
Figure 5.16	Displacement and Piola-Kirchhoff stress of the anisotropic composite with fiber angles by 30° in relaxations	47
Figure 5.17	The components of overstresses in the pure shear deformation	47
Figure 5.18	A sketch scheme of geometry and FE model of an air-spring tube subjected an internal static pressure	48
Figure 5.19	Deformation and stress in the tube inflated by an internal pressure 0,9MPa the angle of fibers $\varphi=30^\circ$, 35° and 40°	49
Figure 5.20	“Inversion phenomenon” happens to a tube reinforced by fibers with $\varphi=40^\circ$	50

Figure 5.21	The internal pressure and the longitudinal stretch with different fiber angles	50
Figure 5.22	External force acts on the tube in a creep	51
Figure 5.23	Deformation and stress of the tube at different time instants in a creep	51
Figure 5.24	The viscous behavior of the tube in the creep process	52
Figure 5.25	Two approaches for the viscous response of the fiber-reinforced composites in relaxations	54
Figure 5.26	Two approaches for the viscous response of the fiber-reinforced composites in creeps	54
Figure 6.1	Compression of a block	61
Figure 6.2	Deformation of the block in horizontal magnetic field	61
Figure 6.3	Deformation of the block in vertical magnetic field	62
Figure 6.4	Loading depends on direction and magnitude of magnetic field	62
Figure 6.5	A geometric model to applied simple shear	63
Figure 6.6	MS block in simple shear	63
Figure 6.7	Variation of magnetic fields H_x , H_y in the deformation body	64
Figure 6.8	Dependency of stress components and displacement on magnetic field	64
Figure 6.9	Geometry of the tube	65
Figure 6.10	Magnetic flux density, magnetic field	65
Figure 6.11	Magnetic traction and Von Misses stress	66
Figure 6.12	Displacement depends on magnetic when loading is constant	66
Figure 6.13	Loading depends on magnetic when applied displacement is constant	67
Figure 6.14	A scheme sketch of the compressive block in a magnetic field	68
Figure 6.15	Deformation of the MS anisotropic block without and with a uniform magnetic field	69
Figure 6.16	Distribution of the magnetic field and the magnetization of the MS anisotropic material	70
Figure 6.17	Displacements of the top surface of the block versus the magnetic flux density	70
Figure 6.18	A geometry of a plate subjected a simple shear state is embedded in a static uniform magnetic field	71
Figure 6.19	Simple shear state of the plate with different magnetic directions	72
Figure 6.20	Distribution of the magnetic field with $\theta = 50^\circ$	72

Figure 6.21	Dependencies of a displacement and a shear stress on the magnetic field	73
Figure A.1	Configuration and motion of a continuum body	A-2
Figure A.2	Traction vectors acting on infinitesimal surface elements	A-8
Figure B.1	The generalized rheological Maxwell model for internal stress-like variables	A-19
Figure B.2	Multiplicative decomposition of deformation gradient	A-20
Figure B.3	Rheological equivalent Maxwell model for internal strain-like variables ...	A-21
Figure C.1	Define “ <i>Structural Mechanics Module</i> ” and “ <i>PDE Modes</i> ” modules	A-23
Figure C.2	Define constitutive equations	A-24
Figure C.3	Modify the definition of free energy function	A-24
Figure C.4	Formulate evolution equations	A-25
Figure C.5	Define a user function	A-25
Figure C.6	Integral volume of an air-spring tube	A-26

List of Tables

Table 4.1	Elastic coefficients of the isotropic material by the simple tensile test	26
Table 4.2	Viscoelastic coefficients of the isotropic material by the simple tensile test	26
Table 4.3	Elastic coefficients of the isotropic material by the pure shear test	29
Table 4.4	Viscoelastic coefficients of the isotropic material by the pure shear test ...	29
Table 4.5	Elastic coefficients of the isotropic material by the biaxial tensile test	30
Table 5.1	Elastic and viscoelastic material parameters of anisotropic composites	53
Table 6.1	Material parameters of an MS anisotropic composite	67

Notation and Symbols

We attempt to employ notations that reflect as clearly as possible differences of kind among mathematical entities. The scalar quantities are denoted by Latin or Greek italic letters while vectors and second-order tensors and/or matrices are represented by the boldface characters and blackboard bold letters denote fourth-order tensors. Subscript indices i, j, \dots of vectors, matrices and tensors signify specific components of the corresponding vectors, matrices and tensors.

\mathbf{a}_0	Unit vector of the first fiber direction in reference configuration
\mathbf{a}_α	Unit vector of the α -th fiber direction in reference configuration
\mathbf{A}	Almansi strain tensor
\mathbf{b}_0	Unit vector of the second fiber direction in reference configuration
\mathbf{b}	Left Cauchy-Green deformation tensor
\mathbf{B}	Magnetic induction vector or magnetic flux in spatial configuration
\mathbf{B}_I	Magnetic induction vector in reference configuration
B_x, B_y	Component of \mathbf{B} in x and y directions
c_1, c_2	Mooney-Rivlin coefficients
\mathbf{C}	Right Cauchy-Green tensor deformation
$\bar{\mathbf{C}}$	Modified right Cauchy-Green deformation tensor
\mathbf{C}_M^e	Elastic component of the right Cauchy-Green tensor of the matrix phase
\mathbf{C}_F^e	Elastic component of the right Cauchy-Green tensor of the fiber phase
\mathbf{C}_M^v	Viscous component of the right Cauchy-Green tensor of the matrix phase
\mathbf{C}_F^v	Viscous component of the right Cauchy-Green tensor of the fiber phase
dl	Current element length
dL	Material element length
\mathbf{e}_i	Orthogonal base vectors
\mathbf{E}	Green-Lagrange strain tensor
E_r	Spring stiffness in the r -th branch of the Maxwell model
\mathbf{f}_b	Body force

F	Deformation gradient
\mathbf{F}_M^e	Elastic component of deformation gradient of the matrix phase
\mathbf{F}_F^e	Elastic component of deformation gradient of the fiber phase
\mathbf{F}_M^v	Viscous component of deformation gradient of the matrix phase
\mathbf{F}_F^v	Viscous component of deformation gradient of the fiber phase
I	Unit tensor
I_1, I_2, I_3	Elastic principal invariants
I_4, I_5, \dots, I_{10}	Pseudo-invariants
$\bar{I}_a, a = 1, 2, 4, \dots$	Modified invariants of the corresponding principal invariants
$I_{M_1}^e, I_{M_2}^e, I_{M_3}^e$	Invariants of \mathbf{C}_M^e in the matrix phase
I_{F_4}, \dots, I_{F_8}	Invariants of \mathbf{C}_F^e in the fiber phase
I	Fourth-order unit tensor
J	Jacobian determinant
H	Magnetic field vector in spatial configuration
\mathbf{H}_I	Magnetic field vector in reference configuration
H_x, H_y	Component of H in x and y directions
k_1	Stress-like material parameter of free energy function
k_2	Dimensionless parameters of free energy function
m	Positive integer
\mathbf{M}_1	Structural tensor representing the first fiber direction
\mathbf{M}_2	Structural tensor representing the second fiber direction
\mathbf{M}_α	Structural tensor representing the α -th fiber direction
$\tilde{\mathbf{M}}_\alpha, \alpha = 1, 2$	structural tensors in the intermediate configuration
n	Positive integer
n	Unit normal vector
p	Hydrostatic pressure
P	First Piola-Kirchhoff stress tensor
\mathbb{P}	Fourth-order projection tensor
\mathbf{Q}_r	Overstress tensor
s_x, s_y	Normal Cauchy stresses in x and y directions
S	Second Piola-Kirchhoff stress tensor

\mathbf{S}_{am}^{EQ}	Anisotropic equilibrium component of the second Piola-Kirchhoff stress tensor
\mathbf{S}_{EQ}	Equilibrium component of the second Piola-Kirchhoff stress tensor
$\bar{\mathbf{S}}_{EQ}$	Fictitious second equilibrium Piola-Kirchhoff stress tensor
\mathbf{S}_{iso}^{EQ}	Isotropic equilibrium component of the second Piola-Kirchhoff stress tensor
\mathbf{S}_{NEQ}	Non-equilibrium component of the second Piola-Kirchhoff stress tensor
\mathbf{S}_{vol}^{EQ}	Volumetric equilibrium component of the second Piola-Kirchhoff stress tensor
t	Time
\mathbf{t}	Cauchy traction vector
\mathbf{T}_F	Anisotropic flow stress for the fiber phase
\mathbf{T}_M	Isotropic flow stress of the matrix
\mathbf{u}	Displacement in spatial configuration
\mathbf{U}	Displacement in reference configuration
v	Volume in spatial configuration
V	Volume in reference configuration
\mathbb{V}_F	Positive-definite, fourth-order, isotropic tensor related to the fiber viscosities and the fiber arrangement
\mathbb{V}_M	Positive-definite, fourth-order, major and minor symmetric tensor related to the matrix phase
\mathbf{x}	Position vector in spatial configuration
\mathbf{X}	Position vector in reference configuration

\mathcal{B}	Continuum body
\mathcal{D}_{int}	Internal dissipation inequality
α, β, γ	Non-dimensional material parameters
β_{ra}	Non-dimensional free-energy factor
δ_{ij}	Kronecker delta
$\mathbf{\varepsilon}$	Infinitesimal strain tensor
$\bar{\gamma}_1, \bar{\gamma}_2, \dots$	Response coefficients
$\mathbf{\Gamma}_r$	Internal variables as inelastic strain tensors
$\bar{\mathbf{\Gamma}}_r$	Modified internal variables of $\mathbf{\Gamma}_r$
$\eta_{F_\alpha}, \alpha = 1, 2$	Fiber viscosities
η_{M_B}	Bulk viscosity of the matrix material
η_{M_S}	Shear viscosity of the matrix material
η_r	Viscosity of dashpot in the r-th branch of the Maxwell model
φ	Fiber angle
λ_α	Stretch ratio of the α -th fiber
$\lambda_{\mathbf{a}_\alpha}$	Stretch vector in the unit vector direction \mathbf{a}_α
$\lambda_1, \lambda_2, \lambda_3$	Principal stretches
$\bar{\lambda}_1, \bar{\lambda}_2, \bar{\lambda}_3$	Modified principal stretches
μ	Shear modulus
μ_0	Universal constant
μ_r	Relative magnetic permeability
θ	Magnetic direction
ρ	Mass density in current configuration
ρ_0	Mass density in material configuration
$\boldsymbol{\sigma}$	Cauchy stress tensor
τ_{ra}	Relaxation time
$\boldsymbol{\tau}$	Kirchhoff stress tensor
$\boldsymbol{\tau}_M$	Maxwell stress
Ψ	Helmholtz free energy function
Ψ_{dis}	Distortional contribution of the free energy function
Ψ_{EQ}	Equilibrium component of the free energy function

Ψ_{ani}^{EQ}	Anisotropic equilibrium contribution of the free energy function
Ψ_F^{EQ}	Equilibrium component of the free energy function of the fiber phase
Ψ_{iso}^{EQ}	Isotropic equilibrium contribution of the free energy function
Ψ_M^{EQ}	Equilibrium component of the free energy function of the matrix phase
Ψ_{vol}^{EQ}	Volumetric equilibrium contribution of the free energy function
Ψ_{NEQ}	Non-equilibrium component of the free energy function
Ψ_F^{NEQ}	Non-equilibrium component of the free energy function of the fiber phase
Ψ_M^{NEQ}	Non-equilibrium component of the free energy function of the matrix phase
Υ_{iso}^{NEQ}	Dissipative potentials determining the r-th viscoelastic contribution

Chapter 1

INTRODUCTION

Fiber-reinforced elastomers (FREs) also well-known as anisotropic hyperelastic composites are widely used in practice, including industrial engineering, automobile, aircraft, biomechanics and medicine, for example gas pipes, automotive tyres, absorbers, belts, man-made (elastomeric) composites, etc., as illustrated in Figure 1.1.

These composites have many potential advantages due to high specific stiffness and strength, good corrosion resistance and thermal insulation. The typical anisotropic behavior is often formed by a number of fiber cords (usually one or two fibers coincide at each point) which are systematically arranged in a rubber-like matrix material. However, these materials not only have a highly non-linear behavior and possess anisotropic mechanical properties but also exhibit viscoelastic material behavior. Furthermore particularly important to this behavior is the heating of the structure because of internal dissipation and the temperature dependence of the material parameters. Therefore the ability to accurately predict the mechanical behavior of these materials is an important technological problem that is still far from being completely understood.

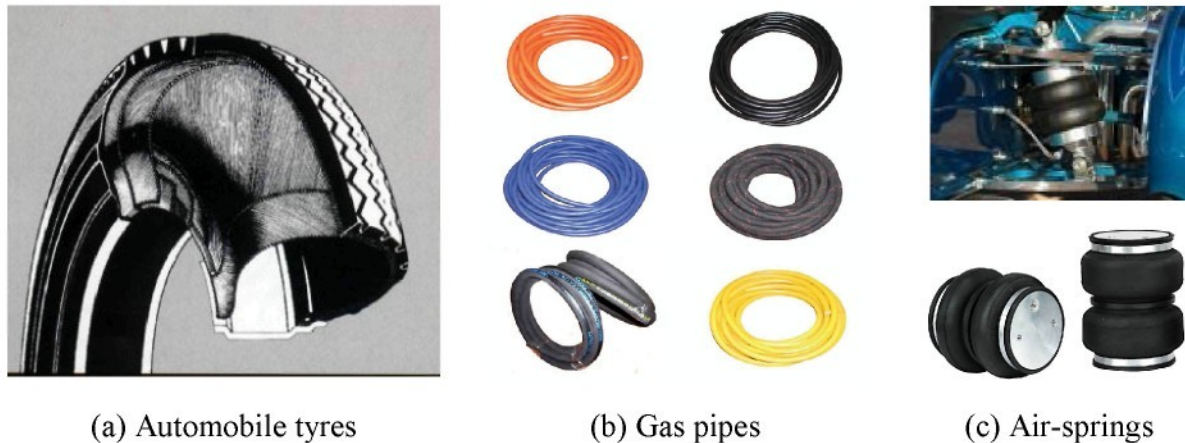


Figure 1.1 – Some applications of FREs

The main objective of the thesis is to identify and simulate the viscous characteristics of the fiber-reinforced composite materials with rubber-like matrix. The identification of the material parameters and the implementation of the numerical simulations that base on the chosen viscoelastic model are presented.

In this work both a mechanical experiment and a numerical simulation have been used in an effort to gain better insight into the mechanics causing the observed behavior and to facilitate ability performance of a viscoelastic model. As introduced in Chapter 2, there are many proposed viscoelastic models to deal viscoelastic problems of isotropic rubber-like materials as well as anisotropic hyperelastic composites with rubber-like matrix. However we focus on an approach in the continuum mechanical point of view.

In particular, to describe a viscoelastic behavior of anisotropic hyperelastic materials the existence of the Helmholtz free-energy functions is postulated. The free energy function is splitted into equilibrium and non-equilibrium parts governing the equilibrium (hyperelastic) and non-equilibrium (viscoelastic) responses, respectively. The non-equilibrium contribution of the free energy function depends not only on external variables, which are measurable and controllable quantities, but also on internal variables (hidden to the external observers). We use two approaches for the viscous response:

The first approach is formulated for internal stress-like variables (so called overstresses) and the formulation of the evolution equations is linear for loading close to thermodynamic equilibrium.

The second approach with nonlinear evolution equations is formulated for internal strain-like variables (so called inelastic strains) by assuming parallel multiplicative decompositions of the deformation gradient into elastic and viscous parts.

We use rheological models such as Kelvin-Voigt or Maxwell models to establish evolution equations for internal variables. More details in fundamental theory of viscoelastic models are described briefly in Appendix B.

Finally, we expand attention to develop constitutive formulations of anisotropic magneto-sensitive (MS) elastomer materials. Owing to the magnetic field is considered as a preferred direction in the reference configuration, hence the MS elastomers are subjected simultaneously to the action of the mechanical loading and magnetic field as similar to composites reinforced by fiber families. The theory of nonlinear magnetoelasticity for MS elastomers is applied to a number of simple boundary-value problems.

In order to achieve the above objectives, many tasks related to experimental and numerical FEM calculations should be implemented, namely some main tasks as follows:

- Propose the free energy functions used in the research.
- Formulate explicit expressions of equilibrium stress in deformation plane.
- Perform experiments in relaxation to measure the forces and the strains.
- Develop a Matlab program for evaluating the material parameters.
- Establish the viscoelastic model in FEM to calculate numerical simulations of viscoelastic materials.
- Extend constitutive equations of the anisotropic MS elastomers.
- Compute numerically some examples of MS elastomers in FEM.

Outline of the dissertation

The dissertation is organized as follows:

Short introduction to the subject of dissertation thesis is in Chapter 1.

The overview of the recent literature concerning the subject of thesis is in Chapter 2.

Some used free energy functions are proposed in Chapter 3. The suitable form of free energy contributions are chosen by means of the decomposition of the free energy function into volumetric, isotropic and anisotropic parts. Additionally in this chapter explicit equilibrium stress responses for both isotropic and anisotropic materials are derived and a finite element formulation with consistent linearization is used for solving evolution equations.

Chapter 4 presents the experimental performance and the evaluation of material parameters for both isotropic and anisotropic materials. Some Matlab programs are developed for fitting the chosen model to experimental data.

In Chapter 5, the numerical simulations of the viscoelastic composite materials are implemented by Comsol MultiphysicsTM. Some basic problems are computed to compare to the experimental results. The effects of fiber directions, loading velocities and material coefficients on the viscous characteristics are also illustrated.

Chapter 6 is devoted to study an elastic behavior of MS elastomers. First relevant constitutive equations of MS elastomers are summarized concisely, some free energy functions are proposed and at the end of this chapter there will be some examples of the MS elastomers implemented in the finite element code Comsol MultiphysicsTM which is suitable for the simulation of coupled-field problems.

Some conclusions, discussions and future perspectives are presented in Chapter 7.

Appendix A summarizes concisely some kinematical aspects of the motion and deformation of a continuum body used in large deformation analyses. The notion of stress, which is responsible for the deformation of materials, is introduced. Some important forms of stress measures, namely Cauchy stress and Piola-Kirchhoff stress tensors, and conjugate strain tensors are shown. A brief review of the mathematical equations of the balance principles governing the motion of a continuum is also presented therein.

In Appendix B constitutive equations for anisotropic rubber-like composite derived by a Helmholtz free-energy function is taken out. Evolution equations are given for both internal variables including inelastic strain and overstress tensors.

The basic implementations of the finite element code in Comsol Multiphysics are included in Appendix C.

Finally, a typical program code developed in Matlab is illustrated in Appendix D.

Chapter 2

OVERVIEW OF LITERATURE

Keeping track of achievements of research of isotropic hyperelastic elastomers we see a large amount of results which were obtained in course of last decades. It can be realized that the formulation of the constitutive theory of the isotropic composites at finite strains has reached a certain completion. Several constitutive models can be derived based on the statistical theory of networks of non-Gaussian flexible chains to study homogeneous deformations of isotropic, incompressible hyperelastic rubber like materials, for example we can refer to Elías- Zúñiga (2006). Even the constitutive model which is derived in Drozdov & Dorfmann (2001) can correctly describe the stress-strain curves up to the break points. Beside that some simplified constitutive models based on macroscopic studies were proposed to be so good enough to predict the nonlinear behavior of isotropic hyperelastic materials. Apart from classical constitutive models such as neo-Hookean, Money-Rivlin and Ogden models (see Holzapfel, 2000), we can find out relatively simpler models such as the model proposed by Gao (1997) and used by Guo & Sluys (2006) which showed a good performance in tension as well as in compression. Alternatively another elasticity model that is based on the logarithmic strain tensor proposed by Hencky and studied in detail by Poživilová (2002) and Plešek & Kruisová (2006), this model represents an extremely effective description of the mechanical behavior of rubber-like materials, but it encounters some computational disadvantages.

Numerous amounts of numerical simulations for large deformation of rubber-like materials have rapidly increased recently. The finite element formulation of isotropic incompressible hyperelastic membranes that was employed simply by means of the Newton-Raphson incremental-iterative method with displacement control was presented in Jiang & Haddow (1995) and Reese & Wriggers (1997). A general formulation of thin incompressible membranes using the finite element method based on the principle of virtual work was discussed by Holzapfel et al. (1996) and Bařar & Itskov (1998). Specially, nonlinear membrane theories for rubber-like membranes or shells accounting for large elastic strains performed by FEM calculations have a significant interest, for instance the study of large deformation of a nonlinear rubber-like membrane concerning inflated structures Guo (2001), Pamplona et al. (2006) or Ibrahimbegović & Gruttmann (1993). These numerical examples demonstrate a very satisfying performance of the proposed formulation. In addition, a comparison between three-dimensional continuum elements and shell elements in solid mechanics has been implemented by Wriggers et al. (1996) and Eberlein & Wriggers (1999) for finite elastoplastic deformations. An innovative brick element formulation for large deformation problems in finite elasticity is discussed by Reese et al. (1998). Then a locking effect as the so-called hourglass instability for large deformation problems was dealt in the

work by Reese et al. (2000) and Reese (2003b) by remaining the stabilization matrix to be always positive definite.

Recent progress in computer-aided polymer processing analysis demonstrates the need for accurate description of the viscoelastic material behaviour. The continuum formulation for viscoelastic isotropic materials at finite strains is based on the multiplicative decomposition of the isochoric component of deformation gradient into elastic and viscous contribution and the generalized Maxwell rheological model, for example a three-dimensional thermo-dynamical model was proposed by Le Tallec et al. (1993). This approach is then applied in some numerical results by Bonet & Profit (2000), Bonet (2001) and Amin et al. (2006). However in this framework a simplification of the formulation when dealing with viscous materials is commonly restricted to small perturbations away from thermodynamical equilibrium means that the strain rate has to be close to zero. Therefore in the work of Reese & Govindjee (1998a) a theory for nonlinear viscoelasticity, which validates for deviations any size away from thermodynamic equilibrium, i.e. valid for large deformation rates is developed. Besides, a micromechanically motivated material model for the thermo-viscoelastic material behavior of rubber-like polymers was derived by extending the transient network theory, see Reese (2003a), it is based on deformation-like internal variables. Alternatively, the problem of Mullins' effect in carbon black-filled rubbers is constructed from a micro-mechanically viewpoint by Govindjee & Simo (1991).

A number of the computational simulation of the inflation membranes in the case of finite viscoelastic materials were implemented in Karamanou et al. (2006). A general variational formulation of finite viscoelasticity models was proposed by Fancello et al. (2005), they focused on comparison of the capacity of Hencky and Ogden type models to reproduce observed nonlinear viscous behavior in shear tests. It showed that Ogden models performed better. In the paper of Kleuter et al. (2007) an algorithm for the identification of material parameters for large strain viscoelasticity in data of multiple experiments was carried out by minimizing a least squares functional. Coupled thermo-mechanical simulations of large cyclic deformations of rubber cylinders were also implemented by the use of the finite element code Johnson & Chen (2002, 2005) to allow accurate predictions of the strain and temperature distributions in rubber components induced by viscoelastic heating. As well as a finite element implementation of a thermo-viscoelastic material behavior of rubber-like polymers that utilizes a nonlinear evolution law to include thermal effects by using the non-equilibrium free energy of the material was presented by Reese & Govindjee (1998b).

The observations and the identification of material parameters which are affected by temperature and strain rate can be found out by fitting the experimental data, such as Drozdov & Christiansen (2009), Oman et al. (2009).

However the approach of viscoelastic response, which is based on the formulation of nonlinear evolution equations in inelastic strains, is complicated relatively in mathematical aspects. Simo (1987), Holzapfel & Reiter (1995) and Holzapfel & Simo (1996) have all proposed linear differential equations to simulate the stress relaxation in the viscous component of the linear rheological mechanical model. The assumption of splitting the elastic and non-equilibrium stresses into volumetric and deviatoric responses respectively by the

multiplicative procedure is discussed by Holzapfel (1996). Moreover the extension of the specific model of finite strain viscoelasticity proposed by Simo (1987) is pointed out in Govindjee & Simo (1992) by the micro-mechanical considerations and simultaneously efficient algorithms for performing numerical computations are exploited to adjust the model for large-scale simulations.

Recently the characterization of the material properties and the development of constitutive laws for anisotropic nonlinearly elastic solids is also a topic of considerable and increasing interest. Constitutive equations of anisotropic materials can be derived by using the free energy function which can be decoupled separately into isotropic and anisotropic contributions, as proposed by Holzapfel (2000). Anisotropic models were proposed by Bonet & Burton (1998) and Chevaugnon et al. (2000) using an isotropic hyperelastic strain energy function that is expressed in terms of 5 invariants to describe orthotropic transversely isotropic materials. A discussion of influence of the fifth invariant I_5 on the response of the transversely isotropic materials is presented in Merodio & Ogden (2005) under simple deformations. Alternatively, an expression for the effective energy-density function of the composite in terms of the properties of the phases was developed by deBotton et al. (2006), Guo et al. (2007) based on theoretical homogenization to capture more accurately the overall response of the transversely isotropic composite under any general loading modes. Constitutive models of anisotropic materials reinforced by two fibers were also studied by using the isotropic free energy function expressed in terms of 8 invariants Holzapfel (2000). The analogy between the material description – usually based on the right Cauchy–Green tensor – and the spatial formulation – typically in terms of the Finger tensor was proven in Menzel & Steinmann (2002). This approach was proved successful to describe the highly nonlinear and anisotropic behavior of biological structures as composites reinforced by two fiber families in FEM, such as Eberlein et al. (2000), Holzapfel et al. (2000a, b), Kroon & Holzapfel (2008), Gasser et al. (2001). The models were demonstrated to be suitable for predicting the anisotropic elastic response of materials in the large strain domain. An application to the modeling of orthotropic hyperelastic cylindrical thick shells under pressure is implemented by Haussy & Ganghoffer (2002).

Otherwise, one orthotropic hyperelastic constitutive model was proposed by Itskov (2001) by using a non-linear extension of the orthotropic St. Venant-Kirchhoff material and it was described in each principal material direction by arbitrary isotropic tensor function coupled with the corresponding structural tensor. An effectual model was developed by Reese (2000, 2003c) and Reese et al. (2001) to describe the hyperelastic behavior of pneumatic membranes reinforced with roven-woven fiber in which the fibers are modeled by means of truss elements.

The mechanical testing of anisotropic nonlinearly elastic solids is also a subject of attractive interest. The results of such testing are important, in particular, for the characterization of the material properties and the development of constitutive laws that can be used for predictive purposes. Bischoff proposed one model (Bischoff et al., 2000) which is derived from an orthotropic unit cell of eight representative fibers by means of the Gaussian statistic theory and the material parameters of the model was evaluated by fitting uniaxial

compression data (Bischoff et al., 2001). We should also note that Holzapfel & Ogden (2008) pointed out some errors prior researchers misled and claimed that planar biaxial testing cannot fully characterize the three-dimensional anisotropic elastic properties of soft tissues. They explained the limitations of biaxial testing to identify the mechanical properties of anisotropic solids capable of large elastic deformations. More about the determination of material models for orthotropic composites from uniaxial extension tests and histostructural data can be referred to Holzapfel (2006). In addition, an essential application for modeling the mechanical response of arterial walls which may consist of two or more concentric layers, in which each layer of the material is regarded as consisting of two families of mechanically equivalent helical fibers, is considered by Ogden & Schulze-Bauer (2000). The nonlinear elasticity theory to obtain general formulas for the pressure and axial load in the symmetrical extension and inflation of a thick-walled tube is derived. Residual stress in the unloaded circular cylindrical configuration is also included in the formulation.

For viscoelastic anisotropic hyperelastic materials a constitutive description is a challenging research topic and the list of publications in this field are quite spare. Generally, in the continuum mechanical point of view to characterize a visco-hyperelastic behavior of anisotropic materials a Helmholtz free-energy function is used, in addition the assumption of the free energy is decoupled in two parts: the first part describing the rate-independent material behavior and the second incorporating time-dependent or viscous effects, for instant see Holzapfel & Gasser (2001), Nguyen et al. (2007). An important point in developing viscous models is the choice of the evolution equation for the internal variables which can be taken either the inelastic strain or the overstress tensors. The formulation of evolution equations in strain variables is based on assuming parallel multiplicative decompositions of the deformation gradient into elastic and viscous parts, for example Diani et al. (2006), Nguyen et al. (2007), Nedjar (2007). Whereas the description of viscous responses in overstresses is considered in the recent papers of Holzapfel & Gasser (2001), Holzapfel et al. (2001) and Kaliske (2000) by means of the split of the stress tensor into volumetric, isotropic and anisotropic contributions corresponding to each compound of the composite materials. All these approaches have in common that the evolution equations are formulated by means of one of two standard viscoelastic models: Maxwell-type (Holzapfel & Gasser, 2001) and Kelvin-Voigt-type (Peña et al., 2007) to exhibit a viscoelastic behavior. Besides, other approaches on the micromechanical theory for the large-deformation time-dependent behavior of the composite can be referred to as Bischoff et al. (2004), Bischoff (2006).

Examples of finite element formulations and numerical computations for modeling nonlinear viscoelastic response of reinforced elastomers can include the works of Holzapfel & Gasser (2001), Areias & Matouš (2008), Peña et al. (2007) and Nguyen et al. (2007).

The comprehensive review of the basic principles, theories and equations in mechanics and electromagnetism can be found in the paper of Pao (1978) where the corresponding constitutive equations for solids and boundary conditions are discussed as well. Modern consistent electromagnetic theory is presented in the recent book by Kovetz (2000) where the complete set of laws of electromagnetism, mechanics and thermodynamics is treated.

While the theory of magnetoelasticity is well-known and advanced, the theoretical basis of most current research in the field of MS elastomers is very recent. The full system of equations suitable for deformable MS solids in an electro-magnetic field was first considered by Brigadnov & Dorfmann (2003) who suggested a simple energy function for isotropic MS elastomers and derived the basic system of constitutive relations. The strain tensor and the magnetic induction vector are chosen as the basic variables. They presented also a numerical simulation of the simple shear of an incompressible MS elastomer between two infinite parallel plates subjected to a magnetic field perpendicular to shear direction.

In the recent series of papers of Dorfmann & Ogden (2003-2005) a theory of nonlinear magnetoelasticity for MS elastomers was developed and applied to a number of simple boundary-value problems. Other recent related theoretical works are those by Steigmann (2004, 2009) and Kankanala & Triantafyllidis (2004, 2008). Important guidelines for the experimentalists and for people involved in numerical simulations of MS elastomer response can be found in further papers of Dorfmann et al. (2005) and Bustamante et al. (2006). In the recent paper of Ottenio et al. (2008) the linearized equations governing incremental effects in a magnetoelastic solid subject to finite deformation in the presence of a magnetic field are derived and the tensors of magnetoelastic moduli are defined. These equations are then used to examine the problem of surface stability of a homogeneously pre-strained half-space.

However for the most part of exact solutions to representative boundary-value problems are idealized in the sense that they apply only to bodies of infinite extent in one or more directions so that edge effects are not considered. The first numerical simulation of a boundary-value problem involving finite geometry is reported by Bustamante et al. (2007). In their paper the problem of a circular cylindrical tube of finite length that is deformed and then subjected to an axial magnetic field is examined.

The unique characteristic of magneto-rheological elastomer (MRE) is that its shear modulus can be continuously controlled by the external magnetic field (Gong et al., 2005). Shearing of the cured composite in the presence of the magnetic field causes particle displacement from their low energy state, thereby requiring additional work. This work rises monotonically with applied magnetic field, thus resulting in a field dependent shear modulus. It has been reported (Jolly et al., 1996) that the maximum increase in the shear modulus due to the MR effect is about 50–60% of the zero-field modulus, depending on the matrix elastomer. For hard elastomers like natural rubber the relative increase has typically been 30–40%. The field-induced modulus increase is substantial even at kilohertz mechanical frequencies (Ginder et al., 2002). Such properties make MREs promising in many applications in automotive industry as variable stiffness suspension systems and active damping components (Carlson & Jolly, 2000; Albanese-Lerner & Cunefer, 2008; Kalio et al., 2007; Deng & Gong, 2007).

In this thesis, the viscoelastic behavior of the isotropic as well as anisotropic rubber-like materials is studied in the continuum mechanical theory by means of the free energy functions which are proposed in Chapter 3. The constitutive equation which interrelate the stress components and the strain components within a nonlinear regime can be found in section B.1 of Appendix B, more details see also, for example, Holzapfel (2000) or Truesdell

& Noll (1992). The viscoelastic models of the anisotropic materials depending on the choice of internal variables and evolution equations are summarized in section B.2 of Appendix B. Evolution equations of overstresses proposed by Holzapfel & Gasser (2001) in the theory of linear viscoelasticity is quite simple to utilize for evaluating material parameters by experimental performances and implementing numerical simulations in FEM. However this model is believed in not credible the general problem of large deformations and large perturbations away from thermodynamic equilibrium, such as full thermo-mechanical coupling or high strain rates. Therefore, for this reason, the nonlinear viscoelastic model proposed by Nguyen et al. (2007) is also given.

The constitutive formulation of magnetic and mechanical equations for MS elastomers is provided in series of recent studies by Brigadnov & Dorfmann (2003) and Dorfmann & Ogden (2003-2005). These governing equations are summarized briefly in section 6.1 of Chapter 6. Specially, the influence of the magnetic field on the mechanical stress in the deforming body is incorporated through a magnetic stress tensor instead of through magnetic body forces included to the mechanical equilibrium equation, because the resulting total Cauchy stress tensor has the advantage of being symmetric, it can be referred to Dorfmann & Ogden (2004). The magnetic induction vector \mathbf{B} and the magnetic field vector \mathbf{H} are regarded as fundamental field variables and defined by the total free energy function.

Chapter 3

FREE ENERGY FUNCTIONS AND CONSTITUTIVE RELATIONS FOR EQUILIBRIUM AND VISCOELASTIC RESPONSE OF RUBBER-LIKE COMPOSITE

An overview of the theory of modelling of anisotropic composites with rubber-like matrix is presented in the Appendix B of this thesis. General constitutive relations are derived there on the basis of a free-energy function Ψ and evolution equations for internal strain-like or stress-like variables are given. Hence, the aim of this chapter is to specify several appropriate forms of strain-energy functions within the constitutive theory of finite hyperelasticity and viscoelasticity and to derive constitutive relations of stress response in two dimensional problems, namely simple tension, pure shear and biaxial tensile deformations. In the first two sections of this chapter we present several free energy functions and constitutive relations for the equilibrium response of isotropic and anisotropic material. In the third section we introduce the numerical formulation of the evolution equations for stress-like and strain-like nonelastic variables.

3.1. Free energy functions

In particular, a selection of representative examples of the equilibrium part Ψ_{EQ} of free energy function (B.2, B.4) within the isothermal regime is presented to describe each contribution (volumetric, isotropic and anisotropic isochoric) which allows to model an isotropic rubber-like material and a composite in which a rubber-like matrix material is reinforced by families of fibers.

3.1.1. Volumetric free energy function

Since we consider only incompressible composite materials hence the volumetric part of the free energy function may be chosen in the following form Holzapfel (2000)

$$\Psi_{vol}^{EQ} = -p(J-1) \quad (3.1)$$

where p is the Lagrange multiplier that can be determined from the equilibrium equations and the boundary conditions.

3.1.2. Isotropic (isochoric) free energy functions

Neo-Hookean model. The strain energy function of neo-Hookean model is the simplest form of the isotropic free energy function which is expressed in a term of the first principal invariant \bar{I}_1 , defined by (B.13)₁, refer to Poživilová (2002)

$$\Psi_{iso}^{EQ} = \mu_{NH} (\bar{I}_1 - 3) \quad (3.2)$$

where the shear modulus is defined by $\mu = 2\mu_{NH}$.

Mooney-Rivlin model. The Mooney-Rivlin model is often employed in the description of the behavior of isotropic rubber-like materials. The strain energy function of this model is expressed in terms of the first two principal invariants \bar{I}_1 and \bar{I}_2 of the modified right Cauchy-Green tensor $\bar{\mathbf{C}}$, refer to (B.3) and (B.13)

$$\Psi_{iso}^{EQ} = \mu_{MR_1} (\bar{I}_1 - 3) + \mu_{MR_2} (\bar{I}_2 - 3) \quad (3.3)$$

where μ_{MR_1} and μ_{MR_2} are the material constants of Mooney-Rivlin model (Holzapfel, 2000). The shear modulus is defined by $\mu = 2(\mu_{MR_1} + \mu_{MR_2})$.

A general form for strain energy function of incompressible rubbers attributable of Mooney-Rivlin can be extended as an infinite series in terms of \bar{I}_1 and \bar{I}_2

$$\Psi_{iso}^{EQ} = \sum_{m=0}^{\infty} \sum_{n=0}^{\infty} c_{mn} (\bar{I}_1 - 3)^m (\bar{I}_2 - 3)^n \quad \text{with } c_{00} = 0 \quad (3.4)$$

where c_{mn} are material constants, Hartmann (2001).

Ogden model. The Ogden model (Holzapfel, 2000) with a strain energy function formulated in terms of principal stretches $\bar{\lambda}_1$, $\bar{\lambda}_2$ and $\bar{\lambda}_3$ has shown to be of grate accuracy in spite of a relatively complicated numerical realization. In which $\bar{\lambda}_1^2$, $\bar{\lambda}_2^2$ and $\bar{\lambda}_3^2$ are well-known as the eigenvalues of the symmetric tensor $\bar{\mathbf{C}}$. It was built originally for incompressible materials where $\bar{\lambda}_1 \bar{\lambda}_2 \bar{\lambda}_3 = 1$. Ogden proposed the strain energy function of the principal stretches $\bar{\lambda}_a$ ($a = 1, 2, 3$) in the form

$$\Psi_{iso}^{EQ} = \Psi_{iso}^{EQ}(\bar{\lambda}_1, \bar{\lambda}_2, \bar{\lambda}_3) = \sum_{r=1}^N \frac{\mu_r}{\alpha_r} (\bar{\lambda}_1^{\alpha_r} + \bar{\lambda}_2^{\alpha_r} + \bar{\lambda}_3^{\alpha_r} - 3) \quad (3.5)$$

where N is a positive integer determining the number of terms in the strain energy function, μ_r are material constants (shear moduli) and α_r are dimensionless constants (determined by experiments), $r = 1, \dots, N$.

For consistency with linear theory the parameter μ denotes the classical shear modulus and material constants μ_r and α_r are related by

$$\mu = \frac{1}{2} \sum_{r=1}^N \mu_r \alpha_r \quad \text{with} \quad \mu_r \alpha_r > 0 \quad (3.6)$$

The neo-Hookean model is considered as a special case of Ogden model with $N = 1$, $\alpha_1 = 2$, we have

$$\Psi_{iso}^{EQ} = \mu_{NH} (\bar{\lambda}_1^2 + \bar{\lambda}_2^2 + \bar{\lambda}_3^2 - 3) \quad (3.7)$$

where the constant $\mu_{NH} = \frac{\mu_1}{2}$.

The Mooney-Rivlin is referred to a special case of Ogden's model for incompressible materials which obtain by setting $N = 2$, $\alpha_1 = 2$, $\alpha_2 = -2$

$$\Psi_{iso}^{EQ} = \mu_{MR1} (\bar{\lambda}_1^2 + \bar{\lambda}_2^2 + \bar{\lambda}_3^2 - 3) + \mu_{MR2} (\bar{\lambda}_1^{-2} + \bar{\lambda}_2^{-2} + \bar{\lambda}_3^{-2} - 3) \quad (3.8)$$

3.1.3. Anisotropic (isochoric) free energy functions

The component of strain energy function for anisotropic properties is related to the free energy stored in fibers. Since \bar{I}_4 and \bar{I}_6 , given by (B.13)₃ and (B.25)₁, equal the square of stretches in two fiber directions (Holzapfel, 2000), for simplicity, the anisotropic free energy is only considered as a function of these two invariants.

The simplest form of the anisotropic free energy is as a polynomial function of pseudo-invariants (Nam, 2004)

$$\Psi_{ani}^{EQ} = \frac{k}{2} (\bar{I}_4 - 1)^2 \quad (3.9)$$

(for one fiber-reinforced composites).

$$\Psi_{ani}^{EQ} = \frac{k_1}{2} (\bar{I}_4 - 1)^2 + \frac{k_2}{2} (\bar{I}_6 - 1)^2 \quad (3.10)$$

(for two fiber-reinforced composites).

On the other hand the energy stored in the fibers is also assumed to be governed by an exponential function, Holzapfel & Gasser (2001), and given in the forms

$$\Psi_{ani}^{EQ} = \frac{k_1}{2k_2} \left\{ \exp \left[k_2 (\bar{I}_4 - 1)^2 \right] - 1 \right\} \quad (3.11)$$

(for one fiber-reinforced composite materials).

$$\Psi_{ani}^{EQ} = \frac{k_1}{2k_2} \left\{ \exp \left[k_2 (\bar{I}_4 - 1)^2 \right] - 1 \right\} + \frac{k_3}{2k_4} \left\{ \exp \left[k_4 (\bar{I}_6 - 1)^2 \right] - 1 \right\} \quad (3.12)$$

(for two fiber-reinforced composite materials).

3.2. Equilibrium stress responses in plane-stress deformations

In order to provide a fundamental theory for evaluating material parameters equilibrium stress expressions need to be defined explicitly. Herein principal stress responses of both isotropic and anisotropic materials in plane stress are formulated in terms of principal stretches undergoing some basic deformation states, namely simple tensile, pure shearing and biaxial tensile deformations. For two fiber-reinforce (anisotropic) composite the arrangement of the fibers in the deformation plane are assumed to be symmetric with respect to loading directions, it means the principal stress directions and the principal stretches are identical.

According to Holzapfel (2000), the principal stress can be defined from the free energy function in terms of principal stretches as follows

$$\sigma_a = \bar{\lambda}_a \frac{\partial \Psi}{\partial \bar{\lambda}_a} - p \quad (a = 1, 2, 3) \quad (3.13)$$

- For isotropic materials:

$$\sigma_a = \bar{\lambda}_a \frac{\partial \Psi_{iso}}{\partial \bar{\lambda}_a} - p \quad (3.14)$$

- For anisotropic materials:

$$\sigma_a = \bar{\lambda}_a \left(\frac{\partial \Psi_{iso}}{\partial \bar{\lambda}_a} + \frac{\partial \Psi_{ani}}{\partial \bar{\lambda}_a} \right) - p \quad (3.15)$$

but since the arrangement of the fibers in the plane strain the third principal stress is out of the plane strain and independent on the anisotropic components so that

$$\sigma_3 = \bar{\lambda}_3 \frac{\partial \Psi_{iso}}{\partial \bar{\lambda}_3} - p = 0 \quad (3.16)$$

leads to

$$p = \bar{\lambda}_3 \frac{\partial \Psi_{iso}}{\partial \bar{\lambda}_3} \quad (3.17)$$

where the constraint of incompressible materials is fulfilled by $\bar{\lambda}_1 \bar{\lambda}_2 \bar{\lambda}_3 = 1$.

3.2.1. Isotropic rubber-like materials

Relationships of isotropic invariants to principal stretches are given by

$$\begin{aligned} \bar{I}_1 &= \bar{\lambda}_1^2 + \bar{\lambda}_2^2 + \bar{\lambda}_3^2 \\ \bar{I}_2 &= \bar{\lambda}_1^2 \bar{\lambda}_2^2 + \bar{\lambda}_2^2 \bar{\lambda}_3^2 + \bar{\lambda}_3^2 \bar{\lambda}_1^2 = \bar{\lambda}_1^{-2} + \bar{\lambda}_2^{-2} + \bar{\lambda}_3^{-2} \end{aligned} \quad (3.18)$$

Using (3.14), (3.17) and (3.18) we obtain explicit principal stress expressions as

- Neo-Hookean model:

$$\begin{aligned}\sigma_1 &= 2\mu_{NH} \left(\bar{\lambda}_1^2 - \frac{1}{\bar{\lambda}_1^2 \bar{\lambda}_2^2} \right) \\ \sigma_2 &= 2\mu_{NH} \left(\bar{\lambda}_2^2 - \frac{1}{\bar{\lambda}_1^2 \bar{\lambda}_2^2} \right)\end{aligned}\quad (3.19)$$

- Mooney-Rivlin model:

$$\begin{aligned}\sigma_1 &= 2(\mu_{MR_1} + \mu_{MR_2} \bar{\lambda}_2^2) \left(\bar{\lambda}_1^2 - \frac{1}{\bar{\lambda}_1^2 \bar{\lambda}_2^2} \right) \\ \sigma_2 &= 2(\mu_{MR_1} + \mu_{MR_2} \bar{\lambda}_1^2) \left(\bar{\lambda}_2^2 - \frac{1}{\bar{\lambda}_1^2 \bar{\lambda}_2^2} \right)\end{aligned}\quad (3.20)$$

- Ogden model:

$$\begin{aligned}\sigma_1 &= \sum_{r=1}^N \mu_r \left(\bar{\lambda}_1^{\alpha_r} - \frac{1}{\bar{\lambda}_1^{\alpha_r} \bar{\lambda}_2^{\alpha_r}} \right) \\ \sigma_2 &= \sum_{r=1}^N \mu_r \left(\bar{\lambda}_2^{\alpha_r} - \frac{1}{\bar{\lambda}_1^{\alpha_r} \bar{\lambda}_2^{\alpha_r}} \right)\end{aligned}\quad (3.21)$$

Note, however, that the first and second principal stresses of simple tensile and biaxial tensile deformations in plane stress problems can be defined by the expressions (3.19) ÷ (3.21), whereas for the pure shearing deformation is merely a special case as setting $\bar{\lambda}_2 = 1$.

3.2.2. Composites reinforced by two families of fibers

The properties of two families of fibers are assumed to be identical. The fiber orientations compared to the first principal direction are defined by angles φ . Then the pseudo-invariants \bar{I}_4, \bar{I}_6 are given by

$$\bar{I}_4 = \bar{I}_6 = \bar{\lambda}_1^2 \cos^2 \varphi + \bar{\lambda}_2^2 \sin^2 \varphi \quad (3.22)$$

When the decomposition of the stress into isotropic and anisotropic parts is used we have

$$\sigma_k = \sigma_{isok} + \sigma_{anik} \quad (k=1,2,3) \quad (3.23)$$

here the isotropic components of the principal stresses σ_{isok} are defined to be identical for the isotropic materials such as expressions (3.19) - (3.21).

The expressions of the anisotropic principal stresses are defined by the chosen anisotropic energy function, particularly for the anisotropic energy functions are

- Polynomial function (3.10):

$$\begin{aligned}\sigma_{am1} &= 4k\bar{\lambda}_1^2(\bar{I}_4 - 1)\cos^2\varphi \\ \sigma_{am2} &= 4k\bar{\lambda}_2^2(\bar{I}_4 - 1)\sin^2\varphi\end{aligned}\quad (3.24)$$

- Exponential function (3.12):

$$\begin{aligned}\sigma_{am1} &= 4k_1 \exp\left[k_2(\bar{I}_4 - 1)^2\right](\bar{I}_4 - 1)\bar{\lambda}_1^2 \cos^2\varphi \\ \sigma_{am2} &= 4k_1 \exp\left[k_2(\bar{I}_4 - 1)^2\right](\bar{I}_4 - 1)\bar{\lambda}_2^2 \sin^2\varphi\end{aligned}\quad (3.25)$$

It can easily realize that at small deformation, i.e. $\bar{I}_4 \rightarrow 1$, the stress response in the exponential form (3.25) is coincident to the response (3.24).

3.3. Non-equilibrium stress responses

Since the total stress is decoupled into equilibrium and non-equilibrium parts, then next task is to indicate how to calculate the non-equilibrium stress from evolution equations of internal variables. Herein, we will present solutions of non-equilibrium stresses for two approaches through overstress or inelastic strain tensors as internal variables.

In a finite-element framework, the time integration of the evolution equations for the internal variables is performed at the integration point level. At time $t_{n+1} = t_n + \Delta t$, the updated variables are evaluated assuming that the values of all variables at previous time t_n are known.

3.3.1. Solution of evolution equations for over stresses

For the formulation of viscoelastic responses in over stresses, the non-equilibrium stress contribution is able to be integrated directly from evolution equations (B.32), in which equilibrium isochoric stress contributions $\mathbf{S}_{iso\alpha}^{EQ}$ are defined from the equilibrium isochoric parts of the free energy function. The closed form solution of the linear evolution equation is given by the convolution integral and the recurrence update formula (Holzapfel & Gasser, 2001) for the internal stresses

$$\mathbf{Q}_{\alpha\alpha} = \exp(-T/\tau_{\alpha\alpha})\mathbf{Q}_{\alpha\alpha}^{0*} + \int_{0^+}^T \exp[-(T-t)/\tau_{\alpha\alpha}] \beta_{\alpha\alpha}^{\infty} \dot{\mathbf{S}}_{iso\alpha}^{\infty}(t) dt \quad (3.26)$$

for $\alpha = 1, \dots, m$, and $a = 1, 2, 4, \dots, 8$.

$$(\mathbf{Q}_{\alpha\alpha})_{n+1} = \exp(2\xi_{\alpha\alpha})(\mathbf{Q}_{\alpha\alpha})_n + \exp(\xi_{\alpha\alpha})\beta_{\alpha\alpha}^{\infty}[(\mathbf{S}_{iso\alpha}^{\infty})_{n+1} - (\mathbf{S}_{iso\alpha}^{\infty})_n] \quad (3.27)$$

with $\xi_{\alpha\alpha} = -\Delta t/2\tau_{\alpha\alpha}$ and $\Delta t = t_{n+1} - t_n$.

3.3.2. Solution of evolution equations for inelastic strains

The approach of viscoelastic responses in inelastic strain variables can derive the non-equilibrium stress from the non-equilibrium contribution of the free energy function, equation (B.9)₂. Therefore the integration of the isotropic evolution equation (B.39) for \mathbf{C}_M^v of the matrix and the anisotropic evolution equation (B.42) for \mathbf{C}_F^v of the fiber phase is required.

The time discretization of evolution equations for \mathbf{C}_M^v and \mathbf{C}_F^v is applied to give nonlinear equations for the updated values as follows

$$\left(\mathbf{C}_M^v\right)_{n+1} - 2\Delta t \left(\mathbb{V}_M^{-1}\right)_{n+1} \left(\mathbf{T}_M\right)_{n+1} - \left(\mathbf{C}_M^v\right)_n = \mathbf{0} \quad (3.28)$$

$$\left(\mathbf{C}_F^v\right)_{n+1} - 2\Delta t \left(\mathbb{V}_F^{-1}\right)_{n+1} \left(\mathbf{T}_F\right)_{n+1} - \left(\mathbf{C}_F^v\right)_n = \mathbf{0} \quad (3.29)$$

where $\mathbb{V}_M^{-1}, \mathbf{T}_M$ are defined by equations (B.40) and (B.41) for the matrix phase and $\mathbb{V}_F^{-1}, \mathbf{T}_F$ are defined by equations (B.43) and (B.44) for the fiber phase, respectively. More in details for the solution algorithms it can be referred to (Nguyen et al., 2007).

Chapter 4

EXPERIMENTS AND MATERIAL PARAMETER IDENTIFICATION

4.1. Experimental equipments and specimens

4.1.1. Universal testing machine TIRatest 2810

The TIRatest 2810 machine (Figure 4.1) can be used for routine tests and investigations by tension, compression and bending with a high level of technology, accuracy and exact measuring results in the shortest time. The maximum of loading is applied up to 10kN. The machine is controlled by either the remote control unit EDC60/120 box or the “PC-control” mode using the “TIRatest” software (Figure 4.2).

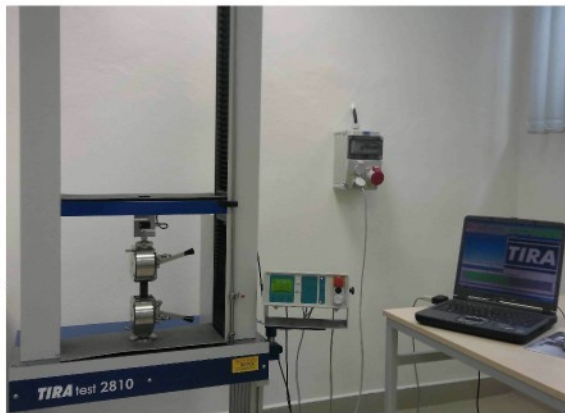


Figure 4.1 – Universal testing machine TIRatest 2810

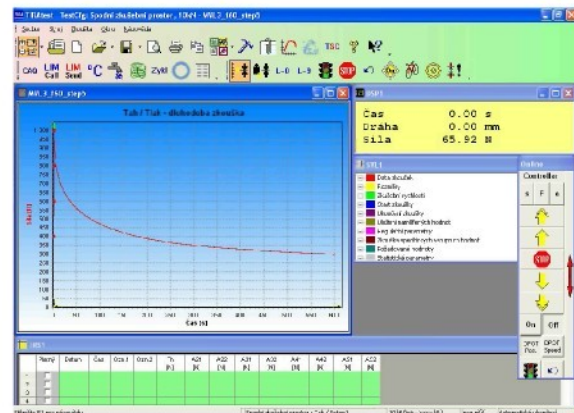


Figure 4.2 – The main window application of TIRatest software

4.1.2. Biaxial testing equipment

The biaxial testing equipment (Figure 4.3) fabricated for testing textile materials therefore has a low capacity of 300N in each perpendicular direction and only in tension. A biaxial specimen ⑤ is fixed by a set of clamps ④. Applying load is turned by the screws ② which are connected to the test frame ① for a requirement of a symmetric strain distribution. The values of the forces are measured by two force sensors ③ that can transmit a signal via the cables ⑥ to a computer.

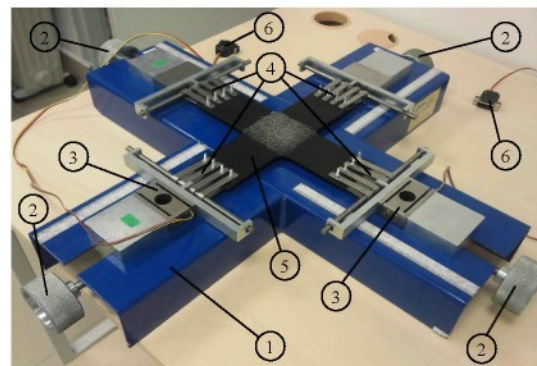


Figure 4.3 – Biaxial testing equipment

4.1.3. System Q-400 digital cameras Dantec Dynamics

The Digital Image Correlation System is an optical instrument for full-field, non-contact and three-dimensional measurement of deformations and strains on components and materials. We use the system with two high resolution digital cameras (Figure 4.4) to record surface changes of the object under investigation while loaded. The recorded images are analyzed and compared by a special correlation technique which allows the determination of the surface displacements with high local resolution. The measuring principle of the Q-400 system is based on digital image correlation. More details of the correlation technique are in the chapter seven of the PhD thesis of Nam (2004).



Figure 4.4 – Digital cameras

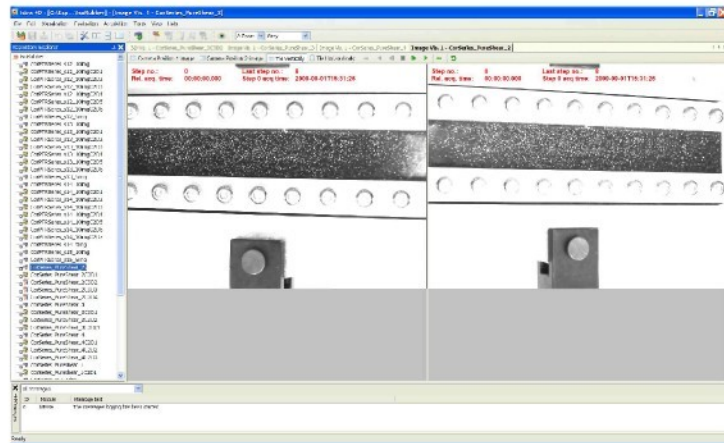


Figure 4.5 – Main window of Istra 4D software

The “Istra 4D” software (as shown in Figure 4.5) is designed for controlling the measurement system Q-400 and for evaluating the data. To use this software we must obey the following steps:

- Step 1: Activation of Hardware. This step is used to connect the cameras to the controlling program.
- Step 2: Calibration of Cameras. A calibration target is chosen that the image must be filled as much as possible. The calibration target must be in the focus of both cameras. It could be necessary to adjust the intensity.
- Step 3: Acquisition of Images. We can capture images either by manual acquisition or by trigger signal acquisition.
- Step 4: Evaluation. We do successively a chain of operations including: start a new evaluation, select the evaluation settings, create a mask, search of start points and perform the evaluation.
- Step 5: Visualization, in order to display results in graphics and analyzing and export data by the Gauge method.

4.1.4. Specimen preparation

We prepared several specimens cut from both isotropic “E-Styrene-Butadiene” rubber-like materials and “Nitrile-Butadiene” rubber-like matrix composites with two families of viscose fiber reinforcements for tensile, pure shear and biaxial tests. The shapes of experimental specimens are shown in Figure 4.6, namely for tensile and pure shear tests the specimens have a rectangular shape whereas the biaxial specimen has a cruciform shape. The interest regions of the specimens are marked randomly by white-painted points that are recorded by video extensimetry to evaluate the deformation and strains by means of the image correlation method as mentioned above.



Figure 4.6 – Shapes of specimens for simple tensile, pure shear and biaxial tests

4.2. Experiments and identification methods

4.2.1. Experimental descriptions

All the tests are performed at a room-temperature about 20°C with isothermal conditions. First for excluding a Mullins effect on the behavior of the material during the test we have performed a preconditioning of all the samples by cyclic tests about eight times loading and unloading, an illustration of Mullins effect shown in Figure 4.7. As can see after the first cycle the Mullins effect is nearly eliminated.

After excluding the Mullins effect the specimens are kept in a stress-free state within 2 to 3 hours before relaxation tests are performed. In order to determine all viscoelastic characteristic of materials, a driven displacement is set-up with many steps to control the tests, namely velocities in loading stages are constant up to 1mm/s and then during each relaxation process the displacement is held constantly for 15 minutes.

For simplifying numerical estimations three assumptions are issued as follows

- Load is applied suddenly.
- Time in a relaxation process is long enough.
- Strain is unchanged throughout a relaxation process.

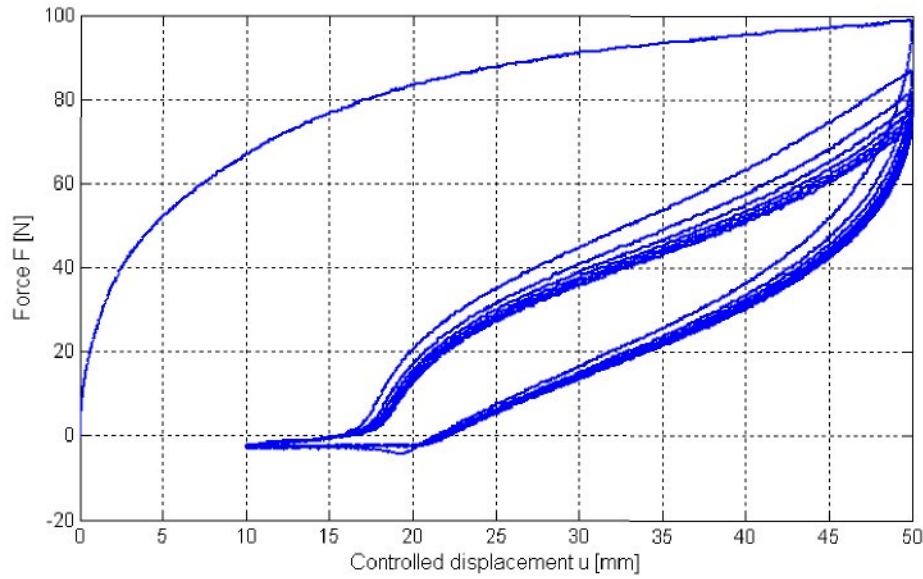


Figure 4.7 – Mullins effect in cyclic tests

Due to the form of the specimen and its boundary conditions during the test are symmetric. We assert that the stress and strain measured in the loading direction are the principal stress and strain respectively. In the second assumption the forces at the end of relaxation processes will play a role as the equilibrium forces. Furthermore the stress distribution in the central region of specimen is supposed to be uniform. The principal Cauchy stress is therefore defined by

$$\sigma_i = \frac{\lambda_i F_i}{A_{0i}} \quad (4.1)$$

where λ_i , F_i are the principal stretch and the applied force, respectively, along to the measured direction and A_{0i} is the initial cross-section area perpendicular to the load F_i .

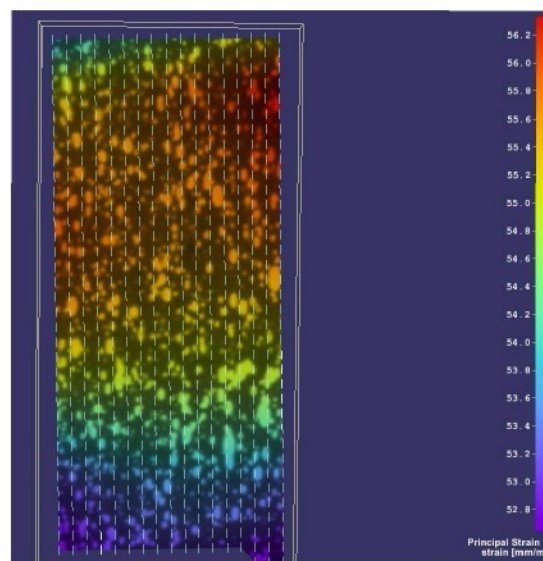


Figure 4.8 – Strain evaluation by the image correlation

Owing to the third assumption, it is only necessary to capture an image of the undeformed specimen as a reference image. Another image of the deformed specimen at the end of each relaxation process is also taken to evaluate the strains by the image correlation method. Figure 4.8 illustrates an evaluation of a strain spectrum.

4.2.2. Identification methods

In order to simulate precisely a viscoelastic characteristic of isotropic rubber-like materials as well as fiber-reinforced composite materials we need to show which model the best is to recur completely the working ability of these materials. For fulfill this desire we start from a numerical evaluation of constant material parameters concerning the model by experimental data.

Every numerical evaluation is divided into two main steps including:

- Estimate constant elastic parameters of composites.
- Estimate constant viscoelastic parameters of composites.

The number of the elastic parameters needs to be estimated depending on a chosen model by means of the free energy function. We have postulated the decomposition of the free energy into volumetric and isochoric parts, i.e.

$$\Psi = \Psi_{vol} + \Psi_{iso} \quad (4.2)$$

For anisotropic composite materials the isochoric free energy is additionally split into isotropic and anisotropic (isochoric) parts, therefore

$$\Psi = \Psi_{vol} + \Psi_{iso} + \Psi_{ani} \quad (4.3)$$

An additional assumption of all the composite materials is incompressible, i.e. the constraint $J = 1$, hence the volumetric part can be chosen in the following form (3.1).

The isotropic (isochoric) component of free energy function may be involved by the strain energy function of Neo-Hookean (3.2), Mooney-Rivlin (3.3) or Ogden (3.5) models.

The anisotropic (isochoric) part of free energy function for fiber-reinforced composites is used to relate to the fiber stretches referred to as a polynomial function of two pseudo-invariants \bar{I}_4 and \bar{I}_6 equation (3.10). Herein the two fiber families are assumed to exhibit the same mechanical properties.

The explicit expressions of the principal Cauchy stresses in the plane deformation are derived in the previous chapter.

For estimating the viscoelastic parameters the linear viscous Maxwell model is used, in which only one element represents a viscous response of the isotropic material and two elements represent separately viscous response of the matrix and fiber phases for fiber-reinforced composites. We suppose that the overstress can be expressed in a Prony series, particularly

$$q = \sum_{\alpha=1}^N q_{\alpha}^0 e^{-\frac{t}{\tau_{\alpha}}} \quad (4.4)$$

where $N=1$ is for the isotropic materials and $N=2$ is for the fiber-reinforced composites, τ_{α} is relaxation time and q_{α}^0 are initial over stresses determined at the beginning $t = 0.0^+$.

We consider the first assumption of suddenly applied load because it determines the initial condition of the over stresses. Let us observe a standard Maxwell element, as shown in Figure 4.9. When a load is applied suddenly it means that the stretches of the elastic springs are identical, therefore

$$q_{\alpha}^0 = E_{\alpha} \varepsilon_{\alpha} = E_{\alpha} \varepsilon \quad (4.5)$$

and

$$\sigma_{iso\alpha}^{eq} = E_{\alpha}^{\infty} \varepsilon \quad (4.6)$$

then

$$q_{\alpha}^0 = \frac{E_{\alpha}}{E_{\alpha}^{\infty}} \sigma_{iso\alpha}^{eq} = \beta_{\alpha} \sigma_{iso\alpha}^{eq} \quad (4.7)$$

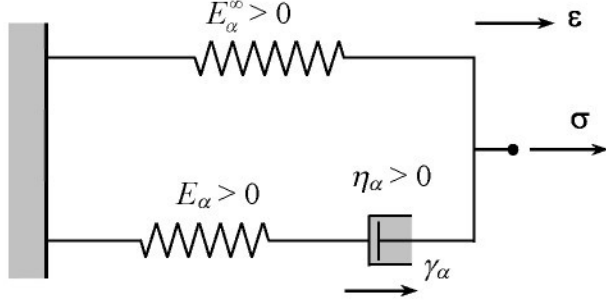


Figure 4.9 – A standard Maxwell element

Substituting equation (4.7) into equation (4.4) we have explicit expressions of over stresses needed to be evaluated as follows

$$q = \beta_{iso} \sigma_{iso}^{eq} e^{-\frac{t}{\tau_{iso}}} \quad (4.8)$$

for the isotropic materials, and

$$q = \beta_{iso} \sigma_{iso}^{eq} e^{-\frac{t}{\tau_{iso}}} + \beta_{ani} \sigma_{ani}^{eq} e^{-\frac{t}{\tau_{ani}}} \quad (4.9)$$

for the anisotropic materials.

These elastic and viscoelastic parameters are classified into 2 types which are linear and nonlinear coefficients. The linear coefficients can be evaluated immediately by using the linear least-square method to fit a linear model to data. An effective operator in Matlab which is the backslash operator “\” is used to solve a system of linear equations for these unknown coefficients. On the other hand, nonlinear models are more difficult to fit than linear models because the coefficients cannot be estimated using simple matrix techniques. Instead, an iterative approach is required by using an available function as “lsqnonlin”. More details for estimating processes it can look at Appendix D.

4.3. Isotropic composite materials

First we will begin evaluating material parameters of the viscoelastic isotropic rubber-like materials via basic experiments, namely simple tension, pure shear and biaxial tests.

4.3.1. Simple tension

The controlled displacement is set-up as presented in Figure 4.10 including 14 loading steps. The displacement in each step is increased by 15 mm up to total displacement 210 mm, each relaxation process lasts 900s.

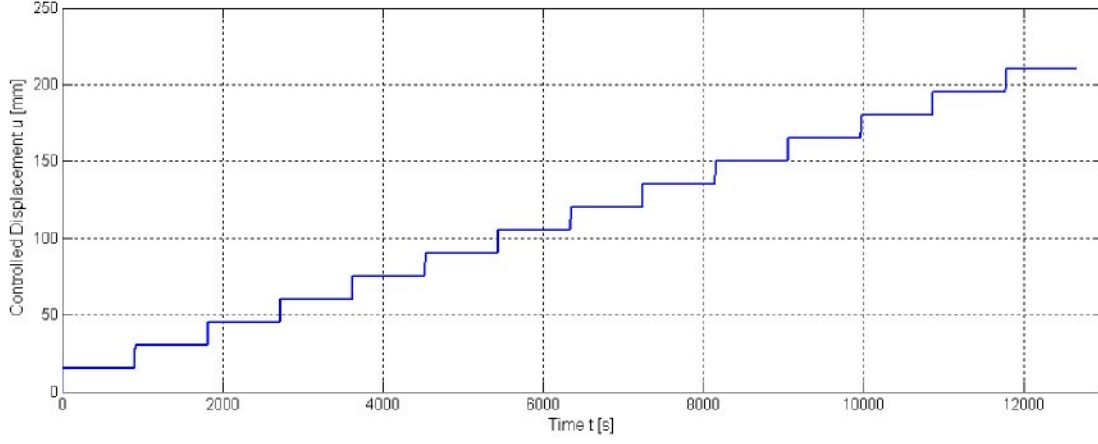


Figure 4.10 – Controlled displacement in the simple tensile test

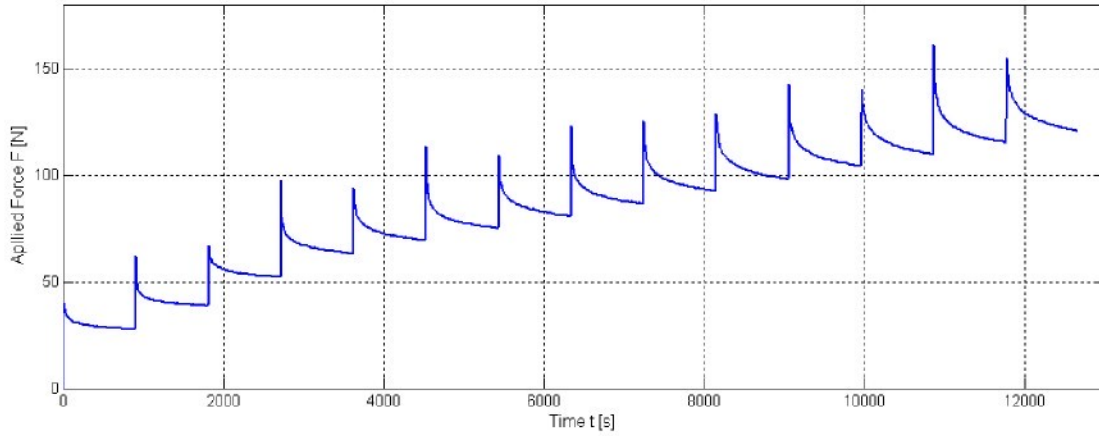


Figure 4.11 – Applied force in the simple tensile test

The force in the simple tensile test is shown in Figure 4.11. From the measured force the first principal Cauchy stress can be defined in equation (4.1). We obtain 14 value sets of stretches and stresses in the equilibrium state.

By using the fundamental theory mentioned in equations (3.19) ÷ (3.21), the evaluation results for chosen elastic models are depicted in Figure 4.12. The evaluated elastic coefficients and corresponding residual estimations are listed in Table 4.1. As it can be seen the Ogden model with 2 terms (corresponding to 4 material parameters) describes the equilibrium behavior of isotropic materials well.

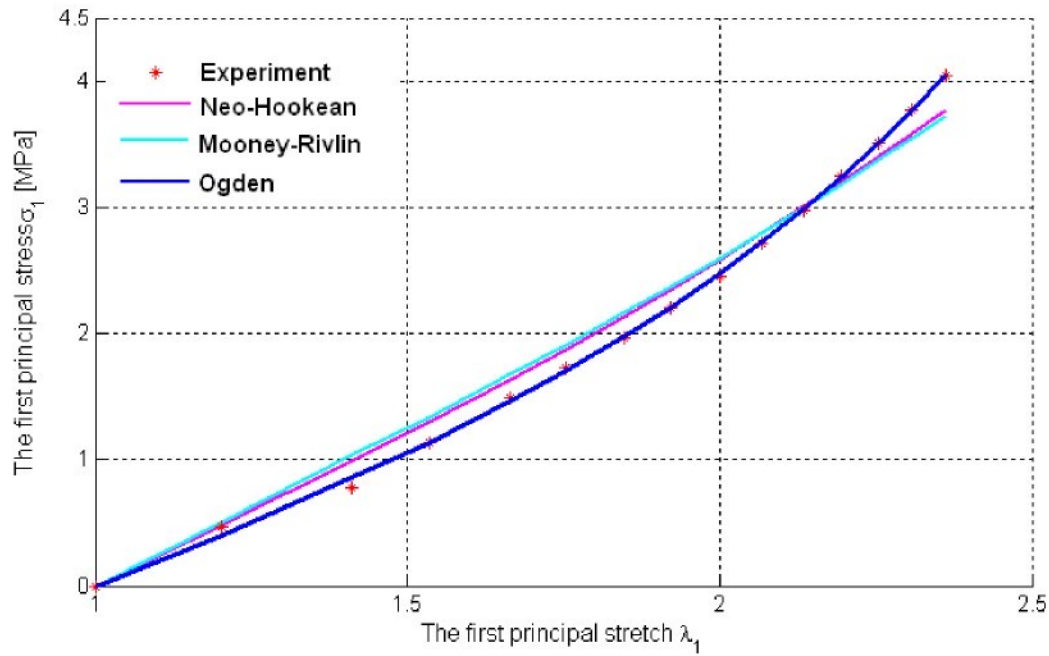


Figure 4.12 – Estimation of elastic coefficients of the isotropic material by a simple tensile test with different models

Table 4.1 – Elastic coefficients of the isotropic material by the simple tensile test

Model	Neo-Hookean	Mooney-Rivlin	Ogden
Material coefficients	$c = 0,3678 \text{ MPa}$	$c_1 = 0,3441 \text{ MPa}$ $c_2 = 0,0492 \text{ MPa}$	$\mu_1 = 0,5428 \text{ MPa}; \alpha_1 = 2,25$ $\mu_2 = 0,00056 \text{ MPa}; \alpha_2 = 7,99$
Shear modulus	$\mu = 0,7356 \text{ MPa}$	$\mu = 0,6883 \text{ MPa}$	$\mu = 0,6115 \text{ MPa}$
Error ($\sum \Delta y_i / \sum y * 100\%$)	5,73%	6,84%	0,89%

For evaluating viscoelastic material coefficients neo-Hookean and Ogden models are used for representing the behavior of the isotropic material, the viscoelastic response is modeled by one Maxwell element. Using expression (4.8) to fit the model to the experimental data the results are presented in Figure 4.13, the viscoelastic coefficients are found out as in Table 4.2.

Table 4.2 – Viscoelastic coefficients of the isotropic material by the simple tensile test

Model	Neo-Hookean	Ogden
Relaxation time	$\tau = 114,2 \text{ [s]}$	$\tau = 118,9 \text{ [s]}$
Scale coefficients	$\beta = 0,278$	$\beta = 0,293$
Residual ($\sum \Delta y_i ^2$)	40,3403	7,4678

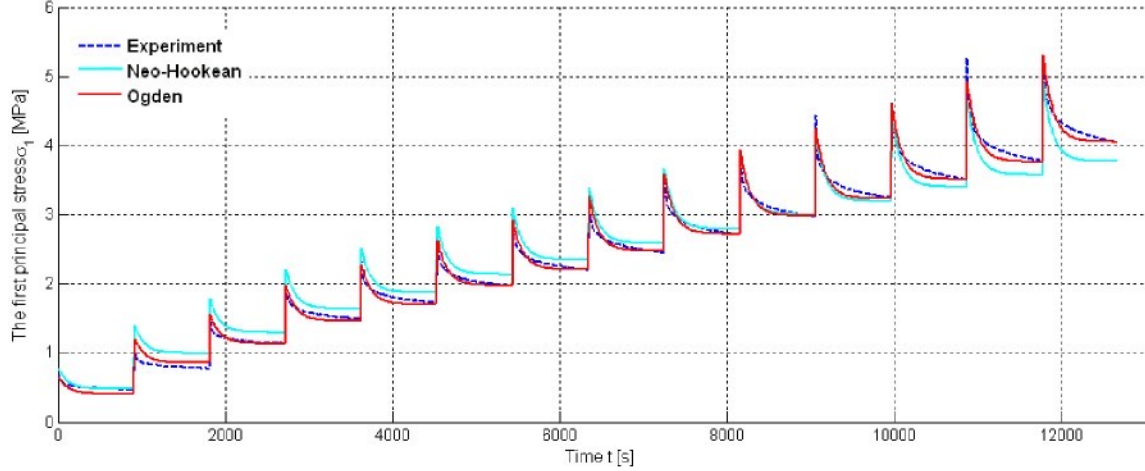


Figure 4.13 – Estimation of viscoelastic coefficients of the isotropic material by a simple tensile test with neo-Hookean and Ogden models

4.3.2. Pure shear test

Pure shear strain state was obtained by using a rectangular sheet about 30mm high and $2,9 \times 220 \text{ mm}^2$ section subjected to uniaxial displacement. Figure 4.14 signifies the controlled displacement with 9 steps, the increasing displacement in each step is 1,5mm. The applied force is measured as in Figure 4.15. Due to a special shape of a specimen the width is much larger than the height ($b/l \sim 7,5$) so that the second principal stretch during the test is close to 1, as illustrated in Figure 4.16.

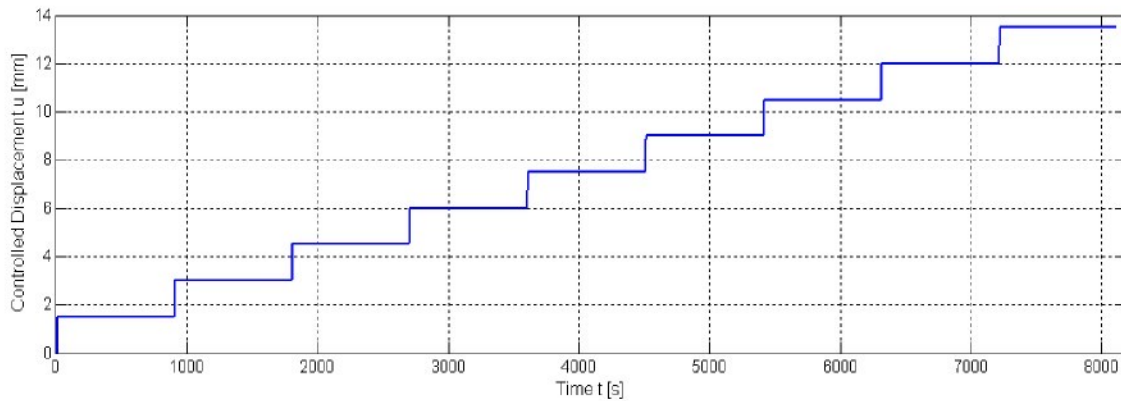


Figure 4.14 – Controlled displacement in the pure shear test

Since $\lambda_2 = 1$ the Mooney-Rivlin is coincident with the neo-Hookean model, hence we only use neo-Hookean and Ogden models for estimating elastic coefficients, in which Ogden models are applied with one and two terms corresponding to 2 and 4 parameters, respectively. The estimation is shown in Figure 4.17, whereas the elastic coefficients are collected in Table 4.3. We can realize that the Ogden model with 4 parameters describes the equilibrium of the isotropic material quite adequately.

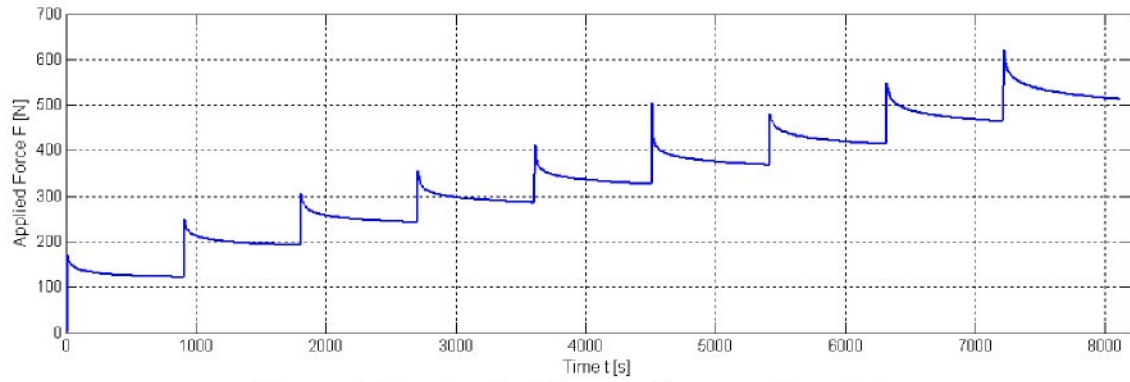


Figure 4.15 – Applied force in the pure shear test

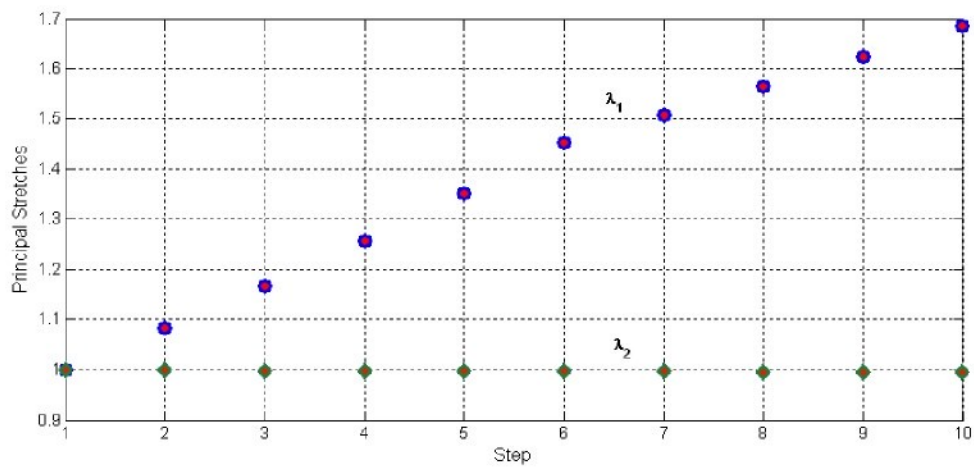


Figure 4.16 – Principal stretches in the pure shear test

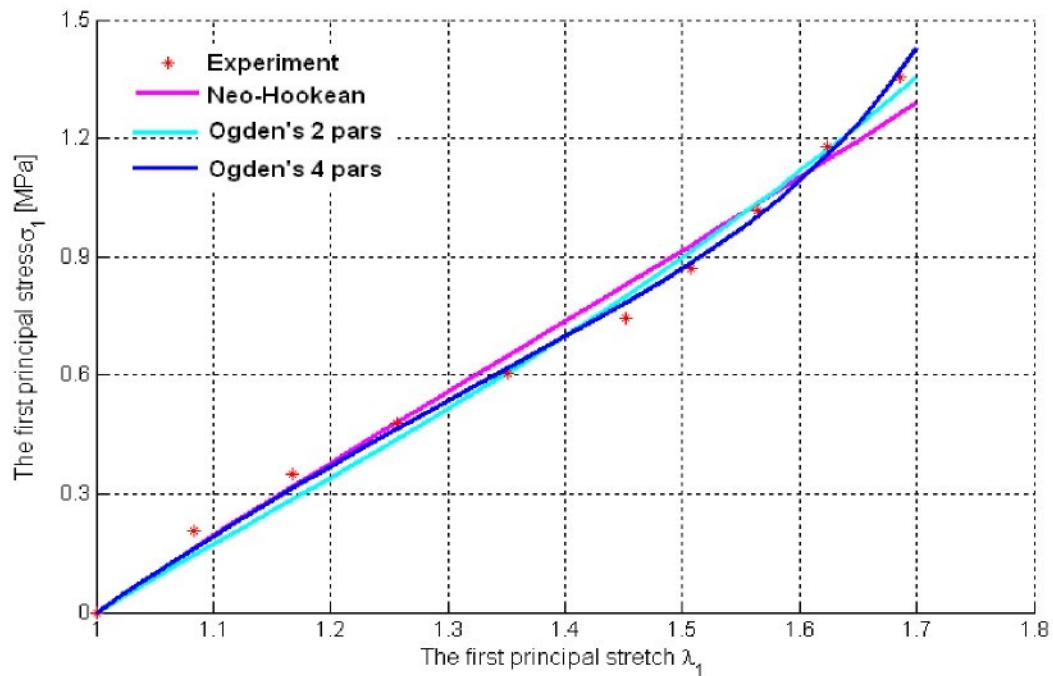


Figure 4.17 – Estimation of elastic coefficients of the isotropic material by a pure shear test with different models

Table 4.3 – Elastic coefficients of the isotropic material by the pure shear test

Model	Neo-Hookean	Ogden's 2 parameters	Ogden's 4 parameters
Material coefficients	$c = 0,2537$ MPa	$\mu_1 = 0,3161$ MPa $\alpha_1 = 2,84$	$\mu_1 = -0,0001$ MPa; $\alpha_1 = -15,41$ $\mu_2 = 64,776$ MPa; $\alpha_2 = 0,016$
Shear modulus	$\mu = 0,5074$ MPa	$\mu = 0,4483$ MPa	$\mu = 0,5054$ MPa
Error ($\sum \Delta y_i / \sum y * 100\%$)	6,02%	4,91%	3,09%

The estimation of viscoelastic material coefficients by means of using different models for representing the purely elastic behavior of isotropic materials is presented in Figure 4.18. The viscoelastic coefficients are summarized in Table 4.4.

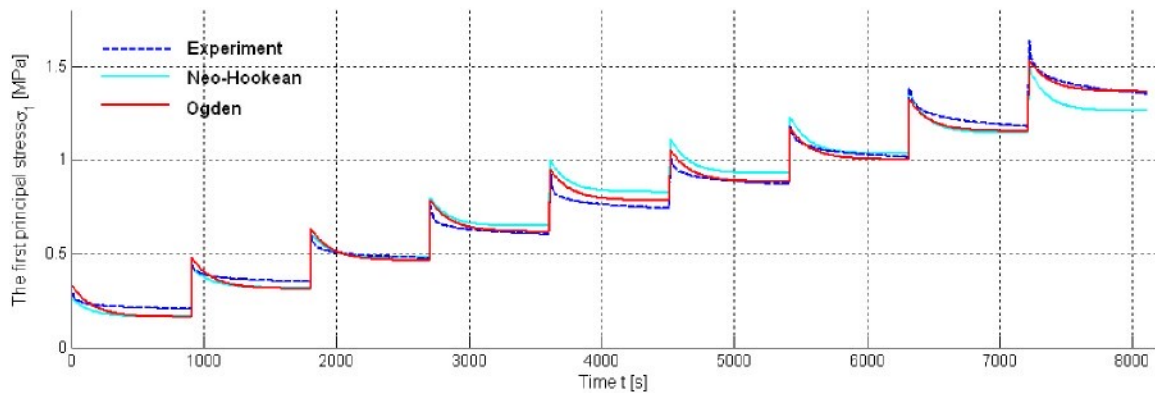


Figure 4.18 – Estimation of viscoelastic coefficients of the isotropic material by a pure shear test with neo-Hookean and Ogden models

Table 4.4 – Viscoelastic coefficients of the isotropic material by the pure shear test

Model	Neo-Hookean	Ogden
Relaxation time	$\tau = 135,4$ [s]	$\tau = 153,9$ [s]
Scale coefficients	$\beta = 0,16$	$\beta = 0,003$
Residual ($\sum \Delta y_i ^2$)	2,7875	0,7707

4.3.3. Biaxial tensile test

By utilizing the biaxial testing apparatus we can control simultaneously the deformation of specimen in two perpendicular directions step-by-step displacement, the equilibrium force is measured after a relaxation in 10 minutes and the corresponding strains are evaluated quite precisely by the two digital cameras.

Three material models that are neo-Hookean, Ogden with 2 parameters and Ogden with 4 parameters are used for estimating constant material coefficients. The estimation results are shown as in Figure 4.19. However, the four calculated parameters of Ogden model

were useless as they did not fulfill the condition (3.6)₂. The elastic coefficients of the remaining models are estimated in Table 4.5.

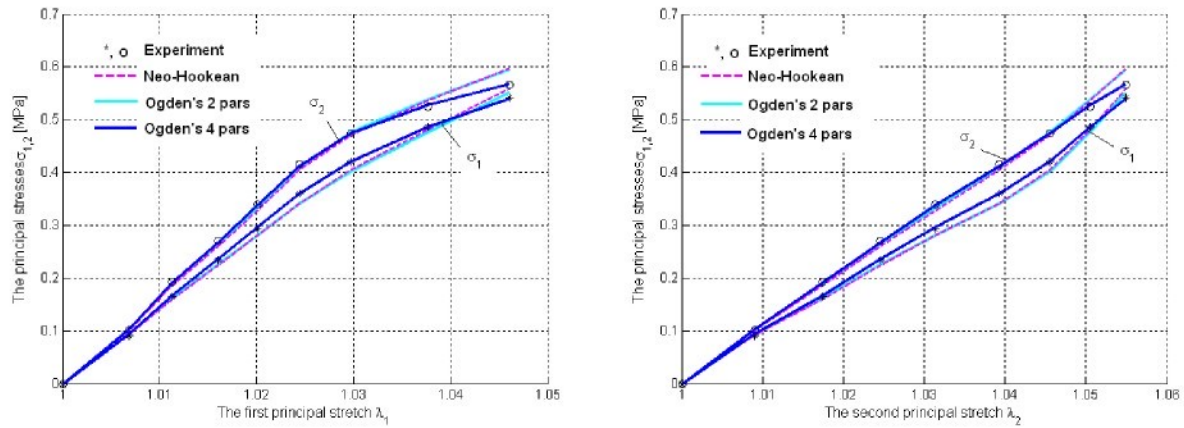


Figure 4.19 – Estimation of elastic coefficients of the isotropic material by a biaxial tensile test with different models

Table 4.5 – Elastic coefficients of the isotropic material by the biaxial tensile test

Model	Neo-Hookean	Ogden's 2 pars	Ogden's 4 pars
Material coefficients	$c = 1,0240 \text{ MPa}$	$\mu_1 = 1,0917 \text{ MPa}$ $\alpha_1 = 3,86$	-
Shear modulus	$\mu = 2,0480 \text{ MPa}$	$\mu = 2,1076 \text{ MPa}$	-
Error ($\sum \Delta y_i / \sum y * 100\%$)	3,09%	2,82%	-

In fact the shear moduli of the same material evaluated by different experiments should be identical. However the shear modulus evaluated by the biaxial tensile test is much bigger than by the other experiments, there are two possible reasons: A subjective reason is caused by the imperfect form of the specimen, specifically the effective cross-sectional area of the specimen arms. This effect can be eliminated by slits made in each of arms as recommended in Kuwabara et al. (1998).

4.4. Fiber-reinforced composite materials

Due to the restriction of the biaxial apparatus is discussed above and since fibers of the composite are cut into short segments for simple tensile test. Hence only a pure shear test is performed for the fiber-reinforced composite material. We implement experiments for composites reinforced with different fiber angles as 30° , 40° , 50° and 60° in multi-step relaxations, in which rectangular sheets with 30mm high and 4,5×220mm cross section. The

values of forces and strains measured at the end of each relaxation process are considered equivalently as the equilibrium quantities.

In this section only neo-Hookean model is used to describe elastic behavior of the matrix, whereas the polynomial function (3.10) of the anisotropic energy component is used for representing anisotropic behavior of fibers. The evaluation result is shown in Figure 4.20, elastic coefficients are identified as follows: shear modulus $\mu = 3,5 \text{ MPa}$, anisotropic constant $k = 8,73 \text{ MPa}$. The numerical results are in good accordance with the experimental data.

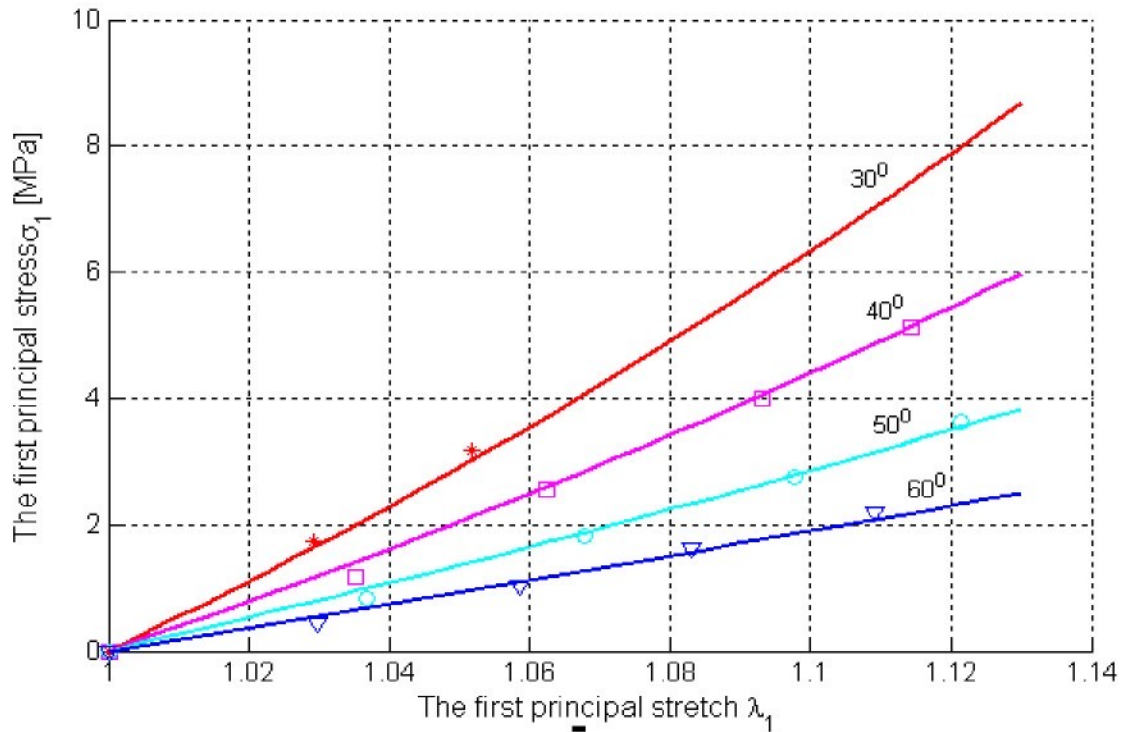
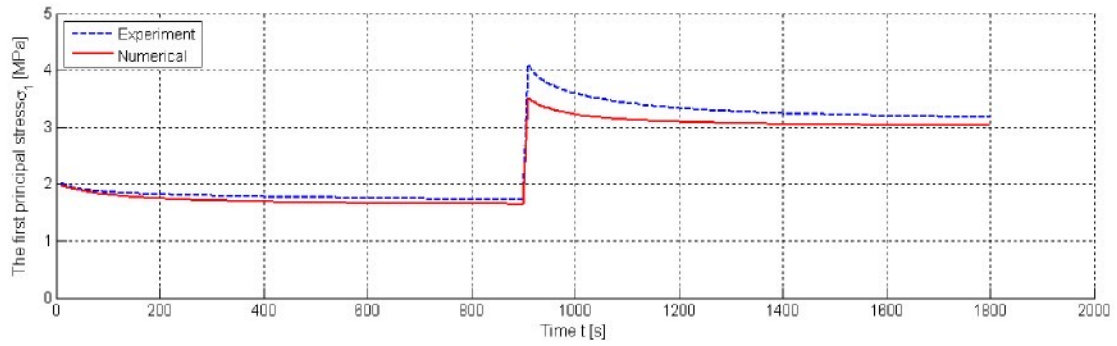


Figure 4.20 – Estimation of elastic coefficients of the composite reinforced with different fiber orientations by a pure shear test

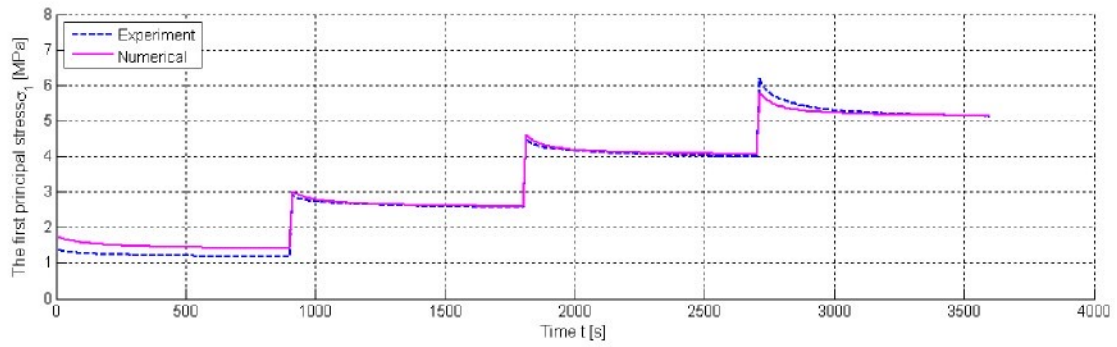
For describing a viscoelastic behavior of fiber-reinforced composites a Maxwell model with two elements is used, therefore over stresses can be expressed in a Prony series by equation (4.9). Since the elastic material parameters were evaluated in the first stage, the equilibrium isotropic and anisotropic stress components are already defined. Applying an iterative approach by means of the nonlinear least-square method in Matlab the estimation result is shown in Figure 4.21 with calculated viscoelastic coefficients as follows

$$\beta_{iso} = 0,06; \quad \tau_{iso} = 269 \text{ s}$$

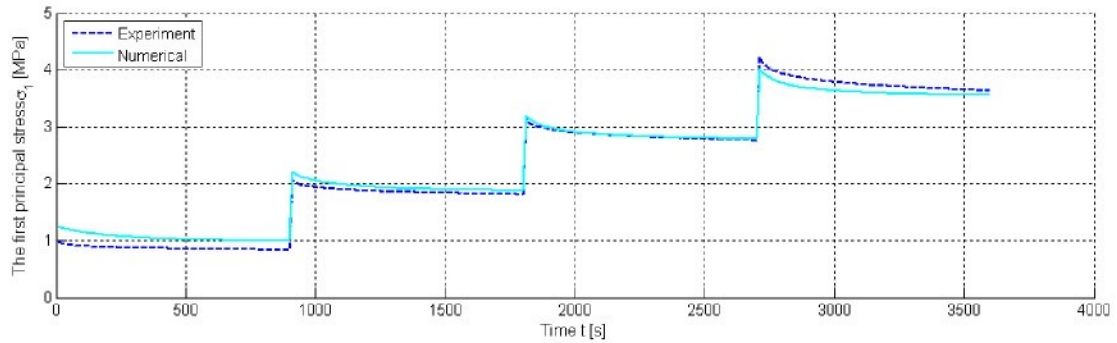
$$\beta_{ani} = 0,11; \quad \tau_{ani} = 54 \text{ s}$$



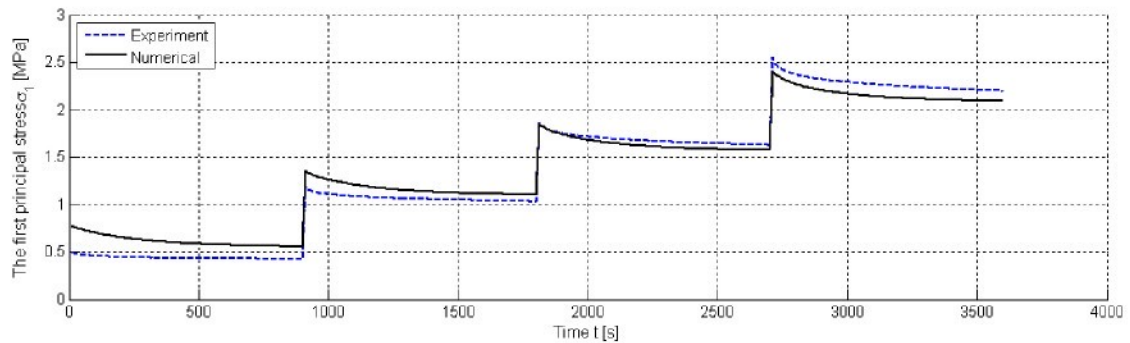
(a) Relaxation processes with fiber angle $\varphi = 30^0$



(b) Relaxation processes with fiber angle $\varphi = 40^0$



(c) Relaxation processes with fiber angle $\varphi = 50^0$



(d) Relaxation processes with fiber angle $\varphi = 60^0$

Figure 4.21 – Estimation of viscoelastic coefficients of the composite reinforced with different fiber orientations by a pure shear test

We see that the estimated curves are quite close to experimental data. The viscoelastic coefficients were assumed to be constant in our simple formulation. However, it is believed that rate-dependent models with constant parameters cannot represent well the experimentally observed rate-dependent phenomena of rubber and rubber composites (Amin et al., 2006). There is a future task to generalize the models and to introduce a dependence of the parameters, for example, on stress, on deformation or on some internal variables. On the other hand, simple models have the advantage that their material parameters can be identified by classical experimental tests and their material equations are well suited to be implemented into computer programs for structural analyses as e.g. finite element programs.

Chapter 5

NUMERICAL SIMULATIONS OF VISCOELASTIC COMPOSITES

In this chapter we will devote to represent some numeric simulations of hyperelastic as well as viscoelastic behavior of composite materials. The main goal is to verify the performance of constitutive viscoelastic models presented in previous chapters associating with the material parameters determined from the evaluation of experiments.

5.1. FEM implementation in COMSOL Multiphysics

The Finite Element Method (FEM) is applied for numerical analysis of viscoelastic fiber-reinforced composite implemented in Comsol Multiphysics which is a scientific and CAE design analysis software environment for the modeling and simulation of any problem of physics described by system of partial differential equations. This software allows the easy modifications or the new definitions of constitutive equations after any user convenience and its main feature is a possibility to solve simultaneously coupled physic problems.

We use the Structural Mechanics Module in combination with PDE modes, in which the Structural Mechanics Module is used to compute a quasi-static behavior of structure whereas the PDE modes are added for the integration of evolution equations of the viscous response that can be referred to section C.1 of Appendix C.

Instead of the common approach, using the conjugate pairs second Piola-Kirchhoff stress and Green-Lagrange strain, Comsol uses the first Piola-Kirchhoff stress \mathbf{P} and its conjugate strain the displacement gradient $\nabla \mathbf{u}$. The reason for this is to utilize the capability of Comsol Multiphysics to automatically differentiate an expression, thus making it easy to modify only the strain energy function. The first Piola Kirchhoff stresses are calculated as

$$\mathbf{P} = \frac{\partial \Psi}{\partial (\nabla \mathbf{u})} \quad (5.1)$$

The Cauchy stress $\boldsymbol{\sigma}$ and the second Piola-Kirchhoff stress \mathbf{S} can then be calculated from the first Piola-Kirchhoff stress by equations (A.33) and (A.34).

Additionally, materials that are nearly incompressible cannot be solved using only displacement variables. The remedy is to introduce the pressure p as a dependent variable. The hyperelastic material model supports both the normal displacement-based formulation and the so-called mixed formulation that includes the pressure.

The definition of the free energy function can be modified directly in a “*Subdomain Settings – Equation System*” table as shown in section C.3 of Appendix C, hence it is easy to define the suitable free energy function corresponding to the chosen model. The constitutive equations as well as the evolution equations can be expressed in the scalar expression table (see sections C.2 and C.4 of Appendix C).

When we study the relaxation problem, a load at the beginning is applied instantaneously, hence we can choose between two approaches: Either the load is applied over a short period of time in the beginning of the time stepping, or a separate static analysis is used for obtaining the initial conditions. However, as the latter method is used for the loading stage, i.e. the load is understood implicitly to be applied suddenly, therefore it will be necessary to create correct initial conditions for the internal variables.

Triangle meshing elements are used for all the simulations in 2-D problems. In addition, an incremental nonlinear Newton-Raphson solution algorithm is used to solve the quasi-static boundary value problem. In order to generate a controlled loading with one- or multi- step values suitable to relaxation and/or creep simulations we use the function definition as mentioned in section C.5 of Appendix C.

5.2. Isotropic (hyperelastic) rubber-like materials

In this work the isotropic rubber-like materials are assumed to be incompressible and able to suffer a nonlinear large deformation that the purely elastic behavior can be described independently by the free energy function, herein neo-Hookean (3.2) and Ogden (3.5) models are used for equilibrium responses. The values of material parameters used in simulations are given in Table 4.1 and Table 4.3.

5.2.1. Equilibrium stress-strain responses

In order to compare numerical and experimental results we will consider two basic problems that have been presented in the previous chapter, namely the simple tensile and pure shear deformations, both of them are studied in quasi-static plane-stress states for isotropic materials.

A schematic sketch of these deformations is depicted in Figure 5.1(a). The thickness of the material is 2,9mm. Due to both the geometries of the body and the loading conditions are symmetric so the symmetric model and loading conditions are used to solve. The finite element (FE) models are shown in Figure 5.1(b). In the both simulations the displacement is controlled at the boundary of the body, for the simple tension case the extension increases up to 167% whereas for the pure shear the maximum extension is 80%.

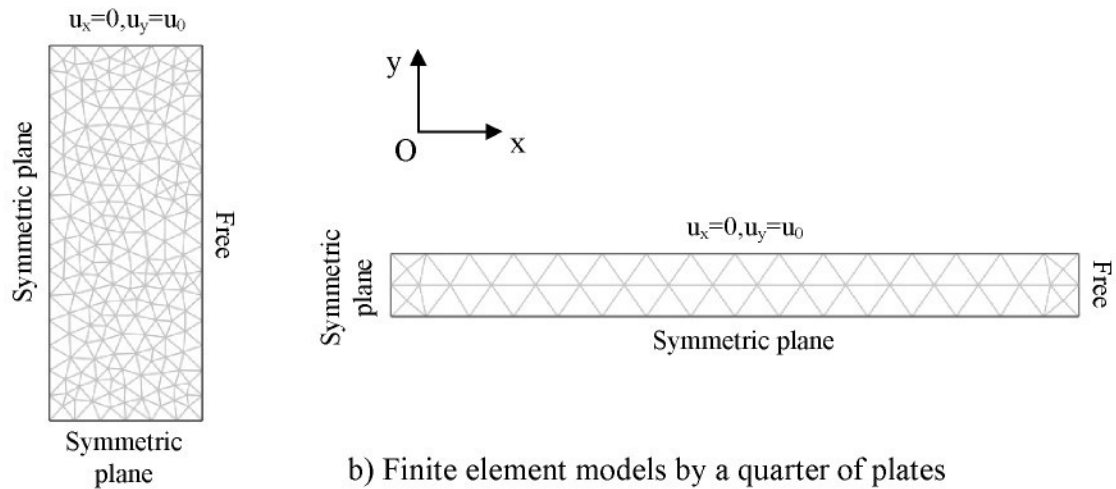
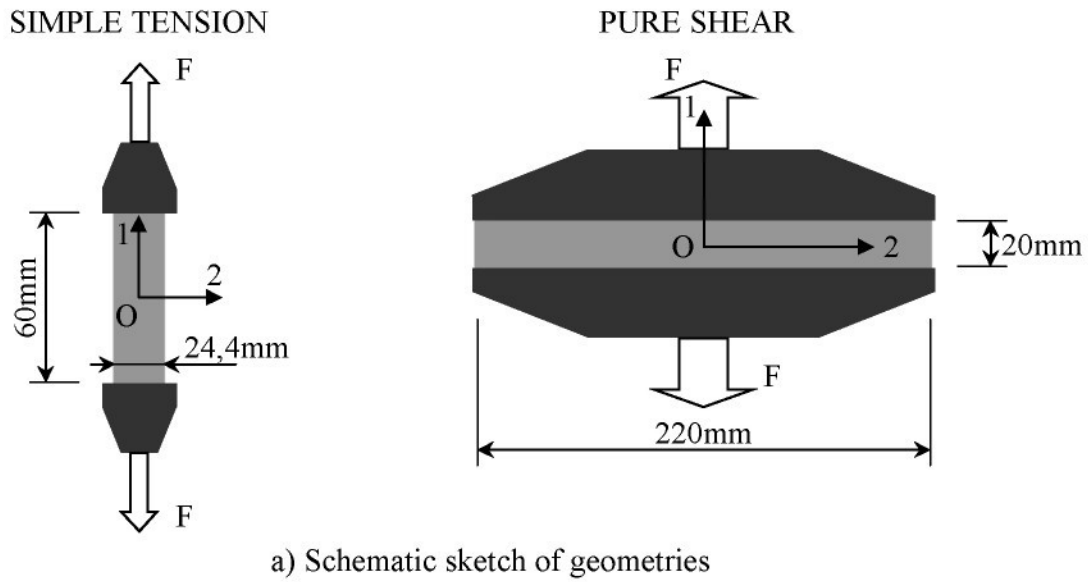


Figure 5.1 – Geometries and FE models in simple tension and pure shear deformations

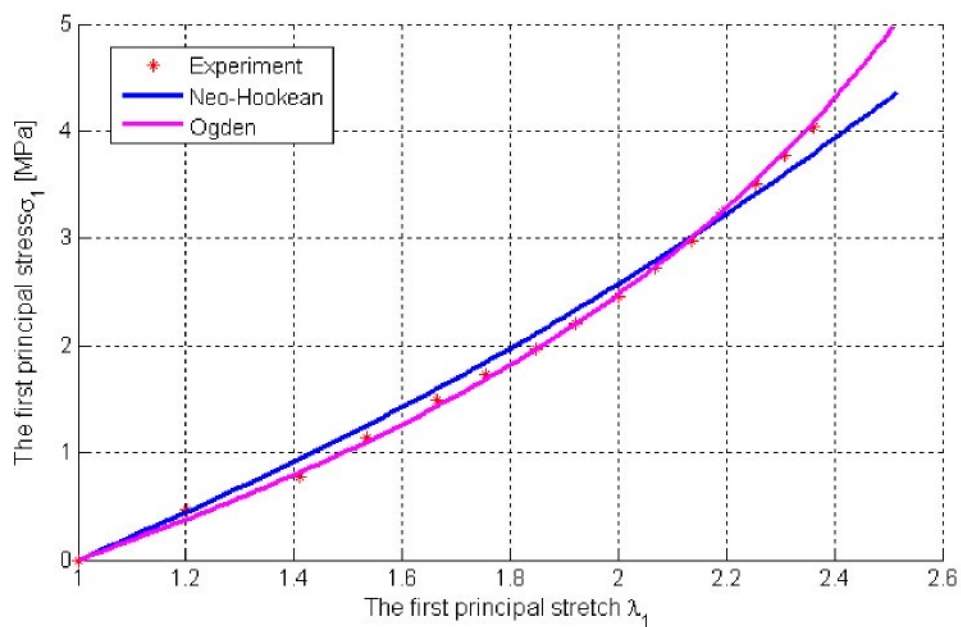


Figure 5.2 – First principal stress versus stretch of simple tension deformation

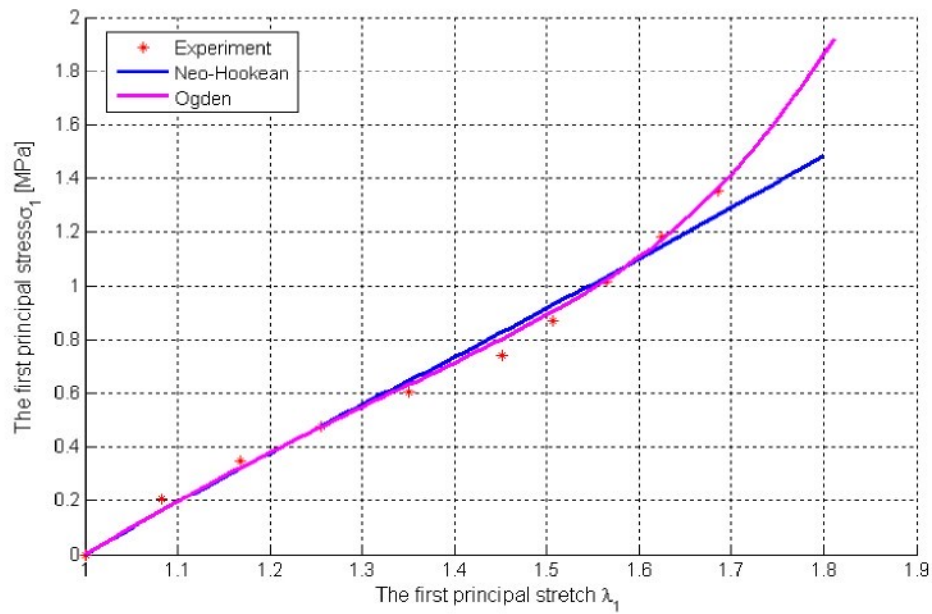
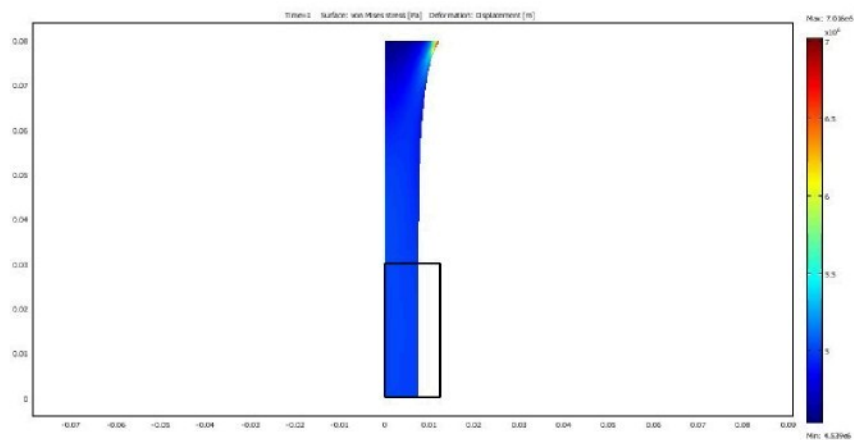
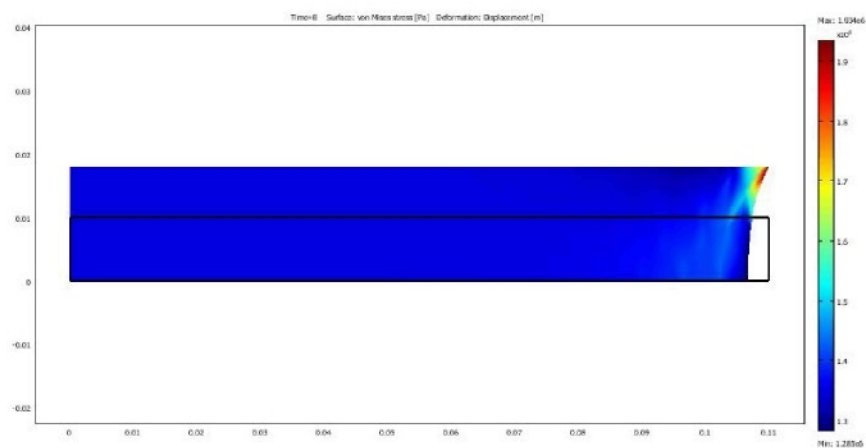


Figure 5.3 – First principal stress versus stretch of pure shear deformation



a) Von Mises stress of simple tension at extension 167% (one quarter of specimen)



b) Von Mises stress of pure shear at extension 80% (one quarter of specimen)

Figure 5.4 – Stress distribution of simple tension and pure shear

The relationships between the principal stress and the principal stretch at a center of the body by means of using neo-Hookean and Ogden models are compared to the experimental data of pure shear and simple tension deformations as shown in Figure 5.2 and Figure 5.3, respectively. The agreement between the numerical results and the experimental data is very good for Ogden's model, nevertheless neo-Hookean model gives good results in the range of small deformations as well.

The distribution of Von Mises stress at large deformations for both simple tension and pure shear states are displayed in Figure 5.4. The state of stress is homogeneous in the whole specimen except at the specimen boundary where the stress concentration is evident owing to the boundary conditions.

5.2.2. Viscoelastic behavior of isotropic materials

In this section we only consider the simple tension problem in order to investigate some viscoelastic responses, particularly effect of loading rates, one- and multi- step relaxations and prediction of creep will be presented. The neo-Hookean model is used to describe the pure elastic behavior of material whereas the evolution equation of over stresses formulated by using Maxwell's model with one spring-dashpot element to represent the viscous characteristic of isotropic material governing the viscous behavior. The chosen material parameters are inferred from the fitting of the experimental data, namely as follows: Shear modulus $\mu = 0,7 \text{ MPa}$, viscous constant coefficient $\beta = 0,27$ and the relaxation time $\tau = 115 \text{ s}$.

5.2.2.1. Effect of loading velocities

The strip of filled rubber of dimensions $60 \times 24,4 \times 2,9 \text{ mm}^3$ is loaded in tension by a series of velocities $v = 1/12, 1/6, 3, \dots \text{ mm/s}$. The applied load is controlled by a displacement of specimen boundary up to the extension 100% with different loading velocities. The results of numerical simulations are compared with the experimental measurements in Figure 5.5. We can realize that the stress increases together with the increasing loading rate owing to the viscoelastic behavior. It means that the stress-strain responses are significantly different due to a viscous material behavior relating to a loading velocity. This coincides with an experimental observation in practice. In addition, the stress curves corresponding to the cases of the infinite loading velocity and no including viscous behavior are upper and lower bounds, respectively.

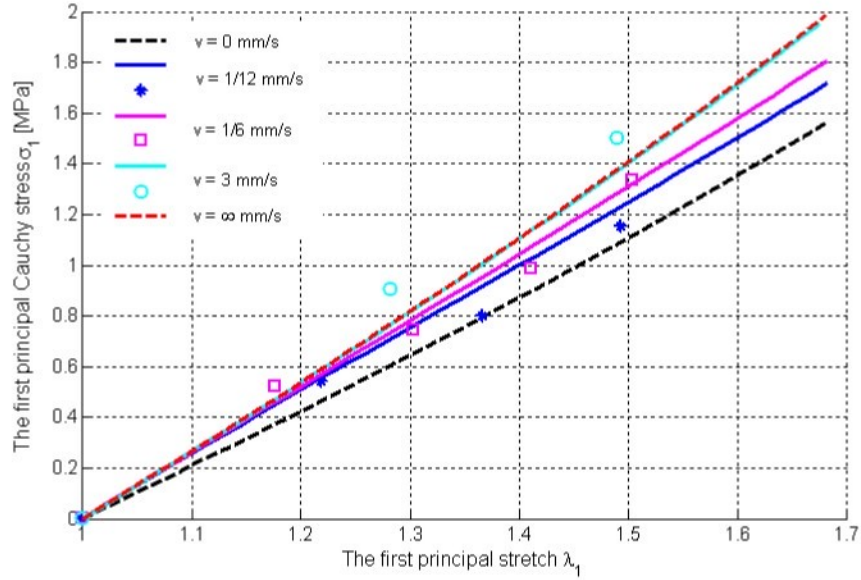


Figure 5.5 – Stress-strain response at different loading velocities (points denote experimental data, solid lines denote numerical results)

5.2.2.2. One-step and multi-step relaxations

Next we simulate a relaxation of isotropic rubber strip of dimensions $60 \times 24,4 \times 2,9$ mm³ undergoing a simple tensile test in a sufficiently long-standing period. The controlled displacement is applied suddenly at different extensions as 20, 40, 60, 80 and 100%, after this stage the displacement is kept constant in course of the relaxation stage. The deformation and the distribution of Von Mises stress by applied different extensions are shown in Figure 5.6. The time dependency of the total Cauchy stress and the viscoelastic part of stress so-called overstress at different stretches are plotted in Figure 5.7. It can be easily realized that after a sufficient holding time the overstresses go to zero and that the stresses reach their equilibrium values. Further, the larger is the stretch the higher is the initial overstress.

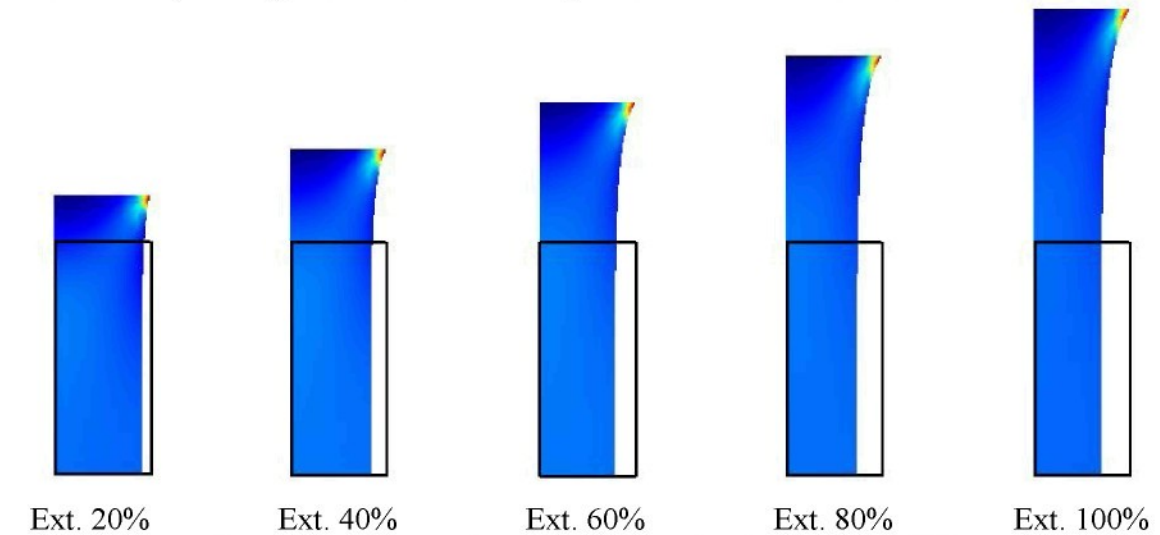


Figure 5.6 – Deformation of isotropic materials in a simple tension at different extensions

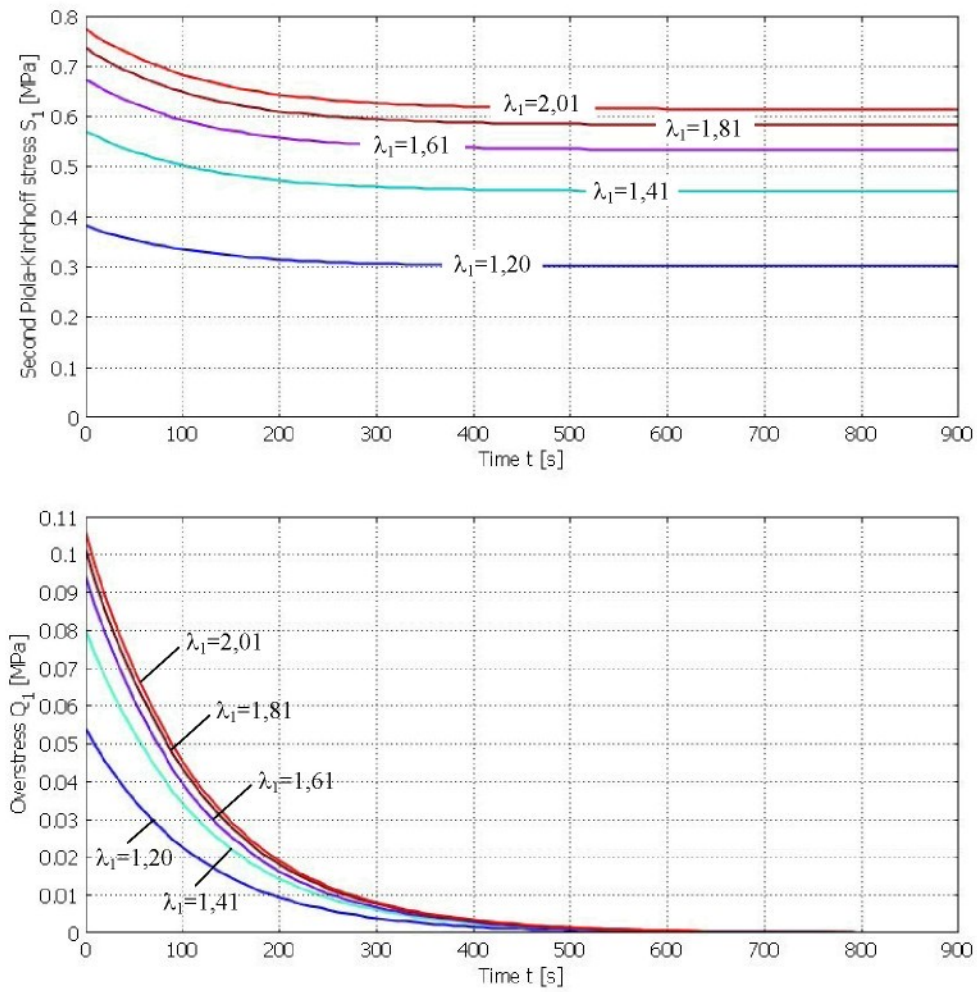


Figure 5.7 – The second Piola-Kirchhoff stresses and overstresses versus time at different stretches

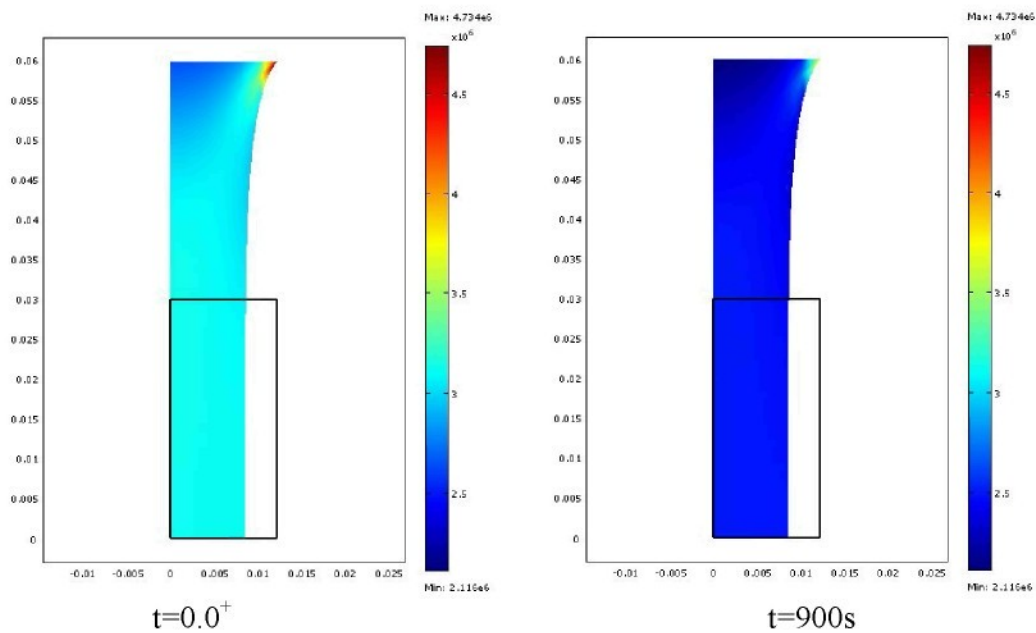


Figure 5.8 – Stress and deformation of simple tension in relaxation

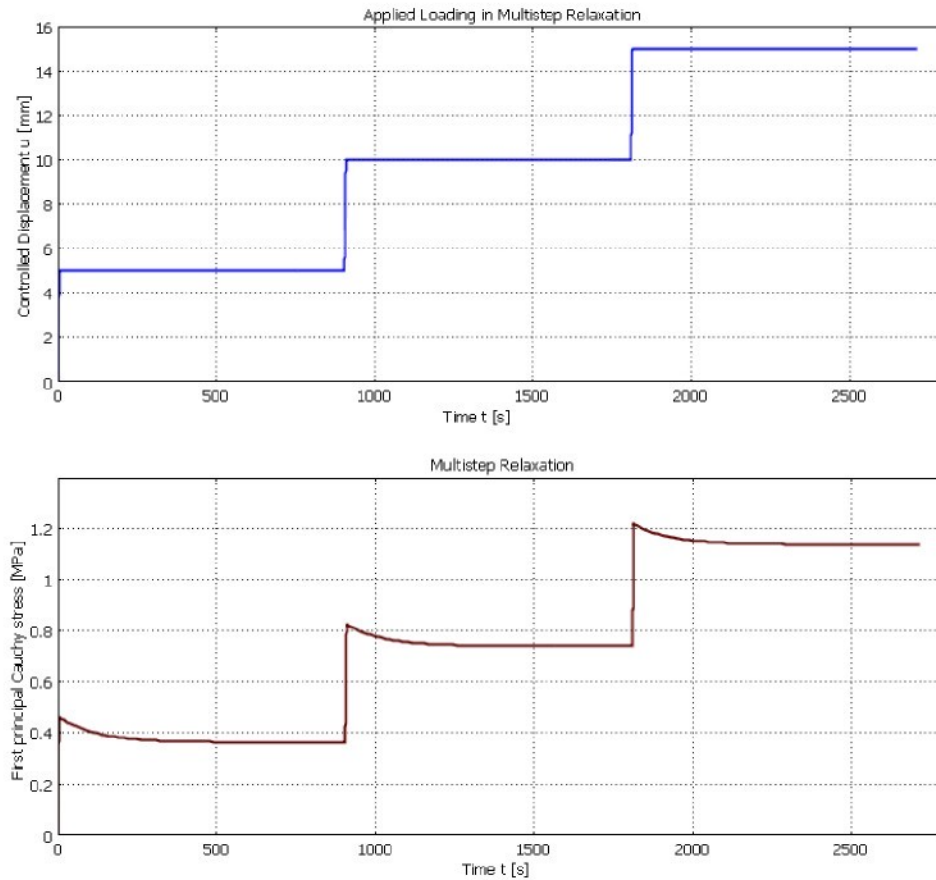


Figure 5.9 – Displacement and Cauchy stress of simple tension in multistep relaxations

The distribution of the Von Mises stress at different times is shown in Figure 5.8. At time $t = 0.0^+$ corresponding to the beginning of the relaxation process the body is deformed by the sudden load, after $t = 900$ s the stress can be identified to be decreasing significantly fluctuating around 20% with respect to the beginning of stresses.

The next simulation is a simple tension where the displacement is set up with three-loading steps in which the loading velocities in every increasing load stage are 3 mm/s. The Cauchy stress in the multi-step relaxation is shown in Figure 5.9.

5.2.2.3. Prediction of creep process

As the controlled load is replaced by a force that is held constantly in a sufficient long time period we have a creep process. Figure 5.10 represents the controlled force and the first principal stretch response of simple tension in a creep, as we can see during the creep the first principal stretch goes to be close to the equilibrium value. The difference between experimental and numerical results is quite significant due to the simplification of chosen viscous model only as a linear viscous model.

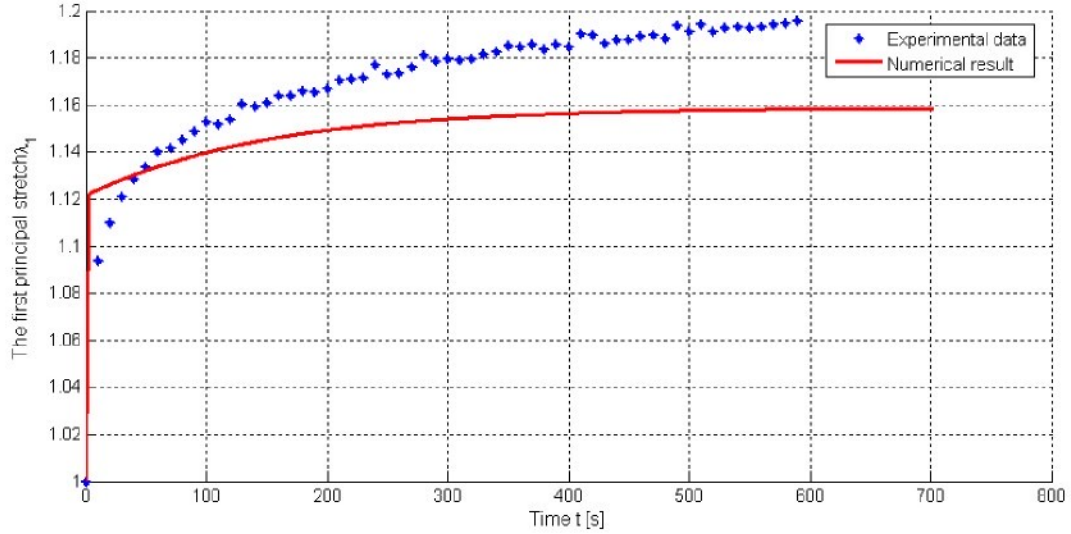


Figure 5.10 – Controlled force and displacement of simple tension in a creep

5.3. Fiber-reinforced composites

5.3.1. Equilibrium response of fiber-reinforced composite in pure shear

A pure shear deformation of two symmetrically fiber-reinforced composites is considered in this subsection in order to compare to the experimental result. As can be seen in Figure 5.11, due to the geometry of the material as well as the loading conditions are designed to be symmetric therefore only a quarter of the body is computed and the symmetric boundary conditions are applied. The fibers are arranged symmetrically with respect to the loading direction and inclined by an angle ϕ . The dimensions of the plate are $220 \times 20 \times 4,5 \text{ mm}^3$.

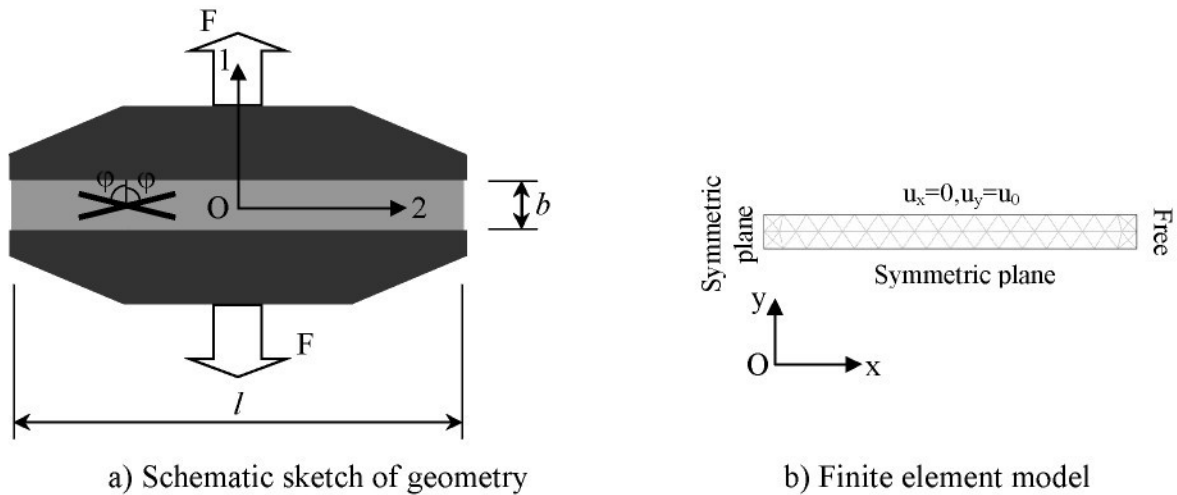


Figure 5.11 – Geometry and FE model of fiber-reinforced composite in pure shear deformation

The neo-Hookean model (3.2) is chosen to represent the equilibrium response of the isotropic part of material. The anisotropic energy contribution of fibers is expressed in a polynomial function (3.10). Here the material parameters includes the shear modulus $\mu = 3,5 \text{ MPa}$, the anisotropic constant $k = 8,73 \text{ MPa}$.

The stress response induced by the same deformation depends on the fiber angles as can be seen in Figure 5.12. The stress decreases along with the increase of the magnitude of the fiber angles. The numerical response in the equilibrium state corresponds to the experimental results as shown in Figure 5.13. It is clear that the change of the stress is nonlinear with respect to the fiber angles.

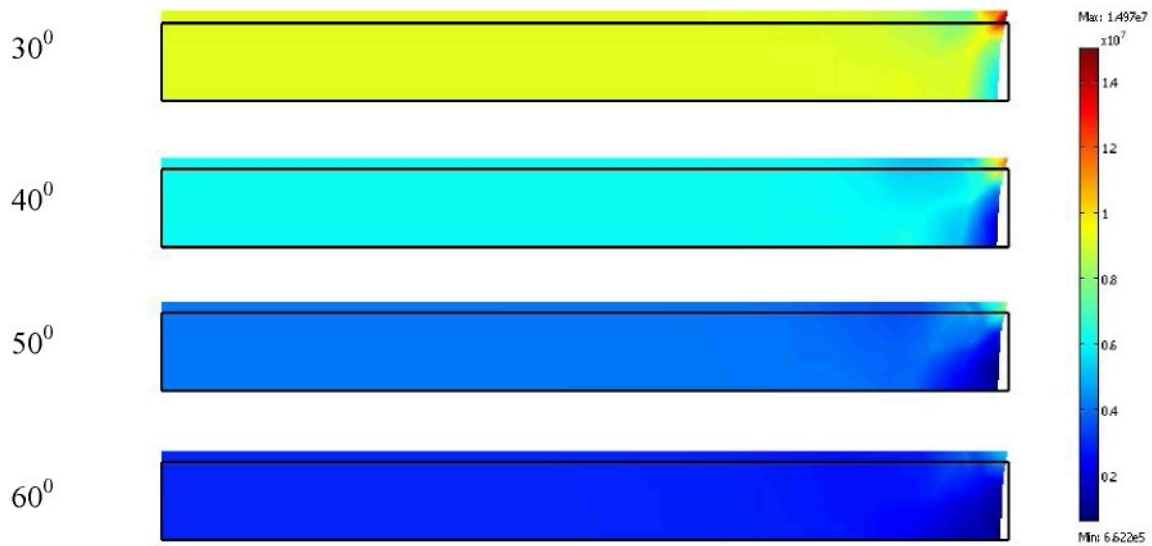


Figure 5.12 – Deformation and stress distribution of composite with different fiber angles

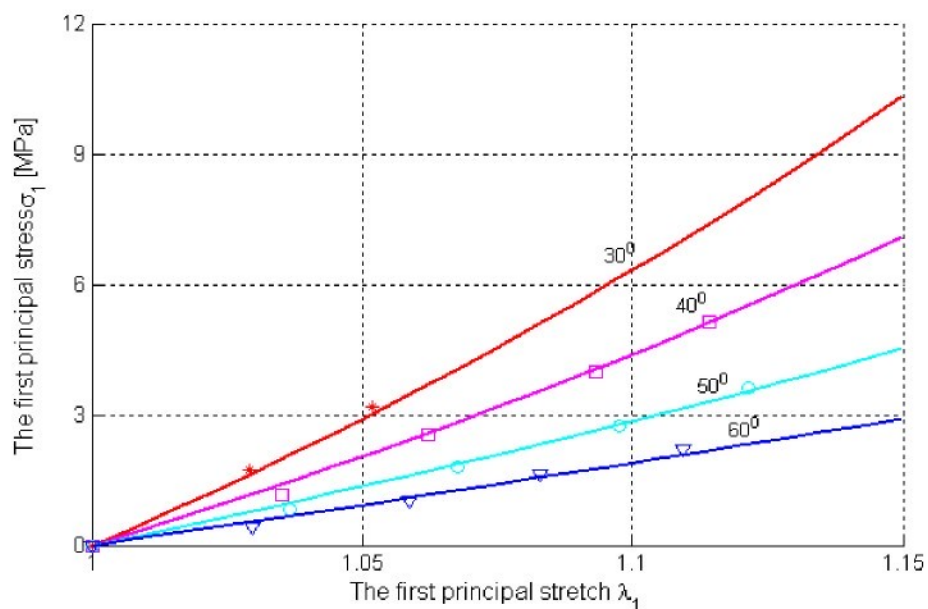


Figure 5.13 – Equilibrium Cauchy stress with different fiber directions in pure shear deformation (points denote experimental data, solid lines denote numerical results)

5.3.2. Elastic response of a rectangular fiber-reinforced composite plate with a hole

We verify our model by calculus of deformation and stress in a rectangular fiber-reinforced composite plate in plane stress state with a centric circular hole. We combine different configurations of the reinforcement fibers. The dimensions of the plate are $100 \times 100 \times 4,5 \text{ mm}^3$ and the radius of the hole is $r=20 \text{ mm}$. The material parameters are shear modulus $\mu = 3,5 \text{ MPa}$ and anisotropic constant $k = 8,73 \text{ MPa}$. We use the symmetric geometry and apply appropriately boundary conditions. The plate is loaded in tension by the displacement u_x at the right boundary (the y displacement here was $u_y = 0$).

The deformed form and the stress distribution of the plate with regard to different fiber configurations are depicted in Figure 5.14.

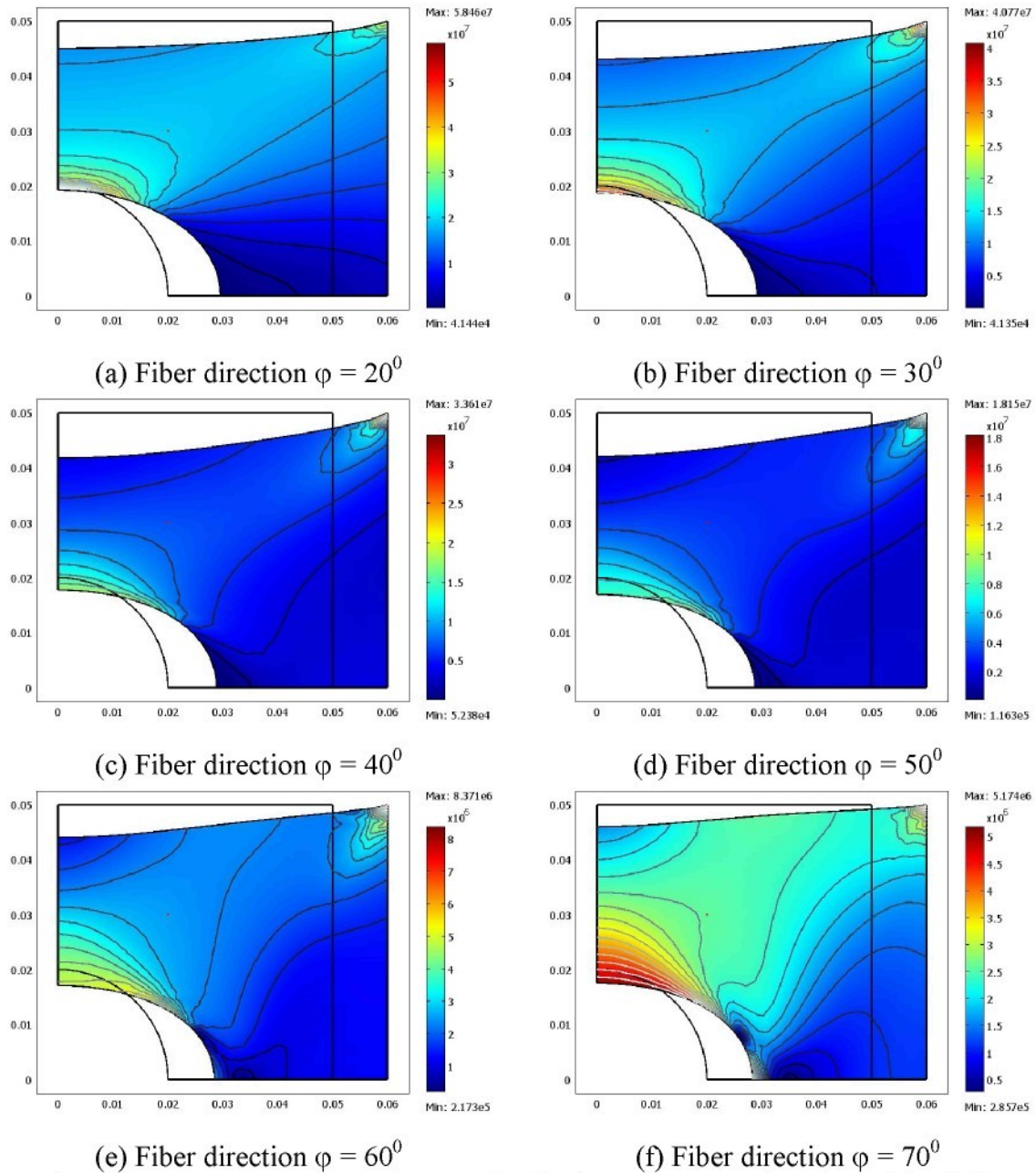


Figure 5.14 – Deformation and stress distribution of a composite plate with a hole

The change of the Cauchy stress at the same position in the plate, denoted by red points in Figure 5.14, with respect to different fiber angles is obvious from Figure 5.15.

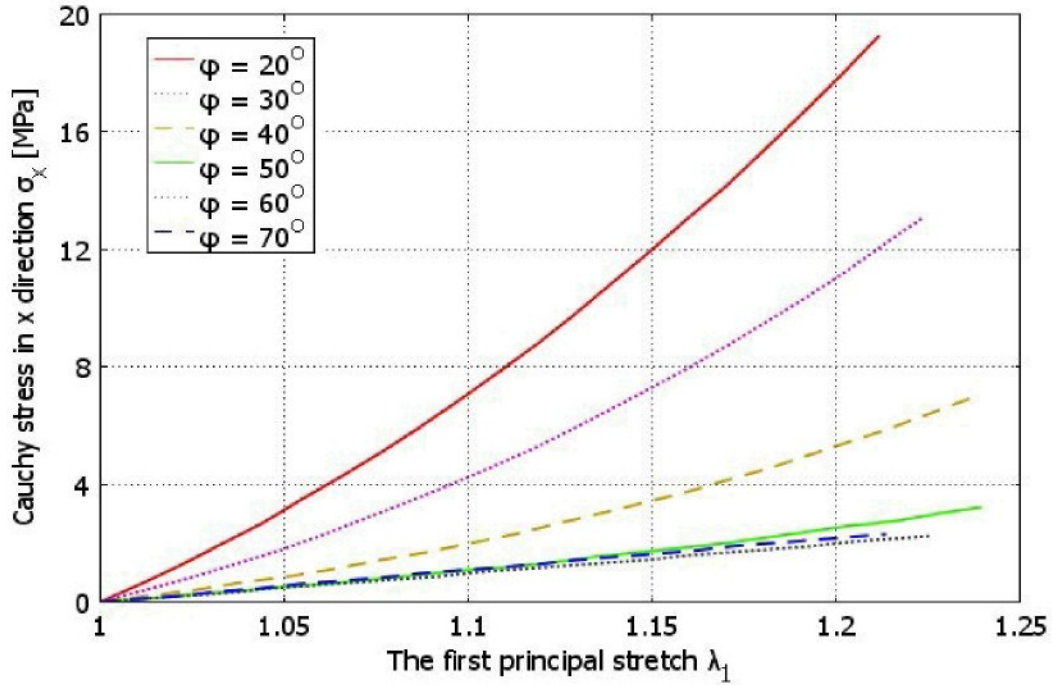


Figure 5.15 – Cauchy stress versus the first principal stretch of a composite with a hole

5.3.3. Viscoelastic response of fiber-reinforced composite

To investigate a viscoelastic behavior of anisotropic hyperelastic materials we simulate numerically the pure shear deformation of the composite strip reinforced by two fiber families, as depicted in Figure 5.11, in several relaxation steps. The fibers are arranged symmetrically with respect to the loading direction and make an angle 30° with the loading axis. The Maxwell model with two spring-dashpot elements is used separately for the matrix and fiber phases to govern isotropic and anisotropic over stresses, respectively. The viscoelastic parameters are $\beta_{iso} = 0,06$; $\tau_{iso} = 269$ s for the matrix phase and $\beta_{ani} = 0,11$; $\tau_{ani} = 54$ s for the fiber phase.

The load is displacement controlled and the displacement is held constant in course of 15 minutes in each of three consecutive relaxation steps. Displacement and stress time histories are shown in Figure 5.16. The Cauchy stress always attempts to reach corresponding equilibrium value in course of the relaxation process. In Figure 5.14 the anisotropic (fiber induced) over stress and the isotropic (intrinsic to rubber) over stress are outlined separately. The anisotropic over stress is largely dominating as expected. The total over stress increases with the increasing deformation.

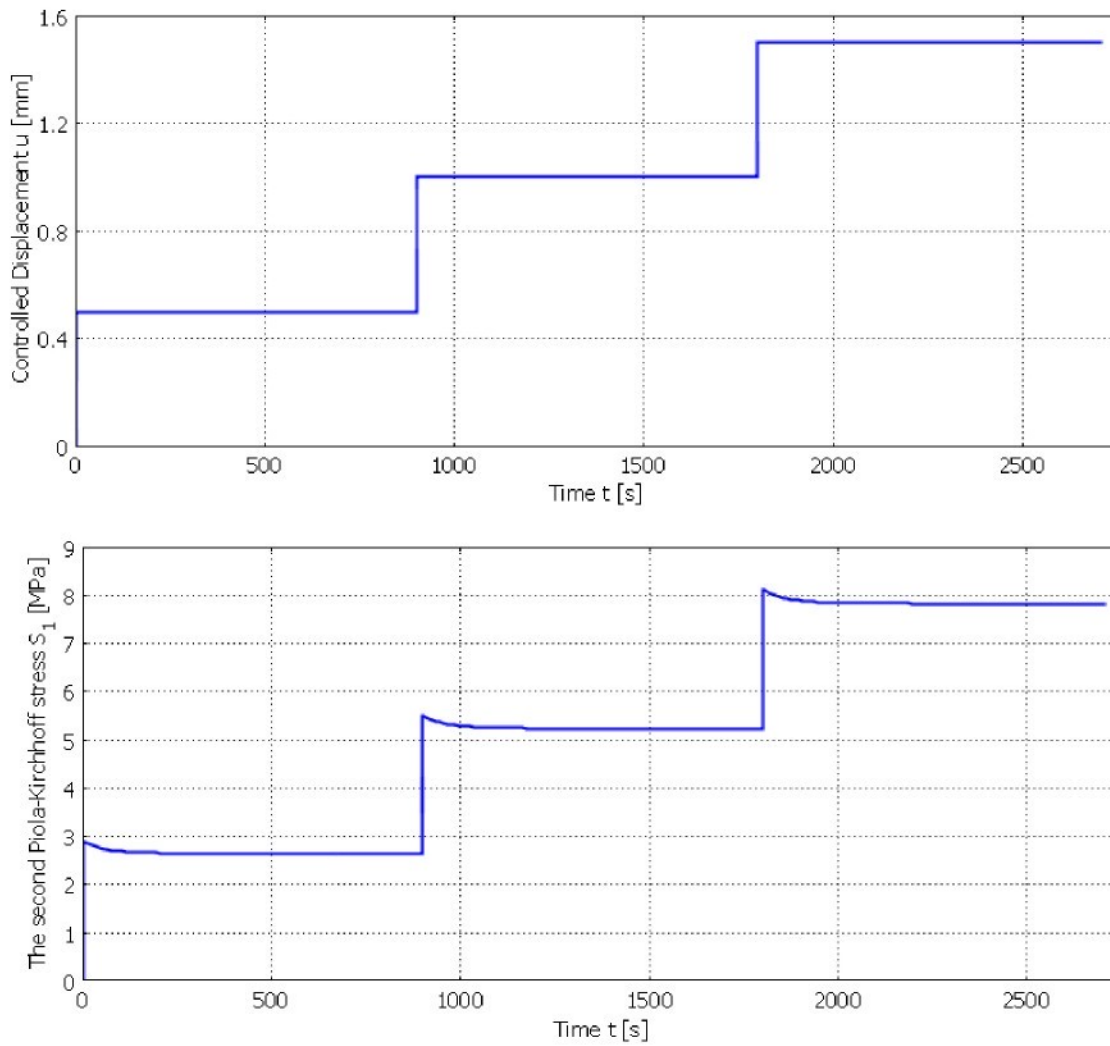


Figure 5.16 – Displacement and Piola-Kirchhoff stress of the anisotropic composite with fiber angles by 30° in relaxations

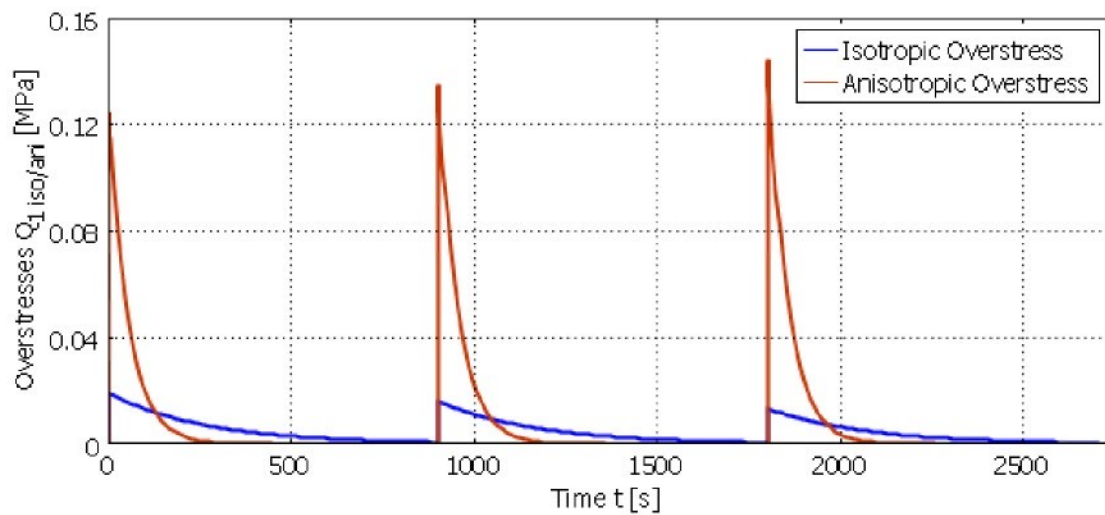


Figure 5.17 – The components of over stresses in the pure shear deformation

5.4. Viscoelastic behavior of an air-spring

In order to study a viscous behavior of a structure in practice we simulate numerically a response of a tubular shell of an air-spring. The material of the tube is assumed to be made from the rubber composite reinforced by two families of fibers. The material parameters were evaluated experimentally in the Chapter 4, specifically the shear modulus $\mu = 3,5 \text{ MPa}$, anisotropic constant $k = 8,73 \text{ MPa}$ and viscoelastic parameters $\beta_{iso} = 0,06$; $\tau_{iso} = 269 \text{ s}$; $\beta_{ani} = 0,11$ and $\tau_{ani} = 54 \text{ s}$.

5.4.1. Equilibrium responses of an air-spring tube

First we consider a case when the tube is subjected to an internal static pressure. An outline of air-spring geometry is depicted in Figure 5.18a. The dimensions of air-spring tube are given as follows: internal radius $r_i = 40 \text{ mm}$, thickness of shell $t = 4,5 \text{ mm}$ and entire length of tube $l = 120 \text{ mm}$, the two fiber arrangements are supposed to be symmetric with respect to the tube axis and the fiber directions are assigned by φ with respect to the circumferential direction of the tube.

The axisymmetric FE model and boundary conditions are used to solve the problem due to axisymmetry of the tube geometry and of the loading conditions. The FE model is shown as in Figure 5.18b.

Notice that while the constant internal pressure is applied in the spatial configuration deformations and stresses are computed in the reference configuration, thus it is necessary to use a mapping transformation for the pressure given by

$$\mathbf{p}_{ref} = p_0 \mathbf{J} \mathbf{F}^{-T} \mathbf{N} \quad (5.2)$$

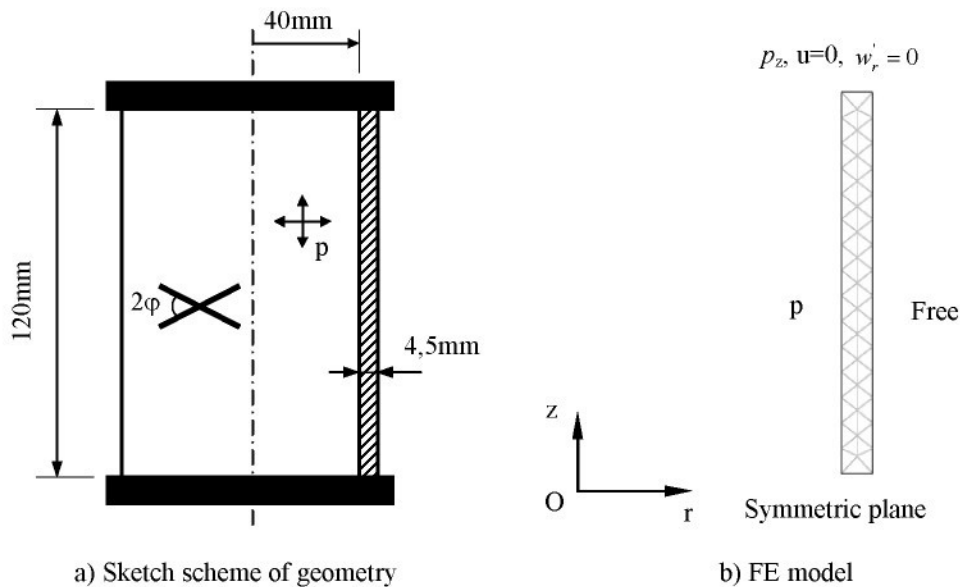


Figure 5.18 – A sketch scheme of geometry and FE model of an air-spring tube subjected an internal static pressure

Since a process of pressure change caused by a volume change inside the tube, which is computed by means of the boundary integration variables referred to section C.6 of Appendix C, is considered to be isothermal obeying the Boyle-Mariotte's law. Hence the internal pressure change corresponding to the volume change is defined by a following expression

$$p_1 V_1 = p_2 V_2 \quad (5.3)$$

We calculate the force acting on the top of the tube from the equilibrium condition in the axial direction

$$P_z = p_s r_i^2 / (r_e^2 - r_i^2) \quad (5.4)$$

where p_s is the pressure inside the tube in the spatial configuration, r_i and r_e are interior and exterior radii of the tube, respectively.

After applying the loading and boundary conditions on the FE model we compute stress-strain responses of the tube reinforced by different fiber angles undergoing a quasi-static pressure, the deformation and Von Mises stress distribution on the tube at an internal pressure by 0,9MPa depending on the fiber angles are illustrated in Figure 5.19. As can see that at the same loading condition the swell of the tube is proportional to the fiber angles.

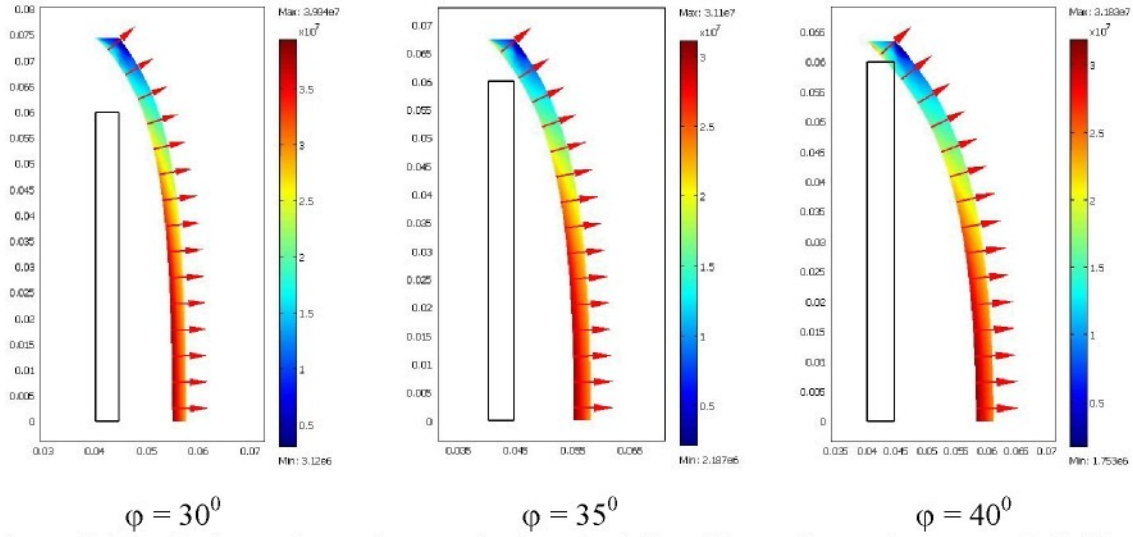


Figure 5.19 – Deformation and stress in the tube inflated by an internal pressure 0,9MPa the angle of fibers (from left to right) $\varphi = 30^\circ$, 35° and 40°

Figure 5.20 shows the deformation and stress distribution in the tube with fiber angle $\varphi = 40^\circ$ at different internal pressures. We can see here a “stretch inversion phenomenon” (in the low pressure domain the tube is shortened during the inflation process).

The “stretch inversion phenomenon” (shortening of the tube when inflated) and the relationship between the internal pressure and the longitudinal stretch are presented in Figure 5.21. We see that if the angle between fibers and the circumferential direction is smaller than $\varphi = 35^\circ$ the tube shortens in the course of inflation. This phenomenon is used in construction of “pneumatic muscles”.

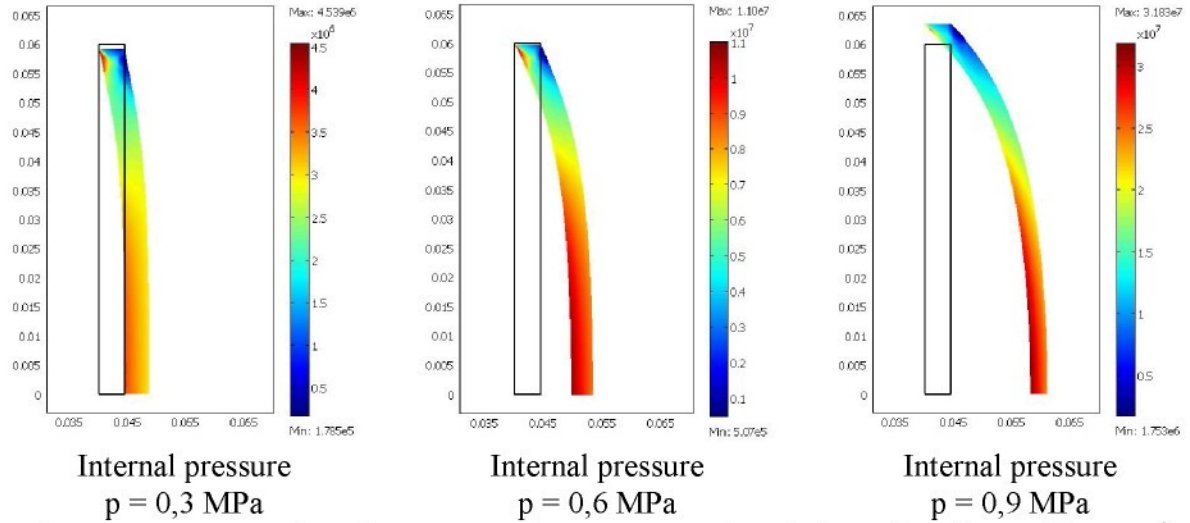


Figure 5.20 – “Inversion phenomenon” happens to a tube reinforced by fibers with $\varphi=40^\circ$

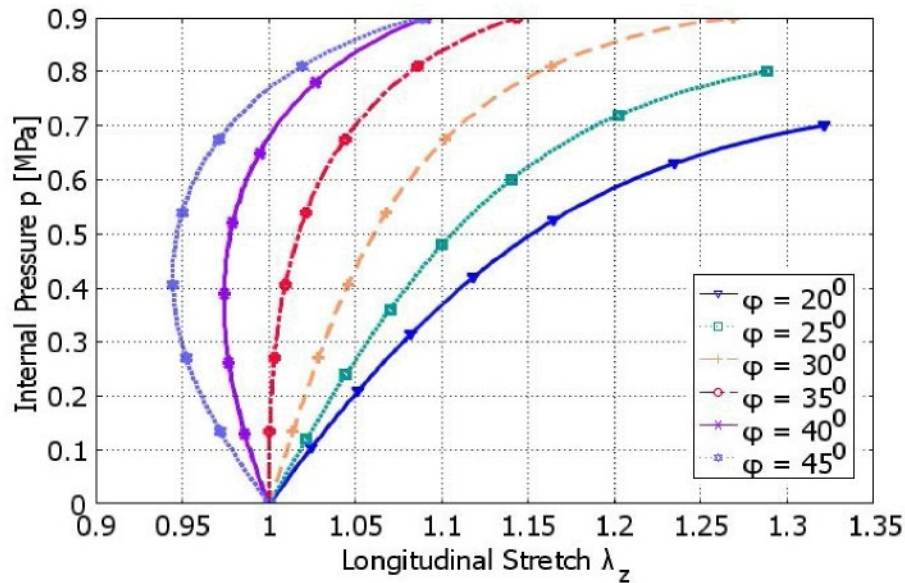


Figure 5.21 – The internal pressure and the longitudinal stretch with different fiber angles

5.4.2. Viscous responses of an air-spring tube

Next we study a viscous behavior of the fiber-reinforced composite tube in a creep process. We assume that the tube inflated by the constant internal pressure 0,9 MPa is subjected additionally to an external force as shown in Figure 5.22. This force is constant for a certain period in course of the creep process.

The deformed shape and the stress of the tube at different time instants in the creep are displayed in Figure 5.23. As observe carefully throughout the creep process we can see that the height of the tube decreases continually while the tube diameter increases.

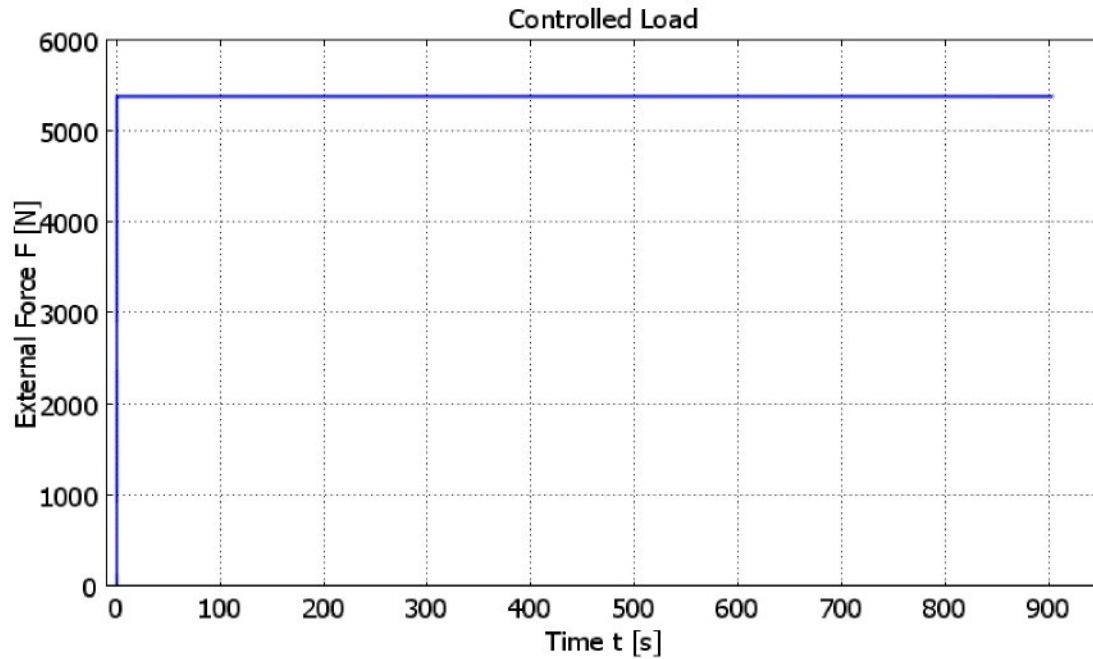


Figure 5.22 – External force acts on the tube in a creep

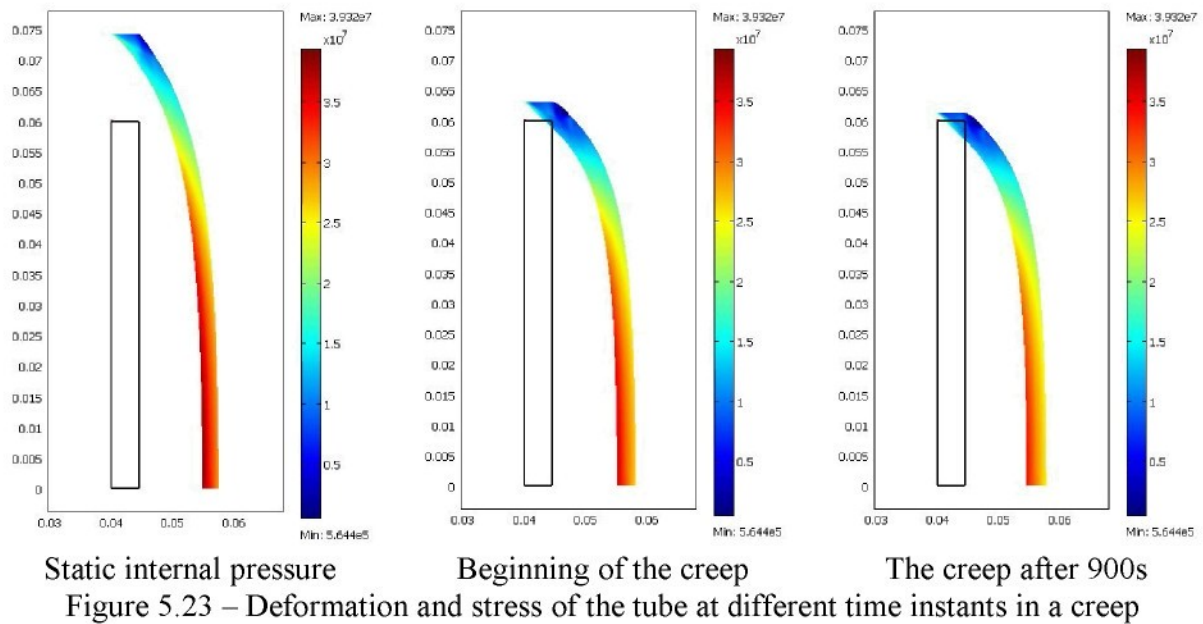


Figure 5.23 – Deformation and stress of the tube at different time instants in a creep

Due to the viscous properties of the material the shape of the tube is changing and this causes a change of internal pressure. Figure 5.24 presents the time dependency of the internal pressure and the displacement of the top of the tube in course of the creep. The internal pressure has been increased by 5% and the top front of spring fell by 1,9 mm which is about 3,2% of the initial length of the tube.

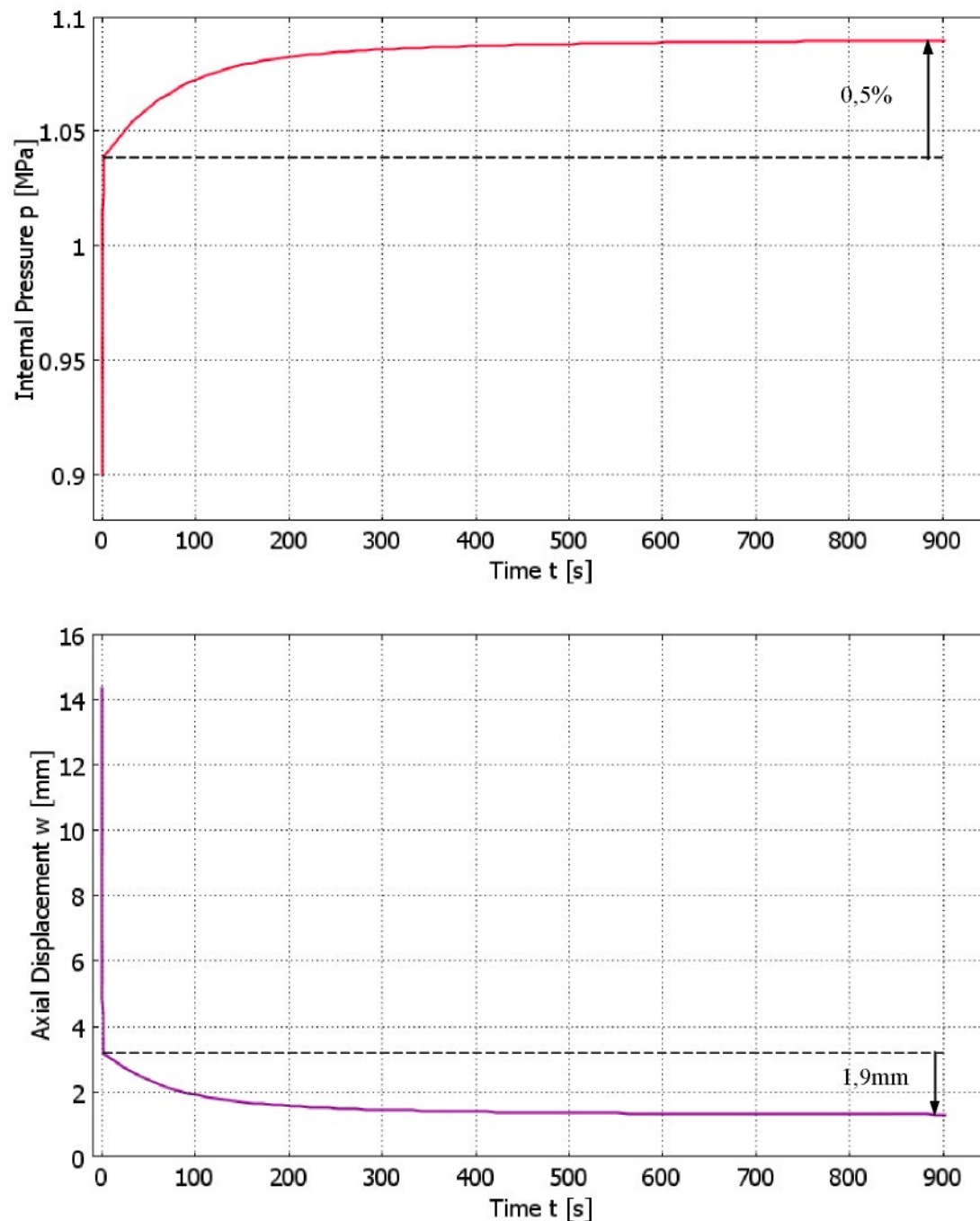


Figure 5.24 – The viscous behavior of the tube in the creep process

5.5. Viscous responses of internal stress-like and strain-like variables

Finally in order to compare two ways of approaches based on internal variables we attempt to implement numerical simulations of viscoelastic fiber-reinforced composites undergoing a simple tensile test by using internal stress-like variables (overstresses) and

internal strain-like variables (inelastic strains). Both of viscous solutions are used two Maxwell elements that represent the viscoelastic response of the (isotropic) matrix and the (anisotropic) fiber phases.

Here the material is considered to be incompressible. The equilibrium components of the free energy function are decomposed separately, specifically volumetric, isotropic and anisotropic parts, refer to Holzapfel & Gasser (2001), given by

$$\Psi_{vol}^{EQ} = -p(J-1) \quad (5.5-a)$$

$$\Psi_{iso}^{EQ} = \frac{\mu_{eq}}{4} \left[(1+\gamma)(\bar{I}_1 - 3) + (1-\gamma)(\bar{I}_2 - 3) \right] \quad (5.5-b)$$

$$\Psi_{ani}^{EQ} = \frac{k_{1eq}}{2k_{2eq}} \left[e^{k_{2eq}(\bar{I}_4 - 1)^2} - 1 \right] + \frac{k_{1eq}}{2k_{2eq}} \left[e^{k_{2eq}(\bar{I}_6 - 1)^2} - 1 \right] \quad (5.5-c)$$

In the first approach the evolution equations (B.32) are solved for the overstress variables representing the viscous characteristics of the matrix and fiber phases. Meanwhile the second approach concerns the evolution equations for inelastic strain variables (B.39) and (B.42) along with the specific non-equilibrium components of the free energy function. Conveniently, the non-equilibrium energy parts are chosen to have the same form of the equilibrium parts, namely as

$$\Psi_{iso}^{NEQ} = \frac{\mu_{neq}}{4} \left[(1+\gamma)(\bar{I}_{M_1}^e - 3) + (1-\gamma)(\bar{I}_{M_2}^e - 3) \right] \quad (5.6-a)$$

$$\Psi_{ani}^{NEQ} = \frac{k_{1neq}}{2k_{2neq}} \left[e^{k_{2neq}(\bar{I}_{F_4}^e - 1)^2} - 1 \right] + \frac{k_{1neq}}{2k_{2neq}} \left[e^{k_{2neq}(\bar{I}_{F_6}^e - 1)^2} - 1 \right] \quad (5.6-b)$$

The material parameters of elastic and viscoelastic are given in Table 5.1.

Table 5.1 – Elastic and viscoelastic material parameters of anisotropic composites

μ_{eq} [MPa]	γ	k_{1eq} [MPa]	k_{2eq}	β_{iso}	τ_{iso} [s]	β_{ani}	τ_{ani} [s]
0,4225	0,6	2	0,5	1	50	1	5

Furthermore, in order to two approaches being equivalent we have relationships between constant material parameters of the equilibrium and non-equilibrium energy parts that $\mu_{neq}/\mu_{eq} = \beta_{iso}$, $k_{1neq}/k_{1eq} = \beta_{ani}$, $k_{2neq} = k_{2eq}$ and $\eta_{M_5} = \tau_{iso}\mu_{neq}$, $\eta_{F_1} = \eta_{F_2} = 4\tau_{ani}k_{1neq}$ (it can be referred to Nguyen et al., 2007).

Both the approaches are applied to study a viscous response of a thin rectangular plate with a reinforcement of two fiber families, its dimensions are $120 \times 50 \times 4,5 \text{ mm}^3$. Hence the deformation response of the plate is considered in a plane stress state. A loading is controlled by three loading steps, in which the controlled loading is held constant within 50s in each step. If the loading is applied by a displacement control, the process will happen under relaxations, inversely the loading control is a force we have creep processes.

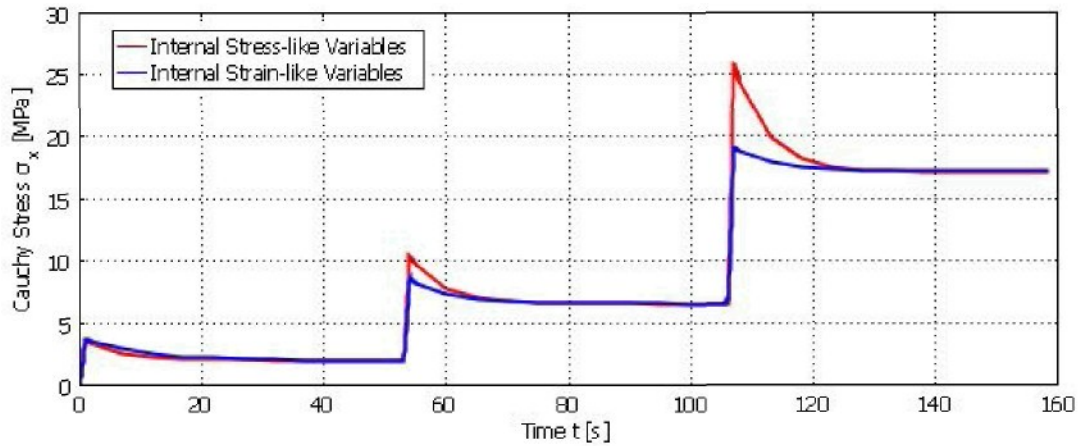


Figure 5.25 – Two approaches for the viscous response of the fiber-reinforced composite in relaxations

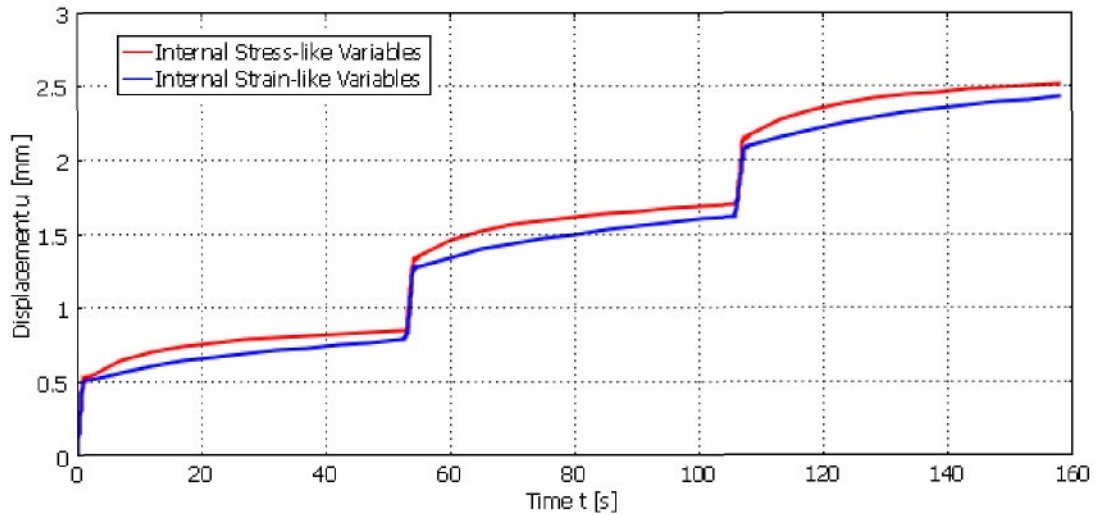


Figure 5.26 – Two approaches for the viscous response of the fiber-reinforced composite in creeps

The viscous responses of the fiber-reinforced composite in relaxations are shown as in Figure 5.25. As a result the equilibrium stresses in two cases are similar, but the distinction of the instant stresses expresses more clearly at a larger deformation. While the viscous responses in creeps with regard to two approaches are nearly similar, it can be observed in Figure 5.26. From observation of experiments in relaxation, for example as can be seen in Figure 4.18, the initial value of the overstress is higher at the larger deformation it seems that the viscoelastic formulation in overstress variables for a relaxation process is more appropriate than in the case for the formulation in inelastic strain variables. However the formulation in overstresses applied to predict the viscoelastic behaviour of the material in a creep process is not exact as we expect, see Figure 5.10, this is coincident the theoretical judgment that this approach is invalid for high strain rates. To resolve this problem the viscoelastic formulation in inelastic strain variable will be considered.

Chapter 6

MAGNETO-SENSITIVE ELASTOMER MATERIALS

Magneto-sensitive elastomers, also called as magneto-rheological elastomers, are smart materials composed of micron-sized ferrous particles dispersed in a polymer matrix. Commonly, magnetic fields are applied to the polymer composite during cross-linking so that chainlike columnar particle structures can be formed and fixed in the matrix after curing. On the contrary in a case of curing without the magnetic field MS materials are obtained to be isotropic. The unique characteristic of MS elastomer is that its shear modulus can be continuously controlled by the external magnetic field (Gong et al., 2005).

The subject of MA thesis (Vlach, 2009) developed recently in our Department has been the design and the implementation of equipment enabling measurement of the response of magnetosensitive elastomers to the mechanical loading in a magnetic field. In this work samples of silicone elastomer with columnar structure of iron particles were made and their magneto-elastic characteristics were measured experimentally.

The constitutive equations of MS elastomers which work in a magnetic field are based on the free energy function depending of two preferred directions parallel with the collums of particles and with the direction of magnetic field respectively (Ottenio et al., 2008; Hoang & Marvalová, 2009). The free energy function depends on invariants which are combinations of the deformation tensor \mathbf{C} , the direction of the collums of particles \mathbf{a}_0 and the vector of magnetic induction \mathbf{B} (see section 6.1.4 of this work) similarly to the modelling of elastomeric composite materials reinforced by families of fibers. In this chapter we employ our experience in the numerical simulation of rubber-like composites considering the experimental findings of Vlach (2009) to develop numerical methods of solution of simple problems of nonlinear magnetoelasticity. We present numerical simulations of the nonlinear coupling between magnetic and mechanical effects which were performed in Comsol Multiphysics.

Our approach is based on the general theory of nonlinear magnetoelasticity incorporated with the theory of fiber-reinforced composites (more details see Kovetz, 2000 and Holzapfel, 2000).

We adopt the formulation of Dorfmann & Ogden (2003-2005) as the starting point. First the relevant magnetic and mechanical balance equations and boundary conditions are summarized. Then the general formulation of constitutive equations for anisotropic magnetoelastic interactions are based on Dorfmann & Ogden (2005) for both compressible and incompressible magnetoelastic materials and then specialized for specific application to incompressible isotropic and anisotropic magnetoelastic materials.

Finally some FEM solutions are implemented in Comsol Multiphysics to illustrate a coupling of the magnetoelastic materials and the external uniform magnetic field. The constitutive equations are based on a modified free-energy function that depends, in addition to the deformation gradient, on the magnetic flux density vector as the independent magnetic variable.

6.1. Governing equations

The balance equations for nonlinear magnetoelastic elastomers in a static magnetic field, as developed generally by Bridgdnov & Dorfmann (2003), Dorfmann & Ogden (2003-2005), are summarized concisely in this section.

6.1.1. Magnetic equations

In the Eulerian description, Maxwell's equations for magnetic induction \mathbf{B} and magnetic field \mathbf{H} vectors in the absence of time dependence, free charges and free currents reduce to

$$\text{div}\mathbf{B} = 0, \quad \text{curl}\mathbf{H} = \mathbf{0} \quad (6.1)$$

which hold both inside and outside a magnetic material (for example, Kovetz, 2000; Bridgdnov & Dorfmann, 2003), where *div* and *curl* relate to the spatial configuration.

Thus, \mathbf{B} and \mathbf{H} can be regarded as fundamental field variables. In the vacuum, we have a basic relation between \mathbf{B} and \mathbf{H} as

$$\mathbf{B} = \mu_0 \mathbf{H} \quad (6.2)$$

where $\mu_0 = 4\pi \times 10^{-7}$ is a universal constant.

Associated with the equations (6.2) are the boundary continuity conditions

$$[\mathbf{B}] \cdot \mathbf{n} = 0, \quad [\mathbf{H}] \times \mathbf{n} = \mathbf{0} \quad (6.3)$$

where $[\bullet]$ signifies a discontinuity across the boundary and \mathbf{n} is its outward unit normal.

Lagrangian counterparts of \mathbf{B} and \mathbf{H} , denoted \mathbf{B}_I and \mathbf{H}_I , respectively, are only considered in material domains to be given by (for example Dorfmann & Ogden, 2005)

$$\mathbf{B}_I = J\mathbf{F}^{-1}\mathbf{B}, \quad \mathbf{H}_I = \mathbf{F}^T \mathbf{H} \quad (6.4)$$

where the superscript T denotes the transpose of a tensor.

And these quantities equations (6.1) become

$$\text{Div}\mathbf{B}_I = 0, \quad \text{Curl}\mathbf{H}_I = \mathbf{0} \quad (6.5)$$

where *Div* and *Curl* are 'div' and 'curl' operators relative to the reference configuration respectively.

The boundary conditions (6.3) can also be expressed in Lagrangian form

$$(\mathbf{B}_I - J\mathbf{F}^{-1}\mathbf{B}_0) \cdot \mathbf{N} = 0, \quad (\mathbf{H}_I - \mathbf{F}^T \mathbf{H}_0) \times \mathbf{N} = \mathbf{0} \quad (6.6)$$

in which \mathbf{B}_0 and \mathbf{H}_0 are the corresponding fields exterior to the material, but evaluated on the boundary in the reference configuration.

6.1.2. Mechanical equations

The conservation of mass equation is written simply as

$$\rho_0 = J\rho \quad (6.7)$$

where J is a volume ratio, $J = \det \mathbf{F}$ and \mathbf{F} is the deformation gradient of the MS body.

The influence of the magnetic field on the mechanical stress in the deforming body may be incorporated through magnetic body forces or through a magnetic stress tensor (see Dorfmann & Ogden, 2005). Herein, we use the latter approach and denote the resulting total Cauchy stress tensor by $\boldsymbol{\tau}$, which has the advantage of being symmetric. In case the absence of mechanical body forces, the equilibrium equation for a magnetoelastic solid in Eulerian configuration has the form

$$\text{div} \boldsymbol{\tau} = \mathbf{0} \quad (6.8)$$

By using the total nominal stress tensor, here denoted \mathbf{T} , which is related to $\boldsymbol{\tau}$ by

$$\mathbf{T} = J\mathbf{F}^{-1}\boldsymbol{\tau} \quad (6.9)$$

then the equilibrium equation (6.8) may be expressed in Lagrangian form as

$$\text{Div} \mathbf{T} = \mathbf{0} \quad (6.10)$$

The boundary condition involving the stress $\boldsymbol{\tau}$, where traction rather than displacement is specified, may be written in the form

$$[\boldsymbol{\tau}]\mathbf{n} = \mathbf{0} \quad (6.11)$$

and it can be noted that the traction $\boldsymbol{\tau}\mathbf{n}$ on the outer boundary includes a contribution from the (symmetric) Maxwell stress outside the material as well as any mechanical traction applied to the surface of the body.

According to Dorfmann & Ogden (2005) as well as Bustamante et al. (2007) that the Maxwell stress outside the material, denoted $\boldsymbol{\tau}_M$, is given by

$$\boldsymbol{\tau}_M = \mathbf{H}^* \otimes \mathbf{B}^* - \frac{1}{2}(\mathbf{H}^* \cdot \mathbf{B}^*)\mathbf{I} \quad (6.12)$$

where \mathbf{I} is the identity tensor and \mathbf{B}^* and \mathbf{H}^* are the corresponding fields exterior to the material evaluated on the boundary in the Lagrangian configuration, of cause $\mathbf{B}^* = \mu_0 \mathbf{H}^*$.

6.1.3. Constitutive equations

For characterize isothermal deformations of MS materials we postulate the existence of a Helmholtz free energy function Ψ . According to Dorfmann & Ogden (2005) for isotropic MS materials the free energy function depends on a deformation gradient tensor \mathbf{F} and on a

magnetic induction \mathbf{B}_l , denoted in the Lagrangian configuration. On the other hand for MS anisotropic MS materials the free energy function additionally depends on a preferred direction of ferrous particles signified by \mathbf{a}_0 . Thus the total free energy function is expressed as

$$\Psi = \Psi(\mathbf{F}, \mathbf{B}_l) \quad \text{or} \quad \Psi = \Psi(\mathbf{F}, \mathbf{a}_0, \mathbf{B}_l) \quad (6.13)$$

From Clausius–Duhem inequality for electro-magnetic media, see Brigadnov & Dorfmann (2003), we can analogously derive constitutive equations which are obtained by differentiation of Ψ with respect to \mathbf{F} and \mathbf{B}_l . The total nominal stress tensor \mathbf{T} and the magnetic field \mathbf{H}_l are given by the simple formulas

$$\mathbf{T} = \frac{\partial \Psi}{\partial \mathbf{F}}, \quad \mathbf{H}_l = \frac{\partial \Psi}{\partial \mathbf{B}_l} \quad (6.14)$$

and for an incompressible material by

$$\mathbf{T} = \frac{\partial \Psi}{\partial \mathbf{F}} - p\mathbf{F}^{-1}, \quad \mathbf{H}_l = \frac{\partial \Psi}{\partial \mathbf{B}_l} \quad (6.15)$$

where p is a Lagrange multiplier associated with the constraint $\det \mathbf{F} = 1$.

The corresponding Eulerian quantities are given by

$$\boldsymbol{\tau} = J^{-1}\mathbf{F} \frac{\partial \Psi}{\partial \mathbf{F}}, \quad \mathbf{H} = \mathbf{F}^{-T} \frac{\partial \Psi}{\partial \mathbf{B}_l} \quad (6.16)$$

and

$$\boldsymbol{\tau} = \mathbf{F} \frac{\partial \Psi}{\partial \mathbf{F}} - p\mathbf{I}, \quad \mathbf{H} = \mathbf{F}^{-T} \frac{\partial \Psi}{\partial \mathbf{B}_l} \quad (6.17)$$

where \mathbf{I} is again the identity tensor.

6.1.4. The free energy function in terms of invariants

For isotropic magnetoelastic materials the material symmetry is similar to that associated with a transversely isotropic elastic material, for which there is a preferred direction in the reference configuration analogous to \mathbf{B}_l . However \mathbf{B}_l is not a unit vector so the theory involves more one invariant than the case for transverse isotropy. Then the free energy function depends on 6 invariants of \mathbf{C} and \mathbf{B}_l , refer to Brigadnov & Dorfmann (2003), Dorfmann & Ogden (2005), in which the invariants are given by

$$\begin{aligned} I_1(\mathbf{C}) &= \text{tr}(\mathbf{C}), & I_2(\mathbf{C}) &= \frac{1}{2}[(\text{tr} \mathbf{C})^2 - \text{tr} \mathbf{C}^2] \\ I_3(\mathbf{C}) &= \det \mathbf{C} = J^2, & I_4(\mathbf{B}_l) &= \mathbf{B}_l \cdot \mathbf{B}_l \\ I_5(\mathbf{C}, \mathbf{B}_l) &= \mathbf{B}_l \cdot \mathbf{C} \mathbf{B}_l, & I_6(\mathbf{C}, \mathbf{B}_l) &= \mathbf{B}_l \cdot \mathbf{C}^2 \mathbf{B}_l \end{aligned} \quad (6.18)$$

Analogously, MS anisotropic elastomers with one preferred direction undergoing an applied magnetic field is similar to composite materials reinforced by two fiber families (more details refer to Holzapfel, 2000), hence the free energy function has to depend on 10 invariants of \mathbf{C} , \mathbf{a}_0 and \mathbf{B}_l , where \mathbf{a}_0 is the direction of the rectified particles. The six invariants I_1, \dots, I_6

are identical to those from the isotropic MS material presented in equation (6.16) and the remaining invariants are defined as follows

$$\begin{aligned} I_7(\mathbf{C}, \mathbf{a}_0) &= \mathbf{a}_0 \cdot \mathbf{C} \mathbf{a}_0, & I_8(\mathbf{C}, \mathbf{a}_0) &= \mathbf{a}_0 \cdot \mathbf{C}^2 \mathbf{a}_0 \\ I_9(\mathbf{C}, \mathbf{a}_0, \mathbf{B}_l) &= (\mathbf{a}_0 \cdot \mathbf{B}_l) \mathbf{a}_0 \cdot \mathbf{C} \mathbf{B}_l, & I_{10}(\mathbf{a}_0, \mathbf{B}_l) &= (\mathbf{a}_0 \cdot \mathbf{B}_l)^2 \end{aligned} \quad (6.19)$$

Since the invariant I_{10} does not depend on the deformation therefore only the nine invariants I_1, \dots, I_9 remain for MS anisotropic materials.

We postulate the decomposition of the free energy function into volumetric, isotropic and anisotropic parts that can be written as

$$\Psi = \Psi_{vol}(J) + \Psi_{iso}(\bar{I}_1, \bar{I}_2) + \Psi_{ani}(I_4, \bar{I}_5, \bar{I}_6) \quad (6.20a)$$

$$\text{or} \quad \Psi = \Psi_{vol}(J) + \Psi_{iso}(\bar{I}_1, \bar{I}_2) + \Psi_{ani}(I_4, \bar{I}_5, \bar{I}_6, \bar{I}_7, \bar{I}_8, \bar{I}_9) \quad (6.20b)$$

where $\bar{I}_1, \dots, \bar{I}_9$ are modified invariants and given by

$$\begin{aligned} \bar{I}_a &= J^{-2/3} I_a \quad (a = 1, 5, 7, 9) \\ \bar{I}_a &= J^{-4/3} I_a \quad (a = 2, 6, 8) \end{aligned} \quad (6.21)$$

For incompressible MS elastomers the volumetric component of the free energy function is chosen in the form

$$\Psi_{vol} = -p(J-1) \quad (6.22)$$

where p is the hydrostatic pressure.

In order to simulate behaviors of the incompressible magnetoelastic elastomer, we refer and inherit a simple form of the free energy function as proposed in Dorfmann's paper (2005). The isotropic and anisotropic contributions of the free energy function are used as follows

$$\Psi_{iso} = \frac{G}{4} \left[(1+\gamma)(\bar{I}_1 - 3) + (1-\gamma)(\bar{I}_2 - 3) \right] \quad (6.23)$$

$$\Psi_{ani} = \frac{1}{\mu_0} (\alpha I_4 + \beta \bar{I}_5) \quad (6.24a)$$

$$\text{or} \quad \Psi_{ani} = \frac{1}{\mu_0} (\alpha I_4 + \beta \bar{I}_5) + \frac{k}{2} (\bar{I}_7 - 1)^2 \quad (6.24b)$$

here we assume that $G = G_0(1 + \eta_G I_4)$ is the shear modulus in the reference configuration, G_0 is the field independent shear modulus (or zero-field modulus) and $k = k_0(1 + \eta_k I_4)$ represents the anisotropic characteristic of MS elastomers. The material parameters α , β and γ are non-dimensional material constants and η_G and η_k are material constants involving the magnetic strength, these parameters need to be determined by coupling magnetic and mechanical experiments.

6.2. Numerical simulations of MS elastomers

To implement the coupled interaction of magnetic field and mechanical material we claim that the magnetic field is solved in the spatial coordinates and the deformation response is computed in the reference coordinates. We also suppose that the external boundary of the surrounding space (vacuum) is far away from the boundary of the MS elastomer body, hence the remote magnetic field is homogeneous.

The influence of the magnetic field on the surface of magnetoelastic body is expressed via the corresponding boundary tractions in the material coordinates and defined as follow (see more Otténio, 2008)

$$\mathbf{T}_a = J\mathbf{F}^{-1}\boldsymbol{\tau}_M\mathbf{N} \quad (6.25)$$

where $\boldsymbol{\tau}_M$ is the Maxwell stress defined by equation (6.12), and \mathbf{N} is a unit outer normal vector on the boundary of the undeformed body.

The stress and strain response of the body is calculated undergoing both magnetic and external forces, the displacement components are passed simultaneously into the magnetic solution by means of an advance technique as the Moving Mesh mode so that the magnetic field domain is changed in compliance with the large deformation of body. Therefore we can investigate the effect of the magnetic field to the magnetoelastic materials during the mechanical loading or vice versa.

6.2.1. FEM solutions of MS isotropic materials

In the following simulations we assume that the MS isotropic elastomer is described by the strain-energy function (6.20a) with contributions given by equations (6.22), (6.23) and (6.24a). The magnetic field inside the material is defined from the strain-energy function by equation (6.17)₂ and by using equation (6.2) for linear homogeneous magnetoelastic material and interconnected to the outer magnetic field through the jump conditions (6.3). The total nominal stress tensor (6.15) in the material is calculated by differentiation of the strain-energy function with respect to \mathbf{F} and satisfies the boundary conditions with the prescribed displacements or the tractions comprising both applied and magnetic forces. All the constitutive relations have been implemented into Comsol Multiphysics FE code.

Some plane strain and axisymmetric problems, namely a plane strain compression of block, a simple shear strain of a plate and a pure shear deformation of a tube, will be investigated in a static magnetic field with an uniform magnetic induction field \mathbf{B} which changes from 0 to 1T while the mechanical loading (displacements or tractions) is held. The material parameters are chosen and bring out specifically in each below part.

6.2.1.1. A plane strain compression of isotropic material block

In order to illustrate an influence of the magnetic field direction to a magnetic material we consider a compressed block in plain strain with a uniform static magnetic field applied subsequently in horizontal and vertical directions. The block has dimensions $20 \times 20 \text{ cm}$ and is compressed by a constant displacement $u_0 = 3 \text{ cm}$ in y- direction (Figure 6.1). Material parameters are chosen as

$$G_0 = 0,4 \text{ MPa}; c_1 = 1,6; c_2 = 0,4$$

$$\alpha = 0,1; \beta = 0,2; \eta_G = 0,9$$

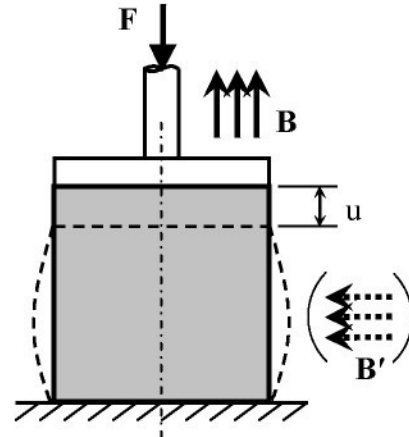


Figure 6.1 – Compression of a block

In Figure 6.2 and Figure 6.3 the deformation shape and the distribution of total stress are displayed in the horizontal magnetic field and in the vertical magnetic field. The magnitude and direction of the magnetic field affect strongly the magnitude of the compressive force necessary to keep the block displacement constant. Figure 6.4 implies that the magnetic direction parallel to the direction of the applied load causes a sharper increase of stiffness.

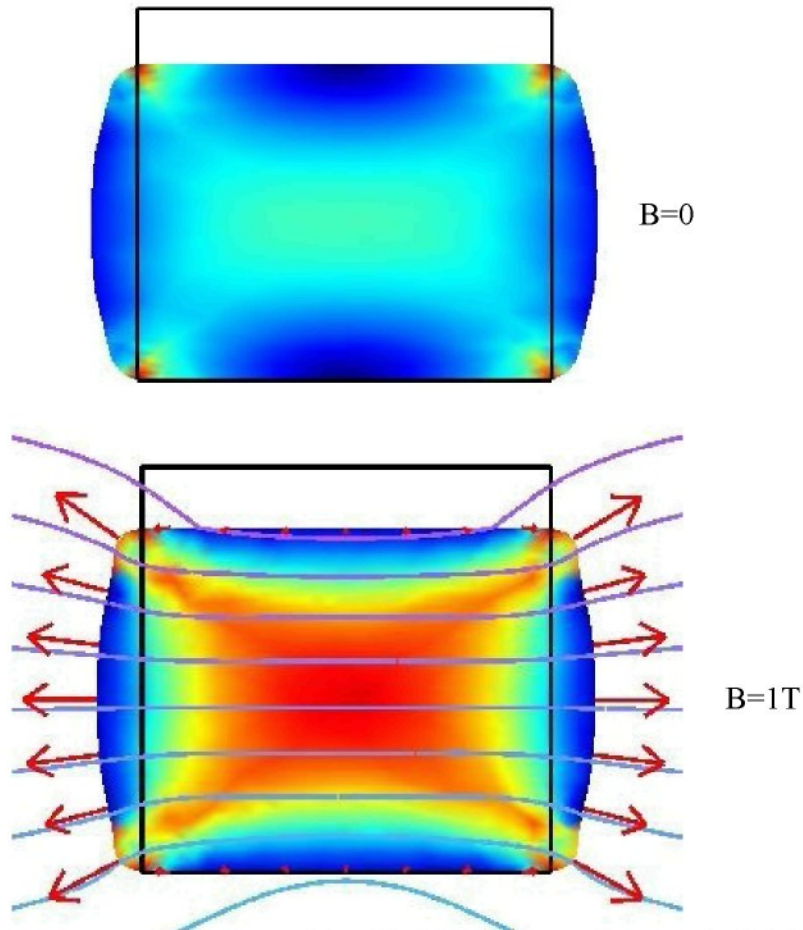


Figure 6.2 – Deformation of the block in horizontal magnetic field

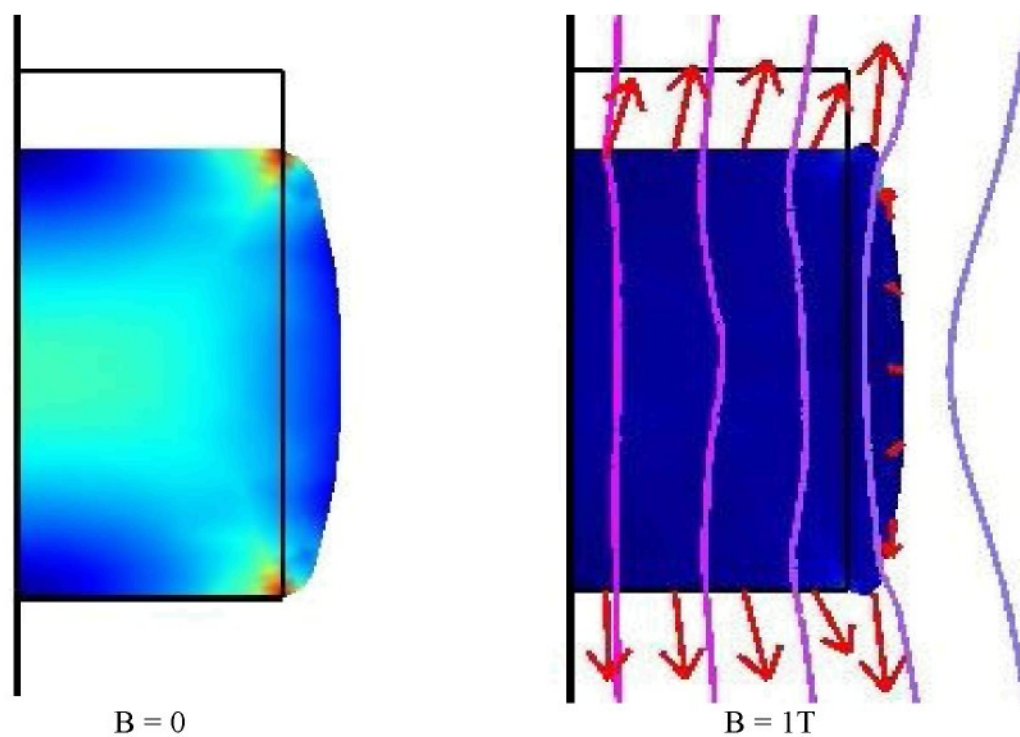


Figure 6.3 – Deformation of the block in vertical magnetic field

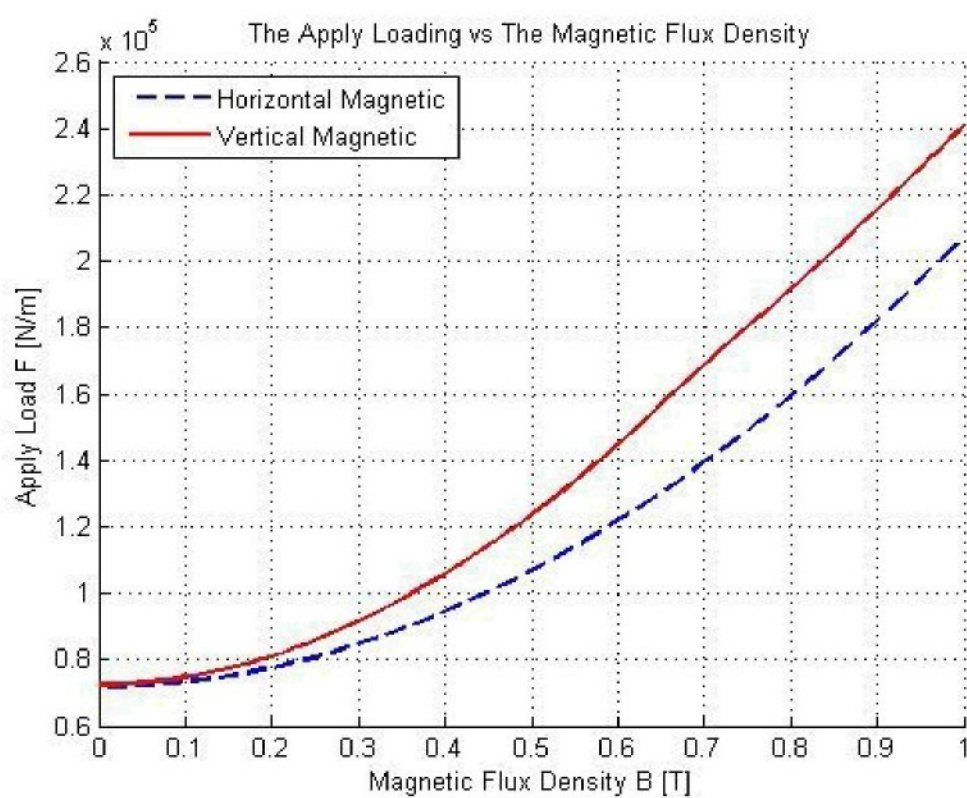


Figure 6.4 – Loading depends on direction and magnitude of magnetic field

6.2.1.2. A simple shear strain of isotropic material plate

A plate of uniform thickness subjected to a unidirectional quasi-static shear deformation along the x-direction (as shown in Figure 6.5). The magnitude of the shear stress applied at the top surface boundary comes up to $\tau_0 = 0,2G_0$, where G_0 is a shear modulus of the plate in the absence of magnetic field. The uniform vertical magnetic induction field \mathbf{B} acts across the plate.

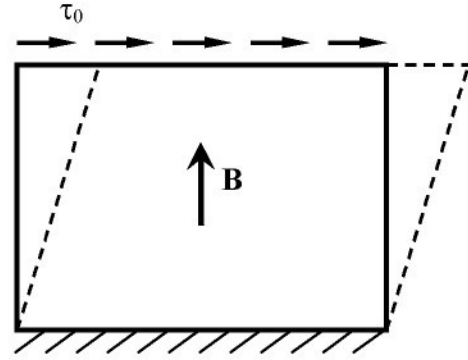


Figure 6.5 – A geometric model to applied simple shear

The material parameters are $G_0 = 0,25\text{MPa}$; $c_1 = 1,6$; $c_2 = 0,4$; $\alpha = 0,1$; $\beta = 0,2$; $\eta_G = 0,9$

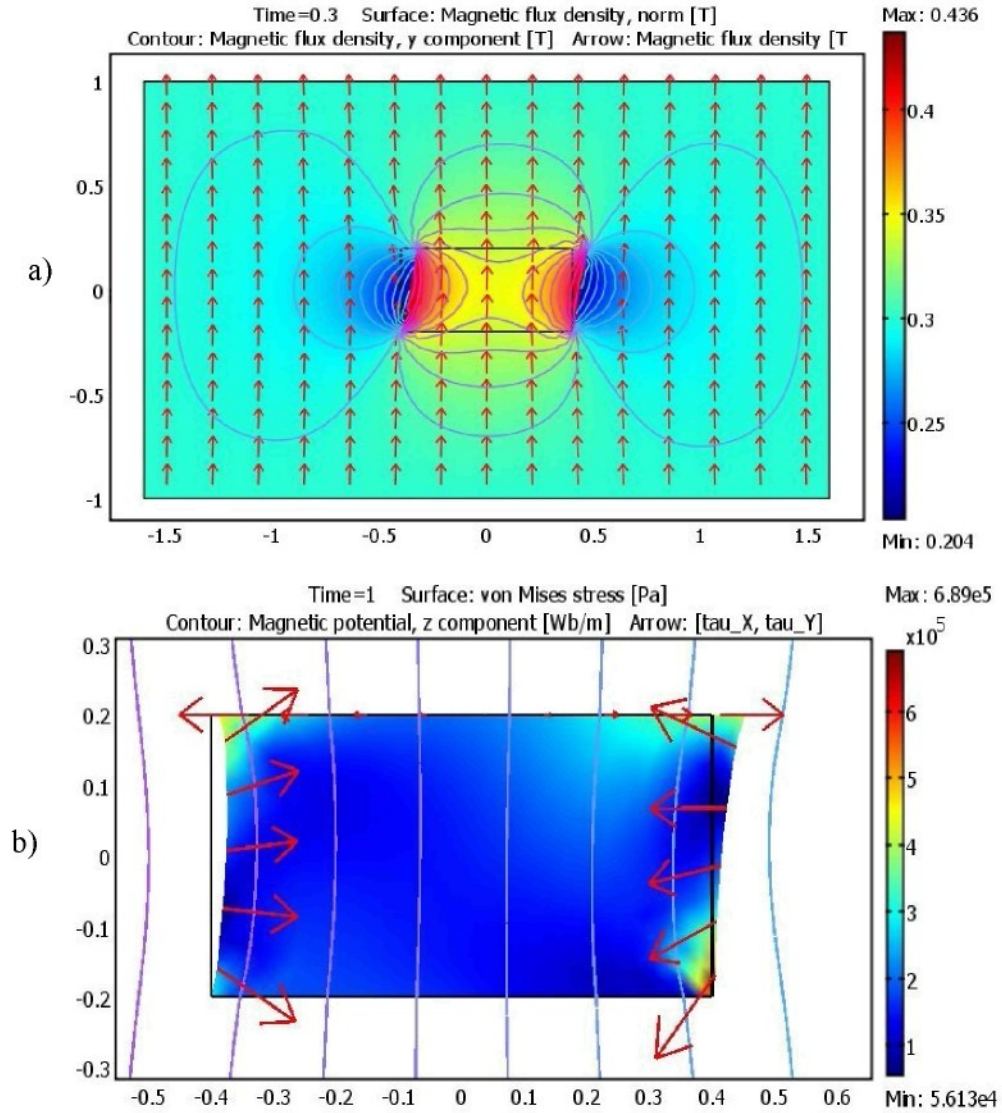


Figure 6.6 – MS block in simple shear: a) Distribution of magnetic field, b) Magnetic traction and Von Mises stress

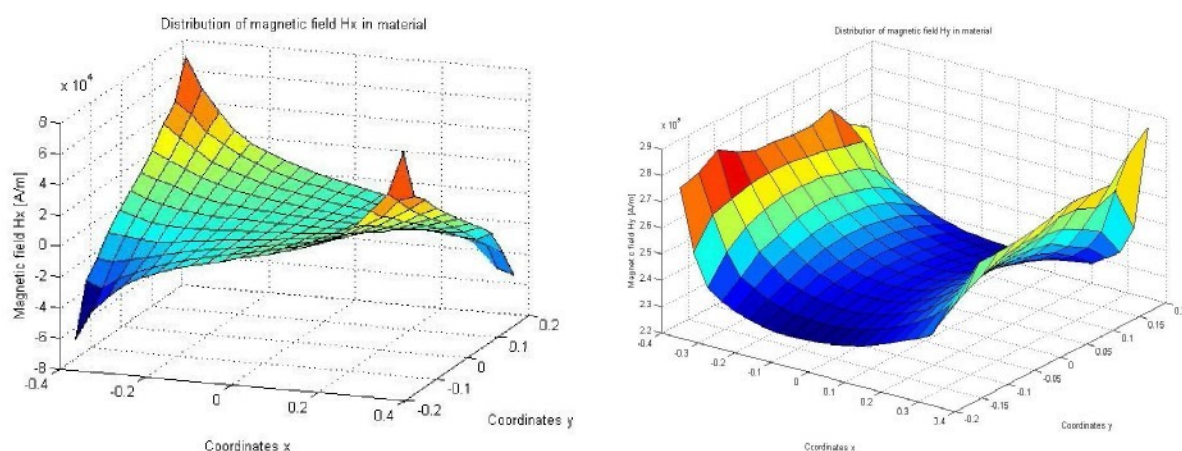


Figure 6.7 – Variation of magnetic fields H_x , H_y in the deformation body

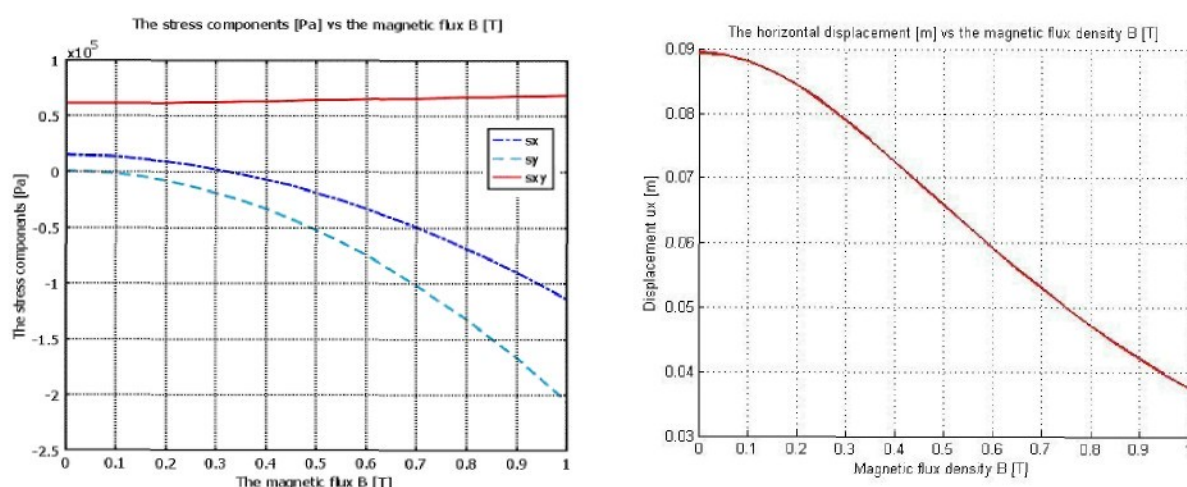


Figure 6.8 – Dependency of stress components and displacement on magnetic field

Figure 6.6 depicts a distribution of magnetic field inside and outside the body and the Von Mises stress due to the application of the horizontal displacement at the top and simultaneous action of a uniform and stationary magnetic field. Owing to the great displacement of the boundary induced by the mechanical load the distribution of magnetic field is not symmetric.

The variation of magnetic fields inside the material is shown in Figure 6.7. The field component H_x perpendicular to the direction of the applied field is antisymmetric and the magnetic field strongly varies close to the body edges.

The dependency of the stress components and the displacement on the applied magnetic field are presented in Figure 6.8. The field affects strongly the increasing normal stresses s_x and s_y , while the component of shear stress is nearly unchanged.

6.2.1.3. A pure shear deformation of isotropic material tube

In this example we consider a thick tube subjected to an axial force and an axial magnetic field. The magnetic far field is assumed to be axial and uniform (Figure 6.9). The linear homogeneous MS elastomer is adopted. The dependence of applied force and displacement on the magnetic quantity \mathbf{B} was determined.

The material parameters are given as following

$$G_0 = 0,4 \text{ MPa}; c_1 = 1,6; c_2 = 0,4$$

$$\mu_r = 2; \alpha = 0,1; \beta = 0,2; \eta_G = 0,9$$

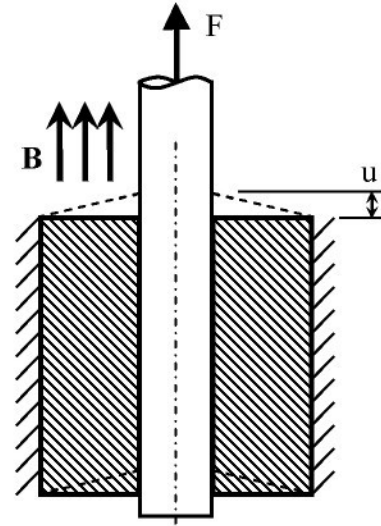


Figure 6.9 – Geometry of the tube

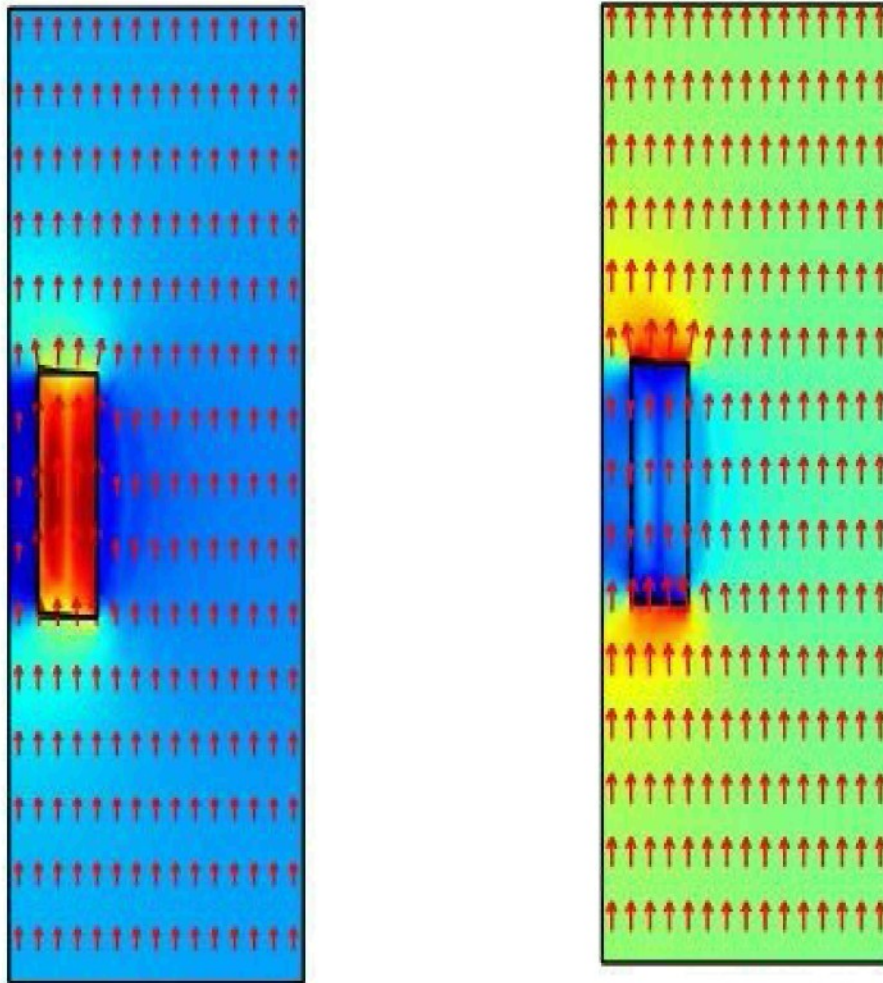


Figure 6.10 – Magnetic flux density (left), magnetic field (right)

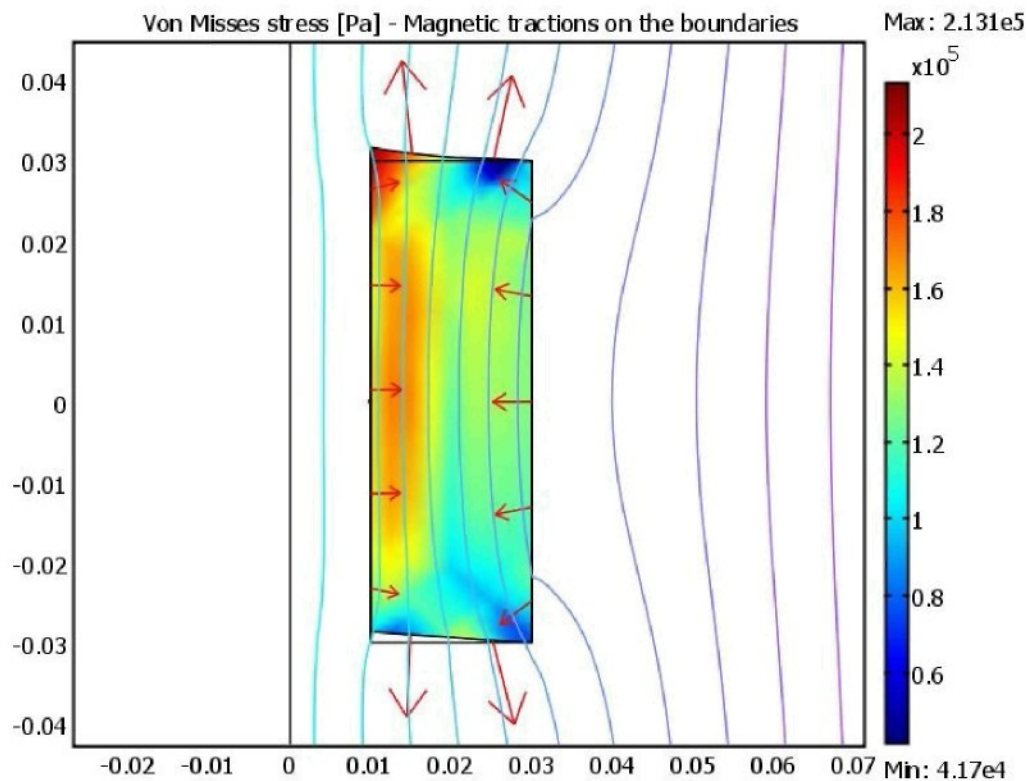


Figure 6.11 – Magnetic traction and Von Misses stress

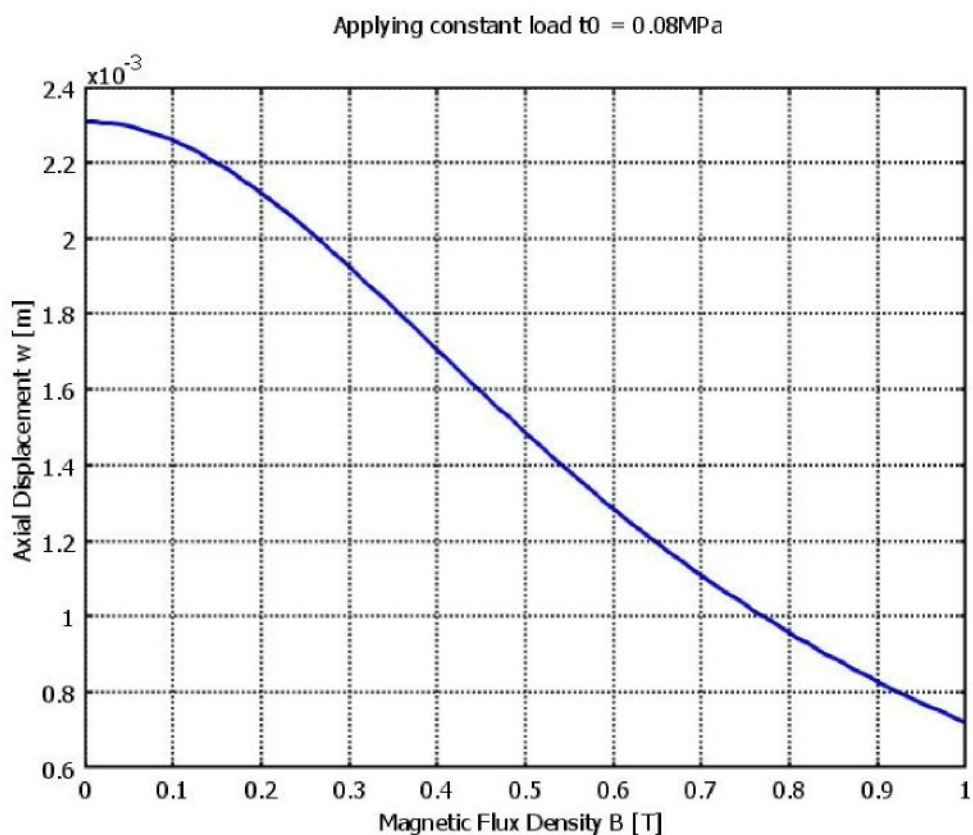


Figure 6.12 – Displacement depends on magnetic when loading is constant

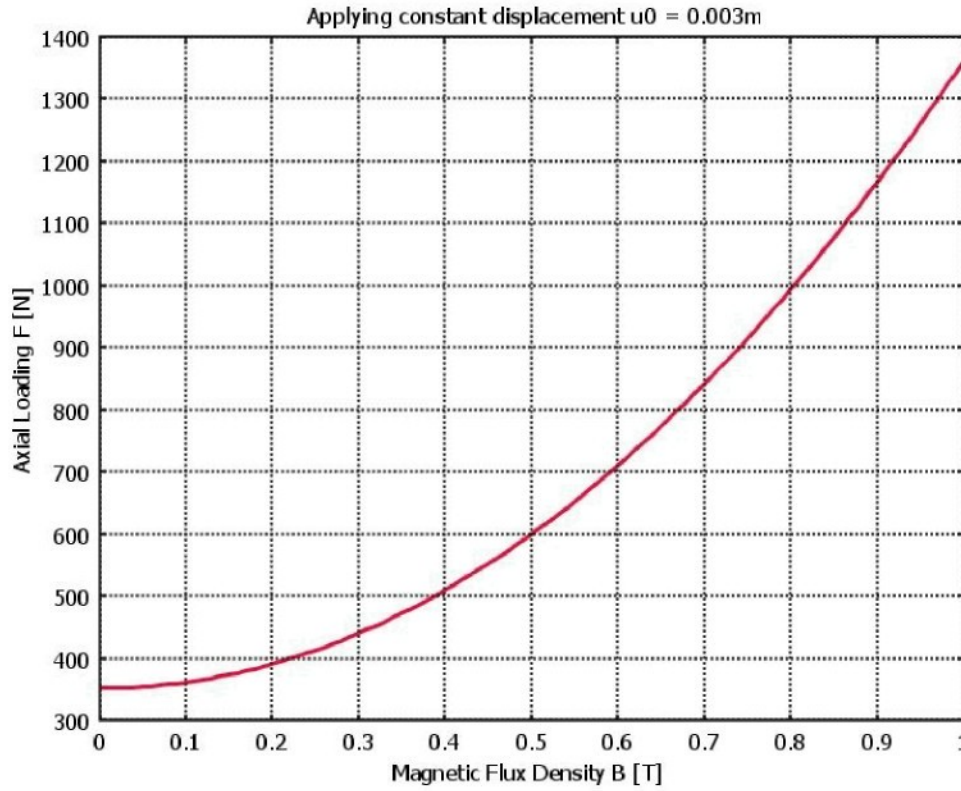


Figure 6.13 – Loading depends on magnetic when applied displacement is constant

The obtained results of axisymmetric problem in Figures 6.10, 6.11, 6.12 and 6.13 are in accordance with the results of Bustamante et al. (2007). The magnetic field changes strongly the material properties of magnetoelastic composites especially when its direction coincides with the direction of applied mechanical loadings.

6.2.2. FEM solutions of MS anisotropic materials

In order to simulate behaviors of incompressible MS anisotropic elastomers, we choose the free energy function defined by equations (6.20b) with contributions given by equations (6.22), (6.23) and (6.24b).

To illustrate the interaction of the MS anisotropic elastomers and the magnetic field we use material parameters as listed in Table 6.1 for all following FEM examples.

Table 6.1 – Material parameters of an MS anisotropic composite

G_0 [MPa]	η_G [T ⁻²]	k_0 [MPa]	η_k [T ⁻²]
1,8	0,6	5,0	0,9
α [-]	β [-]	γ [-]	
0,05	0,1	0,6	

6.2.2.1. Compression of anisotropic material block

First we consider an MS anisotropic block with different aligned directions of ferrous particle chains embedded in a static uniform magnetic field parallel to its axis and simultaneously subjected a compressive load as a constant pressure $p_0=1\text{MPa}$. A scheme sketch of the MS anisotropic block together with an applied magnetic field is depicted in Figure 6.14.

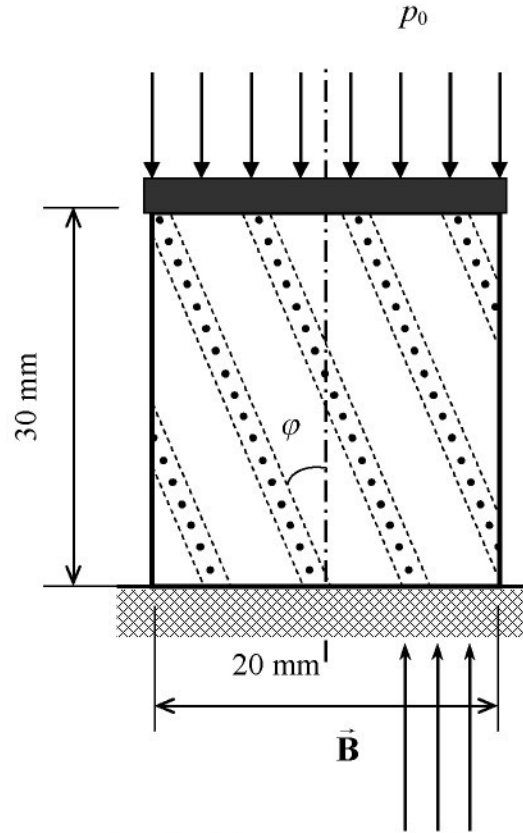
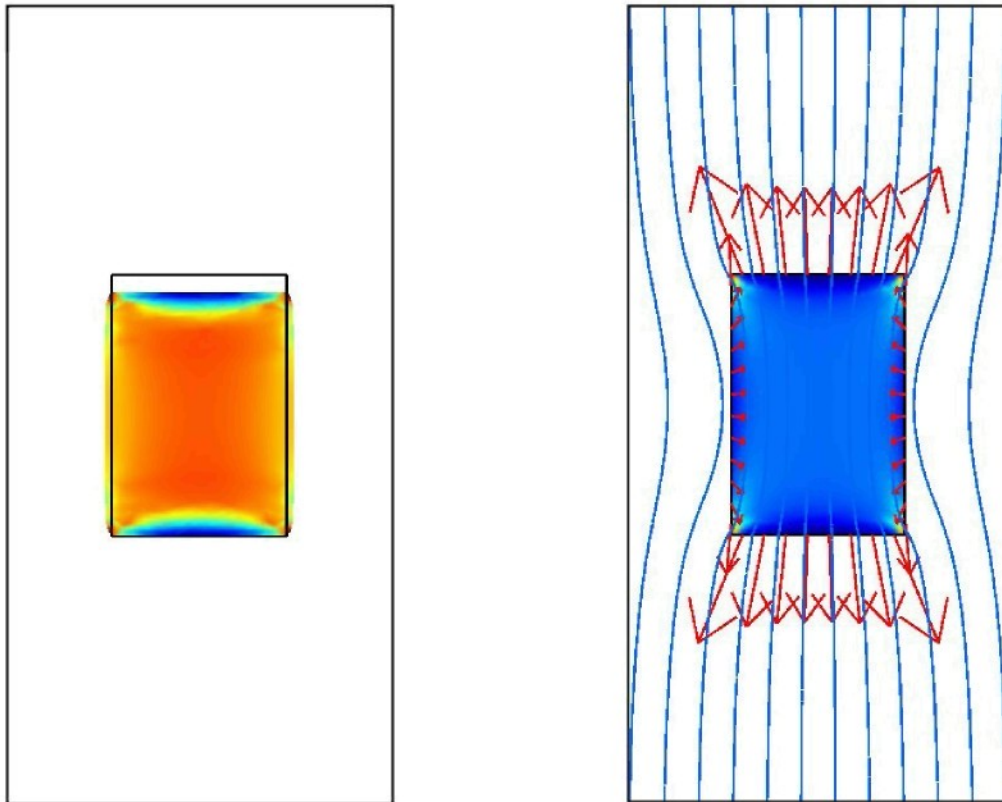
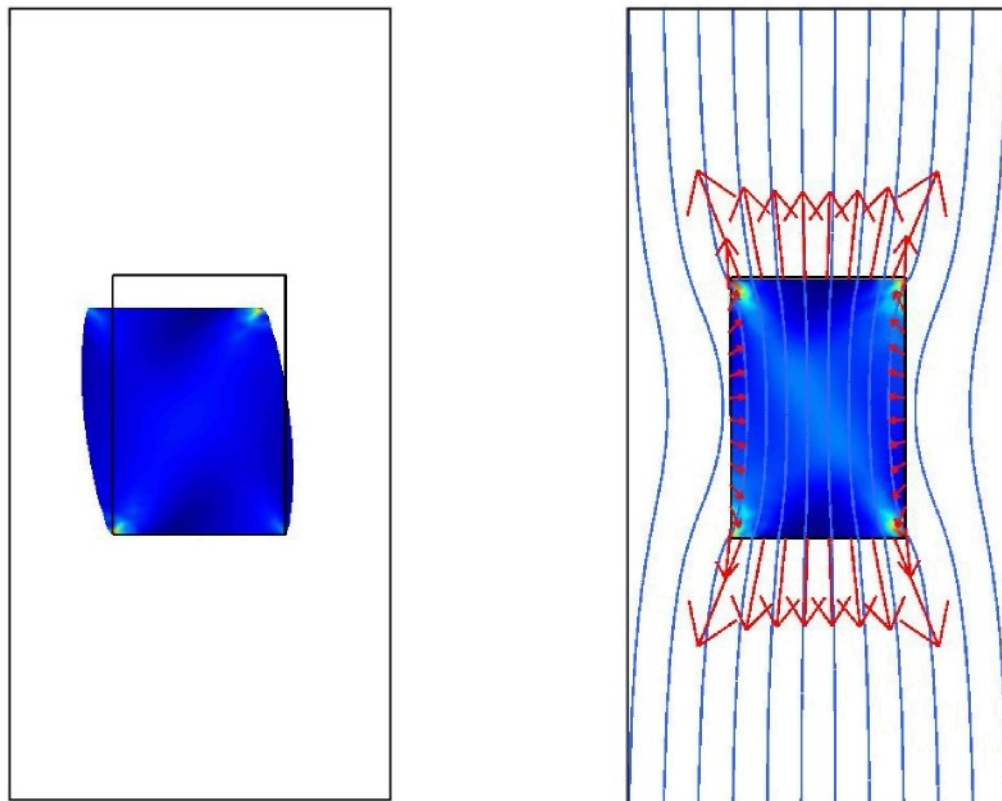


Figure 6.14 – A scheme sketch of the compressive block in a magnetic field

We have obtained series of stress and strain responses of the block as well as the distribution of the magnetic field interior and exterior domains of the MS anisotropic material. In Figure 6.15 illustrates some achieved results of deformations and equivalent stress distributions corresponding to ferrous particle orientations by 0° and 30° without and with the magnetic field applied by $B=1\text{T}$, moreover the direction of the magnetic traction vectors implies the body tends to lengthen along the direction of the applied field. In Figure 6.16 we try to represent a distribution of the magnetic field and a magnetization of the body with the chain orientation by 30° and the magnetic flux density at that time as $0,5\text{T}$, it can be seen that owing to the change of the domains induced by the deformation of the block the distribution of magnetic field does not remain to be symmetric and a strong dependency of the magnetic field on the deformation of the material is still denoted by the distribution of the magnetization inside the material.



a) Orientation of particle chains: $\varphi = 0^\circ$ at $B = 0\text{T}$ and $B = 1\text{T}$



b) Orientation of particle chains: $\varphi = 30^\circ$ at $B = 0\text{T}$ and $B = 1\text{T}$

Figure 6.15 – Deformation of the MS anisotropic block without and with a uniform magnetic field

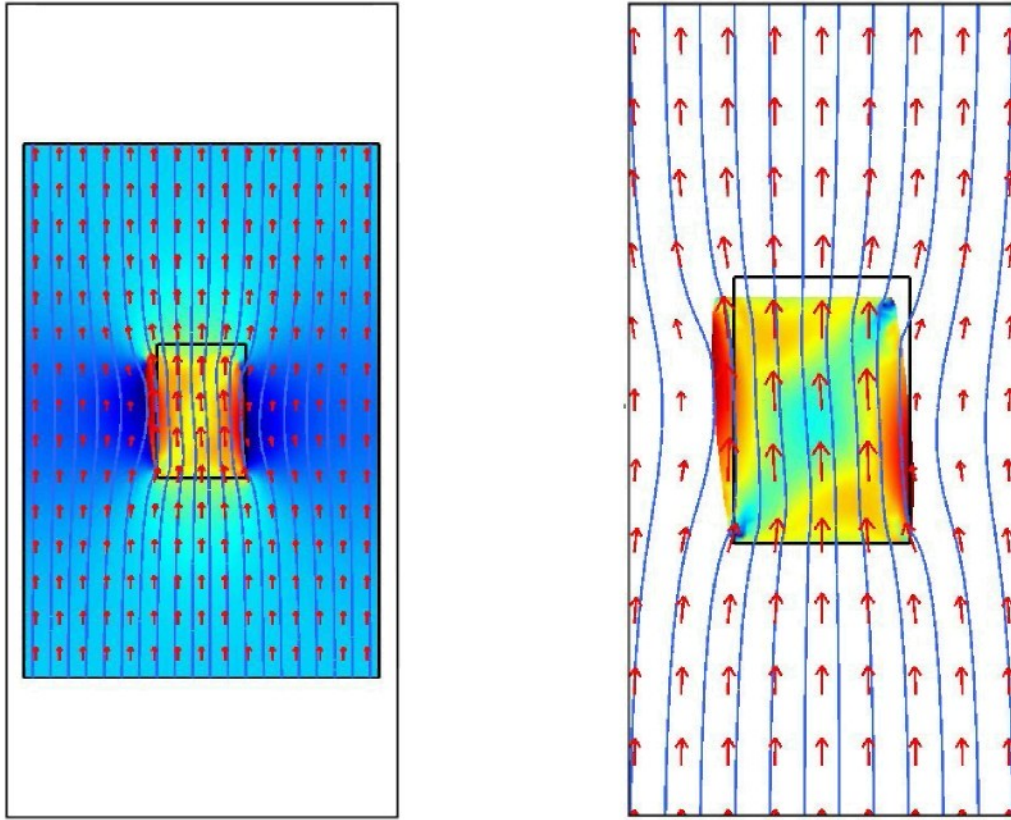


Figure 6.16 – Distribution of the magnetic field and the magnetization of the MS anisotropic material

Next dependencies of horizontal and vertical displacements of the top surface on orientations of ferrous particle chains and on an applied magnetic field are shown as Figure 6.17, the stiffness of the body increases fast that is demonstrated by the deformed block recovered nearly complete when the magnetic field reaches to 1T.

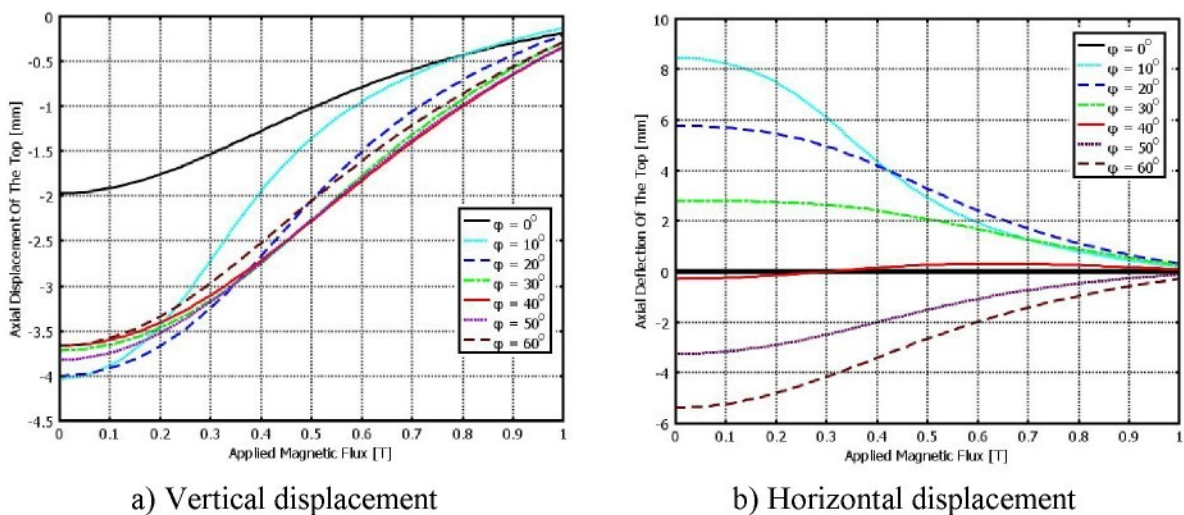


Figure 6.17 – Displacements of the top surface of the block versus the magnetic flux density

6.2.2.2. Simple shear of anisotropic materials

In this subsection a rectangular MS anisotropic composite plate subjected a simple shear state is investigated according to altered directions of an applied magnetic. Here we assume ferrous particles are oriented in a vertical direction, only the modification of the applied magnetic field is considered. The geometry of the plate and loading conditions are represented in Figure 6.18. The direction of the magnetic field is defined by θ compared to the vertical direction. The external loading is set up by a constant traction as $\tau_0 = 1\text{MPa}$.

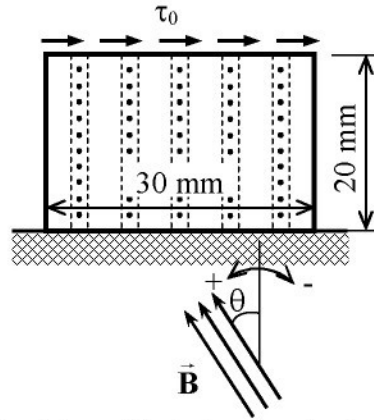
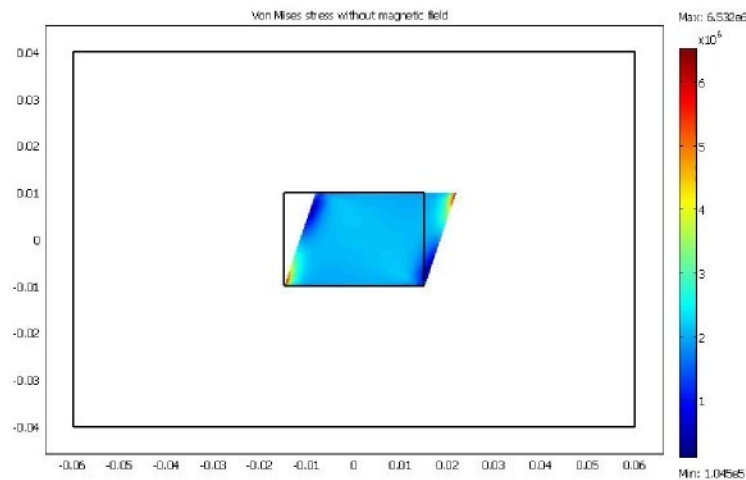
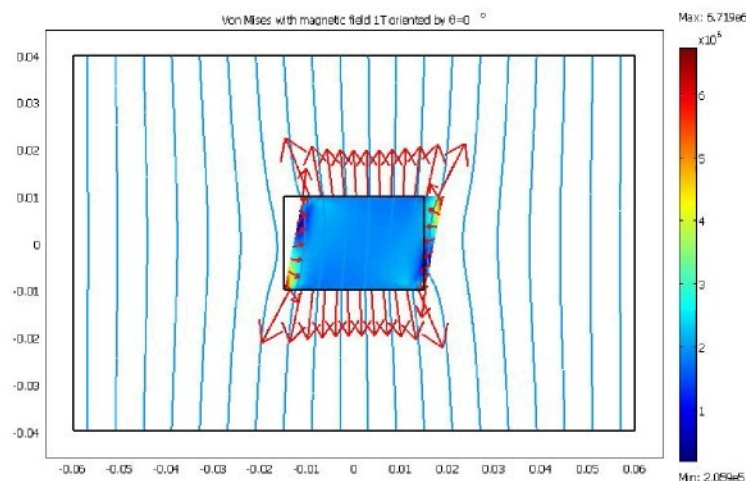


Figure 6.18 – A geometry of a plate subjected a simple shear state is embedded in a static uniform magnetic field

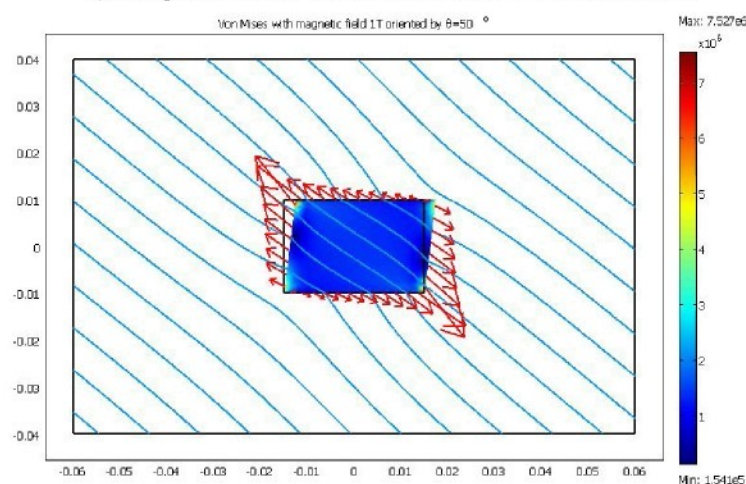
In order to verify effects of the applied magnetic field on the MS body suffered a simple shear state a direction of the magnetic field is changed and some deformation results are obtained as in Figure 6.19. It can conclude that the magnetic forces always affect towards to lengthen the MS body and enhance strongly the stiffness of the material. A high concentration and a large alteration of the magnetic field through the interface of the material and the surrounding space are shown in Figure 6.20. Certainly, inside a dense material the field is distributed higher otherwise it still depends on the deformation of the body.



a) Shear deformation of the plate without magnetic field



b) Magnetic field oriented in a vertical direction



c) Magnetic orientation compared to a vertical direction $\theta=50^\circ$

Figure 6.19 – Simple shear state of the plate with different magnetic directions

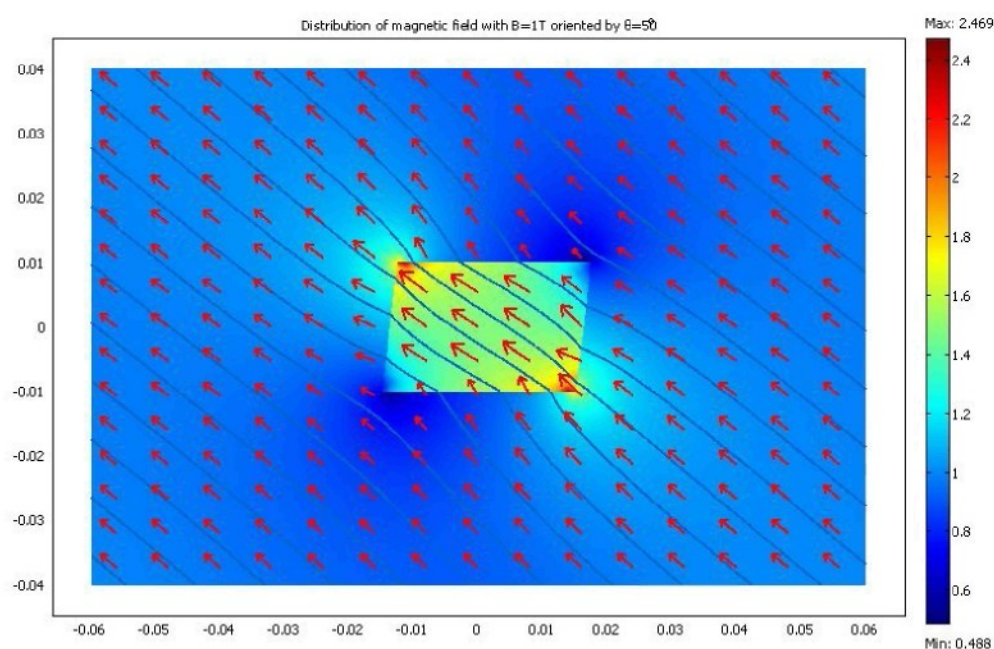
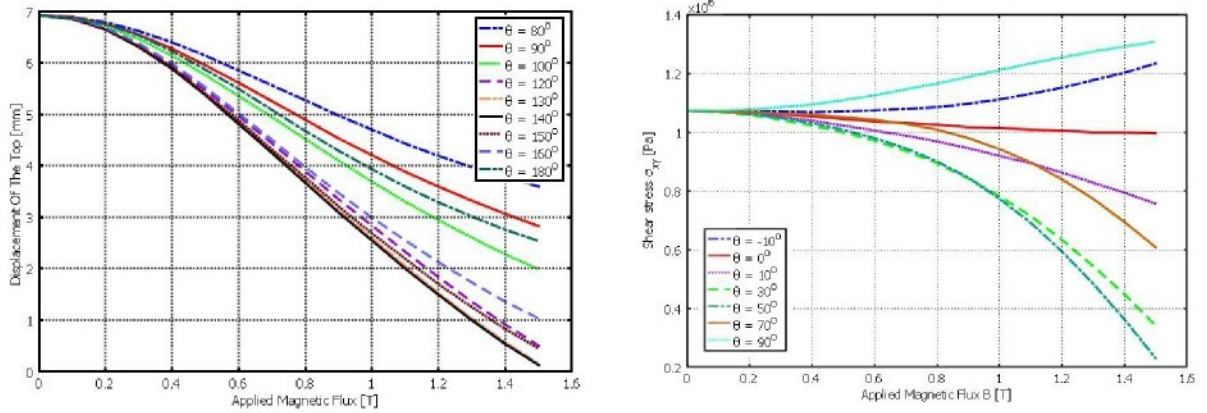


Figure 6.20 – Distribution of the magnetic field with $\theta = 50^\circ$



a) Displacement of the top surface versus different directions of the applied magnetic field
 b) Shear stress at the center of the body versus different directions of the applied magnetic field

Figure 6.21 – Dependencies of a displacement and a shear stress on the magnetic field

Dependencies of a displacement of the top surface applied by the external loading and a shear stress at the central position of the plate on the altered direction of the applied magnetic field are investigated in Figure 6.21. Combination of both the displacement and the shear stress results state that we should apply the contrary direction of the magnetic field against the direction of the deformation in order to enhance a recovery back to the initial form of the deformed MS material.

6.3. Conclusion

In this chapter we have obtained illustrative numerical solutions of simple boundary problems of nonlinear magneto-mechanical response of a body made of isotropic or anisotropic magnetosensitive elastomer subjected to a static magnetic field. The constitutive model that we have used is a simplified model that should be correlated with further experimental data. Nevertheless, the results of the numerical simulations indicate a good qualitative correspondence with experimental findings.

Chapter 7

CONCLUSIONS, DISCUSSIONS AND FUTURE PERSPECTIVES

In this dissertation, the viscoelastic behavior of the fiber-reinforced elastomer has been studied. The viscous characteristics of the anisotropic composites were described by the suitable free energy function and the chosen viscoelastic models. Due to the assumption of the free energy density was decoupled into (elastic) equilibrium and (viscous) non-equilibrium components and then further into volumetric, isotropic and anisotropic components. This allows separate stress relations and viscous flow rules to be specified for the separate constituents of the composite.

The components of the equilibrium stress response were defined directly by the differentiation of the free energy function consisting of volumetric, isotropic and anisotropic parts with respect to the Cauchy-Green deformation tensor. The non-equilibrium response was governed by evolution equations of internal variables which were derived by the use of viscoelastic models. Herein, the generalized Maxwell element model was used in two approaches with either inelastic strains or overstresses playing a role of internal variables. We have mainly focused on describing the viscous response by linear evolution equations of overstresses. Two Maxwell elements corresponding to the viscoelastic representation of the isotropic matrix and anisotropic fiber phases were applied.

Some standard experiments such as simple tensile, pure shear and biaxial tensile tests for isotropic rubber-like materials and composite elastomers reinforced by two families of fibers under many relaxation stages were carried out. The non-contact optical stereo-correlation technique was used to determine precisely for experimental measurements of large deformations and evaluation of strains. Both purely elastic and viscoelastic parameters were determined by fitting the chosen model to experimental data. But for the biaxial tensile test the design optimized form of the specimen need to be improved in order to obtain uniform strain distribution in the interest region. For dealing with this problem, the slits made in each of specimen arms were suggested. In the remaining experiments the evaluation results were in good agreement with experimental data. However, as mentioned, we can enhance a good representation of linear viscoelastic models by introducing a dependence of the material parameters on stress, on strain or on some internal variables as well as increasing the number of elements of the Maxwell model.

The implementation of the set of constitutive equations and evolution equations into a finite element program, Comsol Multiphysics, was established for modeling viscoelastic behaviour of both hyperelastic isotropic and anisotropic composites. The ability of the model to predict nonlinear viscoelastic behavior of isotropic and anisotropic materials was examined

by comparing the theory to experimental results. Several examples relevant to viscoelastic responses, for instance the influence of the loading velocities, one- or multi- step relaxations and a creep were presented. More simulations of complicated boundary value problems of an air-spring tube with two fiber reinforcement were performed using the finite element method. The model provided a very efficient tool to determine realistic predictions of stress, strain and strain rates distributions in the viscoelastic composite materials. Nevertheless as introduced in chapter 1, the formulation of the evolution equations for overstresses is linear for loading close to thermodynamic equilibrium, and then it can be believed that at a high strain rate it is essentially necessary to consider another approach in inelastic strain variables. Consequently, the comparison between two approaches in overstress and inelastic strain variables was considered, this is just the initial step towards the nonlinear approach in inelastic strain variables. However, these approaches are restricted within isothermal regimes, thus thermo-viscoelastic behaviour of anisotropic materials will be a task in future, i.e. an interaction of deformation and temperature in viscoelastic anisotropic materials need to be studied.

The remaining task of the study was to develop a formulation of constitutive equations for anisotropic MS elastomers. Herein, our approach was established basing on the incorporation of the general theory of nonlinear magnetoelasticity and the theory of fiber-reinforced composites by considering an external magnetic field analogous to a preferred direction in the reference configuration. The stress-strain responses were derived by the strain energy function written in terms of invariants. Because a magnetic field is not a unit vector so the MS elastomer placed in a magnetic field depends on more one invariant than in the case without a magnetic field. We implemented several numerical solutions of simple boundary problems of nonlinear magneto-mechanical response of a body made of isotropic or anisotropic magnetosensitive elastomer subjected to a static magnetic field. The finite element software used proved a flexibility and ability of an easy implementation of fairly complicated coupled problem. The FE simulations involved not only the edge effects due to the finite geometry of the body but also the influence of the large displacement of the boundaries. The free energy functions that we have used are very simple forms and represent only a first approach towards a valuable constitutive model. Appropriate experiments which are in preparation will allow the elaboration of the constitutive relations. The constitutive model should involve also the complex dissipative (viscoelastic) behaviour of the material.

As above assessed results, the study of viscoelastic behavior of fiber-reinforced rubber matrix materials in the theory of linear viscoelasticity has reached a certain completion in all three aspects including theory, experiment and numerical simulation. However, the formulation of nonlinear viscoelasticity in internal strain-like variables should be interested to identify material parameters of viscoelastic models proposed and verify through experimental performances. Material parameter identification of MS elastomers corresponding to chosen material models should be also considered. The future studies should include thermal properties of composites with rubber-like matrix.

Literatures

- Albanese-Lerner, A. M., & Cunefare, A. K. (2008). Performance of MRE-based vibration absorbers. *J. Intell. Mater. Syst. Struct.*, Vol. 19, No. 5, pp. 551-563.
- Amin, A. F. M. S., Lion, A., Sekita, S., & Okui, Y. (2006). Nonlinear dependence of viscosity in modeling the rate-dependent response of natural and high damping rubbers in compression and shear: Experimental identification and numerical verification. *International Journal of Plasticity*, Vol. 22, pp. 1610-1657.
- Areias, P., & Matouš, K. (2008). Finite element formulation for modeling nonlinear viscoelastic elastomers. *Comput. Methods Appl. Mech. Engrg.*, Vol. 197, pp. 4702-4717.
- Başar, Y., & Itskov, M. (1998). Finite element formulation of the Ogden material model with application to rubber-like shells. *Int. J. Numer. Meth. Engrg.*, Vol. 42, pp. 1279-1305.
- Bischoff, J. E., Arruda, E. M., & Grosh, K. (2000). A microstructurally-based orthotropic hyperelastic constitutive law for soft tissue. *Journal of Applied Mechanics*, Vol. 60, pp. 570-579.
- Bischoff, J. E., Arruda, E. M., & Grosh, K. (2001). Measurement of orthotropic material properties and constitutive modeling of soft tissue. *Bioengineering Conference, ASME 2001, BED-Vol. 50*, pp. 415-416.
- Bischoff, J. E., Arruda, E. M., & Grosh, K. (2004). A rheological network model for the continuum anisotropic and viscoelastic behavior of soft tissue. *Biomechan Model Mechanobiol*, Vol. 3, pp. 56-65.
- Bischoff, J. E. (2006). Reduced parameter formulation for incorporating fiber level viscoelasticity into tissue level biomechanical models. *Annals of Biomedical Engineering*, Vol. 34, No. 7, pp. 1164-1172.
- Bonet, J., & Burton, A.J. (1998). A simple orthotropic, transversely isotropic hyperelastic constitutive equation for large strain computations. *Comput. Methods Appl. Mech. Engrg.*, Vol. 162, pp. 151-164.
- Bonet, J., & Profit, M.L. (2000). *Nonlinear viscoelastic constitutive modeling of a continuum*. European Congress on Computational Methods in Applied Sciences and Engineering, Barcelona, Spain.
- Bonet, J. (2001). Large strain viscoelastic constitutive models. *International Journal of Solids and Structures*, Vol. 38, pp. 2953-2968.
- Brigadnov, I. A. & Dorfmann, A. (2003). Mathematical modelling of magneto-sensitive elastomers. *Int. J. of Solids Struct.*, Vol. 40, pp. 4659-4674.
- Bustamante, R., Dorfmann, A., & Ogden, R. W. (2006). Universal relations in isotropic nonlinear magnetoelasticity. *Quart. J. Mech. Appl. Math.*, Vol. 59, No. 3, pp. 435-450.

- Bustamante, R., Dorfmann, A., & Ogden, R. W. (2007). A nonlinear magnetoelastic tube under extension and inflation in an axial magnetic field: numerical solution. *J. Eng. Math.*, Vol. 59, pp. 139–153.
- Carlson, J. D., & Jolly, M. R. (2000). MR fluid, foam and elastomer devices. *Mechatronics*, Vol. 10, pp. 555–569.
- Chevaugnon, N., Verron, E., & Peseux, B. (2000). *Finite element analysis of nonlinear transversely isotropic hyperelastic membranes for thermoforming applications*. European Congress on Computational Methods in Applied Sciences and Engineering, Barcelona, Spain.
- deBotton, G., Hariton, I., & Socolsky, E. A. (2006). Neo-Hookean fiber-reinforced composites in finite elasticity. *Journal of the Mechanics and Physics of Solids*, Vol. 54, pp. 533–559.
- Deng, H. X., & Gong, X. L. (2007). Adaptive tuned vibration absorber based on magnetorheological elastomer. *J. Intell. Mater. Syst. Struct.*, Vol. 18, pp. 1205–1210.
- Diani, J., Brieu, M., & Gilormini, P. (2006). Observation and modeling of the anisotropic visco-hyperelastic behavior of rubber-like material. *International Journal of Solids and Structures*, Vol. 43, pp. 3044–3056.
- Dorfmann, A., & Ogden, R. W. (2003). Magnetoelastic modelling of elastomers. *Eur. J. Mech. A/ Solids*, Vol. 22, pp. 497–507.
- Dorfmann, A., & Ogden, R. W. (2004). Nonlinear magnetoelastic deformations of elastomers. *Acta Mechanica*, Vol. 167, No. 1–2, pp. 13–28.
- Dorfmann, A., & Ogden, R. W. (2005). Some problems in nonlinear magnetoelasticity. *Z. angew. Math. Phys. (ZAMP)*, Vol. 56, pp. 718–745.
- Dorfmann, A., Ogden, R. W., & Saccomandi, G. (2005). The effect of rotation on the nonlinear magnetoelastic response of a circular cylindrical tube. *Int. J. of Solids Struct.*, Vol. 42, pp. 3700–3715.
- Drozdov, A. D., & Dorfmann, A. (2001). The stress-strain response and ultimate strength of filled elastomers. *Computational Materials Science*, Vol. 21, pp. 395–417.
- Drozdov, A. D., & Christiansen, J. (2009). Thermo-viscoplasticity of carbon black-reinforced thermoplastic elastomers. *International Journal of Solids and Structures*, Vol. 46, pp. 2298–2308.
- Eberlein, R., & Wriggers, P. (1999). Finite element concepts for finite elastoplastic strains and isotropic stress response in shells: Theoretical and computational analysis. *Comput. Methods Appl. Mech. Engrg.*, Vol. 171, pp. 243–279.
- Eberlein, R., Holzapfel, G. A., & Schulze-Bauer, C. A. J. (2000). An anisotropic constitutive model for annulus tissue and enhanced finite element analyses of intact lumbar disc bodies. *Computer Methods in Biomechanics and Biomedical Engineering*, Vol. 4, pp. 209–229.
- Elías-Zúñiga, A. (2006). A non-Gaussian network model for rubber elasticity. *Polymer*, Vol. 47, pp. 907–914.
- Fancello, E., Stainier, L., & Ponthot, J. P. (2005). A variational formulation of constitutive models and updates in nonlinear finite viscoelasticity. *International Journal for Numerical Methods in Engineering*, Vol. 65, pp. 1831–1864.
- Gasser, T. C., Schulze-Bauer, C. A. J., & Holzapfel, G. A. (2001). A three-dimensional finite element model for arterial clamping. *J. Biomech. Eng.*, Vol. 124, pp. 355–363.

- Gao, Y. C. (1997). Large deformation field near a crack tip in a rubber-like material. *Theoretical and Applied Fracture Mechanics*, Vol. 26, pp. 155–162.
- Ginder, J. M., Clark, S. M., Schlotter, W. F., & Nichols, M. E. (2002). Magnetostrictive phenomena in magnetorheological elastomers. *Int. J. Mod. Phys. B*, Vol. 16, No. 17-18, pp. 2412-2418.
- Gong, X. L., Zhang, X. Z., & Zhang, P. Q. (2005). Fabrication and characterization of isotropic magnetorheological elastomers. *Polymer Testing*, Vol. 24, No. 5, pp. 669-676.
- Govindjee, S., & Simo, J. C. (1991). A micro-mechanically based continuum damage model for carbon black-filled rubbers incorporating Mullins' effect. *J. Mech. Phys. Solids*, Vol. 39, No. 1, pp. 87-112.
- Govindjee, S., & Simo, J. C. (1992). Mullins' effect and the strain amplitude dependence of the storage modulus. *Int. J. Solids Structures*, Vol. 29, No. 14/15, pp. 1737-1751.
- Guo, X. (2001). Large deformation analysis for a cylindrical hyperelastic membrane of rubber-like material under internal pressure. *Rubber Chemistry and Technology*, Vol. 74, pp. 100-115.
- Guo, Z., & Sluys, L. J. (2006). Application of a new constitutive model for the description of rubber-like materials under monotonic loading. *International Journal of Solids Structures*, Vol. 43, pp. 2799-2819.
- Guo, Z., Peng, X., & Moran, B. (2007). Large deformation response of a hyperelastic fibre reinforced composite: Theoretical model and numerical validation. *Composites: Part A*, Vol. 38, pp. 1842–1851.
- Haussy, B., & Ganghoffer, J. F. (2002). *An orthotropic hyperelastic model of cylindrical thick shells under pressure: Application to the modeling of aneurysm*. 15th ASCE Engineering Mechanics Conference, Columbia University, New York, USA.
- Hoang, S. T., & Marvalová, B. (2009). *Magnetoelastic anisotropic elastomers in a static magnetic field: Constitutive equations and FEM solutions*. Proceedings of the sixth European Conference on Constitutive Models for Rubber, Ed.: Taylor & Francis Group. Dresden, September 7-10, 2009, Germany, pp. 453-458.
- Holzappel, G. A., & Reiter, G. (1995). Fully coupled thermo-mechanical behavior of viscoelastic solids treated with finite elements. *Int. J. Engng Sci.*, Vol. 33, No. 7, pp. 1037-1058.
- Holzappel, G. A. (1996). On large strain viscoelasticity: continuum formulation and finite element applications to elastomeric structures. *International Journal for Numerical Methods in Engineering*, Vol. 39, pp. 3903-3926.
- Holzappel, G. A., & Simo, J. C. (1996). A new viscoelastic constitutive model for continuous media at finite thermomechanical changes. *Int. J. Solids Structures*, Vol. 33, No. 20-22, pp. 3019-3034.
- Holzappel, G. A., Eberlein, R., Wriggers, P., & Weizsäcker, H. W. (1996). Large strain analysis of soft biological membranes: Formulation and finite element analysis. *Comput. Methods Appl. Mech. Engrg.*, Vol. 132, pp. 45-61.
- Holzappel, G. A. (2000). *Nonlinear Solid Mechanics, A Continuum Approach for Engineering*. John Wiley, & Son Ltd, Chichester, England.

- Holzappel, G. A., & Gasser, T. C. (2001). A viscoelastic model for fiber-reinforced composites at finite strains: Continuum basis, computational aspects and applications. *Computer Methods in Applied Mechanics and Engineering*, Vol. 190, pp. 4379-4403.
- Holzappel, G. A., Gasser, T. C., & Stadler, M. (2001). A structural model for the viscoelastic behavior of arterial walls: Continuum formulation and finite element simulation. *European Journal of Mechanics A-Solids*, Vol. 21, pp. 441-463.
- Holzappel, G. A. (2006). Determination of material models for arterial walls from uniaxial extension tests and histological structure. *Journal of Theoretical Biology*, Vol. 238, pp. 290-302.
- Holzappel, G. A., & Ogden, R. W. (2008). On planar biaxial tests for anisotropic nonlinearly elastic solids. A continuum mechanical framework. *Mathematics and Mechanics of Solids*, Vol. 14, pp. 474-489.
- Ibrahimbegovic, A., & Gruttmann, F. (1993). A consistent finite element formulation of nonlinear membrane shell theory with particular reference to elastic rubber-like material. *Finite Element in Analysis and Design*, Vol. 12, pp. 75-86.
- Itskov, M. (2001). A generalized orthotropic hyperelastic material model with application to incompressible shells. *Int. J. Numer. Meth. Engng.*, Vol. 50, pp. 1777-1799.
- Jiang, L., & Haddow, J. B. (1995). A finite element formulation for finite static axisymmetric deformation of hyperelastic membranes. *Computers and Structures*, Vol. 57, pp. 401-405.
- Johnson, A. R., & Chen, T. K. (2002). *Thermo-mechanical analyses of dynamically loaded rubber cylinders*. Rubber Division, American Chemical Society, Paper No. 36, Pittsburgh, PA USA.
- Johnson, A. R., & Chen, T. K. (2005). Approximating thermo-viscoelastic heating of largely strained solid rubber components. *Comput. Methods Appl. Mech. Engrg.*, Vol. 194, pp. 313-325.
- Jolly, M. R., Carlson, J. D., Munzo, B. C. & Bullions, T. A. (1996). The magneto-viscoelastic response of elastomer composites consisting of ferrous particles embedded in a polymer matrix. *J. Intell. Mater. Syst. Struct.*, Vol. 7, pp. 613-622.
- Kallio, M., Lindroos, T., Aalto, S., Järvinen, E., Kärnä, T., & Meinander, T. (2007). Dynamic compression testing of a tunable spring element consisting of a magnetorheological elastomer. *Smart Mat. Struct.*, Vol. 16, pp. 506-514.
- Kaliske, M. (2000). A formulation of elasticity and viscoelasticity for fibre reinforced material at small and finite strains. *Comput. Methods Appl. Mech. Engrg.*, Vol. 185, pp. 225-243.
- Kankanala, S. V. & Triantafyllidis, N. (2004). On finitely strained magnetorheological elastomers. *J. Mech.Phys. Solids*, Vol. 52, pp. 2869-2908.
- Kankanala, S. V. & Triantafyllidis, N. (2008). Magnetoelastic buckling of a rectangular block in plane strain. *J. Mech.Phys. Solids*, Vol. 56, pp. 1147-1169.
- Karamanou, M., Warby, M. K., & Whiteman, J. R. (2006). Computational modeling of thermoforming processes in the case of finite viscoelastic materials. *Comput. Methods Appl. Engrg.*, Vol. 195, pp. 5220-5238.
- Kleuter, B., Menzel, A., & Steinmann, P. (2007). Generalized parameter identification for finite viscoelasticity. *Comput. Methods Appl. Mech. Engrg.*, Vol. 196, pp. 3315-3334.
- Kovetz, A. (2000). *Electromagnetic Theory*. Oxford University Press, Oxford, England.

- Kroon, M., & Holzapfel, G. A. (2008). A new constitutive model for multi-layer collagenous tissues. *Journal of Biomechanics*, Vol. 41, pp. 2766–2771.
- Kuwabara, T., Ikeda, S., & Kuroda, K. (1998). Measurement and analysis of differential work hardening in cold-rolled steel sheet under biaxial tension. *Journal of Materials Processing Technology*, Vol. 80–81, pp. 517–523.
- Le Tallec, P., Rahier, C., & Kaiss, A. (1993). Three-dimensional incompressible viscoelasticity in large strains: Formulation and numerical approximation. *Computer Methods in Applied Mechanics and Engineering*, Vol. 109, pp. 233–258.
- Merodio, J., & Ogden, R. W. (2005). Mechanical response of fiber-reinforced incompressible non-linearly elastic solids. *International Journal of Non-linear mechanics*, Vol. 40, pp. 213–227.
- Menzel, A., Steinmann, P. (2002). A view on anisotropic finite hyper-elasticity. *European journal of mechanics. A. Solids*, Vol. 22, No. 1, pp. 71–87.
- Nam, T. H. (2004). *Mechanical properties of the composite material with elastomeric matrix reinforced by textile cords*. Unpublished Ph. D. Thesis, Technical University of Liberec, Czech Republic.
- Nedjar, B. (2007). An anisotropic viscoelastic fibre-matrix model at finite strains: Continuum formulation and computational aspects. *Computer Methods in Applied Mechanics and Engineering*, Vol. 196, pp. 1745–1756.
- Nguyen, T. D., Jones, R. E., & Boyce, B. L. (2007). Modeling the anisotropic finite-deformation viscoelastic behavior of soft fiber-reinforced composites. *International Journal of Solids and Structures*, Vol. 44, pp. 8366–8389.
- Ogden, R. W., & Schulze-Bauer, C. A. J. (2000). Phenomenological and structural aspects of the mechanical response of arteries. J. Casey, and G. Bao, (Eds.), *Mechanics in Biology*, AMD-Vol. 242, BED-Vol. 46, pp. 125–140.
- Oman, S., Nagode, M., & Fajdiga, M. (2009). The material characterization of the air spring bellow sealing layer. *Materials and Design*, Vol. 30, pp. 1141–1150.
- Ottenio, M., Destrade, M., & Ogden, R. W. (2008). Incremental magnetoelastic deformations, with application to surface instability. *Journal of Elasticity*, Vol. 90, No. 1, pp. 19–42.
- Pamplona, D. C., Gonçalves, P. B., & Lopes, S. R. X. (2006). Finite deformations of cylindrical membrane under internal pressure. *International Journal of Mechanical Sciences*, Vol. 48, pp. 683–696.
- Pao, Y. H. (1978). Electromagnetic forces in deformable continua. *Mechanics Today*, Vol. 4, pp. 209–305.
- Peña, E., Calvo, B., Martínez, M. A., & Doblaré, M. (2007). An anisotropic visco-hyperelastic model for ligaments at finite strains. Formulation and computational aspects. *International Journal of Solids and Structures*, Vol. 44, pp. 760–778.
- Plešek, J., & Kruisová, A. (2006). Formulation, validation and numerical procedures for Hencky's elasticity model. *Computers and Structures*, Vol. 84, pp. 1141–1150.
- Poživilová, A. (2002). *Constitutive modeling of hyperelastic materials using the logarithmic description*. Unpublished Ph. D. Thesis, Czech Technical University in Prague, Czech Republic.

- Reese, S., & Wriggers, P. (1997). A material model for rubber-like polymers exhibiting plastic deformation: computational aspects and a comparison with experimental results. *Comput. Methods Appl. Mech. Engrg.*, Vol. 148, pp. 279-298.
- Reese, S., & Govindjee, S. (1998a). A theory of finite viscoelasticity and numerical aspects. *Int. J. Solids Structures*, Vol. 35, No. 26-27, pp. 3455-3482.
- Reese, S., & Govindjee, S. (1998b). Theoretical and numerical aspects in the thermo-viscoelastic material behavior of rubber-like polymers. *Mechanics of Time-Dependent Materials*, Vol. 1, pp. 357-396.
- Reese, S., Wriggers, P., & Reddy, B. D. (1998). A new locking-free brick element formulation for continuous large deformation problems. In *Computational and Applied Mechanics*, pp. 1-20. Retrieved June 13, 2002, from <http://www.mth.uct.ac.za/~bdr/stefwccm.pdf>.
- Reese, S. (2000). *Large deformation FE modeling of the orthotropic elastoplastic material behavior in pneumatic membranes*. European Congress on Computational Methods in Applied Sciences and Engineering, Barcelona, Spain.
- Reese, S., Wriggers, P., & Reddy, B. D. (2000). A new locking-free brick element technique for large deformation problems in elasticity. *Computers and Structures*, Vol. 75, pp. 291-304.
- Reese, S., Raible, T., & Wriggers, P. (2001). Finite element modeling of orthotropic material behavior in pneumatic membranes. *International Journal of Solids and Structures*, Vol. 38, pp. 9525-9544.
- Reese, S. (2003a). A micromechanically motivated material model for the thermo-viscoelastic material behaviour of rubber-like polymers. *International Journal of Plasticity*, Vol. 19, pp. 909-940.
- Reese, S. (2003b). On a consistent hourglass stabilization technique to treat large inelastic deformations and thermo-mechanical coupling in plane strain problems. *International Journal for Numerical Methods in Engineering*, Vol. 57, pp. 1095-1127.
- Reese, S. (2003c). Meso-macro modelling of fibre-reinforced rubber-like composites exhibiting large elastoplastic deformation. *International Journal of Solids and Structures*, Vol. 40, pp. 951-980.
- Simo, J. C. (1987). On a fully three-dimensional finite-strain viscoelastic damage model: Formulation and computational aspects. *Computer Methods in Applied Mechanics and Engineering*, Vol. 60, pp. 153-173.
- Truesdell, C., & Noll, W. (1992). *The Non-Linear Field Theories of Mechanics*. Springer-Verlag, Berlin, Germany.
- Vlach, J. (2009). *Návrh experimentální metody pro stanovení mechanických a magnetických vlastností kompozitů složených ze silikonových elastomerů plněných magneticky polarizovatelnými mikročásticemi*. Unpublished Master Thesis, Technical University of Liberec, Czech Republic.
- Wriggers, P., Eberlein, R., & Reese, S. (1996). A comparison of three-dimensional continuum and shell elements for finite plasticity. *Int. J. Solids Structures*, Vol. 33, pp. 3309-3326.

Publications

- Tuong N.V., Tuan H.S., Pokorny P.: *Matlab-based programming for free-form surfaces*. International Conference 2009 Manufacturing systems today and tomorrow. TUL, Liberec, November 19-20, 2009, Czech, pp. 17, ISBN 978-80-7372-541-9.
- H. S. Tuan, B. Marvalová: *Magnetoelastic anisotropic elastomers in a static magnetic field: Constitutive equations and FEM solutions*. Proceedings of the sixth European Conference on Constitutive Models for Rubber, Ed.: Taylor & Francis Group. Dresden, September 7-10, 2009, Germany, pp. 453-458, ISBN 978-0-415-56327-7.
- Jarmil Vlach, Hoang Sy Tuan, Bohdana Marvalová: *Experimental and numerical research of Magneto-sensitive elastomers*. 47th International Conference of Experimental Stress Analysis. Syrchov, June 8-11, 2009, Czech Republic, pp.283-290, ISBN 978-80-7372-483-2.
- Hoang Sy Tuan, Marvalová Bohdana: *Simulation of Viscoelastic Fiber-Reinforced Composites at Finite Strains in Comsol Multiphysics*. Applied Mechanics 2009, 11th International Scientific Conference. Smolenice, April 6-8, 2009, Slovak Republic, pp. 45-46, ISBN 978-80-89313-32-7.
- Hoang Sy Tuan, B. Marvalová: *Relaxation of Fiber-reinforced Composites: FEM Simulations*. Conference Mechanical Composite Material and Structure. Pilsen, March 12-13, 2009, Czech Republic, pp. 70-77, ISBN 978-80-7043-782-7.
- Sy Tuan Hoang, Bohdana Marvalová: *Coupling of magnetoelastic material and magnetic field in Comsol Multiphysics*. Výpočty Konstrukcí Metodou Konečných Prvků. Pilsen, November 20, 2008, Czech Republic, pp. 8-18, ISBN 978-80-7043-735-3.
- Hoang S. T., Marvalová B.: *Numerical Differentiation of Experimentally Measured Displacements*. 16th Annual Conference Proceedings. Prague, November 11, 2008, Czech Republic, pp. 40, ISBN 978-80-7080-692-0.
- Hoang S.T., Marvalová B.: *Magneto-hyperelastic material in a uniform magnetic field: FEM Calculation of Stress and Strain*. Engineering Mechanics 2008, National Conference with International Participation. Svatka, May 12-15, 2008, Czech Republic, pp. 86-87, ISBN 978-80-87012-11-6.

- Jan Růžička, Hoang Sy Tuan, Bohdana Marvalová: *Dynamic measuring methods of viscoelastic properties of materials*. 14th International Conference, Structure and Structural Mechanics of Textiles. TU of Liberec, November 26-28, 2007, Czech Republic, pp. 97-104. ISBN 978-80-7372-271-5.
- Hoang Sy Tuan, Bohdana Marvalová: *FE analysis of cord-reinforced rubber composites at finite strains*. Výpočty Konstrukcí Metodou Konečných Prvků. Prague, November 22, 2007, Czech Republic, pp. 9-20, ISBN 978-80-01-03942-7.
- Hoang. S.T., Marvalová B.: *Constitutive Material Model of Fiberreinforced Composites in Comsol Multiphysics*. Technical Computing Prague 2007, 15th Annual Conference Proceedings. Prague, November 14, 2007, Czech Republic, pp. 53, ISBN 978-80-7080658-6.
- Tuan Hoang Sy, Marvalová B.: *Relaxation of the Rubber Plate with Central Hole – FEM Simulation in Comsol Multiphysics*. Applied Mechanics 2007, 9th International Scientific Conference. Malenovice, April 16-19, 2007, Czech Republic, pp. 214-215, ISBN 978-80-248-1389-9.

Appendix A

OVERVIEW OF CONTINUUM MECHANICS

The method of continuum mechanics is used as a powerful and effective tool to explain various physical phenomena successfully without detailed knowledge of the complexity of their internal microstructures. From the physical point of view this is an approximation in which the very large numbers of particles are replaced by a few quantities; we consider a macroscopic system. Hence, the primary interface with nature is through these quantities which represent averages over dimensions that are small enough to capture high gradients and to reflect some micro-structural effects.

In order to explain the macroscopic behavior of physical objects, first of all we must understand the motion and deformation that are caused by stresses in a material undergoing forces and moments. Thus, we will focus to study the motion and finite deformation of a continuum mechanics in this chapter.

The approach is introduced with both the notion ‘Lagrangian’ (material) and ‘Eulerian’ (spatial) descriptions. First the kinematical definitions and formulae are considered in finite strains. The strain tensors in material and spatial configuration are defined. Next the stresses and forces are presented in the deformable body during a finite motion. For that body the concept of stress is introduced and the properties of traction vector and stress tensors in different descriptions are discussed. Finally the balance or conservation of mass, linear momentum, moment of momentum and energy are summarized concisely.

A.1. Finite strain kinematics

In this section, a brief outline of those concepts and principles of finite strain kinematics are summarized. The aim of this section is to introduce some basic kinematics to study the motion and finite deformation of a deformable body. More comprehensive continuum kinematics overview can be referred to many textbooks, such as Truesdell & Noll (1992) and Holzapfel (2000).

A.1.1. Motions of continuum bodies

The macroscopic study is to concern with the mechanics of a body in which both *mass* and *volume* are continuous functions of continuum particles. Such a body is called a **continuum body**, or just a continuum.

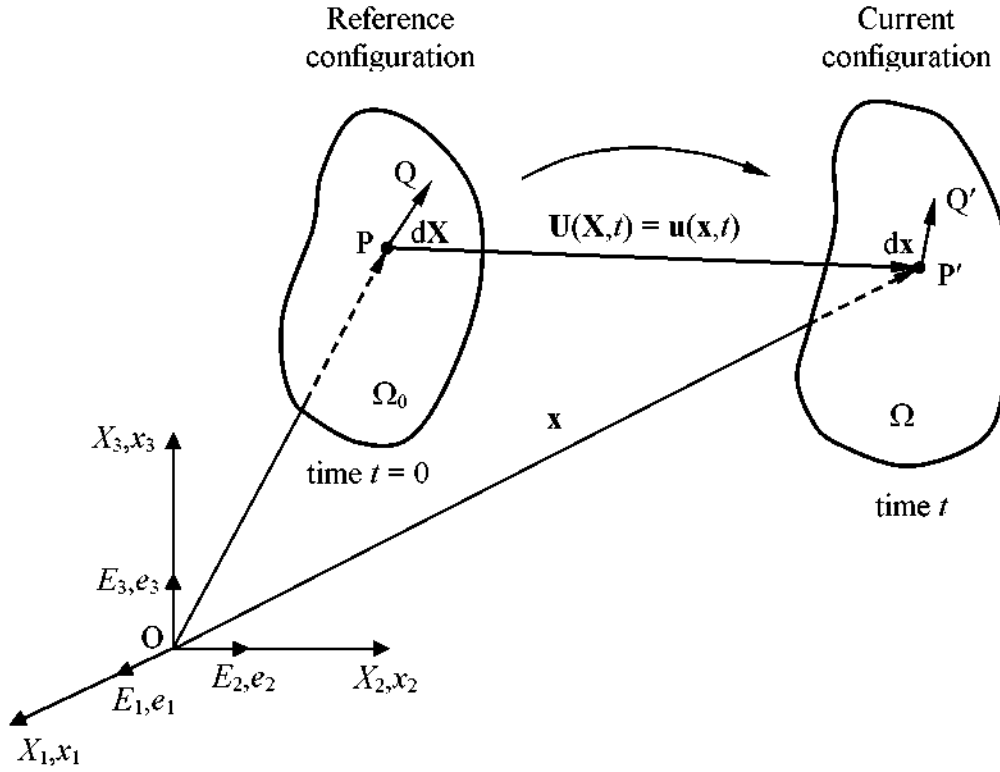


Figure A.1 – Configuration and motion of a continuum body

A continuum body \mathcal{B} with particle $P \in \mathcal{B}$ which is embedded in the three-dimensional Euclidean space referred to a rectangular Cartesian coordinate system with a fixed origin O and orthogonal base vectors \mathbf{e}_i ($i=1,2,3$), as shown in Figure A.1, is considered at a given instant of time t .

The continuum body \mathcal{B} occupies a geometrical region in undeformed state at time $t = 0$ denoted by Ω_0 . The configuration of such body is referred to as an initial, reference or also undeformed configuration. In reference configuration, a typical particle of the body occupying the point P can be represented by the position vector \mathbf{X} with respect to fixed origin of the coordinate system. Now assume that the region Ω_0 moves to a new region Ω which is occupied by the continuum body \mathcal{B} at a time $t > 0$. The configuration of \mathcal{B} at time t is so-called current (or deformed) configuration. The point P of the reference configuration moves to a point P' of the current configuration. The position vector \mathbf{x} serves as a label for the associated point P' with respect to the fixed origin O . The motion may be mathematically described by equation between reference and current particle position as

$$\mathbf{x} = \mathbf{x}(\mathbf{X}, t) \quad (\text{A.1})$$

The motion \mathbf{x} carries point P located at Ω_0 to places P' in the current configuration Ω . The parametric equation (A.1) determines successive positions \mathbf{x} of a typical particle P in space. The function \mathbf{x} is the trajectory of the point P .

Since no two distinct particles can have the same position in any configuration and no two distinct points in a given configuration can be position of the same particle, the function (A.1) is specified uniquely and the unique inverse function exists

$$\mathbf{X} = \mathbf{X}(\mathbf{x}, t) \quad (\text{A.2})$$

The component of vector $\mathbf{X} = X_i \mathbf{E}_i$ and $\mathbf{x} = x_i \mathbf{e}_i$ are considered as being along the axes introduced. Denote that X_i , $i=1,2,3$, as the *material (referential) coordinates* of point P and x_i , as the *spatial (current) coordinates* of point P' . Since the same reference frame is agreed for the reference and current configurations, which is why the basis vectors $\{\mathbf{E}\}$ and $\{\mathbf{e}\}$ are identical.

Material and spatial descriptions

Problems in continuum mechanics may be formulated either with material coordinates as independent variables - using the so-called *material description* of the problem or with spatial coordinates as independent variables - using the *spatial description*. In the finite strain analysis a careful distinction has to be made between the coordinate systems that can be chosen to describe the behavior of the body whose motion is above consideration.

Both description of the motion (A.1) and (A.2) are equivalent, but not identical and they are described by different functions. The material description in the first equation (A.1) is a characterization of the motion with respect to the material coordinates and the time t , the independent variables (\mathbf{X}, t) are referred to as *material variables*. A material description refers to the behavior of a material particle as it moves. On the other hand, in the description of motion given by (A.2) attention is paid to a point in space. This description is called the spatial description and the independent variables (\mathbf{x}, t) are referred to as *spatial variables*. Traditionally, the material description is referred to as the **Lagrangian** and spatial description is referred to as **Eulerian**. Due to the fact that the constitutive behavior of solids is often given in terms of material coordinates we often prefer the **Lagrangian description**.

Displacement field

The vector field

$$\mathbf{U}(\mathbf{X}, t) = \mathbf{x}(\mathbf{X}, t) - \mathbf{X} \quad (\text{A.3})$$

represents the displacement field of a typical particle and relates its position \mathbf{X} in the undeformed configuration to its position \mathbf{x} in the deformed configuration at time t . The displacement field \mathbf{U} which characterizes the material (Lagrangian) description of the displacement field, is a function of the referential position \mathbf{X} and time t .

The displacement field in the spatial (Eulerian) description, denoted \mathbf{u} , is a function of the current position \mathbf{x} and time t , as

$$\mathbf{u}(\mathbf{x}, t) = \mathbf{x} - \mathbf{X}(\mathbf{x}, t) \quad (\text{A.4})$$

The vectors \mathbf{U} and \mathbf{u} have the same values. They represent functions of different arguments.

A.1.2. Deformation gradient

Deformation of a continuum body (i.e. the changes of size and shape) occur when moved from the reference configuration Ω_0 to current configuration Ω . To qualify the deformation of a material particle P, the changes of the immediate neighborhood of the particle have to be analyzed. Consider a material particle Q in the neighborhood of a material P, see Figure A.1. The position Q relative to P is given by the element vector $d\mathbf{X}$ as

$$d\mathbf{X} = \mathbf{X}_Q - \mathbf{X}_P \quad (\text{A.5})$$

After deformation the material particles P and Q have deformed to current spatial positions P' and Q' and the corresponding element vector become

$$d\mathbf{x} = \mathbf{x}_{Q'} - \mathbf{x}_{P'} \quad (\text{A.6})$$

A key quantity in finite deformation analysis is the deformation gradient \mathbf{F} , which is involved in all equations quantities before deformation to corresponding quantities after (or during) deformation. Defining the *deformation gradient tensor* as

$$\mathbf{F} = \frac{\partial \mathbf{x}(\mathbf{X}, t)}{\partial \mathbf{X}} \quad (\text{A.7})$$

In indicial notation the deformation gradient tensor is expressed as

$$F_{ij} = \frac{\partial x_i}{\partial X_j} \quad (i, j = 1, 2, 3) \quad (\text{A.8})$$

The inverse of \mathbf{F} is

$$\mathbf{F}^{-1} = \frac{\partial \mathbf{X}}{\partial \mathbf{x}} \quad (\text{A.9})$$

In general, the nonsingular (invertible, i.e. $\det \mathbf{F} \neq 0$) tensor \mathbf{F} depends on \mathbf{X} which denotes a so-called *inhomogeneous deformation*. A deformation of a body in question is said to be *homogeneous* if \mathbf{F} does not depend on the space coordinates. The components F_{ij} ($i, j = 1, 2, 3$) depend only on time.

Displacement gradient tensor

To combine the deformation gradient with the displacement vector we deduce from (A.3) and definition (A.7) that

$$\text{Grad} \mathbf{U} = \text{Grad} \mathbf{x}(\mathbf{X}, t) - \text{Grad} \mathbf{X} = \mathbf{F}(\mathbf{X}, t) - \mathbf{I} \quad (\text{A.10})$$

The second-order tensor $\text{Grad}\mathbf{U}$ is called the displacement gradient tensor in the material description.

The displacement gradient tensor in the spatial description is given from (A.4) and definition (A.9) as

$$\text{grad}\mathbf{u} = \text{grad}\mathbf{x} - \text{grad}\mathbf{X}(\mathbf{x}, t) = \mathbf{I} - \mathbf{F}^{-1}(\mathbf{X}, t) \quad (\text{A.11})$$

Jacobian determinant

The determinant of the deformation gradient \mathbf{F} will be denoted by

$$J(\mathbf{X}, t) = \det \mathbf{F}(\mathbf{X}, t) \quad (\text{A.12})$$

in which J is also known as the volume ratio of the change in volume between the reference and the current configuration at time t

$$dv = J(\mathbf{X}, t) dV \quad (\text{A.13})$$

In the relation (A.13), dV and dv are denoted infinitesimal volume elements defined in the reference and current configuration.

Because \mathbf{F} is nonsingular, so that $J = \det \mathbf{F} \neq 0$. Because of the impenetrability of matter, i.e. volume elements cannot have negative volumes, $J < 0$ will be rejected. Consequently, the volume ratio must be greater than zero for all particles in undeformed configuration and for all time t ,

$$J = \det \mathbf{F} > 0 \quad (\text{A.14})$$

therefore the inverse of deformation gradient \mathbf{F} exists.

A.1.3. Strain tensors

In the previous subsection the deformation gradient is presented as the fundamental kinematical tensor in finite deformation kinematics that characterizes changes of material elements during motion. The purpose of this section is to determine these changes in the forms of *strain tensors* related to either the reference or current configuration.

Infinitesimal strain tensor used in small strain analysis can be expressed in terms of the derivatives of displacement field as

$$\boldsymbol{\varepsilon} = \frac{1}{2} \left[\left(\frac{\partial \mathbf{u}}{\partial \mathbf{X}} \right) + \left(\frac{\partial \mathbf{u}}{\partial \mathbf{X}} \right)^T \right] \quad (\text{A.15})$$

The reason, why this tensor cannot be used in nonlinear mechanics is that for rigid body rotation this strain measure does not vanish. It means that stresses arise in the body during the rigid body rotation. For infinitesimal strains these stresses can be neglected but for large strain analysis this tensor is usually useless.

Material strain tensors are determined by the change along the length between two neighborhood point P and Q with the element vector $d\mathbf{X}$ which is located in material configuration, occurring during a motion to the new point P' and Q' with the element vector $d\mathbf{x}$, located in current configuration. The material and current elemental lengths squared to be determined as (see Figure A.1)

$$dL^2 = d\mathbf{X} \cdot d\mathbf{X}, \quad dl^2 = d\mathbf{x} \cdot d\mathbf{x} \quad (\text{A.16})$$

The change in the squared lengths that occurs as the body deform the reference to current configuration can be written in terms of the element material vector $d\mathbf{X}$ as

$$\begin{aligned} \frac{1}{2}(dl^2 - dL^2) &= (d\mathbf{x} \cdot d\mathbf{x} - d\mathbf{X} \cdot d\mathbf{X}) = \frac{1}{2}(\mathbf{F}d\mathbf{X} \cdot \mathbf{F}d\mathbf{X} - d\mathbf{X} \cdot d\mathbf{X}) \\ &= \frac{1}{2}(d\mathbf{X} \mathbf{F}^T \mathbf{F} d\mathbf{X} - d\mathbf{X} \cdot d\mathbf{X}) = d\mathbf{X} \cdot \frac{1}{2}(\mathbf{F}^T \mathbf{F} - \mathbf{I}) d\mathbf{X} \\ &= d\mathbf{X} \cdot \frac{1}{2}(\mathbf{C} - \mathbf{I}) d\mathbf{X} = d\mathbf{X} \cdot \mathbf{E} d\mathbf{X} \end{aligned} \quad (\text{A.17})$$

where \mathbf{C} is the *right Cauchy–Green strain tensor*, which is given in terms of the deformation gradient \mathbf{F} as

$$\mathbf{C} = \mathbf{F}^T \mathbf{F} \quad (\text{A.18})$$

Tensor \mathbf{E} is known as the *Green-Lagrange strain tensor*, which is given as

$$\mathbf{E} = \frac{1}{2}(\mathbf{C} - \mathbf{I}) \quad (\text{A.19})$$

Alternatively, **spatial strain tensors** are determined by the change in the squared lengths that occurs as the body deform the current to reference configuration can now be written in terms of the element spatial vector $d\mathbf{x}$ as

$$\frac{1}{2}(dL^2 - dl^2) = \frac{1}{2}(d\mathbf{x} \cdot d\mathbf{x} - d\mathbf{x} \cdot \mathbf{F}^{-T} \mathbf{F}^{-1} d\mathbf{x}) = d\mathbf{x} \cdot \frac{1}{2}(\mathbf{I} - \mathbf{b}^{-1}) d\mathbf{x} = d\mathbf{x} \cdot \mathbf{A} d\mathbf{x} \quad (\text{A.20})$$

where \mathbf{b} is *left Cauchy–Green strain tensor (or Finger deformation tensor)*, which is given in terms of the deformation gradient \mathbf{F} as

$$\mathbf{b} = \mathbf{F} \mathbf{F}^T \quad (\text{A.21})$$

Tensor \mathbf{A} is known as the *Almansi strain tensor (or Eulerian)*, which is given as

$$\mathbf{A} = \frac{1}{2}(\mathbf{I} - \mathbf{b}^{-1}) \quad (\text{A.22})$$

Tensor \mathbf{C} is related to the undeformed configuration Ω_0 and tensor \mathbf{b} is related to the deformed configuration Ω . Both tensors \mathbf{C} and \mathbf{b} are symmetric and positive definite, i.e. for every arbitrary non-zero vector and it holds that

$$\mathbf{C} = \mathbf{F}^T \mathbf{F} = (\mathbf{F}^T \mathbf{F})^T = \mathbf{C}^T \quad \text{and} \quad \mathbf{b} = \mathbf{F} \mathbf{F}^T = (\mathbf{F} \mathbf{F}^T)^T = \mathbf{b}^T \quad (\text{A.23})$$

$$\mathbf{x}^T \mathbf{C} \mathbf{x} > 0 \quad \text{and} \quad \mathbf{x}^T \mathbf{b} \mathbf{x} > 0 \quad (\text{A.24})$$

A.1.4. Structural tensor

For anisotropic materials we introduce the stretch vector $\lambda_{\mathbf{a}_\alpha}$ in the unit vector direction \mathbf{a}_α characterizing the α -th fiber direction in each point $\mathbf{X} \in \Omega_0$ which is defined by

$$\lambda_{\mathbf{a}_\alpha}(\mathbf{X}, t) = \mathbf{F}(\mathbf{X}, t) \mathbf{a}_\alpha \quad (\text{A.25})$$

with length $\lambda_\alpha = |\lambda_{\mathbf{a}_\alpha}|$ called stretch ratio or simply the stretch of a fiber. Then the square of λ is computed according to

$$\lambda_\alpha^2 = \lambda_{\mathbf{a}_\alpha} \cdot \lambda_{\mathbf{a}_\alpha} = \mathbf{F} \mathbf{a}_\alpha \cdot \mathbf{F} \mathbf{a}_\alpha = \mathbf{a}_\alpha \cdot \mathbf{C} \mathbf{a}_\alpha = \mathbf{C} : \mathbf{M}_\alpha \quad (\text{A.26})$$

in which $\mathbf{M}_\alpha = \mathbf{a}_\alpha \otimes \mathbf{a}_\alpha$ (with Cartesian components $(\mathbf{M}_\alpha)_{IJ} = a_{\alpha I} a_{\alpha J}$) is defined to be a *structural tensor* of order two in the reference configuration and $\alpha = 1$ with one fiber-reinforced composites (*transversely isotropic materials*) or $\alpha = 1, 2$ with two fiber-reinforced composites (*orthotropic hyperelastic materials*).

A.2. Stress tensors

Stress tensors for a deformable body undergoing a finite motion are presented in this section. A motion and deformations described by kinematics are generally caused by external forces acting on a body. Stress is firstly defined in the current configuration in the standard way as force per unit area. This leads to the well-known Cauchy stress tensor as used in linear analysis. In contrast to linear small displacement analysis, stress quantities that refer back to the initial body configuration can also be defined. This will be archived using work conjugate concepts that will lead to the Piola-Kirchhoff stress tensors.

A.2.1. Cauchy stress tensor and equilibrium equation

There exists unique second-order tensor field $\boldsymbol{\sigma}$ and \mathbf{P} so that

$$\mathbf{t} = \boldsymbol{\sigma} \mathbf{n} \quad \text{or} \quad t_i = \sigma_{ij} n_j \quad (\text{A.27})$$

where \mathbf{t} represents the *Cauchy traction vector* (force measures per unit surface area defined in the current configuration, Figure A.2), exerted on ds with outward normal \mathbf{n} , $\boldsymbol{\sigma}$ denotes a symmetric spatial tensor field called the **Cauchy stress tensor** (or Cauchy stress)

$$\boldsymbol{\sigma} = \boldsymbol{\sigma}^T \quad \text{or} \quad \sigma_{ij} = \sigma_{ji} \quad (\text{A.28})$$

In terms of Cartesian coordinates the Cauchy stress tensor $\boldsymbol{\sigma}$ is comprised of the components of the traction vectors on three mutually orthogonal planes:

$$\boldsymbol{\sigma} = [\sigma_{ij}] = \begin{bmatrix} \sigma_{11} & \sigma_{12} & \sigma_{13} \\ \sigma_{21} & \sigma_{22} & \sigma_{23} \\ \sigma_{31} & \sigma_{32} & \sigma_{33} \end{bmatrix} \quad (\text{A.29})$$

The equilibrium equation of a deformable body in the current configuration is expressed as

$$\text{div} \boldsymbol{\sigma} + \mathbf{f}_b = \mathbf{0} \quad \text{in } V \quad (\text{A.30})$$

where \mathbf{f}_b is a body force.

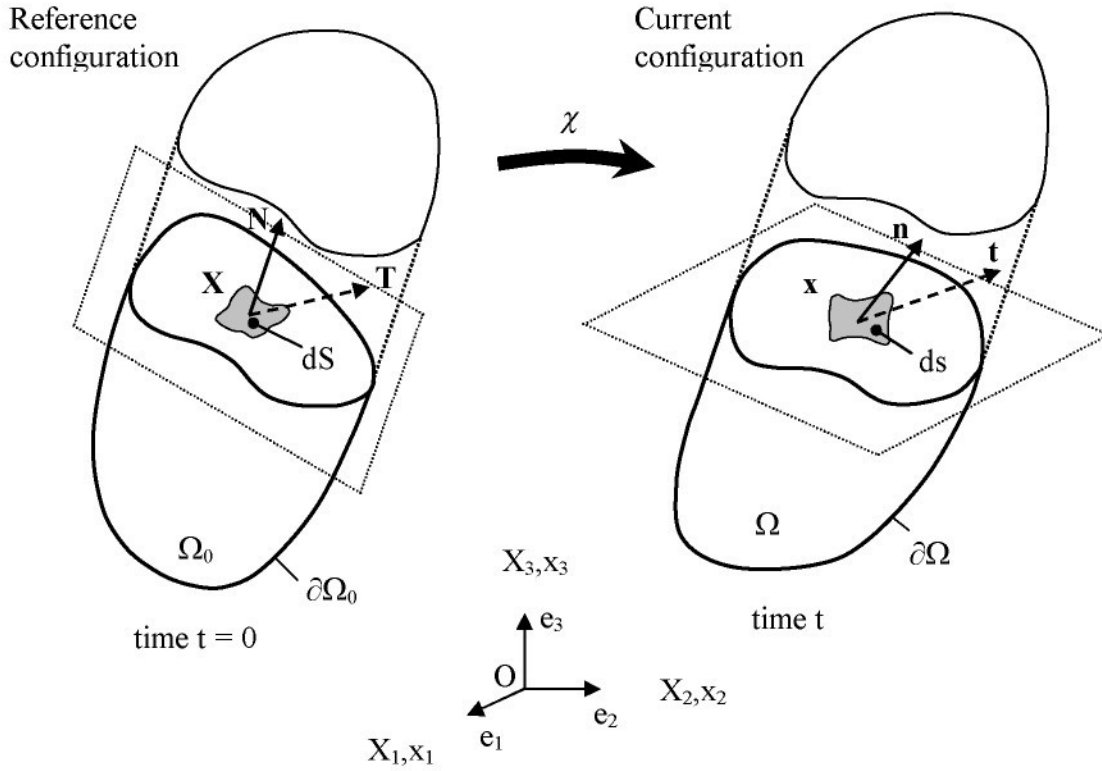


Figure A.2 – Traction vectors acting on infinitesimal surface elements

A.2.2. Alternative stress tensors

In the finite deformation theory we have to take into account the change of geometrical body and the stresses should be somehow related to strains. So if we are working with Green-Lagrange strain tensor (which is related to original configuration) we must defined stresses similarly with respect to original configuration. In this subsection the stress tensors used for practical nonlinear analysis are presented.

Most of their components do not have a direct physical interpretation. Often it is convenient to work with the so-called **Kirchhoff stress tensor** $\boldsymbol{\tau}$, which differs from the Cauchy stress tensor by the volume ratio J . It is a contravariant spatial tensor field parameterized by spatial coordinates, and is defined by

$$\boldsymbol{\tau} = J\boldsymbol{\sigma} \quad \text{or} \quad \tau_{ij} = J\sigma_{ij} \quad (\text{A.31})$$

The vector which described the *first Piola-Kirchhoff traction vector* (force measures per unit surface area defined in the reference configuration (Figure A.2)) can be expressed as following form

$$\mathbf{T} = \mathbf{P}\mathbf{N} \quad \text{or} \quad T_i = P_{ij}N_j \quad (\text{A.32})$$

in which \mathbf{N} is outward normal to boundary surface while \mathbf{P} characterizes a tensor field called the **first Piola-Kirchhoff stress tensor** (or Piola stress), in general, is not symmetric tensor.s

In the finite strain analysis, the Cauchy stress tensor is not the most suitable stress tensor, however it is the only one which is of interest from engineering point of view. The constitutive relations for finite strain follow from the equilibrium equations and the balance of energy. The relation between the Cauchy stress tensor $\boldsymbol{\sigma}$ and the first Piola-Kirchhoff stress tensor \mathbf{P} may be written in the form

$$\boldsymbol{\sigma} = J^{-1} \mathbf{P} \mathbf{F}^T \text{ or } \mathbf{P} = J \boldsymbol{\sigma} \mathbf{F}^{-T} \quad (\text{A.33})$$

The stress tensor work conjugate with the Green-Lagrange strain is the **second Piola-Kirchhoff stress tensor** \mathbf{S} which is related to the Cauchy stresses

$$\mathbf{S} = J \mathbf{F}^{-1} \boldsymbol{\sigma} \mathbf{F}^{-T} = \mathbf{F}^{-1} \mathbf{P} = \mathbf{S}^T \quad (\text{A.34})$$

with its inverse

$$\boldsymbol{\sigma} = J^{-1} \mathbf{F} \mathbf{S} \mathbf{F}^T \quad (\text{A.35})$$

It should be noted that the second Piola-Kirchhoff stress tensor has little physical meaning. The second Piola-Kirchhoff stress tensor is invariant under rigid-body motion. However, it plays an important role in expressing the basic principles of continuum mechanics.

The first and second Piola-Kirchhoff stress tensors are established basing on conservation of mass principle and mathematical consistent consideration accounting the forces which are transformed from one configuration to another. These tensors are independent on choosing a coordinate system and insensitive towards motion of total rigid bodies.

From equation of (A.34) a fundamental relationship between the first Piola-Kirchhoff stress tensor \mathbf{P} and symmetric second Piola-Kirchhoff stress tensor \mathbf{S} is

$$\mathbf{P} = \mathbf{F} \mathbf{S} \quad (\text{A.36})$$

A.2.3. Conjugate pairs of stress and strain tensors

The so-called energy conjugate stress and strain tensors play an important role in formulation of the internal energy of deformable bodies. The stress measures described in the previous sections can be used to express the internal energy of a body. However, if a decision is made about the use of a certain strain measure, the stress tensor to be used in combination can not be selected arbitrar. Therefore, choosing appropriate conjugate pairs of stress and strain tensors is needed.

The tensor which conjugates to the Green-Lagrange strain tensor \mathbf{E} is the second Piola-Kirchhoff stress tensor \mathbf{S}

$$\mathbf{S} = J \mathbf{F}^{-1} \boldsymbol{\sigma} \mathbf{F}^{-T} \Leftrightarrow \mathbf{E} = \frac{1}{2} (\mathbf{C} - \mathbf{I}) \quad (\text{A.37})$$

The stress tensor conjugates to the Almansi strain tensor is called **Hill's stress tensor** $J \mathbf{F}^T \boldsymbol{\sigma} \mathbf{F}$

$$J\mathbf{F}^T \boldsymbol{\sigma} \mathbf{F} \Leftrightarrow \mathbf{A} = \frac{1}{2}(\mathbf{I} - \mathbf{B}^{-1}) \quad (\text{A.38})$$

One of the conjugate pairs of stress and strain tensors above which is described by the Green-Lagrange strain tensor and the second Piola-Kirchhoff stress tensor is the best-known.

A.3. Balance principles

The fundamental balance principles, i.e. conservation of mass, the momentum balance principles and balance of energy, are valid in all branches of continuum mechanics. They are applicable to any particular material and must be satisfied for all time.

A.3.1. Conservation of mass

In non-relativistic physics mass cannot be produced or destroyed, so that the mass m of a body is a conserved quantity. Hence, if a particle has certain mass in the reference configuration it must stay the same during a motion. Additionally

$$\text{From the definition of the mass densities at the points } \mathbf{X} \text{ and } \mathbf{x} \text{ we can get}$$

$$dm(\mathbf{X}) = \rho_0 dV \quad \text{and} \quad dm(\mathbf{x}, t) = \rho(\mathbf{x}, t) dv \quad (\text{A.39})$$

Substituting equation (A.42) into (A.41) we obtain

$$\rho_0 dV = \rho(\mathbf{x}, t) dv \quad (\text{A.40})$$

By recalling $dv = JdV$ we can deduce that

$$\rho_0 = \rho J \quad (\text{A.41})$$

It represents the continuity mass equation in the material description which is the appropriate description in solid mechanics.

A.3.2. Momentum balance principles

The balance of linear momentum is postulated as

$$\frac{D}{Dt} \int_{\Omega} \rho \mathbf{v} dv = \frac{D}{Dt} \int_{\Omega_0} \rho_0 \mathbf{V} dV = \mathbf{F}(t) \quad (\text{A.42})$$

By computing the integral form of Cauchy's stress theorem and by using divergence theorem we find out **Cauchy's first equation of motion** in the local form with respect to the current configuration as

$$\text{div } \boldsymbol{\sigma} + \mathbf{b} = \rho \dot{\mathbf{v}} \quad \text{or} \quad \frac{\partial \sigma_{ij}}{\partial x_j} + b_i = \rho \dot{v}_i \quad (\text{A.43})$$

where $\boldsymbol{\sigma}$ is the Cauchy stress tensor, \mathbf{b} is the body force in the current configuration, \mathbf{v} is a spatial velocity field.

The equation of motion in the reference configuration is also obtained in the local form

$$\text{Div } \mathbf{P} + \mathbf{B} = \rho_0 \dot{\mathbf{V}} \quad \text{or} \quad \frac{\partial P_{ij}}{\partial X_j} + B_i = \rho_0 \dot{V}_i \quad (\text{A.44})$$

where \mathbf{P} is the first Piola-Kirchhoff stress tensor, \mathbf{B} is the body force in the reference configuration and \mathbf{V} denotes the material description of the velocity field.

The **balance of angular momentum** (or **balance of moment of momentum** or **balance of rotational momentum**) is given by

$$\frac{D}{Dt} \int_{\Omega} \mathbf{r} \times \rho \mathbf{v} dv = \frac{D}{Dt} \int_{\Omega_0} \mathbf{r} \times \rho_0 \mathbf{V} dV = \mathbf{M}(t) \quad (\text{A.45})$$

where \mathbf{r} is the position vector.

From the global form of balance of angular momentum in the current configuration and by means of Cauchy's stress theorem and the divergence theorem we are able to deduce the satisfaction of the Cauchy stress tensor to be symmetric, i.e.

$$\boldsymbol{\sigma}^T = \boldsymbol{\sigma} \quad \text{or} \quad \sigma_{ij} = \sigma_{ji} \quad (\text{A.46})$$

It is a local consequence of the balance of angular momentum, often referred to as Cauchy's second equation of motion.

A.3.3. Balance of mechanical energy

The balance of mechanical energy in the spatial description is a consequence of Cauchy's first equation of motion (balance of linear momentum) and described as following

$$\frac{D}{Dt} \int_{\Omega} \frac{1}{2} \rho \mathbf{v}^2 dv + \int_{\Omega} \boldsymbol{\sigma} : \mathbf{d} dv = \int_{\partial\Omega} \mathbf{t} \cdot \mathbf{v} ds + \int_{\Omega} \mathbf{b} \cdot \mathbf{v} dv \quad (\text{A.47})$$

where \mathbf{d} denotes the rate of deformation tensor.

It states that the rate of change of kinetic energy $\frac{1}{2} \rho \mathbf{v}^2$ of a mechanical system plus the rate of internal mechanical work done by internal stresses $\boldsymbol{\sigma}$ equals the rate of external mechanical work done on that system by surface traction \mathbf{t} and body force \mathbf{b} .

Equivalently to (A.47) we have the balance of mechanical energy

$$\frac{D}{Dt} \int_{\Omega_0} \frac{1}{2} \rho_0 \mathbf{V}^2 dV + \int_{\Omega_0} \mathbf{P} : \dot{\mathbf{F}} dV = \int_{\partial\Omega_0} \mathbf{T} \cdot \mathbf{V} dS + \int_{\Omega_0} \mathbf{B} \cdot \mathbf{V} dV \quad (\text{A.48})$$

in the material description.

A.3.4. Balance of energy in continuum thermodynamics

In many problems of physics and engineering both mechanical and thermal energy are essentially considered. A continuum which possesses both mechanical and thermal energy is called a thermodynamic continuum. In the case thermal power is added to a thermodynamic continuum, the rate of internal energy equals the sum of the rate of internal mechanical work and the rate of thermal work. Consequently, equation (A.47) becomes

$$\frac{D}{Dt} \int_{\Omega} \left(\frac{1}{2} \rho \mathbf{v}^2 + e_c \right) dv = \int_{\partial\Omega} (\mathbf{t} \cdot \mathbf{v} + q_n) ds + \int_{\Omega} (\mathbf{b} \cdot \mathbf{v} + r) dv \quad (\text{A.49})$$

where e_c is the internal energy per unit current volume and defined from

$$\dot{e}_c = \boldsymbol{\sigma} : \mathbf{d} - \text{div} \mathbf{q} + r \quad (\text{A.50})$$

in which \mathbf{q} is the so-called Cauchy heat flux (or true heat flux) defined per unit surface area in the spatial configuration.

Equation (A.49) is also known as the first law of thermodynamics in the spatial description.

The first law of thermodynamics in the material description reads

$$\frac{D}{Dt} \int_{\Omega_0} \left(\frac{1}{2} \rho_0 \mathbf{V}^2 + e \right) dV = \int_{\partial\Omega_0} (\mathbf{T} \cdot \mathbf{V} + Q_N) dS + \int_{\Omega_0} (\mathbf{B} \cdot \mathbf{V} + R) dV \quad (\text{A.51})$$

in which e is the internal energy per unit material volume and determined by

$$\dot{e} = \mathbf{P} : \dot{\mathbf{F}} - \text{Div} \mathbf{Q} + R \quad (\text{A.52})$$

It is referred as the local form of the balance of energy in the material description. Here \mathbf{Q} is the so-called Piola-Kirchhoff heat flux (or nominal heat flux) determining per unit surface area in the reference configuration.

In equations (A.49) and (A.50), q_n and Q_n denote heat fluxes, determining heat per unit time and per unit current and material surface area, respectively, whereas r and R denote heat sources per unit time and per unit current and material volume, respectively.

The first-order partial differential equation is due to Kirchhoff and holds at any particle of the body for all times.

Appendix B

ANISOTROPIC VISCOELASTIC MODELS

In this part we will show constitutive equations for anisotropic viscoelastic rubber-like composite derived by a free energy function and evolution equations of internal stress- and strain- like variables. Both of these formulations are formed by using the generalized Maxwell model. However, the linear evolution equations for overstresses are formulated by means of each branch of the Maxwell model equivalent to separate components of the total stress tensor (for example, Holzapfel & Gasser, 2001). On the other hand the evolution equations for inelastic strains are based on assuming parallel multiplicative decompositions of the deformation gradient into elastic and viscous (or inelastic) parts for both matrix and fiber phases (Nedjar, 2007 and Nguyen et al., 2007). The formulation in inelastic strains is proposed in the nonlinear viscoelastic theory far perturbations away from thermodynamic equilibrium (refer to Reese & Govindjee, 1998a, b).

B.1. Constitutive equations

B.1.1. The decomposition of the free energy function

To characterize a viscoelastic behavior of anisotropic materials the uniquely defined Helmholtz free-energy function Ψ was postulated, measured per unit reference volume.

In the following only homogeneous materials are considered, which means that the associated free-energy functions are independent of position in the medium. Therefore, in an isothermal condition, the value of the free energy can be determined by the changes of the $(1+n+m)$ variables, refer to Holzapfel & Gasser (2001) and Nguyen et al. (2007).

$$\Psi = \Psi(\mathbf{C}, \mathbf{M}_\alpha, \mathbf{\Gamma}_r), \quad \alpha = \overline{1, n}, r = \overline{1, m} \quad (\text{B.1})$$

where the right Cauchy-Green deformation tensor \mathbf{C} , n structural tensors \mathbf{M}_α denoting the n fiber orientations in the reference configuration and m (second order) internal state variables $\mathbf{\Gamma}_r$ (not accessible to direct observation). The internal variables $\mathbf{\Gamma}_r$ are considered as inelastic (viscous) strains akin to the strain measure \mathbf{C} .

From experimental observations of elastomeric materials it is known that their deformation response is almost isochoric in nature since the bulk modulus considerably exceeds the shear modulus, then the influence of the bulk viscosity on the stress field is small. For this physical reason it seems to be most beneficial to choose a decoupled representation of

the free-energy function Ψ which describes separately volumetric and distortional (or isochoric, or volume-preserving) contributions, therefore

$$\Psi(\mathbf{C}, \mathbf{M}_\alpha, \mathbf{\Gamma}_r) = \Psi_{vol}^{EQ}(J) + \Psi_{dis}(\bar{\mathbf{C}}, \mathbf{M}_\alpha, \bar{\mathbf{\Gamma}}_r) \quad (\text{B.2})$$

valid for some closed time interval $t \in [0, T]$. Here Ψ_{vol}^{EQ} represents the volumetric response to be fully elastic of sufficiently slow processes, while the second part Ψ_{dis} of the decoupled free energy describes the purely isochoric response. Furthermore $\bar{\mathbf{C}}$ and $\bar{\mathbf{\Gamma}}_r$ are the modified quantities of \mathbf{C} and $\mathbf{\Gamma}_r$, respectively, associated with volume-preserving deformations of the material and given by

$$\bar{\mathbf{C}} = J^{-2/3} \mathbf{C}, \quad \bar{\mathbf{\Gamma}}_r = J^{-2/3} \mathbf{\Gamma}_r \quad (\text{B.3})$$

Now we split the free energy Ψ_{dis} into

$$\Psi_{dis}(\bar{\mathbf{C}}, \mathbf{M}_\alpha, \bar{\mathbf{\Gamma}}_r) = \Psi_{iso}^{EQ}(\bar{\mathbf{C}}) + \Psi_{ani}^{EQ}(\bar{\mathbf{C}}, \mathbf{M}_\alpha) + \sum_{r=1}^m \Upsilon_{isor}^{NEQ}(\bar{\mathbf{C}}, \mathbf{M}_\alpha, \bar{\mathbf{\Gamma}}_r) \quad (\text{B.4})$$

where $\Psi_{iso}^{EQ}(\bar{\mathbf{C}}, \mathbf{M}_\alpha)$ and $\Psi_{ani}^{EQ}(\bar{\mathbf{C}}, \mathbf{M}_\alpha)$ describe the isotropic and anisotropic (isochoric) elastic response as $t \rightarrow \infty$ respectively, responsible for the *thermodynamic equilibrium state*, and $\Upsilon_{isor}^{NEQ}(\bar{\mathbf{C}}, \mathbf{M}_\alpha, \bar{\mathbf{\Gamma}}_r)$ which may be seen as dissipative potentials determine the viscoelastic contribution, responsible for the *thermodynamic non-equilibrium state* of the material.

The free energy function therefore becomes

$$\Psi = \Psi_{EQ} + \Psi_{NEQ} = \underbrace{\Psi_{vol}^{EQ}(J) + \Psi_{iso}^{EQ}(\bar{\mathbf{C}}) + \Psi_{ani}^{EQ}(\bar{\mathbf{C}}, \mathbf{M}_\alpha)}_{\text{equilibrium parts}} + \underbrace{\sum_{r=1}^m \Upsilon_{isor}^{NEQ}(\bar{\mathbf{C}}, \mathbf{M}_\alpha, \bar{\mathbf{\Gamma}}_r)}_{\text{non-equilibrium parts}} \quad (\text{B.5})$$

For a detailed discussion of this issue it can be referred to Holzapfel (2000), Holzapfel & Gasser (2001) and Reese & Govindjee (1998b).

B.1.2. Constitutive equations of stress responses

The stress response may directly be derived from the Clausius–Duhem inequality which only considers for the case of an isothermal condition as (see Truesdell & Noll, 1992 and Holzapfel, 2000)

$$\mathcal{D}_{int} = -\dot{\Psi} + \mathbf{S} : \frac{1}{2} \dot{\mathbf{C}} \geq 0 \quad (\text{B.6})$$

here \mathcal{D}_{int} the internal dissipation inequality, \mathbf{S} the second Piola–Kirchhoff stress tensor, a colon denotes the scalar product of two tensors, whereas the dot written above a quantity represents its material time derivative.

The second Piola–Kirchhoff are defined from

$$\mathbf{S} = 2 \frac{\partial \Psi}{\partial \mathbf{C}} \quad (\text{B.7})$$

For a detail on the derivation of constitutive equations for hyperelastic materials see, for example, Holzapfel (2000).

Due to the decoupled free energy function into equilibrium and non-equilibrium parts (B.5), therefore from equation (B.7) we can obtain the decoupled stress given by

$$\mathbf{S} = 2 \frac{\partial \Psi}{\partial \mathbf{C}} = 2 \frac{\partial}{\partial \mathbf{C}} (\Psi_{EQ} + \Psi_{NEQ}) = \mathbf{S}_{EQ} + \mathbf{S}_{NEQ} \quad (\text{B.8})$$

where

$$\mathbf{S}_{EQ} = 2 \frac{\partial \Psi_{EQ}}{\partial \mathbf{C}} \quad \text{and} \quad \mathbf{S}_{NEQ} = 2 \frac{\partial \Psi_{NEQ}}{\partial \mathbf{C}} \quad (\text{B.9})$$

Furthermore, it is advantageous to carry out a split of the equilibrium free energy into volumetric, isotropic and anisotropic (isochoric) parts, such that we have

$$\mathbf{S}_{EQ} = \mathbf{S}_{vol}^{EQ} + \mathbf{S}_{iso}^{EQ} + \mathbf{S}_{ani}^{EQ} = 2 \frac{\partial \Psi_{vol}^{EQ}}{\partial \mathbf{C}} + 2 \frac{\partial \Psi_{iso}^{EQ}}{\partial \mathbf{C}} + 2 \frac{\partial \Psi_{ani}^{EQ}}{\partial \mathbf{C}} \quad (\text{B.10})$$

B.1.2.1. Transversely isotropic materials

Numerous materials are composed of a matrix material and one or more families of fibers. These types of composites have strong directional properties and their mechanical responses are regarded as anisotropic. A material which is reinforced by only one family of fiber has a single preferred direction. The stiffness of this type of composite material in the fiber direction is typically much greater than in the directions orthogonal to the fibers. It is the simplest representation of material anisotropy, which we call **transversely isotropic** with respect to this preferred direction.

For a transversely isotropic material, the equilibrium free energy can finally be written in terms of the five independent scalar invariants $(I_1, I_2, I_3, I_4, I_5)$ of the right symmetric Cauchy-Green tensor \mathbf{C} and the structural tensor \mathbf{M}_1 , that $\mathbf{M}_1 = \mathbf{a}_0 \otimes \mathbf{a}_0$, describing the fiber direction. These invariants are defined as follows

$$\begin{aligned} I_1 &= \text{tr} \mathbf{C}, \quad I_2 = \frac{1}{2} \left[\text{tr} (\mathbf{C}^2) - (\text{tr} \mathbf{C})^2 \right] \\ I_3 &= \det \mathbf{C}, \quad I_4 = \mathbf{C} : \mathbf{M}_1, \quad I_5 = \mathbf{C}^2 : \mathbf{M}_1 \end{aligned} \quad (\text{B.11})$$

Therefore the free energy function is decoupled into

$$\Psi_{EQ}(I_1, I_2, I_3, I_4, I_5) = \Psi_{vol}^{EQ}(J) + \Psi_{iso}^{EQ}(\bar{I}_1, \bar{I}_2) + \Psi_{ani}^{EQ}(\bar{I}_4, \bar{I}_5) \quad (\text{B.12})$$

where \bar{I}_a are referred to as the modified invariants and are related to

$$\begin{aligned} \bar{I}_1 &= J^{-2/3} I_1, \quad \bar{I}_2 = J^{-4/3} I_2 \\ \bar{I}_4 &= J^{-2/3} I_4, \quad \bar{I}_5 = J^{-4/3} I_5 \end{aligned} \quad (\text{B.13})$$

Then, by use of the chain rule, the volumetric and isochoric parts of the second Piola-Kirchhoff equilibrium stress tensor are derived on the definitions (B.10)

$$\mathbf{S}_{vol}^{EQ} = 2 \frac{\partial \Psi_{vol}^{EQ}(J)}{\partial \mathbf{C}} = 2 \frac{\partial \Psi_{vol}^{EQ}(J)}{\partial J} \frac{\partial J}{\partial \mathbf{C}} = J \frac{\partial \Psi_{vol}^{EQ}(J)}{\partial J} \mathbf{C}^{-1} = J p \mathbf{C}^{-1} \quad (\text{B.14})$$

$$\mathbf{S}_{iso}^{EQ} = 2 \frac{\partial \Psi_{iso}^{EQ}(\bar{I}_1, \bar{I}_3)}{\partial \mathbf{C}} = 2 \sum_{a=1}^2 \frac{\partial \Psi_{iso}^{EQ}}{\partial \bar{I}_a} \left(\frac{\partial \bar{I}_a}{\partial \bar{\mathbf{C}}} : J^{-2/3} \mathbb{P}^T \right) \quad (\text{B.15})$$

$$\mathbf{S}_{ani}^{EQ} = 2 \frac{\partial \Psi_{ani}^{EQ}(\bar{I}_4, \bar{I}_5)}{\partial \mathbf{C}} = 2 \sum_{a=4}^5 \frac{\partial \Psi_{ani}^{EQ}}{\partial \bar{I}_a} \left(\frac{\partial \bar{I}_a}{\partial \bar{\mathbf{C}}} : J^{-2/3} \mathbb{P}^T \right) \quad (\text{B.16})$$

in which \mathbb{P}^T defines the transpose of the fourth-order tensor \mathbb{P} called as the **projection tensor** with respect to the reference configuration, therefore expressed through \mathbf{C} . The definition of the projection tensor \mathbb{P} is given by

$$\mathbb{P} = \mathbb{I} - \frac{1}{3} \mathbf{C}^{-1} \otimes \mathbf{C} \quad (\text{B.17})$$

where \mathbb{I} denotes the fourth-order unit tensor, $\mathbb{I}_{ijkl} = \delta_{ik} \delta_{jl}$, δ_{ij} is the **Kronecker delta**.

By using the fictitious second equilibrium Piola-Kirchhoff stress tensor $\bar{\mathbf{S}}_{EQ}$, which is here defined as

$$\bar{\mathbf{S}}_{EQ} = 2 \frac{\partial \Psi_{iso}^{EQ}}{\partial \bar{\mathbf{C}}} + 2 \frac{\partial \Psi_{ani}^{EQ}}{\partial \bar{\mathbf{C}}} = 2 \sum_{a=1}^2 \frac{\partial \Psi_{iso}^{EQ}}{\partial \bar{I}_a} \frac{\partial \bar{I}_a}{\partial \bar{\mathbf{C}}} + 2 \sum_{a=4}^5 \frac{\partial \Psi_{ani}^{EQ}}{\partial \bar{I}_a} \frac{\partial \bar{I}_a}{\partial \bar{\mathbf{C}}} \quad (\text{B.18})$$

Finally we arrive

$$\mathbf{S}_{EQ} = Jp\mathbf{C}^{-1} + J^{-2/3} \mathbb{P} : \bar{\mathbf{S}}_{EQ} \quad (\text{B.19})$$

with the constitutive equations for the **hydrostatic pressure** (or an indeterminate Lagrange multiplier) p and the fictitious second Piola-Kirchhoff stress $\bar{\mathbf{S}}_{EQ}$ defined by

$$p = \frac{d\Psi_{vol}^{EQ}(J)}{dJ} \quad (\text{B.20})$$

$$\bar{\mathbf{S}}_{EQ} = 2 \frac{\partial \Psi_{iso}^{EQ}(\bar{I}_1, \bar{I}_2, \bar{I}_4, \bar{I}_5)}{\partial \bar{\mathbf{C}}} = \bar{\gamma}_1 \mathbf{I} + \bar{\gamma}_2 \bar{\mathbf{C}} + \bar{\gamma}_4 \mathbf{M}_1 + \bar{\gamma}_5 (\mathbf{M}_1 \bar{\mathbf{C}} + \bar{\mathbf{C}} \mathbf{M}_1) \quad (\text{B.21})$$

with the response coefficients

$$\begin{aligned} \bar{\gamma}_1 &= 2 \left(\frac{\partial \Psi_{iso}^{EQ}}{\partial \bar{I}_1} + \bar{I}_1 \frac{\partial \Psi_{iso}^{EQ}}{\partial \bar{I}_2} \right), & \bar{\gamma}_2 &= -2 \frac{\partial \Psi_{iso}^{EQ}}{\partial \bar{I}_2} \\ \bar{\gamma}_4 &= 2 \frac{\partial \Psi_{iso}^{EQ}}{\partial \bar{I}_4}, & \bar{\gamma}_5 &= 2 \frac{\partial \Psi_{iso}^{EQ}}{\partial \bar{I}_5} \end{aligned} \quad (\text{B.22})$$

Note that in the case we assume incompressibility of the isotropic matrix material, i.e. $I_3 = 1$, we are able to postulate a free energy in terms of the remaining four independent invariants which is enhanced by an indeterminate *Lagrange multiplier* $p/2$ to be identified as a reaction pressure.

B.1.2.2. Two fiber-reinforced composite materials

In this section the constitutive equations for composite material with two families of fibers are presented. The matrix rubber-like material is assumed to be hyperelastic and reinforced by two families of fibers (textile cords). The preferential fiber directions in the

reference configuration are denoted by the unit vector fields \mathbf{a}_0 and \mathbf{b}_0 , relating with the structural tensors $\mathbf{M}_1 = \mathbf{a}_0 \otimes \mathbf{a}_0$ and $\mathbf{M}_2 = \mathbf{b}_0 \otimes \mathbf{b}_0$, respectively.

According to Holzapfel (2000) the strain energy function may be expressed in terms of set of principal invariants $I_1 \rightarrow I_8$. The first three invariants I_1 , I_2 and I_3 are presented in the isotropic case, the pseudo-invariants I_4, \dots, I_8 are associated with the anisotropy generated by the two families of fibers. By use of the decoupled representation of the equilibrium free energy we have

$$\Psi_{EQ}(\mathbf{C}, \mathbf{M}_1, \mathbf{M}_2) = \Psi_{vol}^{EQ}(J) + \Psi_{iso}^{EQ}(\bar{I}_1, \bar{I}_2, \bar{I}_4, \dots, \bar{I}_8) \quad (\text{B.23})$$

The invariants $I_1 \rightarrow I_3$ are identical to those from transversely isotropic materials in equation (B.11) and the remaining invariants are defined by

$$\begin{aligned} I_6 &= \mathbf{C} : \mathbf{M}_2, \quad I_7 = \mathbf{C}^2 : \mathbf{M}_2 \\ I_8 &= \text{tr}(\mathbf{C} \mathbf{M}_1 \mathbf{M}_2) \end{aligned} \quad (\text{B.24})$$

and these corresponding modified invariants are

$$\bar{I}_6 = J^{-2/3} I_6, \quad \bar{I}_7 = J^{-4/3} I_7, \quad \bar{I}_8 = J^{-2/3} I_8 \quad (\text{B.25})$$

Using arguments similar to those used for deriving the stress relation (B.19), we obtain the explicit expressions

$$\mathbf{S}_{EQ} = Jp\mathbf{C}^{-1} + J^{-2/3}\mathbb{P} : \bar{\mathbf{S}}_{EQ} \quad (\text{B.26})$$

where

$$\begin{aligned} \bar{\mathbf{S}}_{EQ} &= 2 \frac{\partial \Psi_{iso}^{EQ}(\bar{I}_1, \bar{I}_2, \bar{I}_4, \bar{I}_5)}{\partial \bar{\mathbf{C}}} = \bar{\gamma}_1 \mathbf{I} + \bar{\gamma}_2 \bar{\mathbf{C}} + \bar{\gamma}_4 \mathbf{M}_1 + \bar{\gamma}_5 (\mathbf{M}_1 \bar{\mathbf{C}} + \bar{\mathbf{C}} \mathbf{M}_1) + \\ &\quad + \bar{\gamma}_6 \mathbf{M}_2 + \bar{\gamma}_7 (\mathbf{M}_1 \bar{\mathbf{C}} + \bar{\mathbf{C}} \mathbf{M}_1) + \bar{\gamma}_8 (\mathbf{M}_1 \mathbf{M}_2 + \mathbf{M}_2 \mathbf{M}_1) \end{aligned} \quad (\text{B.27})$$

with the response coefficients

$$\begin{aligned} \bar{\gamma}_1 &= 2 \left(\frac{\partial \Psi_{iso}^{EQ}}{\partial \bar{I}_1} + \bar{I}_1 \frac{\partial \Psi_{iso}^{EQ}}{\partial \bar{I}_2} \right), \quad \bar{\gamma}_2 = -2 \frac{\partial \Psi_{iso}^{EQ}}{\partial \bar{I}_2} \\ \bar{\gamma}_4 &= 2 \frac{\partial \Psi_{iso}^{EQ}}{\partial \bar{I}_4}, \quad \bar{\gamma}_5 = 2 \frac{\partial \Psi_{iso}^{EQ}}{\partial \bar{I}_5}, \quad \bar{\gamma}_6 = 2 \frac{\partial \Psi_{iso}^{EQ}}{\partial \bar{I}_6} \\ \bar{\gamma}_7 &= 2 \frac{\partial \Psi_{iso}^{EQ}}{\partial \bar{I}_7}, \quad \bar{\gamma}_8 = \frac{\partial \Psi_{iso}^{EQ}}{\partial \bar{I}_8} \end{aligned} \quad (\text{B.28})$$

In one specific case of composite materials with two families of fibers if $\mathbf{a}_0 \cdot \mathbf{b}_0 = 0$, the two families of fibers have orthogonal directions. Then, this material is said to be **orthotropic** in the reference configuration with respect to the planes normal to the fibers and the surface in which the fibers lie. The Helmholtz free energy function is a function of first seven invariants.

All explicit expressions of principal invariants as well as modified invariants and the partial derivatives of them with respect to $\bar{\mathbf{C}}$ can be found out in Holzapfel (2000).

B.2. Evolution equations with internal variables

The existence of non-equilibrium states that do evolve with time is an essential feature of inelastic materials. The Maxwell model (a dashpot is arranged in series with a spring) and the Kelvin-Voigt model (a dashpot is arranged in parallel with a spring), two mechanical models known from linear viscoelasticity, are frequently used to discuss relaxation and creep behavior. In this work we only study the generalized Maxwell scheme with a free spring on one end and a Maxwell elements arranged in parallel. There are two possible way to formulate evolution equations which can be derived directly from this model depending on used internal variables, namely internal strain-like variables (inelastic strains) and internal stress-like variables (overstresses). The evolution equations have to satisfy with the inequality equation (B.6).

B.2.1. Internal stress-like variables

According to Holzapfel (2000) the split of the free energy function into equilibrium and non-equilibrium contributions whereas the equilibrium components of the free energy can be written in terms of invariants, in particular

$$\Psi = \Psi_{EQ}(I_\alpha) + \sum_{r=1}^m \Upsilon_{isor}^{NEQ}(\bar{\mathbf{C}}, \mathbf{M}_\alpha, \bar{\Gamma}_r) \quad (\text{B.29})$$

with $\alpha=1,2,\dots,5$; $\alpha=1$ for one fiber-reinforced composites and $\alpha=1,2,\dots,8$; $\alpha=1,2$ for two fiber-reinforced composites.

Therefore the second Piola-Kirchhoff stress tensor is also decomposed into equilibrium and non-equilibrium stress parts

$$\mathbf{S} = \mathbf{S}_{EQ} + \sum_{r=1}^m \mathbf{Q}_r \quad (\text{B.30})$$

here the internal variables $\mathbf{Q}_r, r=1,\dots,m$ are used to be akin to stress-like tensors, which are non-equilibrium stresses (or overstress) in the sense of non-equilibrium thermodynamics. They are to be interpreted as conjugate variables to Γ_r , with the *internal constitutive equations* $\mathbf{Q}_r = -2\partial\Upsilon_{isor}^{NEQ}/\partial\Gamma_r, r=1,\dots,m$. At thermodynamic equilibrium the viscoelastic anisotropic material responds as perfectly elastic recover the general finite anisotropic elasticity.

In order to consider different contributions of the matrix material and families of fibers on the non-equilibrium part, we divide the internal variables in

$$\mathbf{Q}_r = \sum_{\alpha=1, \alpha \neq 3}^{5 \text{ (or } 8)} \mathbf{Q}_{ra} \quad (\text{B.31})$$

Hence the evolution equations are assumed to be linear and formulated separately for each equilibrium isochoric stress contribution $\mathbf{S}_{iso\alpha}^{EQ}$ corresponding to each branch of the Maxwell model, as shown in Figure B.1, $\alpha = \overline{1,5}$ or $\overline{1,8}$ and $\alpha \neq 3$, as in the form

$$\dot{\mathbf{Q}}_{ra} + \frac{\mathbf{Q}_{ra}}{\tau_{ra}} = \beta_{ra} \dot{\mathbf{S}}_{isoa}^{EQ} \quad (\text{B.32})$$

for $r = 1, \dots, m$, where $\beta_{ra} \in [0, \infty)$ are given non-dimensional free-energy factors, which are associated with the relaxation times $\tau_{ra} \in (0, \infty)$. We assume a stress-free reference configuration which requires the stress values $\mathbf{Q}_{ra}|_{t=0} = \mathbf{0}$ to be zero at reference time $t=0$.

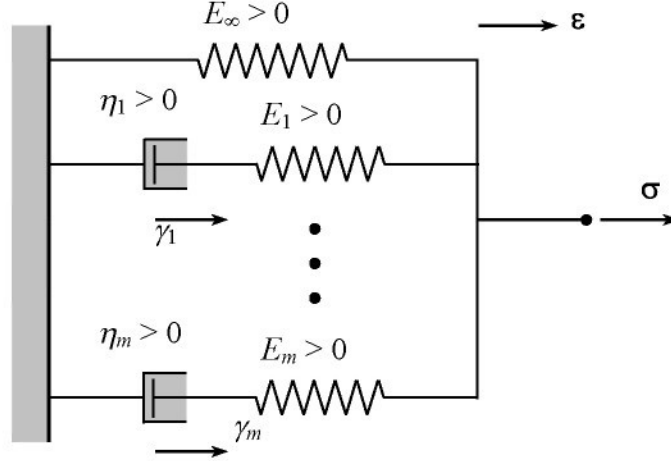


Figure B.1. The generalized rheological Maxwell model for internal stress-like variables

In equation (B.32) τ_{ra} and β_{ra} relate to material parameters in the viscoelastic model as

$$\tau_{ra} = \frac{\eta_r}{E_r} \quad \text{and} \quad \beta_{ra} = \frac{E_r}{E_\infty} \quad (\text{B.33})$$

B.2.2. Internal strain-like variables

As considering the over-stresses as internal variables by virtue of the linearized evolution equations, these models are restricted to small perturbations away from thermodynamic equilibrium, in this subsection the inelastic strains will therefore be considered as the internal variables.

The evolution equations of the internal-strain variables are formulated properly for two orthogonal fiber-families in Nguyen et al. (2007) and let us review constitutive equations in the following.

An essential assumption of the models is that both the fiber reinforcements and matrix can exhibit distinct time-dependent behavior. As such, the constitutive formulation attributes a different viscous stretch measure and free energy density to the matrix and fiber phases by assuming parallel multiplicative decompositions of the deformation gradient into elastic and

viscous (or inelastic) parts, refer to Diani et al. (2006), Nguyen et al. (2007). This decomposition introduces the so-called inelastic intermediate configuration as sketched in Figure B.2,

$$\mathbf{F} = \mathbf{F}_M^e \mathbf{F}_M^v = \mathbf{F}_F^e \mathbf{F}_F^v \quad (\text{B.34})$$

where the M, F subscripts represent respectively the matrix and fiber phases. From this, the elastic and viscous right and left Cauchy–Green deformation tensors can be defined for the matrix and fiber phases as

$$\mathbf{C}_M^e = (\mathbf{F}_M^e)^T \mathbf{F}_M^e, \mathbf{C}_M^v = (\mathbf{F}_M^v)^T \mathbf{F}_M^v, \mathbf{C}_F^e = (\mathbf{F}_F^e)^T \mathbf{F}_F^e, \mathbf{C}_F^v = (\mathbf{F}_F^v)^T \mathbf{F}_F^v \quad (\text{B.35})$$

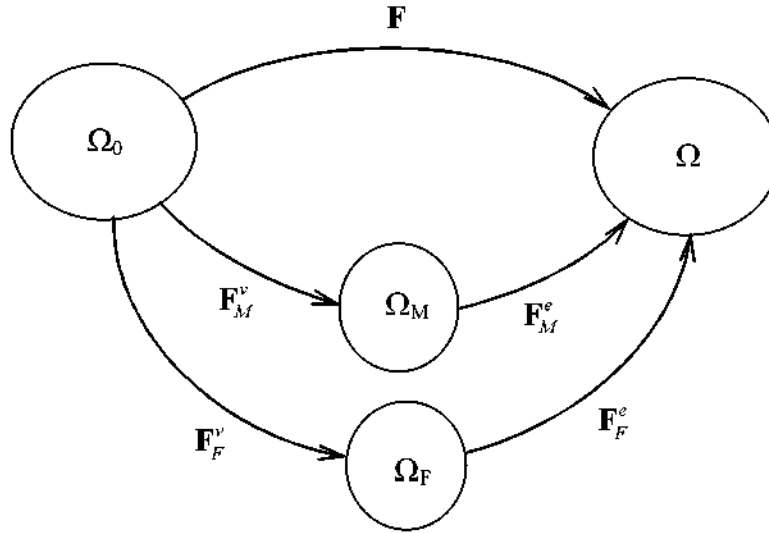


Figure B.2 – Multiplicative decomposition of deformation gradient

In addition, the free energy function is postulated as an isotropic function of the objective Cauchy–Green deformation tensor \mathbf{C} , the structural tensors denoting the fiber orientations \mathbf{M}_α in the reference configuration, and internal state variables ($m=2$) $\mathbf{\Gamma}_1 = \mathbf{C}_M^v$ and $\mathbf{\Gamma}_2 = \mathbf{C}_F^v$ for the viscous relaxation of the matrix and fiber phases. The free energy function is additively assumed to be split into an equilibrium and non-equilibrium contributions and then both the equilibrium and non-equilibrium components of the free energy function are decomposed further into isotropic and anisotropic components in terms of invariants (this formulation is analogous to the rheological model shown in Figure B.3)

$$\Psi(\mathbf{C}, \mathbf{M}_\alpha, \mathbf{F}_M^v, \mathbf{F}_F^v) = \underbrace{\Psi_M^{EQ}(\mathbf{C}) + \Psi_F^{EQ}(\mathbf{C}, \mathbf{M}_\alpha)}_{\text{Equilibrium parts}} + \underbrace{\Psi_M^{NEQ}(\mathbf{C}_M^e) + \Psi_F^{NEQ}(\mathbf{C}_F^e)}_{\text{Non-equilibrium parts}} \quad (\text{B.36})$$

For a composite material with two fiber-families the components of the free energy are expressed as isotropic functions of invariants

$$\begin{aligned} \Psi_M^{eq} &= \Psi_M^{eq}(I_1, I_2, I_3), & \Psi_F^{eq} &= \Psi_F^{eq}(I_4, I_5, I_6, I_7, I_8) \\ \Psi_M^{neq} &= \Psi_M^{neq}(I_{M_1}^e, I_{M_2}^e, I_{M_3}^e), & \Psi_F^{neq} &= \Psi_F^{neq}(I_{F_4}^e, I_{F_5}^e, I_{F_6}^e, I_{F_7}^e, I_{F_8}^e) \end{aligned} \quad (\text{B.37})$$

in which I_1, \dots, I_8 are the invariants of \mathbf{C} , $I_{M_1}, I_{M_2}, I_{M_3}$ are invariants of \mathbf{C}_M^e in the matrix phase, I_{F_4}, \dots, I_{F_8} are invariants of \mathbf{C}_F^e in the fiber phase and given by

$$\begin{aligned}
 I_{M_1}^e &= \mathbf{C}_M^e : \mathbf{I} = \mathbf{C} : \mathbf{C}_M^{v^{-1}}, \\
 I_{M_2}^e &= \frac{1}{2} \left(I_{M_1}^{e^2} - \mathbf{C}_M^{e^2} : \mathbf{I} \right) = \frac{1}{2} \left(I_{M_1}^{e^2} - \mathbf{C} \mathbf{C}_M^{v^{-1}} : \mathbf{C} \mathbf{C}_M^{v^{-1}} \right) \\
 I_{M_3}^e &= \det \mathbf{C}_M^e = \det \left(\mathbf{C} \mathbf{C}_M^{v^{-1}} \right) \\
 I_{F_4}^e &= \mathbf{C}_F^e : \tilde{\mathbf{M}}_1 = \frac{\mathbf{C} : \mathbf{M}_1}{\mathbf{C}_F^v : \mathbf{M}_1}, \quad I_{F_5}^e = \mathbf{C}_F^{e^2} : \tilde{\mathbf{M}}_1 = \frac{\mathbf{C} \mathbf{C}_F^{v^{-1}} \mathbf{C} : \mathbf{M}_1}{\mathbf{C}_F^v : \mathbf{M}_1} \\
 I_{F_6}^e &= \mathbf{C}_F^e : \tilde{\mathbf{M}}_2 = \frac{\mathbf{C} : \mathbf{M}_2}{\mathbf{C}_F^v : \mathbf{M}_2}, \quad I_{F_7}^e = \mathbf{C}_F^{e^2} : \tilde{\mathbf{M}}_2 = \frac{\mathbf{C} \mathbf{C}_F^{v^{-1}} \mathbf{C} : \mathbf{M}_2}{\mathbf{C}_F^v : \mathbf{M}_2} \\
 I_{F_8}^e &= \text{tr} \left(\mathbf{C}_F^e \tilde{\mathbf{M}}_1 \tilde{\mathbf{M}}_2 \right) = \frac{\mathbf{M}_1 \mathbf{C} : \mathbf{C}_F^v \mathbf{M}_2}{(\mathbf{C}_F^v : \mathbf{M}_1)(\mathbf{C}_F^v : \mathbf{M}_2)}
 \end{aligned} \tag{B.38}$$

where $\tilde{\mathbf{M}}_\alpha$ are the structural tensors in the intermediate configuration, $\alpha = 1, 2$.

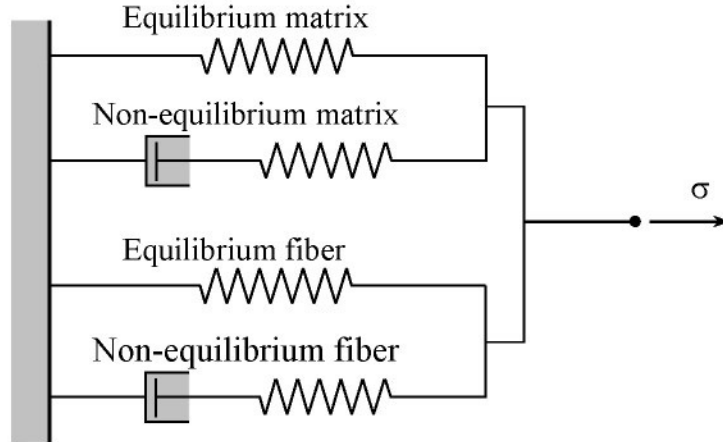


Figure B.3 – Rheological equivalent Mawell model for internal strain-like variables

The evolution equation for \mathbf{C}_M^v is proposed to satisfy (B.6) respectively for the matrix phase as

$$\frac{1}{2} \dot{\mathbf{C}}_M^v = \mathbb{V}_M^{-1} : \mathbf{T}_M \tag{B.39}$$

$$\mathbb{V}_M^{-1} = \frac{1}{2\eta_{M_s}} \left(\mathbf{C}_M^v \odot \mathbf{C}_M^v - \frac{1}{3} \mathbf{C}_M^v \otimes \mathbf{C}_M^v \right) + \frac{1}{9\eta_{M_b}} \mathbf{C}_M^v \otimes \mathbf{C}_M^v \tag{B.40}$$

$$\mathbf{T}_M = -2 \frac{\partial \Psi_M^{neq}}{\partial \mathbf{C}_M^v} \tag{B.41}$$

where $(\mathbf{C}_M^v \odot \mathbf{C}_M^v)_{IJKL} = \frac{1}{2}(\mathbf{C}_{M_{IK}}^v \mathbf{C}_{M_{JL}}^v + \mathbf{C}_{M_{IL}}^v \mathbf{C}_{M_{JK}}^v)$ and η_{M_B} and η_{M_S} are, respectively, the bulk and shear viscosities of the matrix material. The parameter \mathbb{V}_M^{-1} is the inverse of a positive-definite, fourth-order, major and minor symmetric tensor.

The evolution equation (B.39) for describing a viscous behavior of the matrix phase was also proven to be identical to the evolution equation proposed by Reese & Govindjee (1998a, b) for isotropic nonlinear viscoelasticity, see Nguyen et al. (2007).

The evolution equation for \mathbf{C}_F^v of the fiber phase applying to the two orthogonal fiber-families proposed to fulfill the satisfaction of the positive dissipation criteria for the fiber phase is

$$\frac{1}{2} \dot{\mathbf{C}}_F^v = \mathbb{V}_F^{-1} : \mathbf{T}_F \quad (\text{B.42})$$

$$\mathbb{V}_F^{-1} = \sum_{\alpha=1}^2 \frac{1}{4\eta_{F_\alpha}} (\mathbf{M}_\alpha \mathbf{C}_F^v + \mathbf{C}_F^v \mathbf{M}_\alpha) \otimes (\mathbf{M}_\alpha \mathbf{C}_F^v + \mathbf{C}_F^v \mathbf{M}_\alpha) \quad (\text{B.43})$$

$$\mathbf{T}_F = -2 \frac{\partial \Psi_F^{neq}}{\partial \mathbf{C}_F^v} \quad (\text{B.44})$$

where \mathbb{V}_F^{-1} is also the inverse of a positive-definite, fourth-order, isotropic tensor possessing both major and minor symmetry and related directly to the fiber viscosities η_{F_α} and the fiber arrangement.

Note that, for the case of two non-orthogonal fiber families the evolution equations are still used by means of defining orthogonal direction vectors

$$\hat{\mathbf{P}}_1 = \frac{\mathbf{P}_1 + \mathbf{P}_2}{\|\mathbf{P}_1 + \mathbf{P}_2\|} \text{ and } \hat{\mathbf{P}}_2 = \frac{\mathbf{P}_1 - \mathbf{P}_2}{\|\mathbf{P}_1 - \mathbf{P}_2\|} \quad (\text{B.45})$$

Appendix C

IMPLEMENTATION OF USER MATERIAL MODELS IN COMSOL MULTIPHYSICS

C.1. Definition of modules for viscoelastic problems

“*Structural Mechanics Module*” and “*PDE Modes*” modules are included in the project, as shown in Figure C.1, for solving a viscoelastic response of composite structures. The “*Structural Mechanics Module*” is applied for studying all mechanical problems in 2D, 3D and axial symmetrical coordinate systems. The “*PDE Modes*” is utilized to solve partial differential equations, namely herein evolution equations of internal variables (inelastic strains or overstresses).

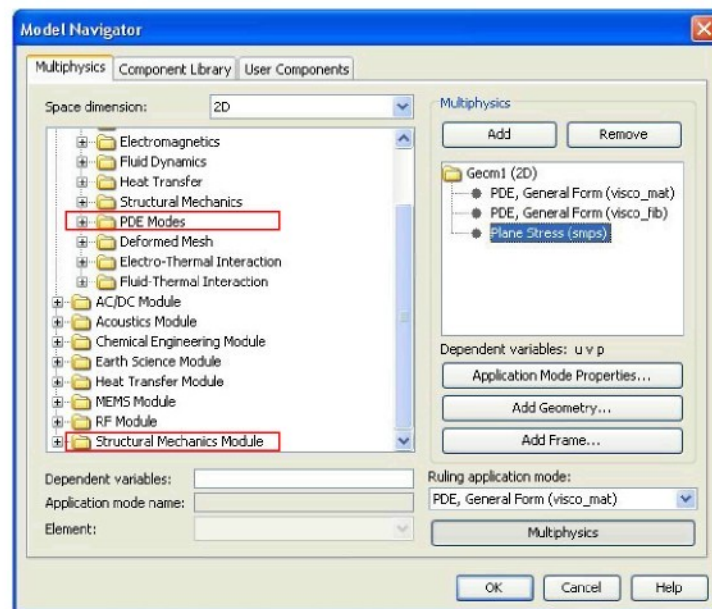



Figure C.1 – Define “*Structural Mechanics Module*” and “*PDE Modes*” modules

C.2. Definition of constitutive equations

To define constitutive equations in COMSOL, first we can write all equations in txt files then we import directly these files in a “*Global Expressions*” table via an icon open  as in Figure C.2.

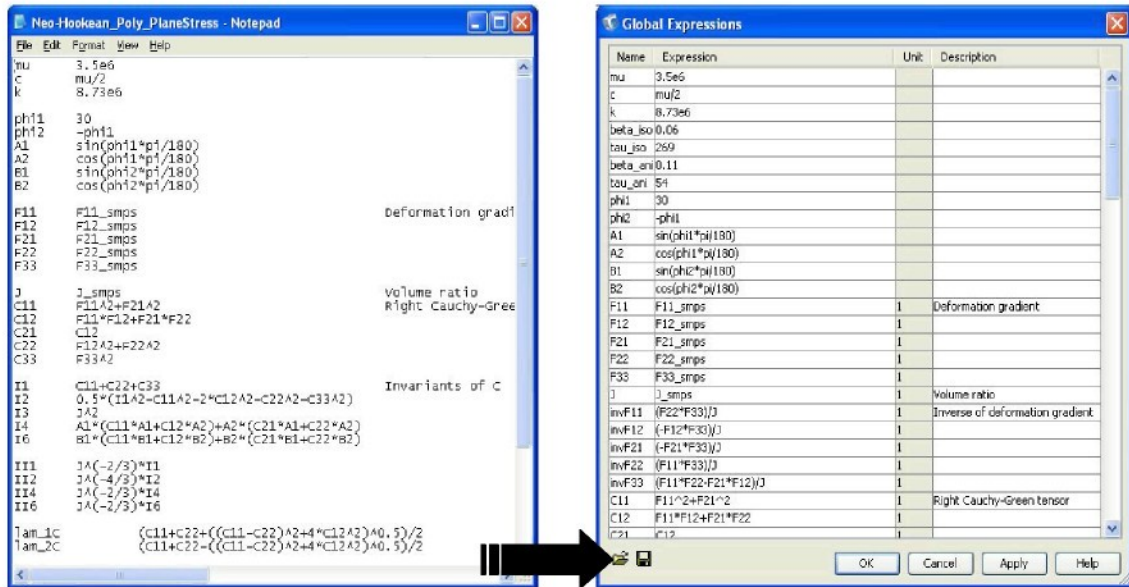


Figure C.2 – Define constitutive equations in “Global Expressions”

C.3. Redefine free energy functions

We must change the definition of free energy function to be suitable to a model which we need. It can be easily performed in a “Subdomain Settings – Equation System” table shown in Figure C.3.

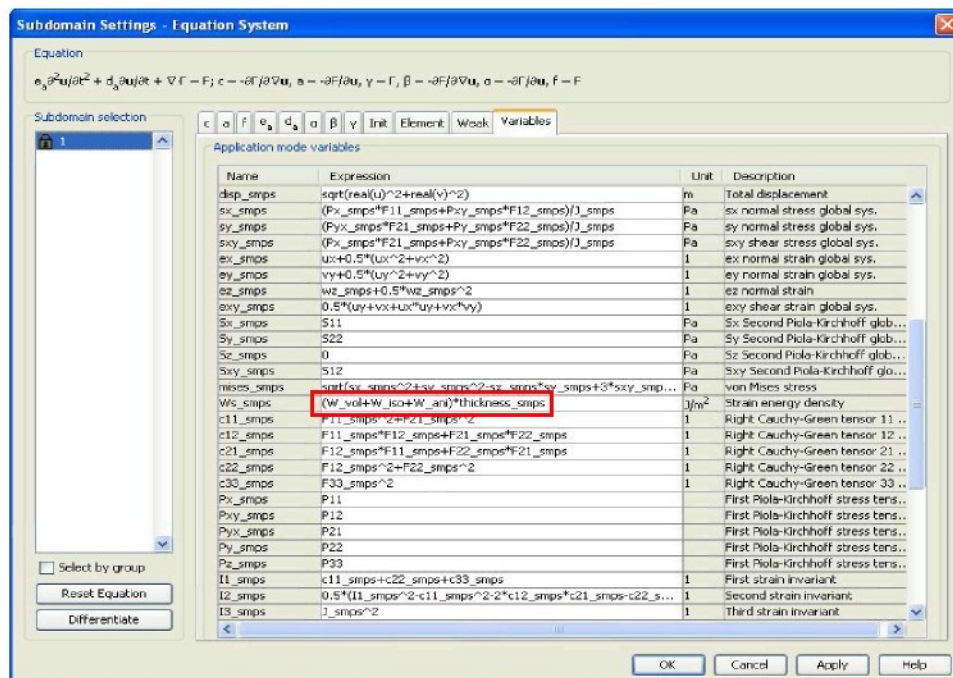


Figure C.3 – Modify the definition of free energy function

C.4. Formulation of evolution equations

Evolution equations of internal variables need to formulate in the “*PDE Modes*” by means of “*Subdomain Settings - PDE, General Form*” as denoted in Figure C.4.

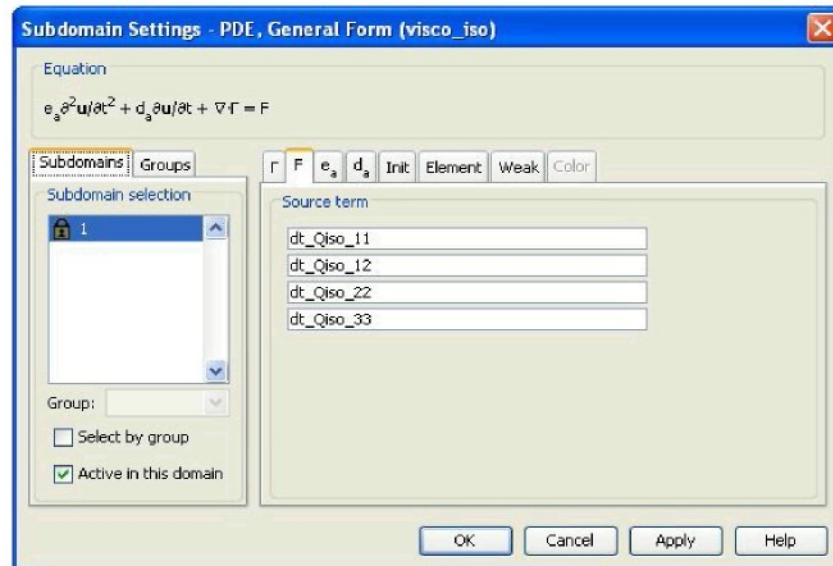


Figure C.4 – Formulate evolution equations

C.5. Define a function in COMSOL

In order to create a controlled step load we use a mode of defining function in COMSOL, shown in Figure C.5.

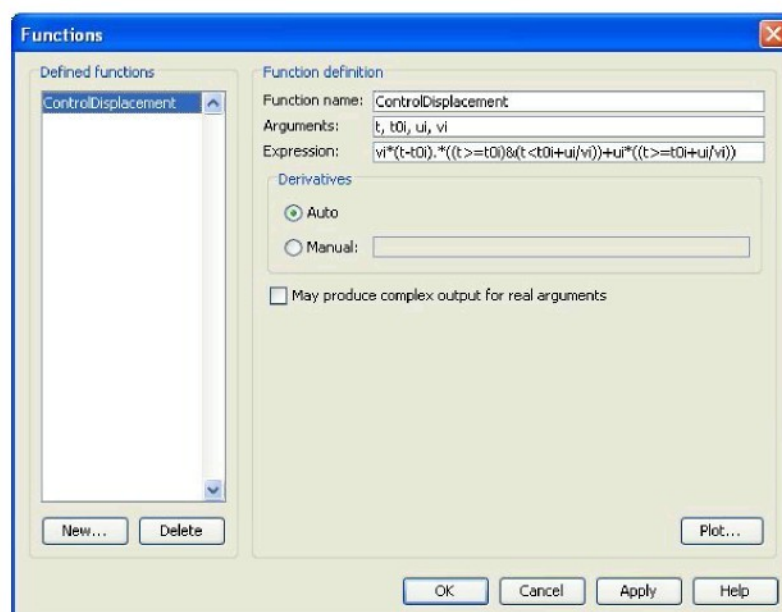


Figure C.5 – Define a user function

C.6. Integration of volume

“Integration Coupling Variables” on a boundary is applied to calculate a volume inside an air-spring tube in which the expression of integral is defined as a scalar quantity as can see in Figure C.6.

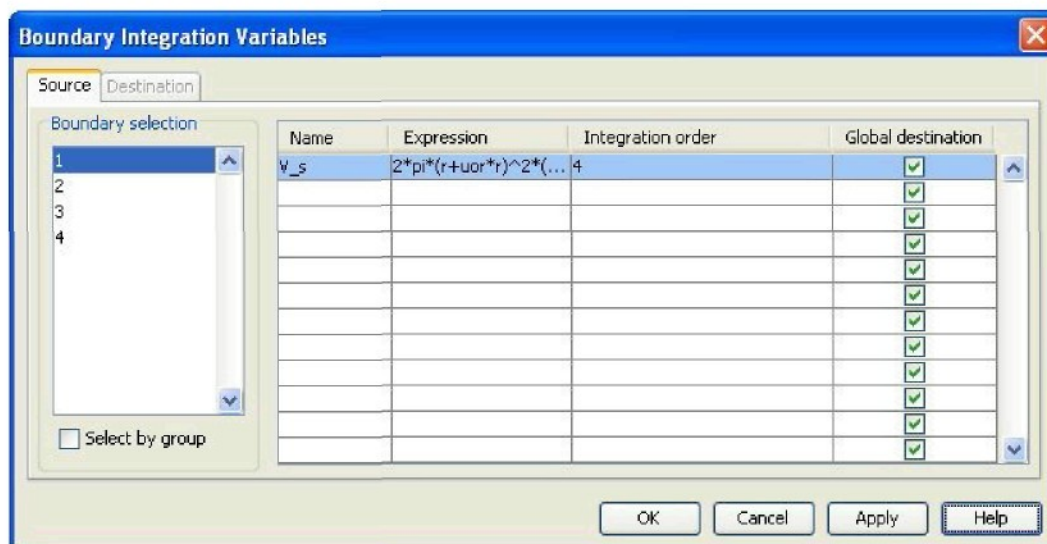


Figure C.6 – Integral volume of an air-spring tube

Appendix D

SOME M-FUNCTION AND SCRIPT FILES IN MATLAB®

In this appendix we would like to show some typical functions programmed in Matlab in order to attend to evaluate all material parameters basing on the experimental data. One evaluation process is apportioned to three steps including: Analyzing data, estimating purely elastic parameters and estimating viscoelastic parameters. While each evaluating step is separated into many functions to conveniently manage.

D.1. Some functions of analyzing data

D.1.1. “ConnectDataSteps” function

Due to the data amount in each relaxation experiment is quite big therefore the experimental performance is split into many steps. Hence this function has a task to connect many experimental steps together and seek equilibrium forces corresponding to every step.

```
function [gdata,data_eq,data_rel]=ConnectDataSteps(angle,fileload,filestrain,step,A0)

gdata = [];
data_end = [0,0,0];
for i = 1:length(fileload)
    data = load(fileload{i});
    data(:,1) = data_end(1) + data(:,1);
    data(:,2) = data_end(2) + data(:,2);
    data(:,3) = data_end(3) + data(:,3);
    gdata = [gdata; data];
    data_end = gdata(end,:);
end
gdata = gdata(1:500:end,:);
data_str = load(filestrain);
e1 = data_str(:,1);
lam1 = 1+e1*1e-3;

i = 0;
k = 1;
j = 1;
data_eq = [0];
temp = [];
data_rel = [];
while i<size(gdata,1)
    i = i+1;
    if gdata(i,2)>k*step
        k = k+1;
        data_eq = [data_eq;F_eq];
        j=1;
        row_st = [size(temp,1),angle;lam1(k),0];
        data_rel = [data_rel;row_st];
        data_rel = [data_rel;temp];
        temp = [];
    end
    if gdata(i,2) == k*step
```

```
F_eq = gdata(i,3);
stress = gdata(i,3)*lam1(k+1)/A0;
temp(j,:) = [gdata(i,1),stress];
j = j+1;
end
end
data_eq = [data_eq;F_eq];
lam1 = lam1(1:length(data_eq));
data_eq = data_eq.*lam1/A0;
data_eq = [lam1,data_eq];
row_st = [size(temp,1),angle;lam1(k+1),0];
data_rel = [data_rel;row_st];
data_rel = [data_rel;temp];
```

D.1.2. Main program of analyzing data

Applying the “ConnectDataSteps” function to connect, analyze and save experimental data in “*mat*” files.

```
clc; clear all;
A0 = 4.5*220; %Cross-section area of specimen [mm2]

%angle = 30;
%name_step = [12];
angle = [40,50,60]'; %Angle of fibers
name_step = [12,34];
step_disp = 1;

Xdat = [];
for st = 1:length(angle)
for i=1:length(name_step)
file_load{i}=strcat('MVL_f',num2str(angle(st)),'_step',...
num2str(name_step(i)),'.txt');
end
file_strain = strcat('Strain_Fiber',num2str(angle(st)),'.txt');

[data_load,data_eq,data_rel] = ConnectDataSteps(angle(st),file_load,file_strain,step_disp,A0);

fileload = strcat('Loading_Fiber',num2str(angle(st)));
fileequilibrium = strcat('Equil_StretchStress_Fiber',num2str(angle(st)));
filerelax = strcat('Relax_TimeStress_Fiber',num2str(angle(st)));
save(fileload,'data_load');
save(fileequilibrium,'data_eq');
save(filerelax,'data_rel');
figure(1); hold on;

plot(data_eq(:,1),data_eq(:,2),'-r*');

end
```

D.2. Estimation of purely elastic coefficients

D.2.1. “VolStress” function

We use this function to calculate the volumetric stress contribution.

```
function s_vol = VolStress(coef,lam1)
```

```
c = coef(1);  
s_vol = -2*D./(lam1.^2);
```

D.2.2. “IsoStress” function

We use this function to calculate the isotropic (isochoric) stress contribution.

```
function s_iso = IsoStress(coef,lam1)  
  
c = coef(1);  
s_iso = 2*c*lam1.^2;
```

D.2.3. “AniStress” function

We use this function to calculate the anisotropic (isochoric) stress contribution.

```
function s_anis = AniStress(coef,lam1,phi)  
  
k = coef(2);  
a01 = cos(phi*pi/180);  
a02 = sin(phi*pi/180);  
  
I4 = lam1.^2.*a01.^2+a02.^2;  
s_anis = 4*k*lam1.^2.*(I4-1).*a01.^2;
```

D.2.4. “FitElasticParameter” function

In order to use it for evaluating elastic material parameters by means of the linear least square method.

```
function [coef,fval,error] = FitElasticParameter(Xdat)  
  
data = Xdat;  
index = 0;  
yreal = [];  
while (isempty(data)==0)  
    n = data(1,1);  
    beta = data(1,2);  
    lam1 = data(2:n+1,1);  
    yreal = [yreal;data(2:n+1,2)];  
    a01 = cos(beta*pi/180);  
    a02 = sin(beta*pi/180);  
  
    for i = 1:length(lam1)  
        I4 = lam1(i)^2*a01^2+a02^2;  
        A(i+index,1) = 2*(lam1(i)^2-1/lam1(i)^2);  
        A(i+index,2) = 4*lam1(i)^2*(I4-1)*a01^2;  
    end  
  
    index = index+n;  
    data = data(n+2:end,:);  
end  
coef = A\yreal;
```

```
fval = yreal - A*coef;  
error = sum(abs(fval))/sum(abs(yreal))*100;
```

D.2.5. The main program of evaluation of purely elastic parameters

```
%This evaluation uses Neo-Hookean model for the isotropic part and polynomial function for the  
anisotropic part  
clc; clear all;  
  
angle = [30,40,50,60];  
Xdat = [];  
for st = 1:length(angle)  
    fileequilibrium = strcat('Equil_StretchStress_Fiber',num2str(angle(st)));  
    load(fileequilibrium);  
    row_add = [size(data_eq,1),angle(st)];  
    Xdat = [Xdat;row_add;data_eq];  
end  
  
[coef_elas,fval,err] = FitElasticParameterter(Xdat);  
save('NeoHookean_Polynomial','coef_elas');  
  
muy=2*coef_elas(1);  
  
style_point = {'*r','sm','oc','vb','<k'};  
style_line = {'-r','-m','-c','-b','-k'};  
  
figure;  
hold on; %title('Data points');  
grid on;  
Ydat = Xdat;  
step = 0;  
while (isempty(Ydat)==0)  
    step = step + 1;  
    n = Ydat(1,1);  
    beta = Ydat(1,2);  
    lam1 = Ydat(2:n+1,1);  
    y_real = Ydat(2:n+1,2);  
    plot(lam1,y_real(:,1),style_point{step});  
    Ydat = Ydat(n+2:end,:);  
end  
  
lamlap = [linspace(1,1.13,30)]';  
for i=1:length(angle)  
    beta = angle(i);  
    yap =  
    VolStress(coef_elas,lamlap)+IsoStress(coef_elas,lamlap)+AniStress(coef_elas,lamlap,beta);  
    plot(lamlap,yap,style_line{i},'linewidth',2);  
end  
xlabel('The first principal stretch \lambda_1');  
ylabel('The first principal stress \sigma_1 [MPa]');
```

D.3. Estimation of viscoelastic coefficients

D.3.1. “OverStress” function

We program it to define overstress components


```
function Q = OverStress(beta,s_eq,tau,time)

Q = beta*s_eq*exp(-time/tau);
```

D.3.2. “FitLinearViscousCoeff” function

We program it for fitting linear viscous coefficients.

```
function [fval,coef_lin] = FitLinearViscousCoeff(coef_nonlin,Xdat,coef_m,scale_coef)
taul = coef_nonlin;
tau2 = taul/scale_coef(2);
data = Xdat;
index = 0;
q_real = [];
A = [];
while (isempty(data)==0)
    n = data(1,1);
    phi = data(1,2);
    lam1 = data(2,1);
    time = data(3:n+2,1);
    time = time-time(1);
    s_iso = IsoStress(coef_m,lam1);
    s_vol = VolStress(coef_m,lam1);
    s_anis = AniStress(coef_m,lam1,phi);
    q_real = [q_real;data(3:n+2,2)-s_vol-s_iso-s_anis];

    Ai = [s_iso*exp(-time/taul)+1/scale_coef(1)*s_anis*exp(-time/tau2)];
    A = [A;Ai];

    index = index+n;
    data = data(n+3:end,:);
end

coef_lin = A\q_real;
fval = q_real-A*coef_lin;
```

D.3.3. “FitViscousParameterter” function

We use it for evaluating all viscous parameters in which non-linear viscous coefficients are estimated by the nonlinear least square method.

```
function [coef,fval] = FitViscousParameterter(Xdat,coef_m,scale_coef)

coef_0 = [1];
fobj = @(x) norm(FitLinearViscousCoeff(x,Xdat,coef_m,scale_coef));
coef_nonlin = lsqnonlin(fobj,coef_0);
[fval,coef_lin] = FitLinearViscousCoeff(coef_nonlin,Xdat,coef_m,scale_coef);
coef = [coef_lin;coef_nonlin];
```

D.3.4. Main program of evaluation of viscoelastic material parameters

```
clc; clear all;
```

```
load 'NeoHookean_Polynomial';

angle = [30,40,50,60];
Xdat = [];
for st = 1:length(angle)
    fileequilibrium = strcat('Relax_TimeStress_Fiber',num2str(angle(st)));
    load(fileequilibrium);
    Xdat = [Xdat;data_rel];
end

scale_tau = 5;
scale_beta = 1/2;
scale_coef = [scale_beta;scale_tau];
coef_vis = FitViscousParameterter(Xdat,coef_elas,scale_coef);
beta1 = coef_vis(1);
beta2 = beta1/scale_beta;
tau1 = coef_vis(2);
tau2 = tau1/scale_tau;

style_point = {'*r','sm','oc','vb','<k'};
style_line = {'-r','-m','-c','-k','-y'};

for st = 1:length(angle)
    fileequilibrium = strcat('Relax_TimeStress_Fiber',num2str(angle(st)));
    load(fileequilibrium);
    data = data_rel;
    time = [];
    s_real = [];
    index = 0;
    s_app = [];
    while (isempty(data)==0)
        n = data(1,1);
        phi = data(1,2);
        lam1 = data(2,1);
        t_step = data(3:n+2,1)-data(3,1);
        time = [time;data(3:n+2,1)];
        s_real = [s_real;data(3:n+2,2)];
        s_iso = IsoStress(coef_elas,lam1);
        s_vol = VolStress(coef_elas,lam1);
        s_anis = AniStress(coef_elas,lam1,phi);
        s_eq = s_vol+s_iso+s_anis;

        over_s = OverStress(beta1,s_iso,tau1,t_step)+OverStress(beta2,s_anis,tau2,t_step);
        s_app = [s_app;over_s+s_eq];
        index = index+n;
        data = data(n+3:end,:);
    end

    figure(st);hold on;grid on;
    plot(time,s_real,'--','linewidth',1.5);
    plot(time,s_app,style_line{st},'linewidth',2);
    xlabel('Time t [s]');
    ylabel('The first principal stress \sigma_1 [MPa]');
    legend('Experiment','Numerical',2);
end
```

List of Publications

- Tuong N.V., Tuan H.S., Pokorny P.: *Matlab-based programming for free-form surfaces*. International Conference 2009 Manufacturing systems today and tomorrow. TUL, Liberec, November 19-20, 2009, Czech, pp. 17, ISBN 978-80-7372-541-9.
- H. S. Tuan, B. Marvalová: *Magnetoelastic anisotropic elastomers in a static magnetic field: Constitutive equations and FEM solutions*. Proceedings of the sixth European Conference on Constitutive Models for Rubber, Ed.: Taylor & Francis Group. Dresden, September 7-10, 2009, Germany, pp. 453-458, ISBN 978-0-415-56327-7.
- Jarmil Vlach, Hoang Sy Tuan, Bohdana Marvalová: *Experimental and numerical research of Magneto-sensitive elastomers*. 47th International Conference of Experimental Stress Analysis. Syrchov, June 8-11, 2009, Czech Republic, pp.283-290, ISBN 978-80-7372-483-2.
- Hoang Sy Tuan, Marvalová Bohdana: *Simulation of Viscoelastic Fiber-Reinforced Composites at Finite Strains in Comsol Multiphysics*. Applied Mechanics 2009, 11th International Scientific Conference. Smolenice, April 6-8, 2009, Slovak Republic, pp. 45-46, ISBN 978-80-89313-32-7.
- Hoang Sy Tuan, B. Marvalová: *Relaxation of Fiber-reinforced Composites: FEM Simulations*. Conference Mechanical Composite Material and Structure. Pilsen, March 12-13, 2009, Czech Republic, pp. 70-77, ISBN 978-80-7043-782-7.
- Sy Tuan Hoang, Bohdana Marvalová: *Coupling of magnetoelastic material and magnetic field in Comsol Multiphysics*. Výpočty Konstruktí Metodou Konečných Prvků. Pilsen, November 20, 2008, Czech Republic, pp. 8-18, ISBN 978-80-7043-735-3.
- Hoang S. T., Marvalová B.: *Numerical Differentiation of Experimentally Measured Displacements*. 16th Annual Conference Proceedings. Prague, November 11, 2008, Czech Republic, pp. 40, ISBN 978-80-7080-692-0.
- Hoang S.T., Marvalová B.: *Magneto-hyperelastic material in a uniform magnetic field: FEM Calculation of Stress and Strain*. Engineering Mechanics 2008, National Conference with International Participation. Svratka, May 12-15, 2008, Czech Republic, pp. 86-87, ISBN 978-80-87012-11-6.
- Jan Růžička, Hoang Sy Tuan, Bohdana Marvalová: *Dynamic measuring methods of viscoelastic properties of materials*. 14th International Conference, Structure and Structural Mechanics of Textiles. TU of Liberec, November 26-28, 2007, Czech Republic, pp. 97-104. ISBN 978-80-7372-271-5.

Hoang Sy Tuan, Bohdana Marvalová: *FE analysis of cord-reinforced rubber composites at finite strains*. Výpočty Konstrukcí Metodou Konečných Prvků. Prague, November 22, 2007, Czech Republic, pp. 9-20, ISBN 978-80-01-03942-7.

Hoang. S.T., Marvalová B.: *Constitutive Material Model of Fiberreinforced Composites in Comsol Multiphysics*. Technical Computing Prague 2007, 15th Annual Conference Proceedings. Prague, November 14, 2007, Czech Republic, pp. 53, ISBN 978-80-7080658-6.

Tuan Hoang Sy, Marvalová B.: *Relaxation of the Rubber Plate with Central Hole – FEM Simulation in Comsol Multiphysics*. Applied Mechanics 2007, 9th International Scientific Conference. Malenovice, April 16-19, 2007, Czech Republic, pp. 214-215, ISBN 978-80-248-1389-9.

V Liberci 26.1.2010

Ing. Hoang Sy Tuan

Prof. Ing. Petr Louda, CSc.
Děkan strojí fakulty
TUL v Liberci

Věc: doporučení školitele

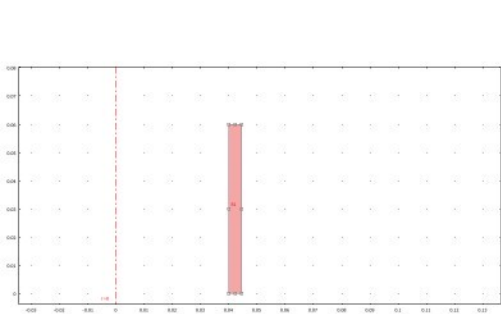
Vážený pane děkane,

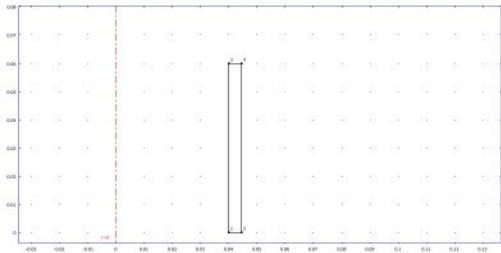
Doporučuji k obhajobě disertační práci svého doktoranda pana Ing. Hoang Sy Tuan s názvem
Elastické a viskoelastické chování kompozitů s elastomerickou maticí.
Doktorand má splněny všechny studijní povinnosti.

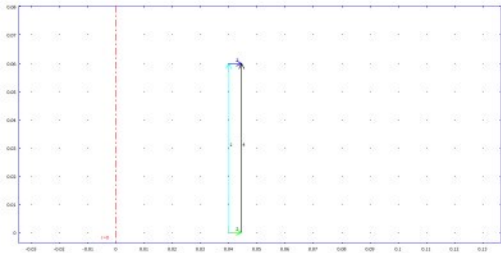
V Liberci 25.1.2010

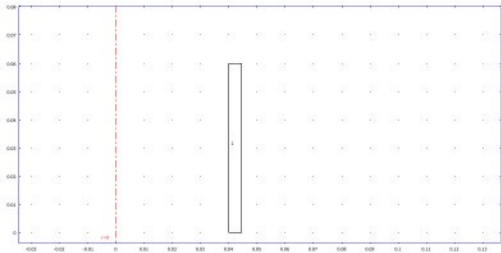
doc. Ing. Bohdana Marvalová
školitelka

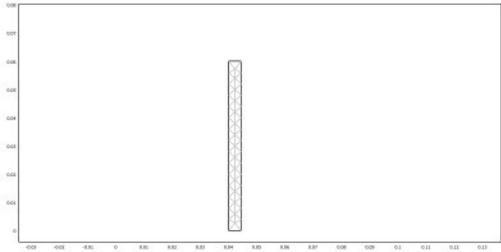




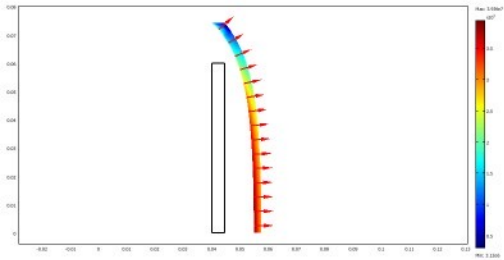




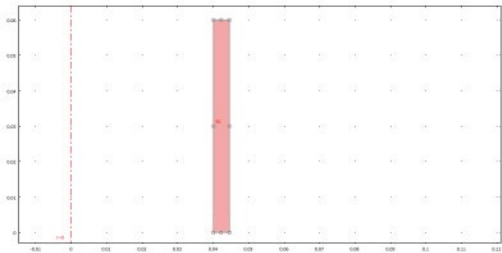


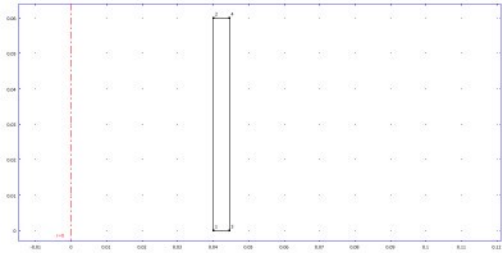


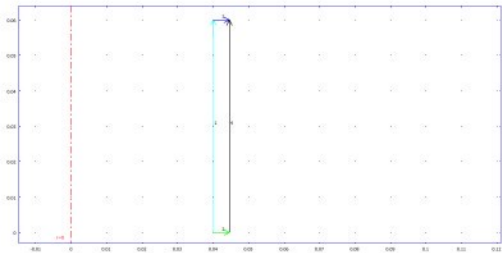


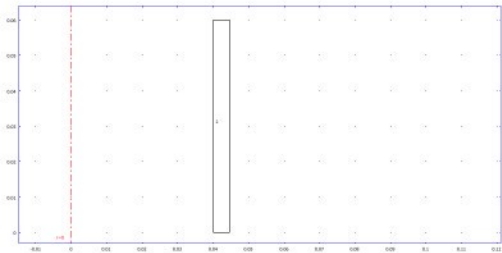


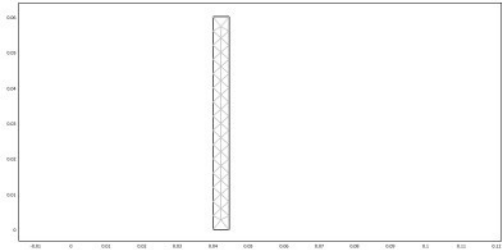












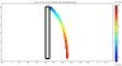
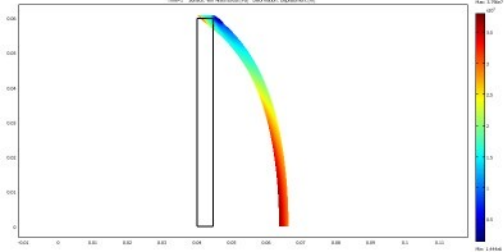
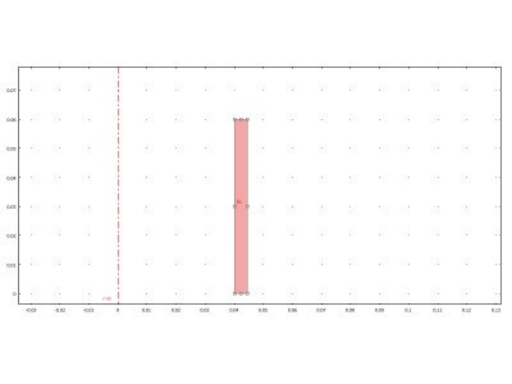
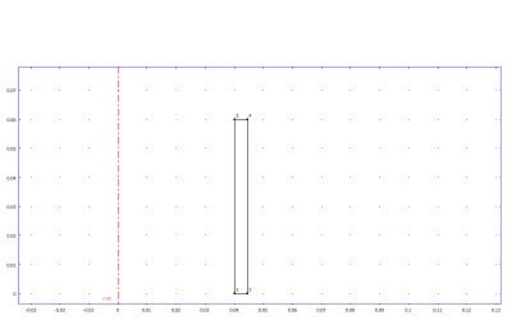


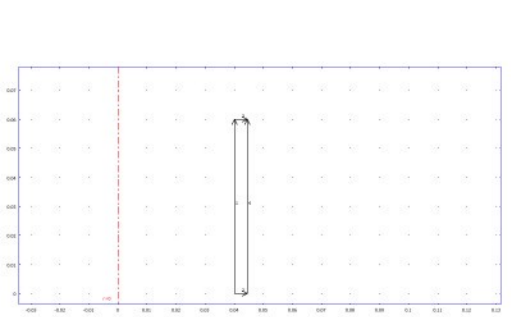
Figure 2: Surface of the function $f(x, y, z)$ defined by the equation $f(x, y, z) = 0$.

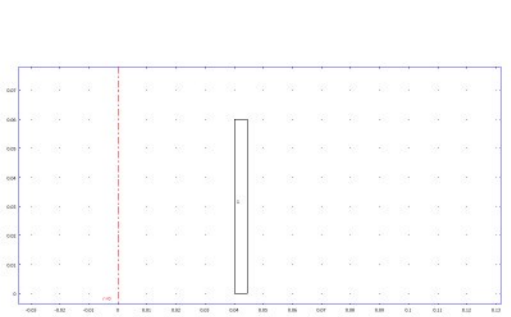


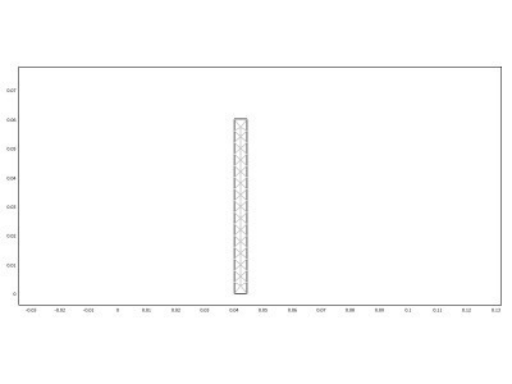




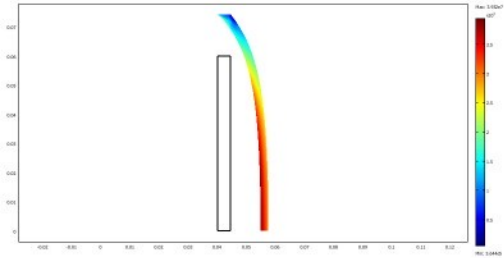




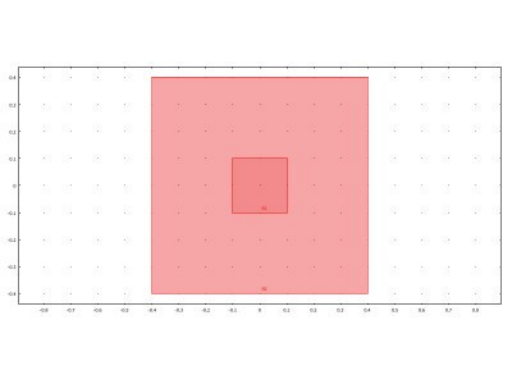


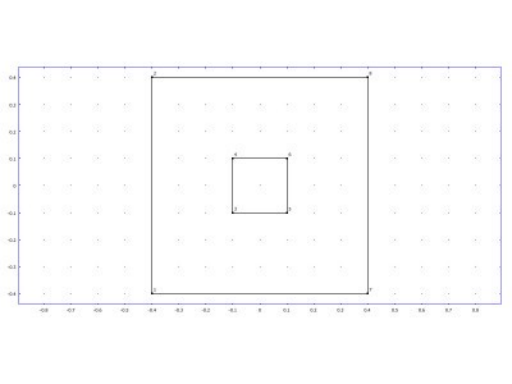


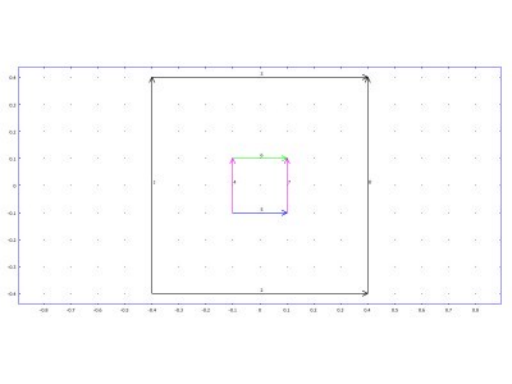


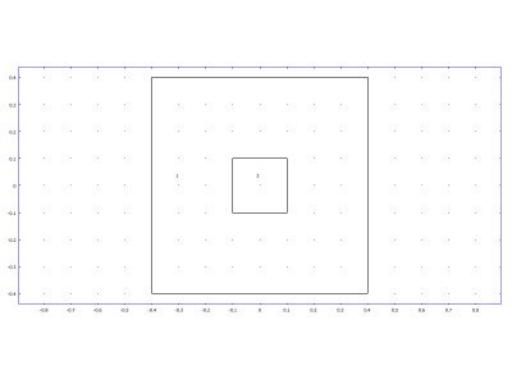


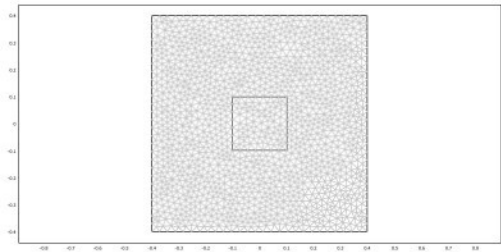






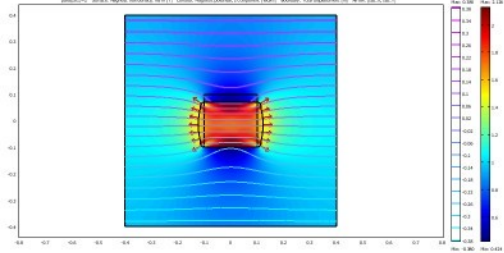




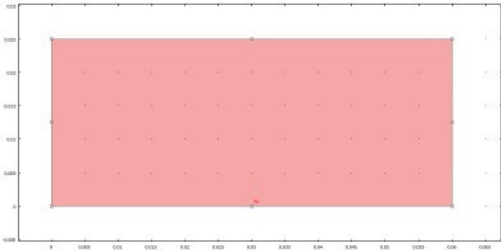


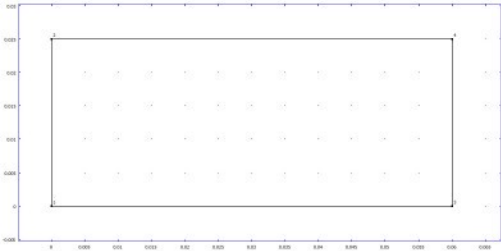


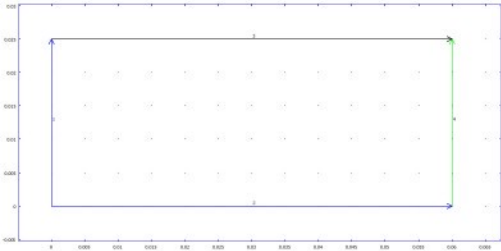
2016/02/10 Surface: Magnitude: function: norm (T) Contour: Magnitude: potential, component: (T) Boundary: total displacement: (u) Axes: [x,u,v]

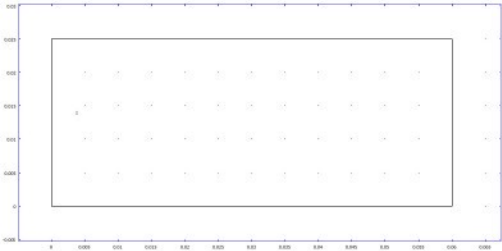


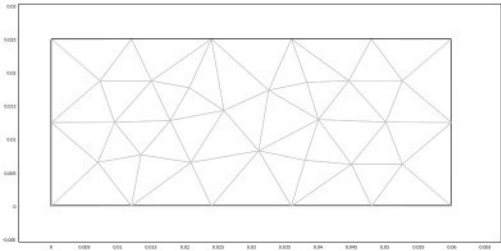


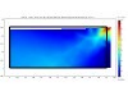




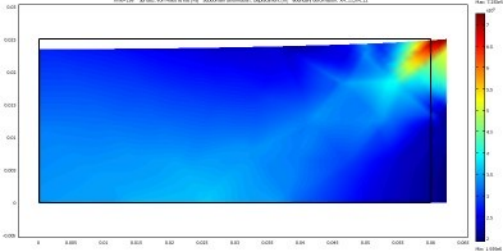




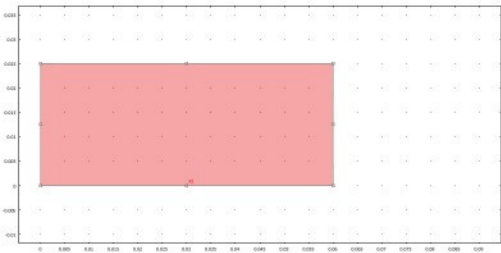


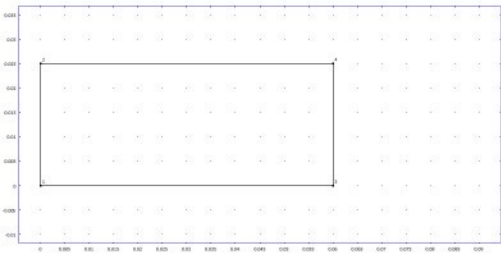


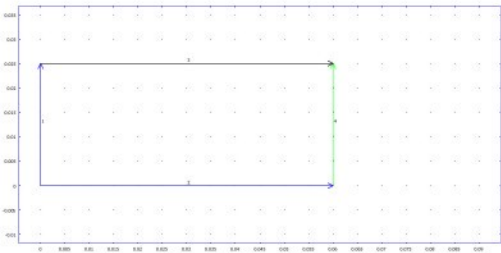
Time=150 Surface warpage stress (MPa) Subduction deformation Dipacament (MPa) Boundary deformation RR_11_P1_11

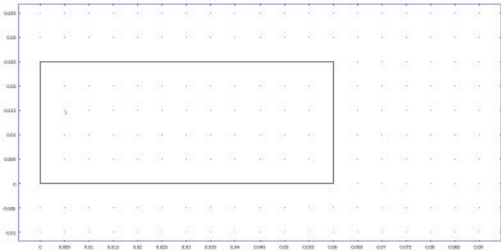


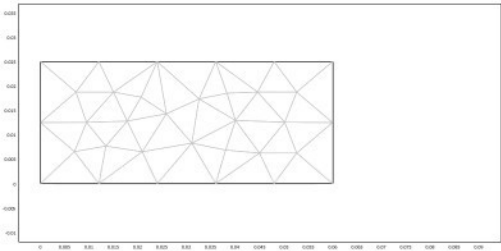


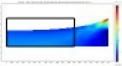




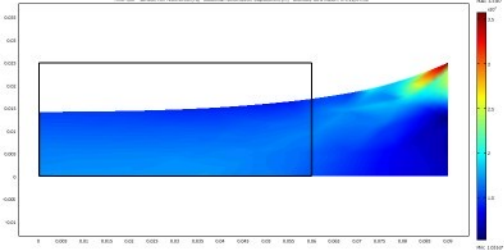




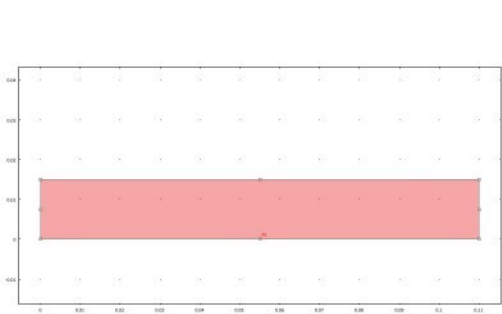


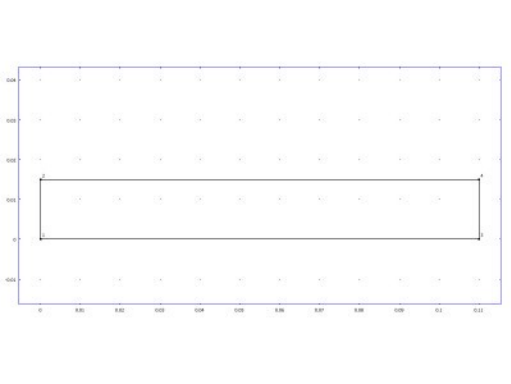


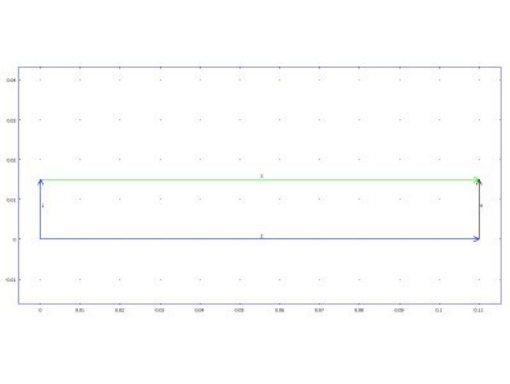
Time=0.00 Surface von Mises stress (Pa) Subdomain deformation: Displacement (m) Boundary deformation: 0.011, 0.011, 0.011

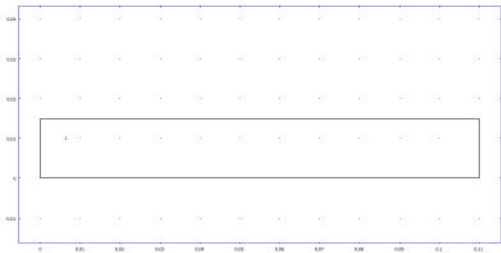


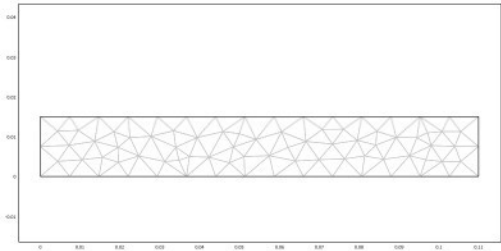












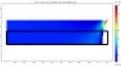
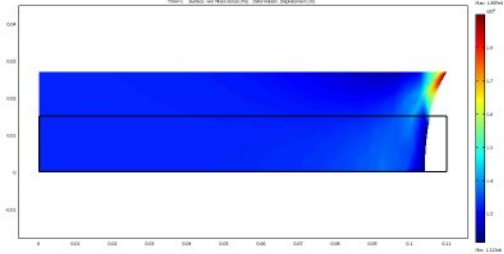
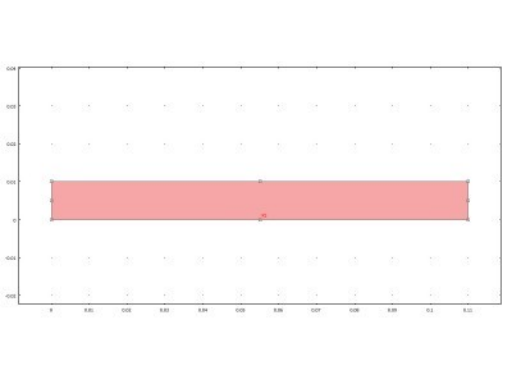
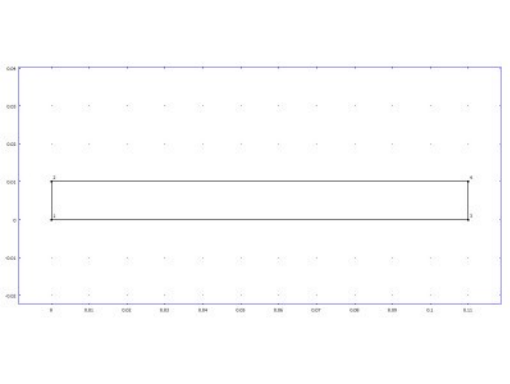


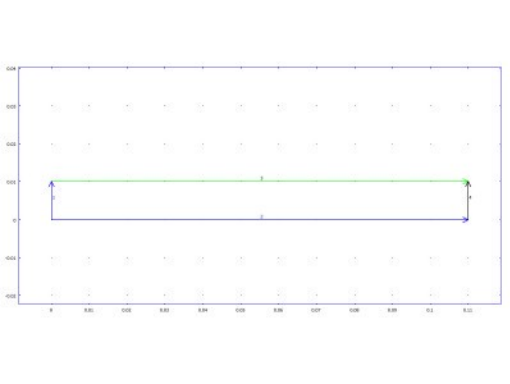
Figure 2: Surface velocity distribution (m/s) on the airfoil.

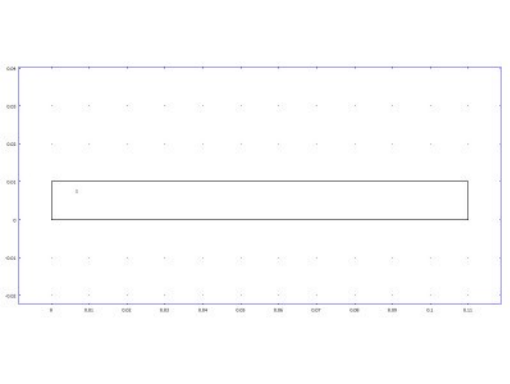


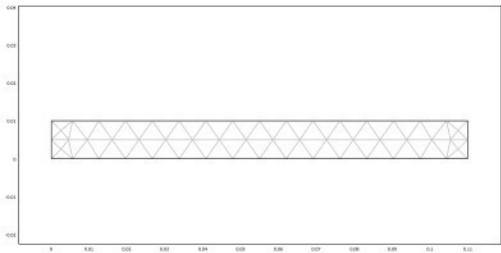


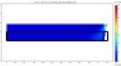




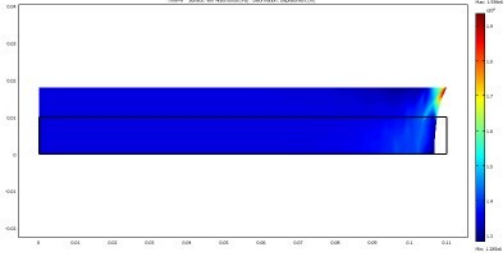




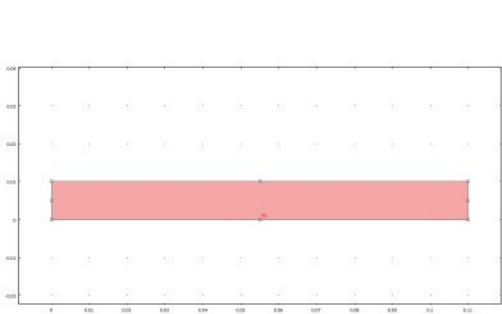


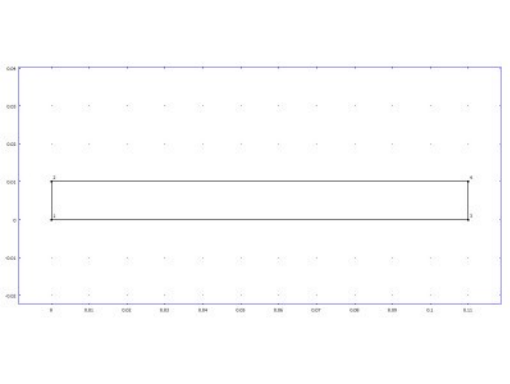


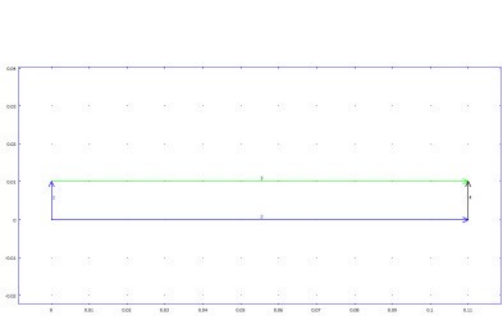
time=8 surfloc via Nao-2000-P2 deformation exponential

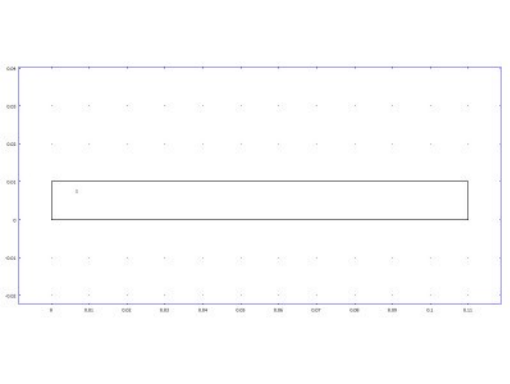












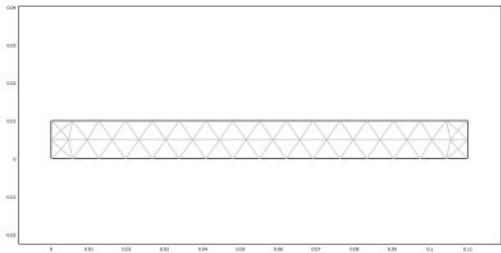
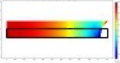
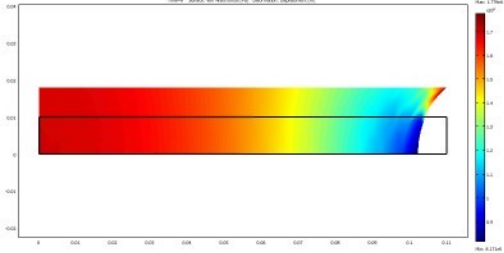


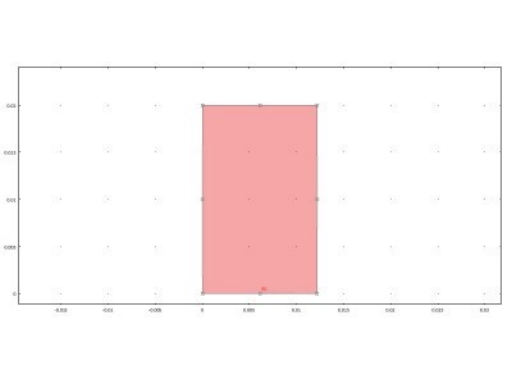
Figure 1.10: A color bar for the color map.

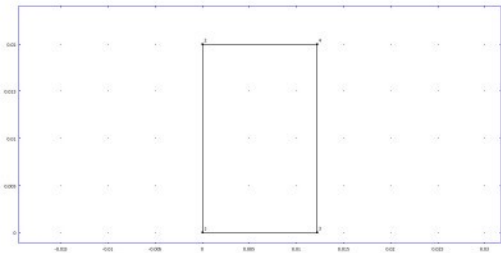


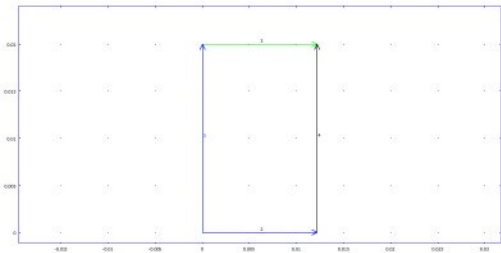
time=8 surfoz von Hsu-zoo(74) deformation exponential

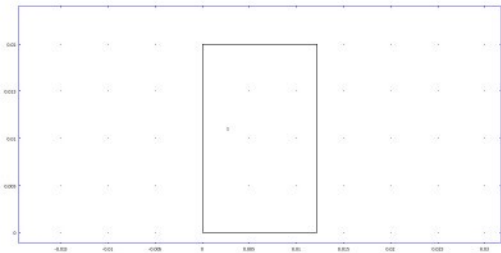


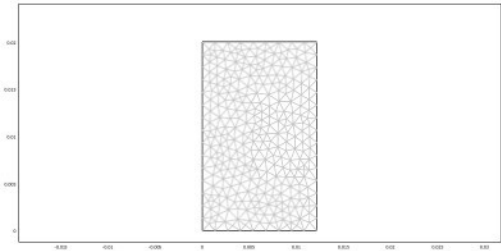












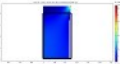
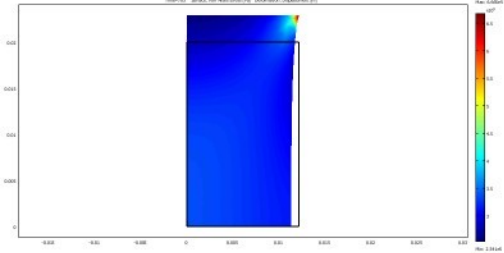
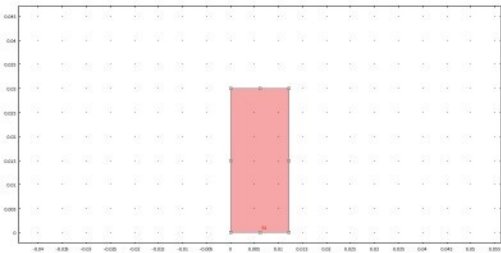
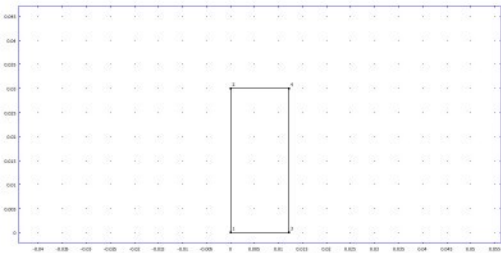


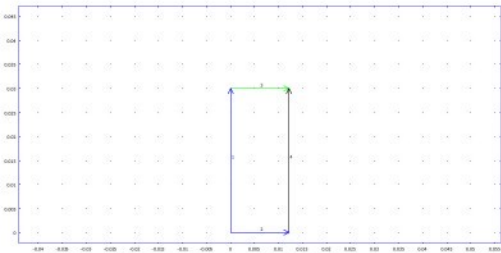
Figure 763: Surface plot of Maximum Principal Strain (MPa) deformation: displacement (m)

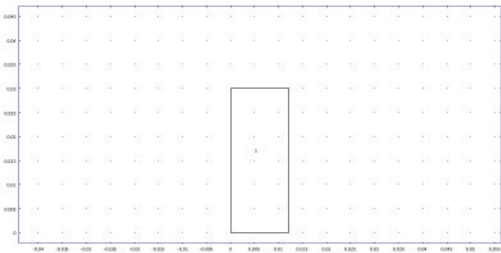


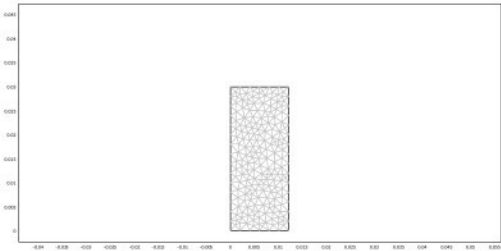


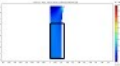




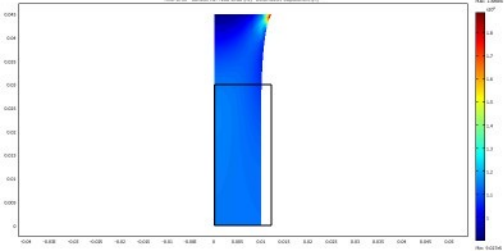




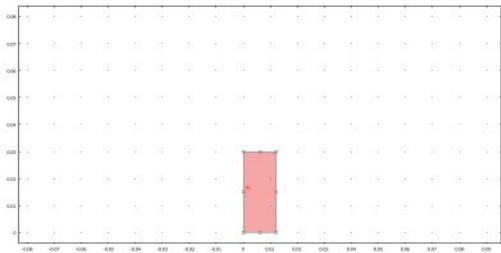


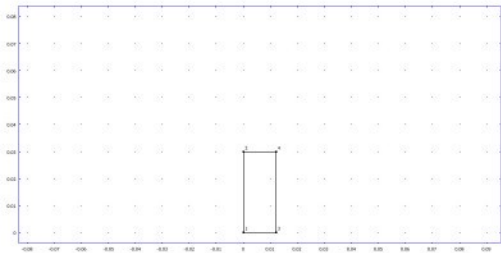


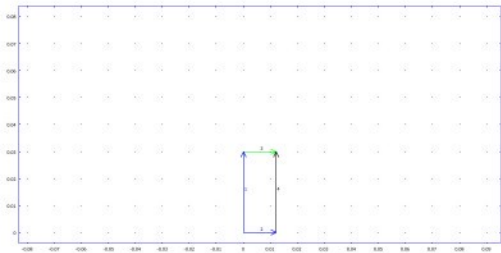
Flow=270.0 Surface: von Mises stress (Pa) bottom: von Mises stress (Pa)

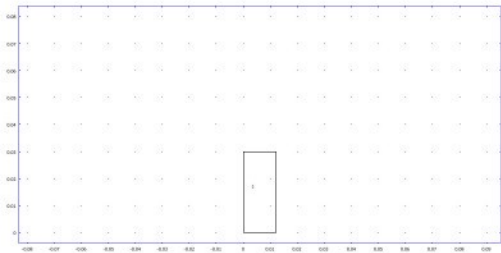


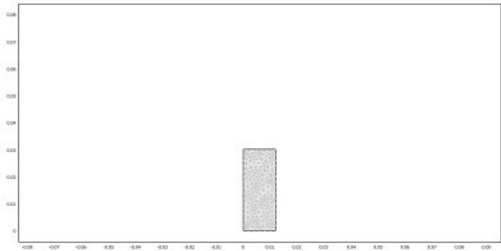












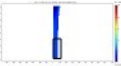
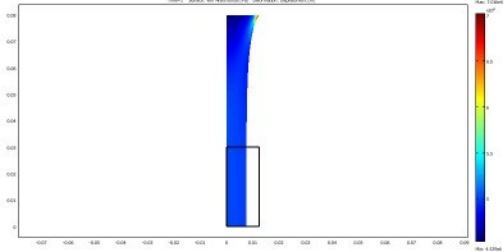
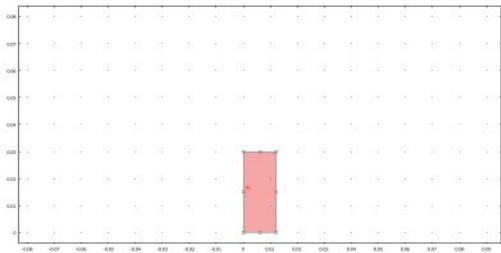
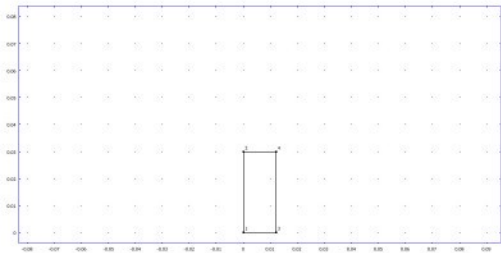


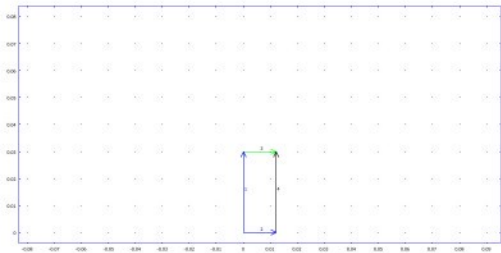
Figure 2: Surface of the deformation displacement

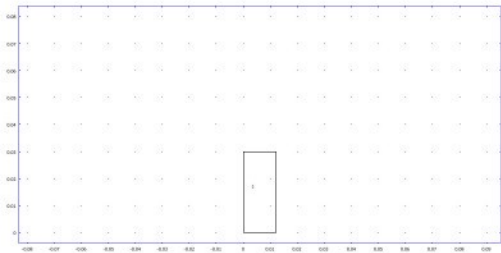


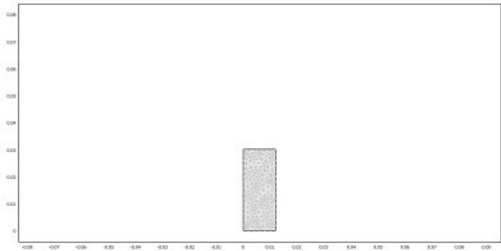


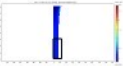




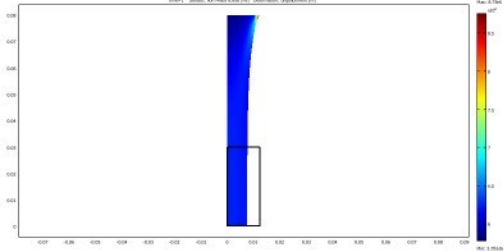




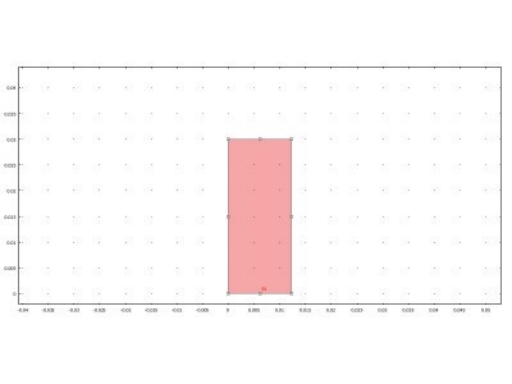


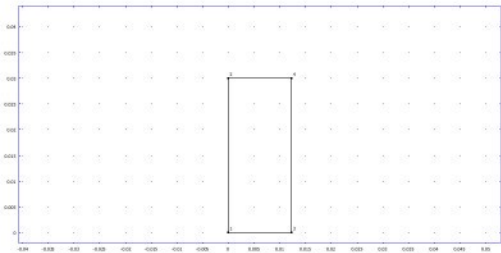


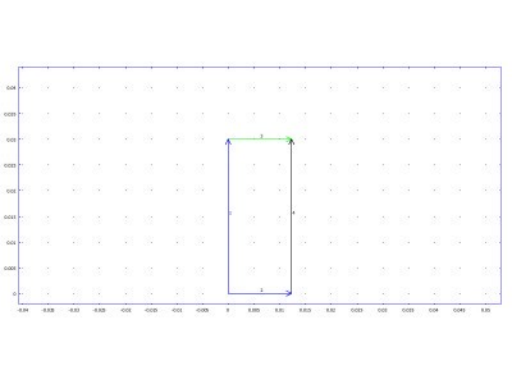
Time=1 Surface: von-Mises Stress [MPa] Deformation, Displacement [m]

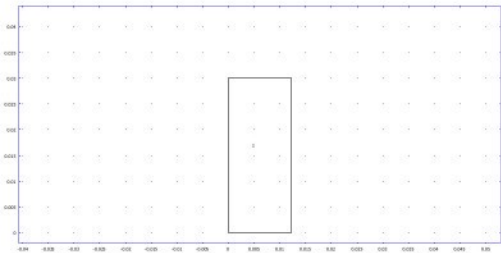


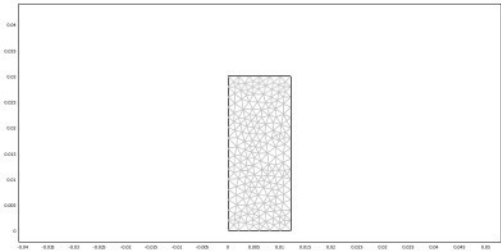


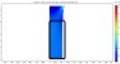




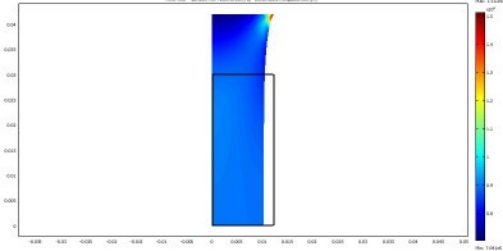




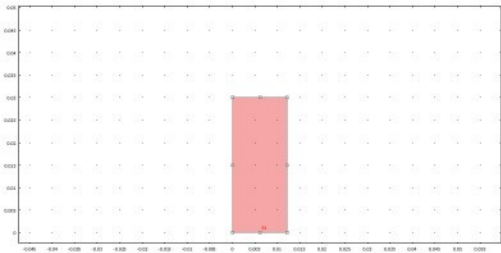


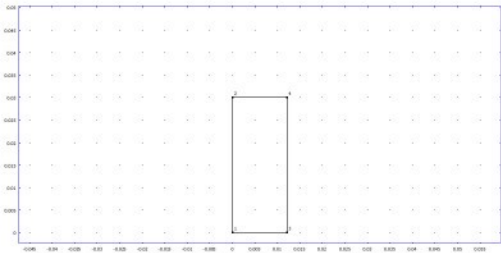


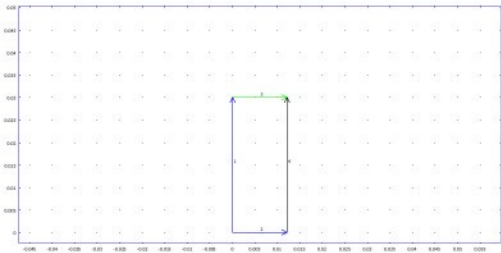
Time=0.02 Surface: von Mises stress (Pa) deformation: displacement (m)

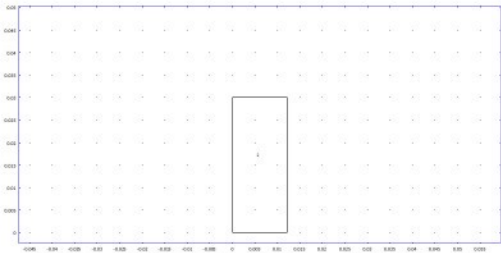


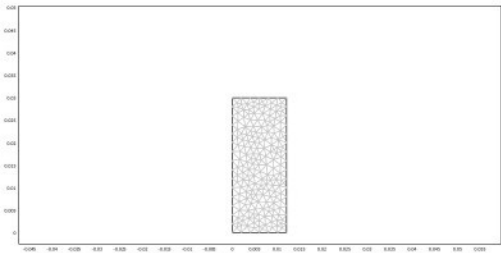


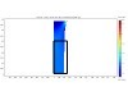




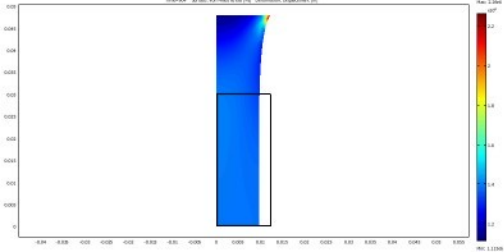




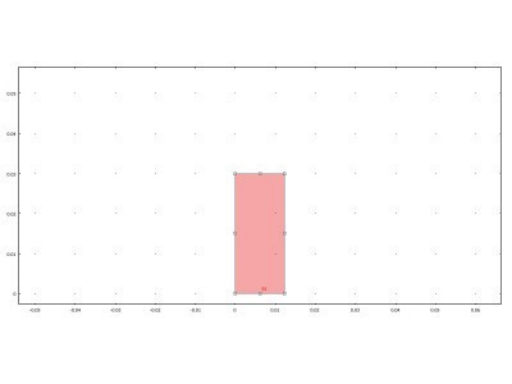


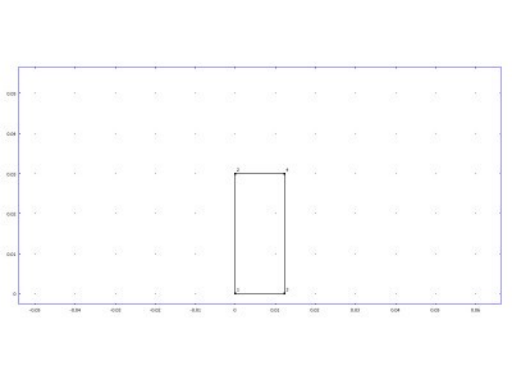


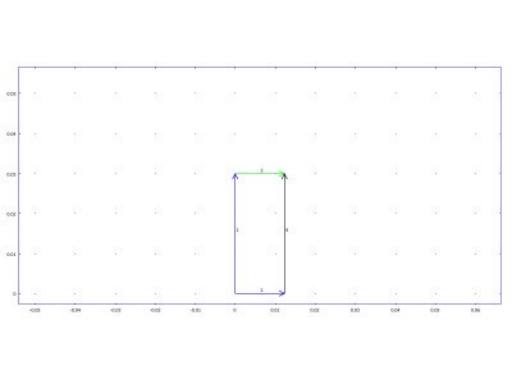
Step=904 Surface von Mises stress [MPa] Deformation Displacement [mm]

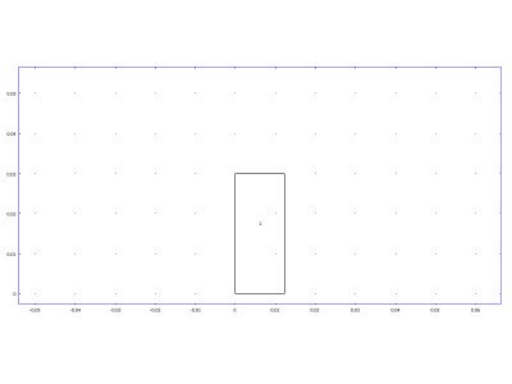


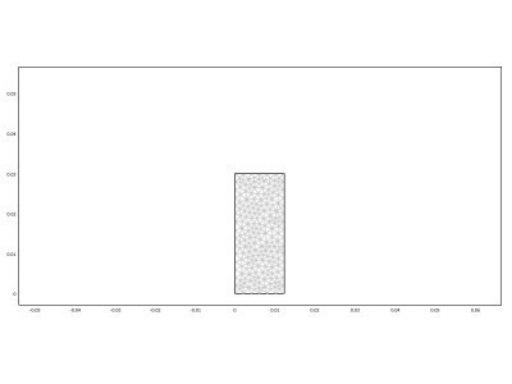


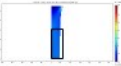




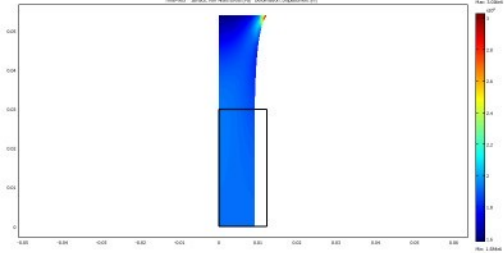




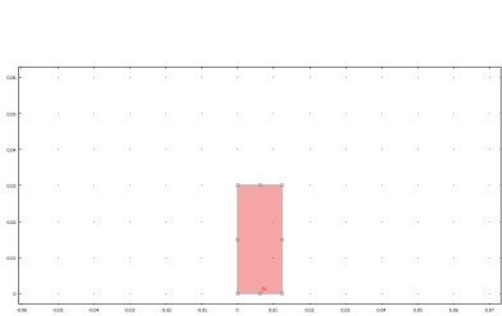


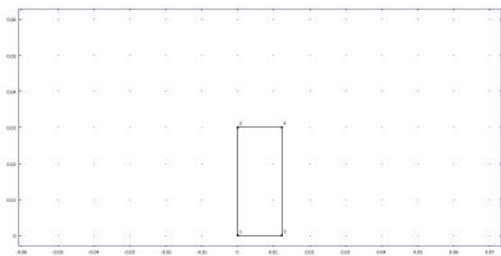


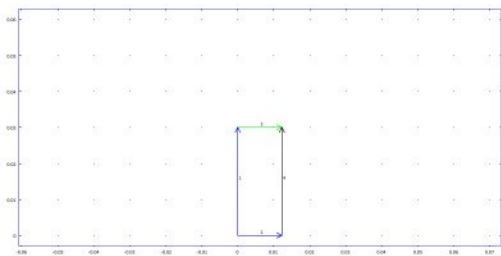
Time=0.0 Surface: von Mises stress (Pa) deformation: displacement (m)

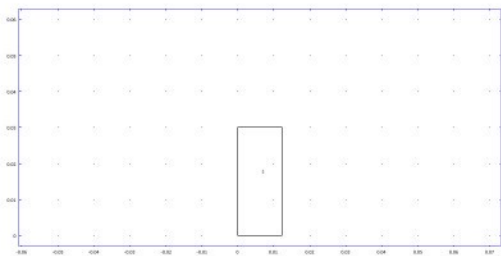


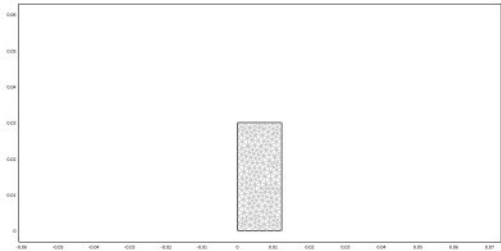


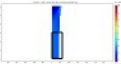




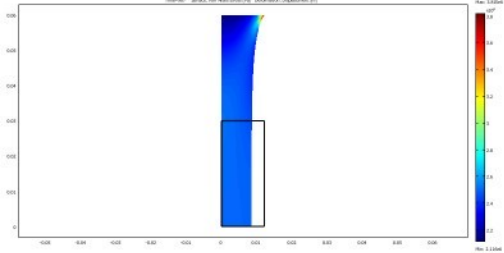




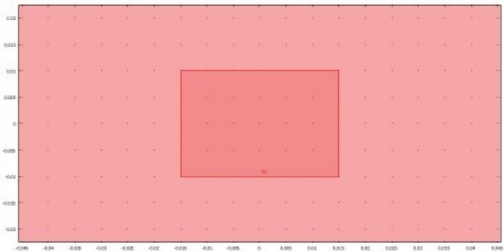


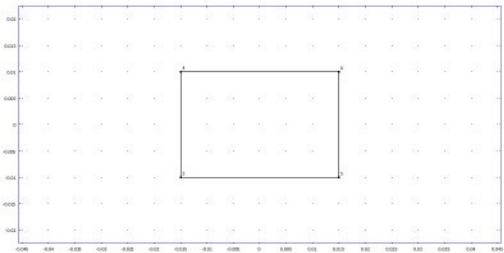


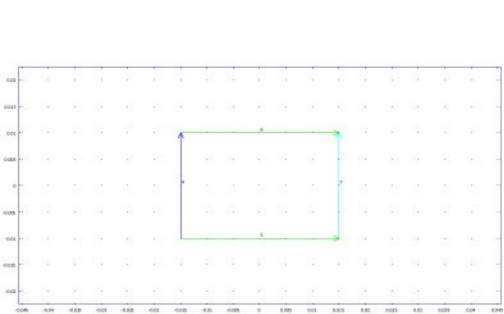
Plot=887 Surface Plot Mass (kg) deformation: displacement (m)

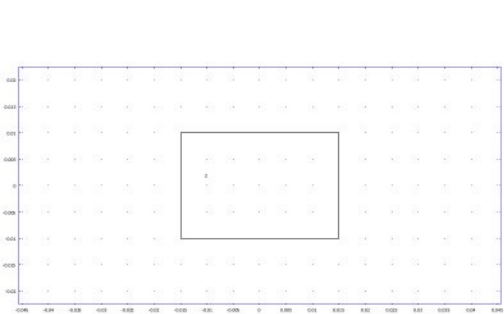


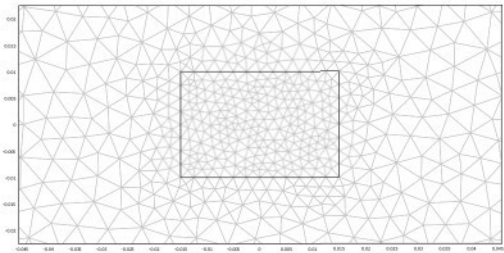


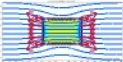




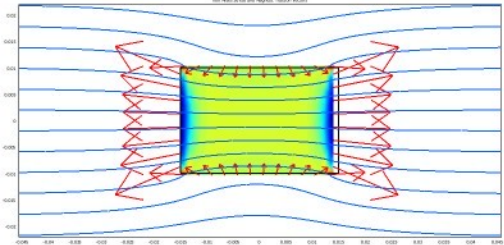




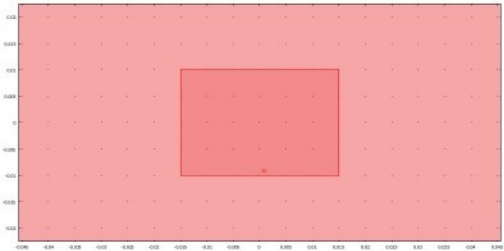


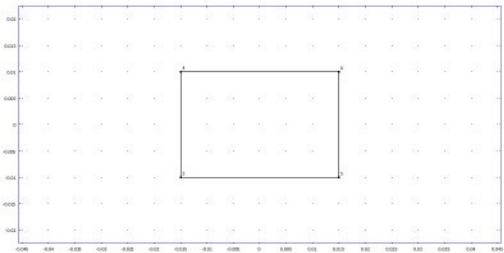


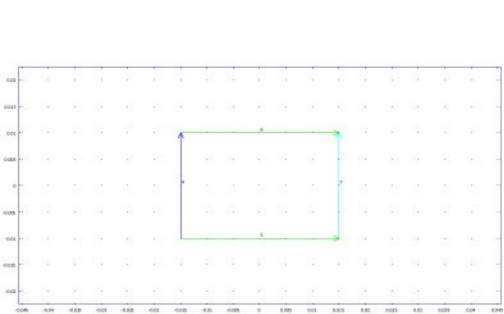
Plot of Magnetic Field and Magnetic Vector Potential

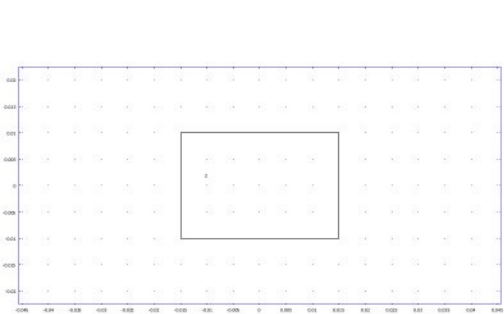


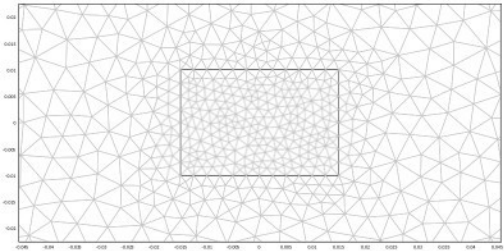


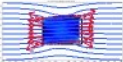




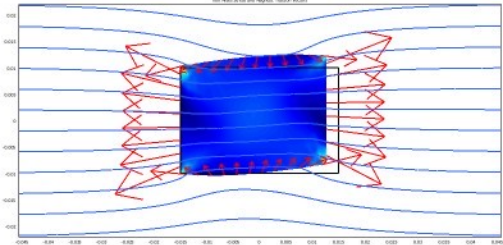




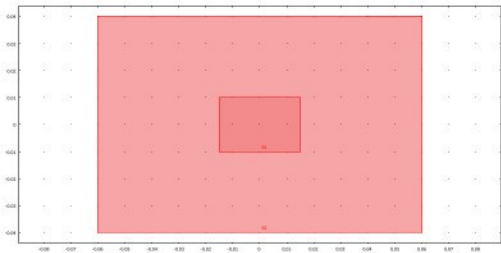


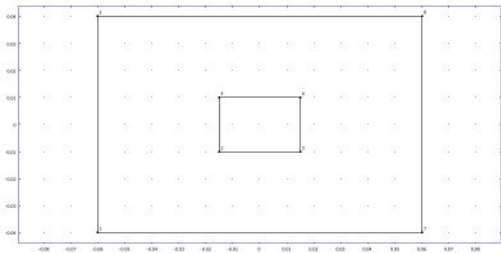


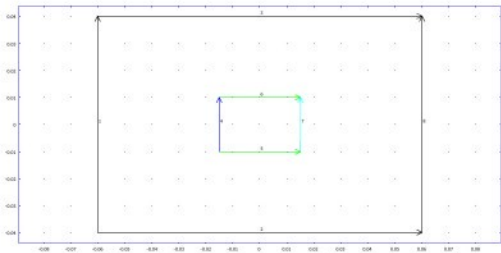
Plot of Magnetic Field and Magnetic Field Vector

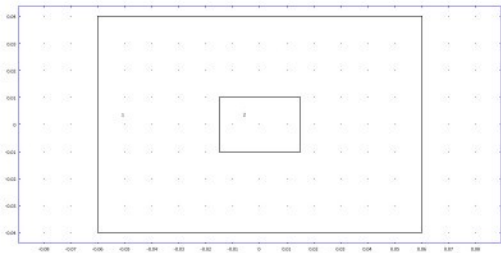


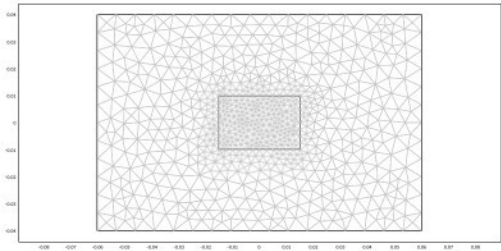






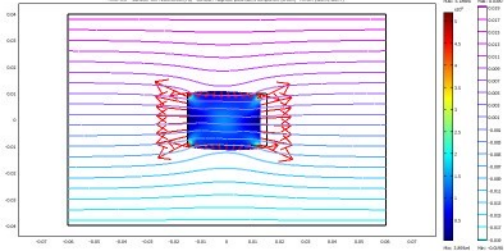




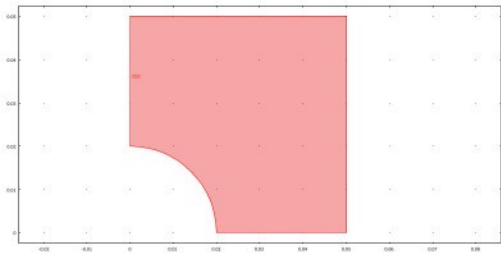


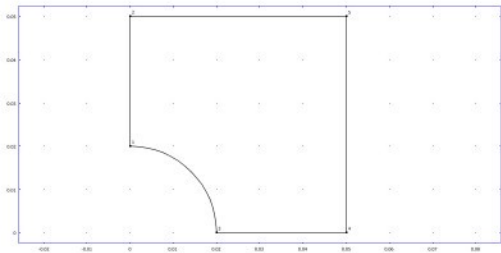


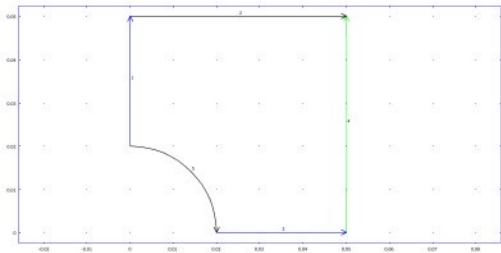
Time=0.5 Surface: wt Magnetic field [Pa] contour: Magnetic potential, z component (A/m) Axes: (x,z,y)

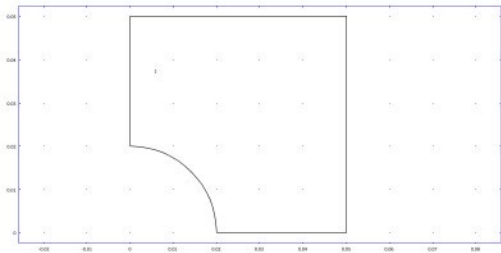


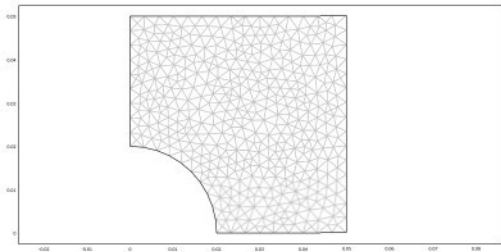


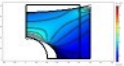


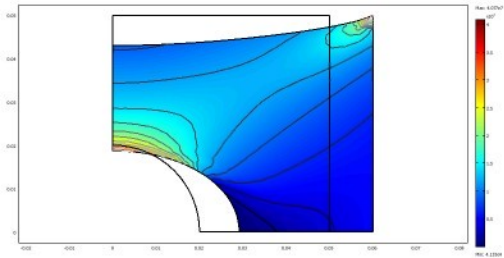




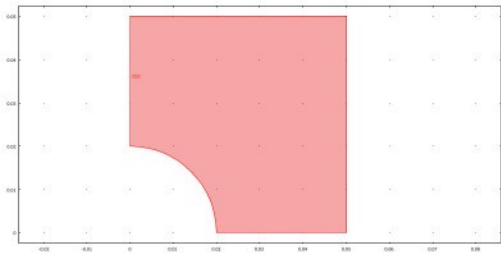


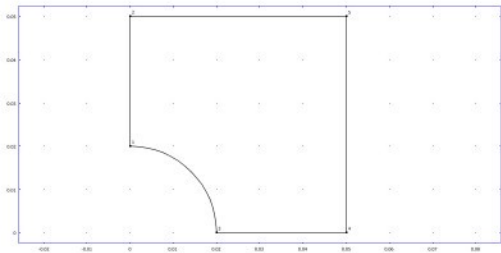


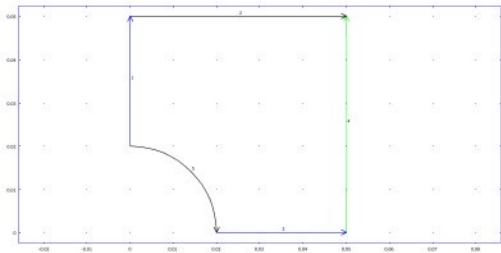


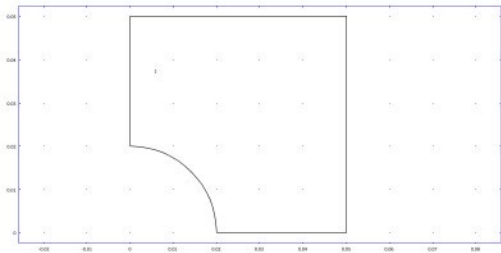


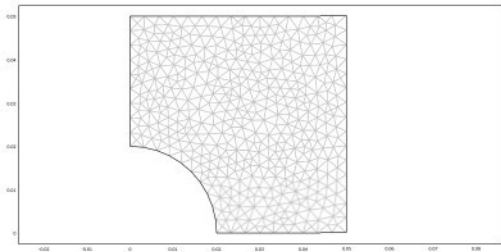




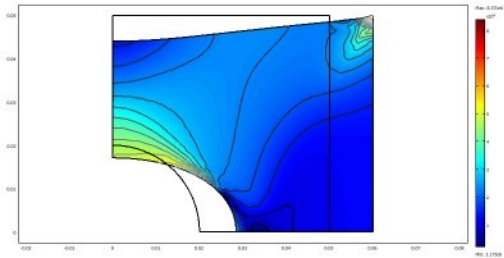




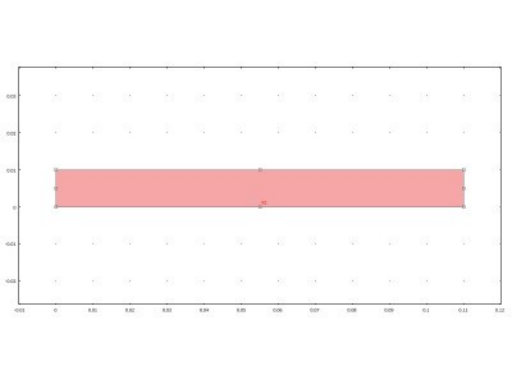


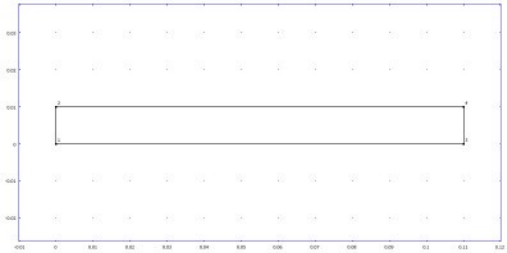


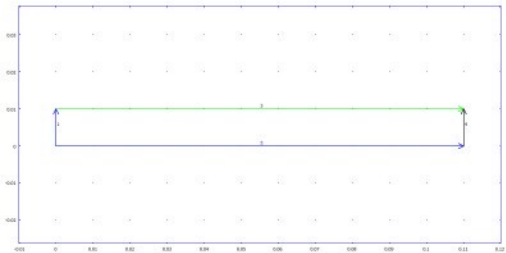


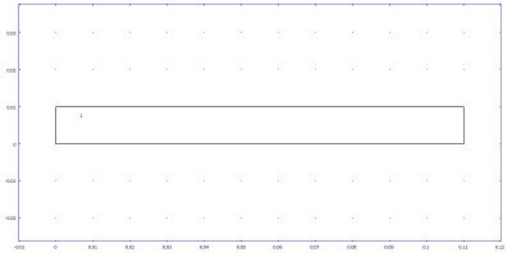


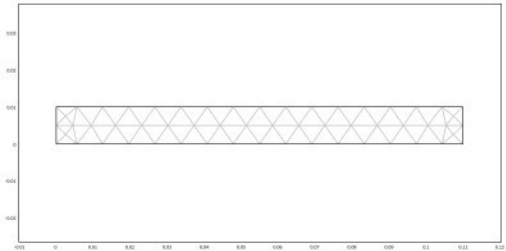




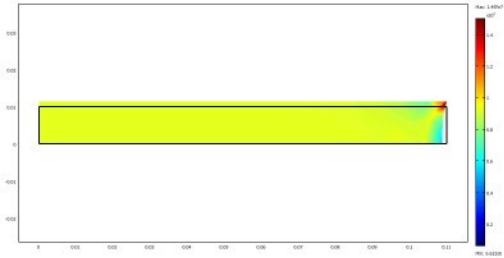




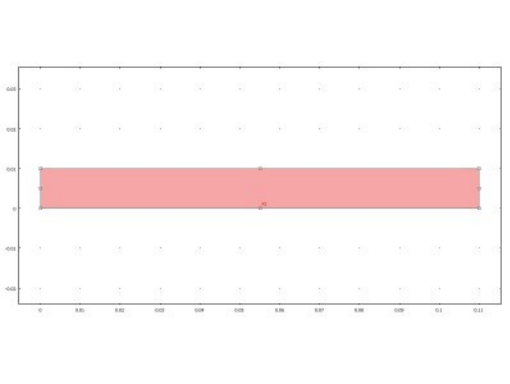


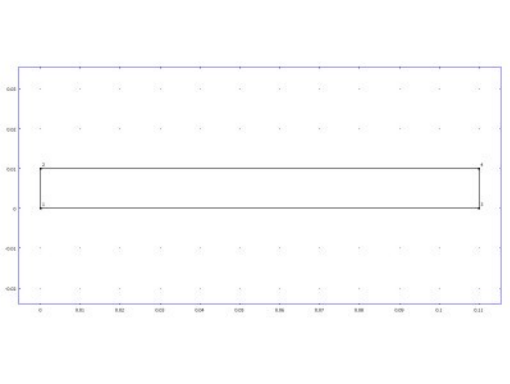


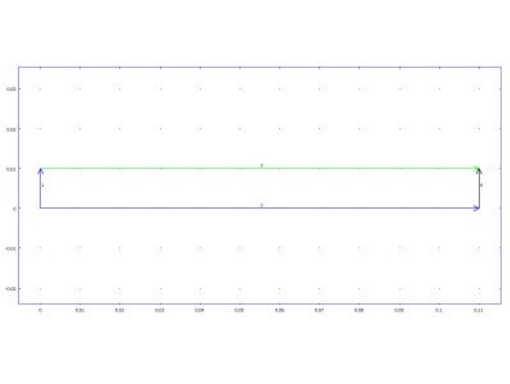


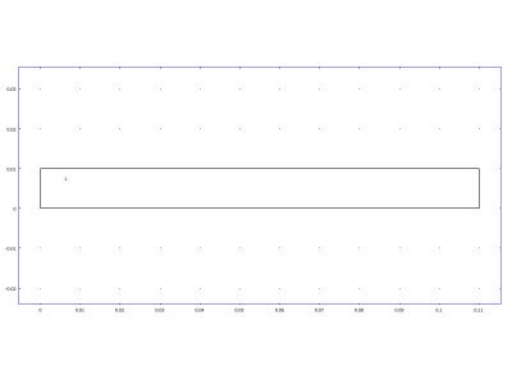


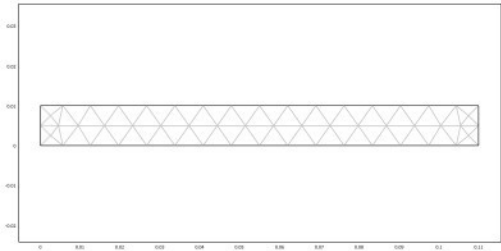












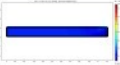
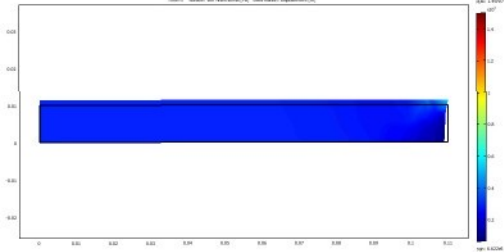
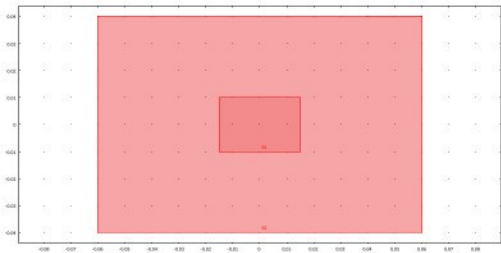
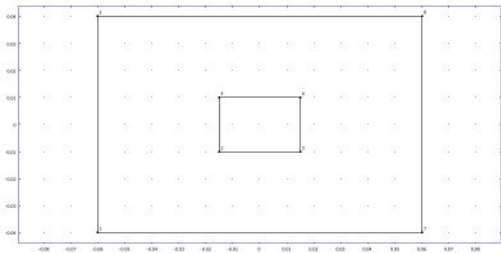


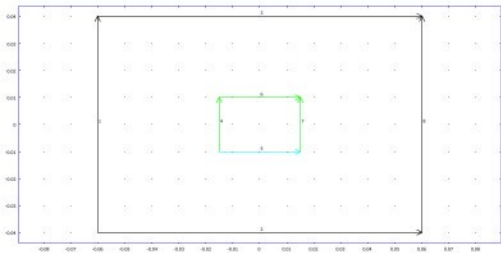
Diagram: Simulation von Materialverhalten (Pd) - Deformation: Displacement (m)

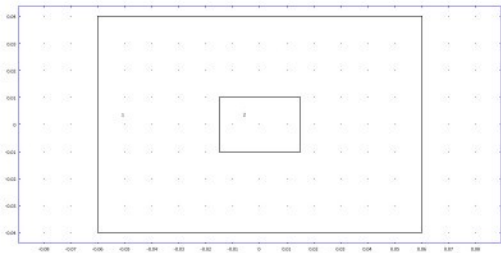












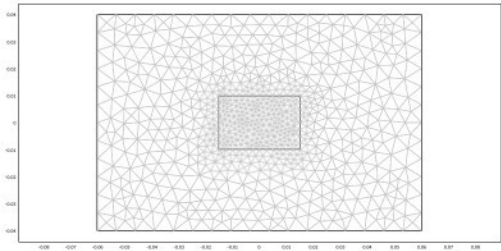
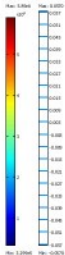
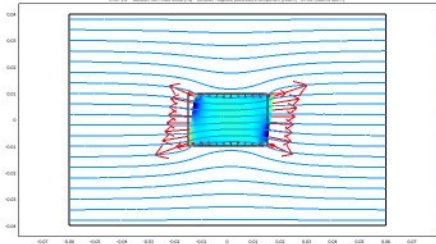


Figure 1: A 2D plot showing the distribution of a variable, with a color bar on the right indicating the scale from 0 to 100.

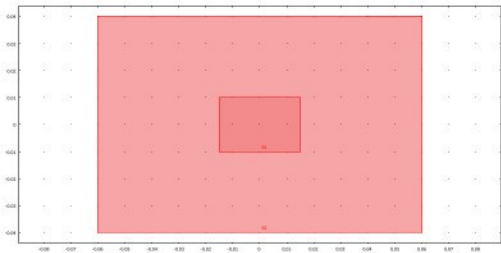


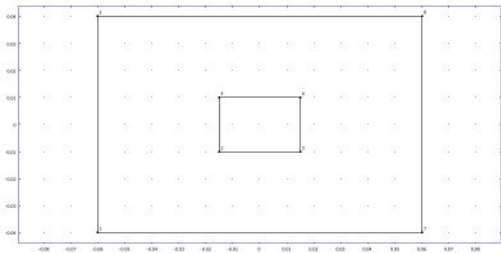
Figure 1: A 2D plot showing the distribution of a variable, with a color bar on the right indicating the scale from 0 to 100.

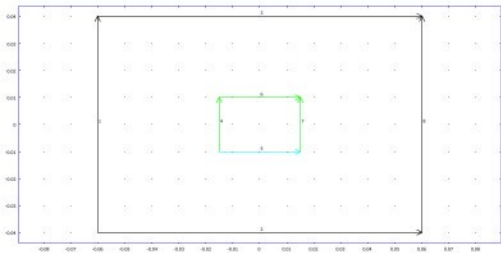
Time=1.0 Surface: kv1(kv1) (kV) Contour Magnetic (current, z-component) (mA) B/H (T/m, A, tesla)

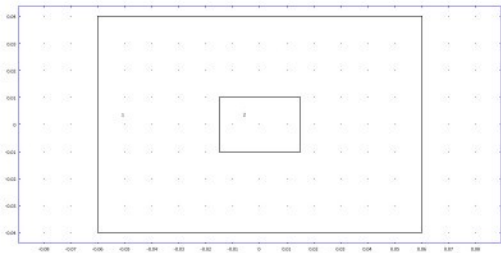


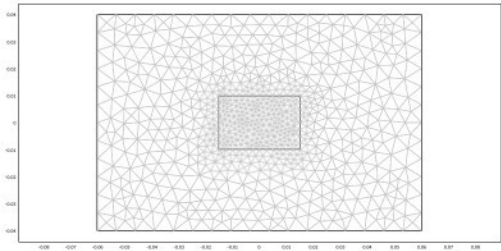


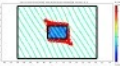


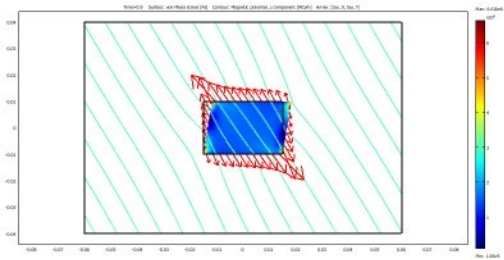




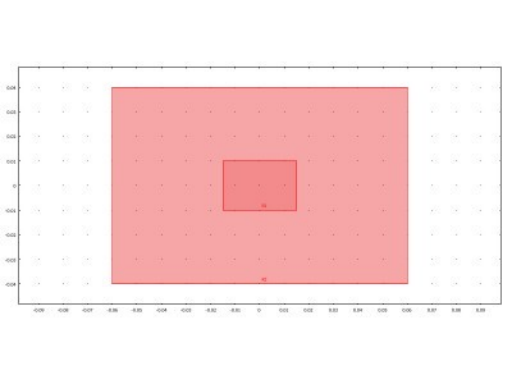


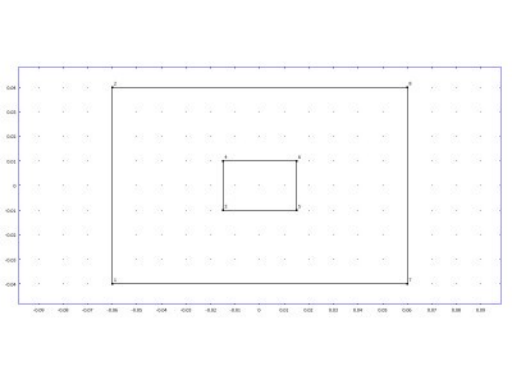


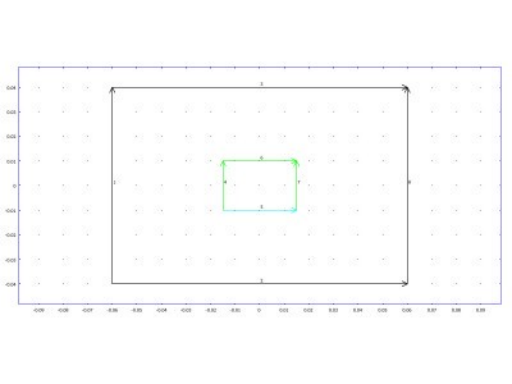


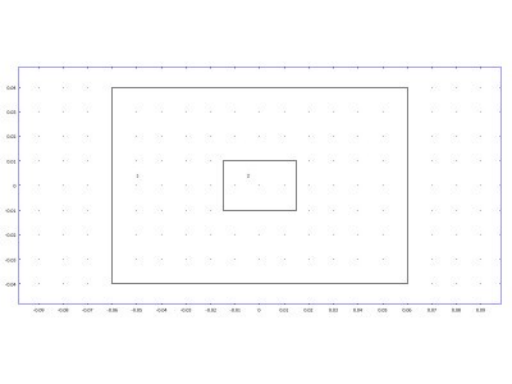


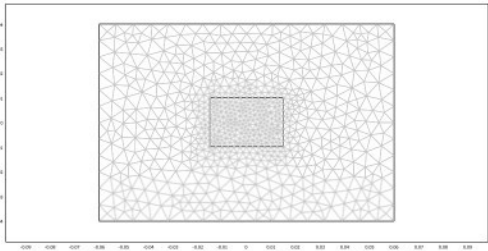






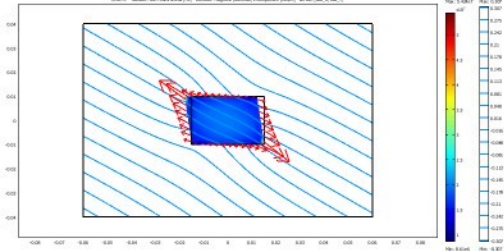




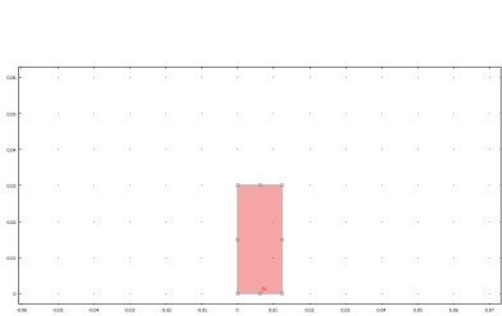


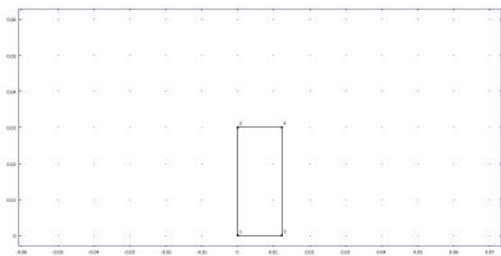


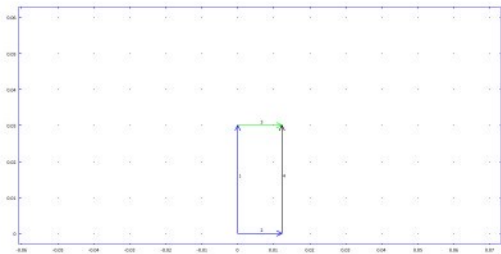
Topic 1: Surface: air flow over a wing [Pa] Contour: Pressure potential, components [N/m²] Streamlines: u, v, w, ρ

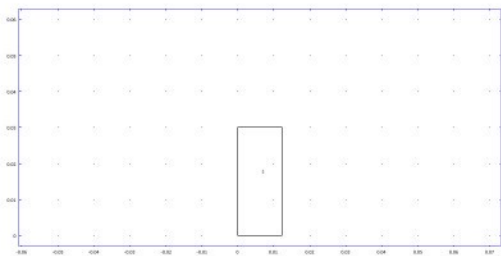


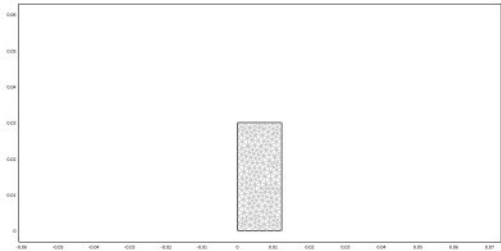












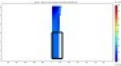
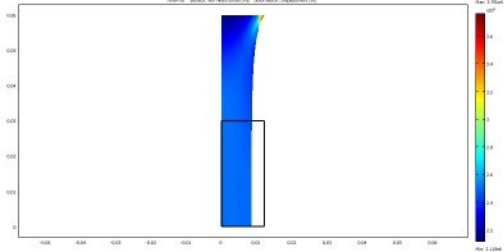
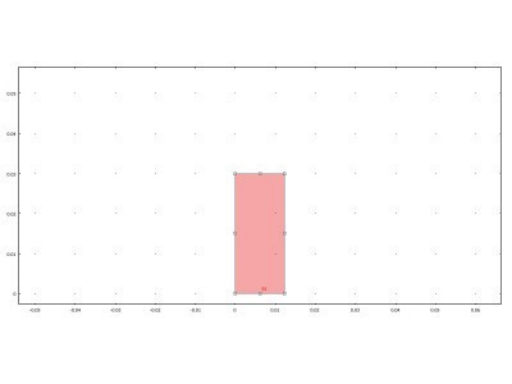
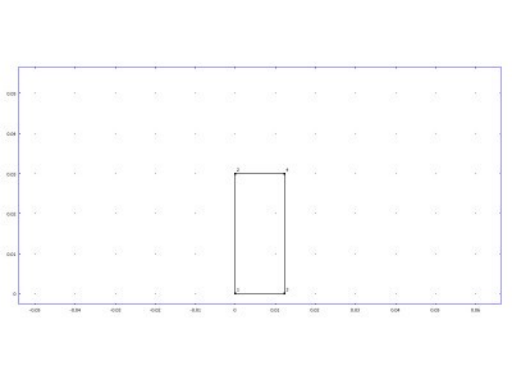


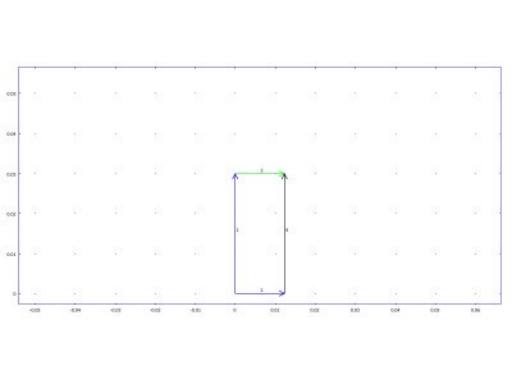
Figure 28 Surface von Mises stress (Pa) deformation displacement (m)

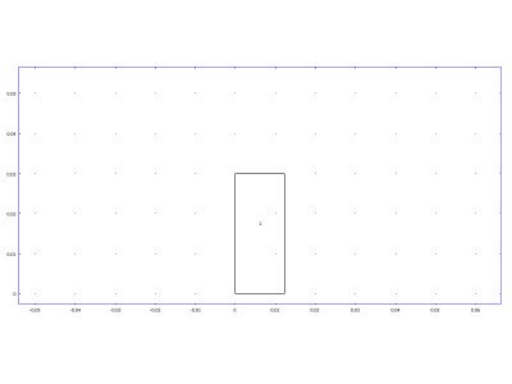


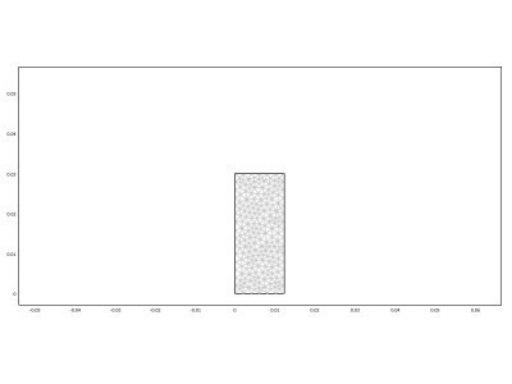


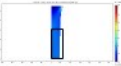




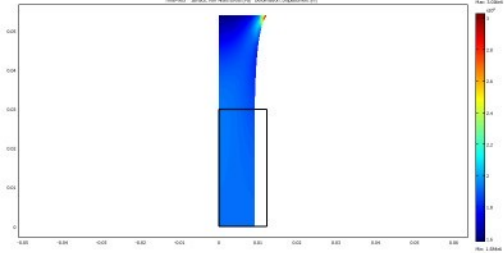




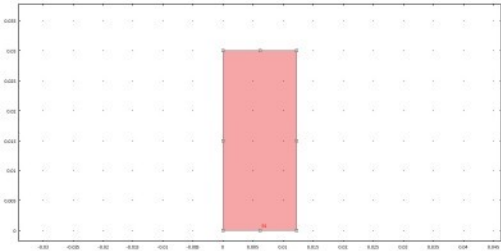


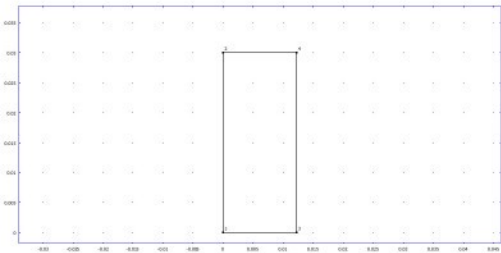


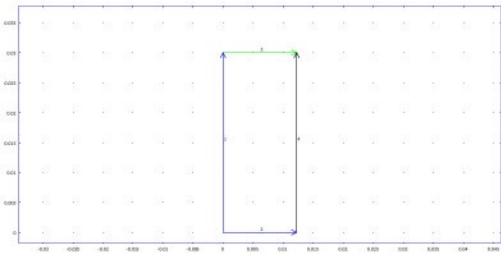
Time=0.0 Surface: von Mises stress (Pa) deformation: displacement (m)

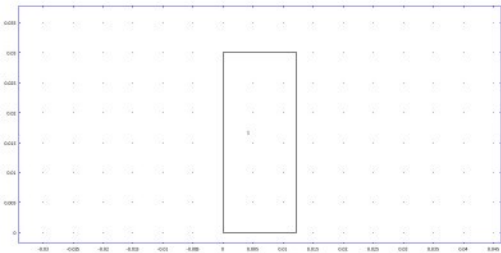


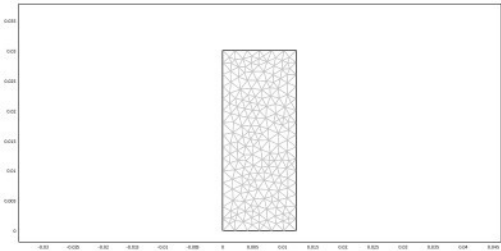


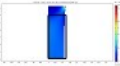




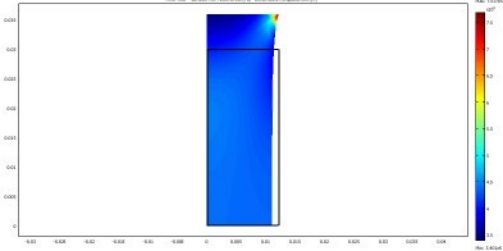




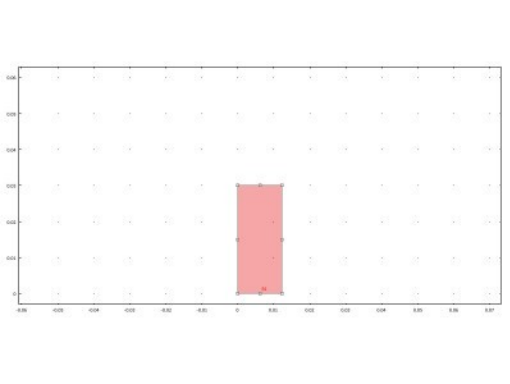


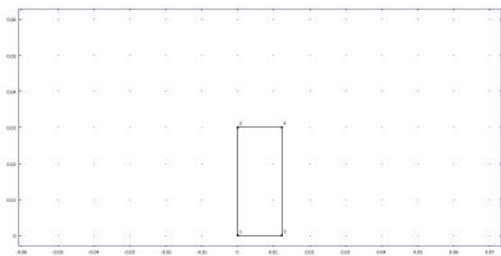


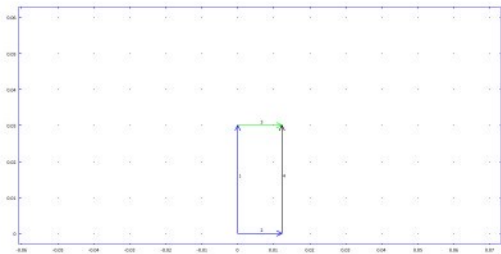
Time=0.02 Turbulent Kinetic Energy (Pa) deformation: displacement (in)

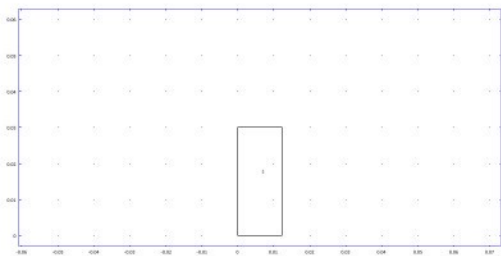


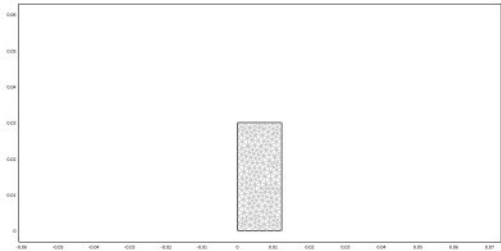












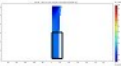
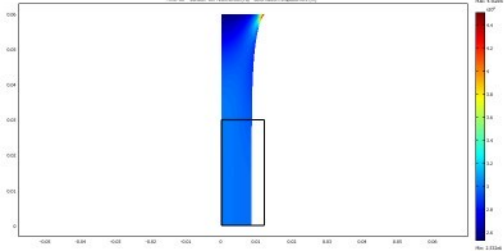
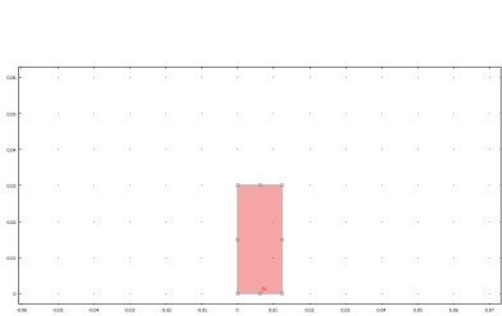
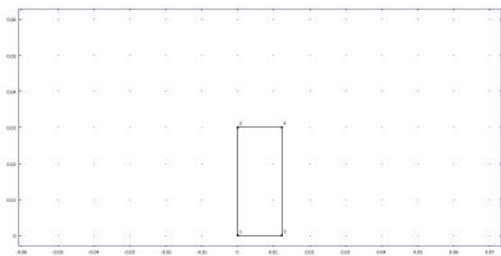


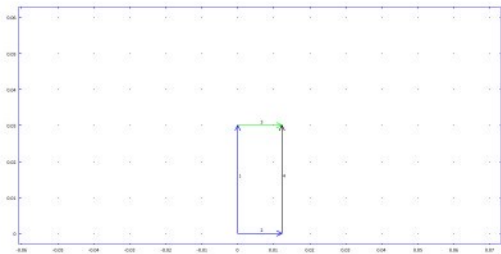
Figure 48 Surface von Mises stress (Pa) deformation displacement (m)

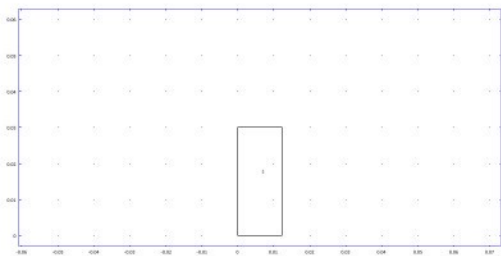


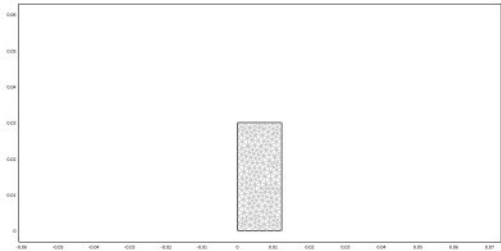


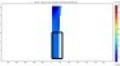




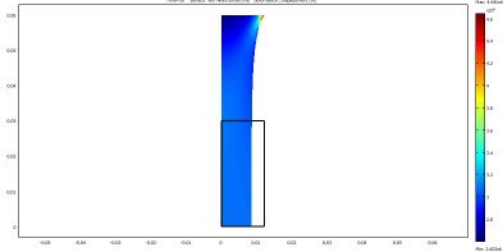




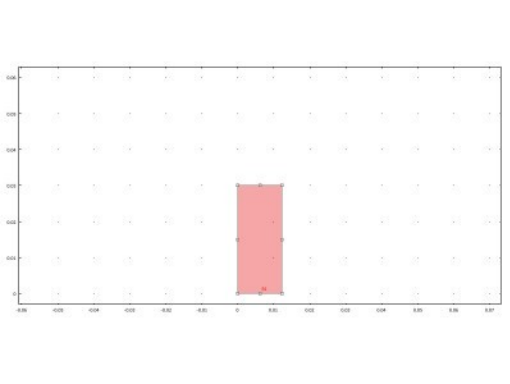


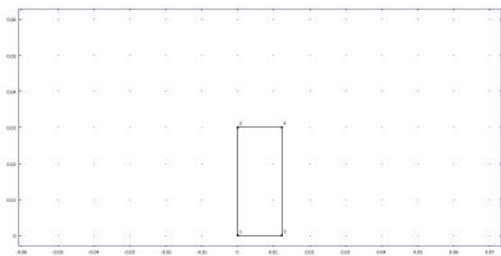


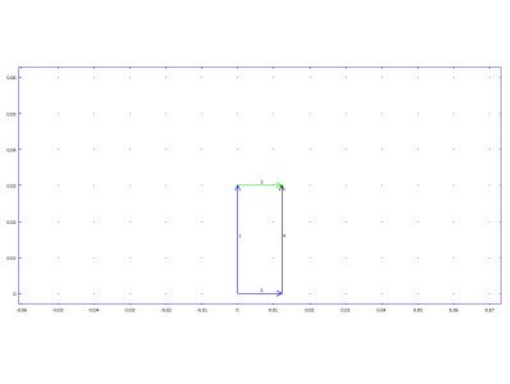
Result: Surface von Maximum (Pa) Deformation, Displacement (m)

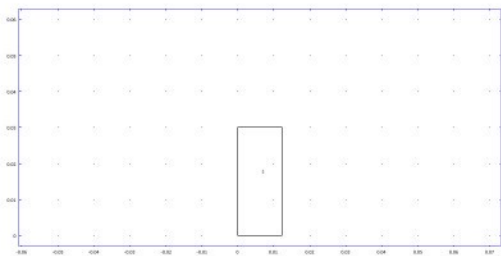


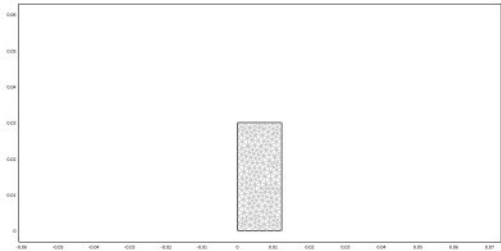


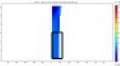




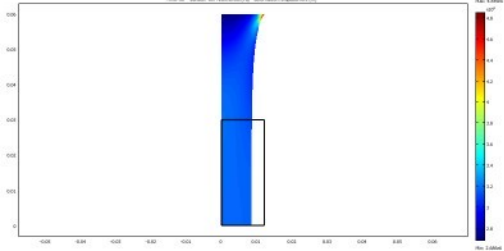




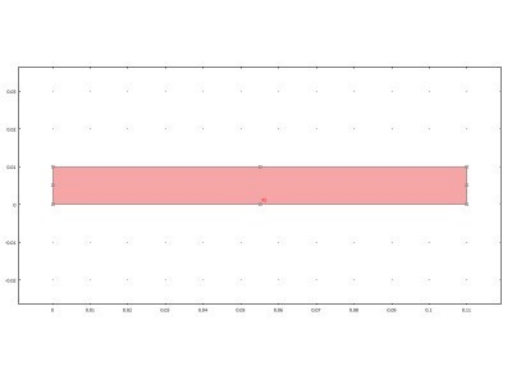


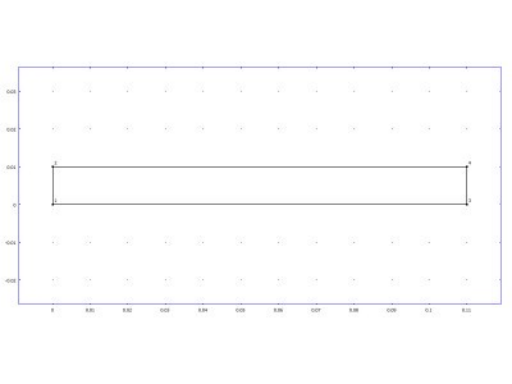


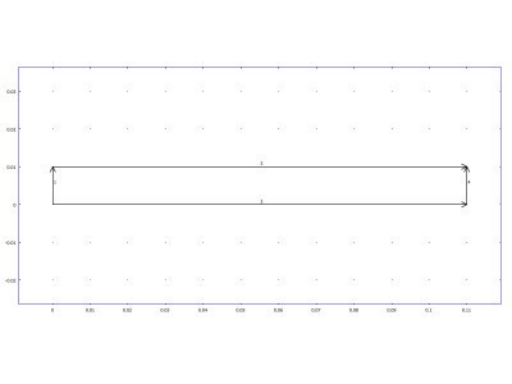
Time=20 Surface von Max (m/s) [Pa] Deformation (displacement) [m]

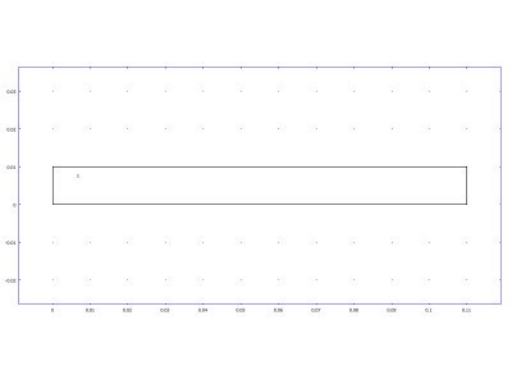












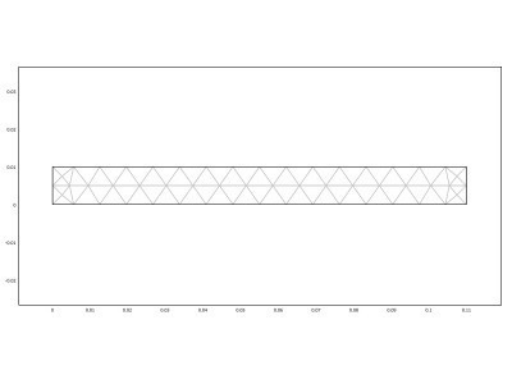
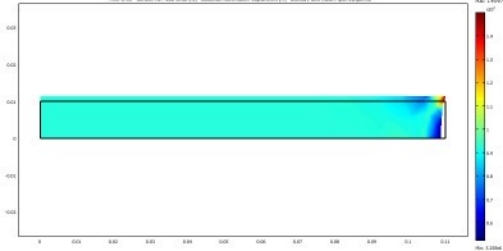


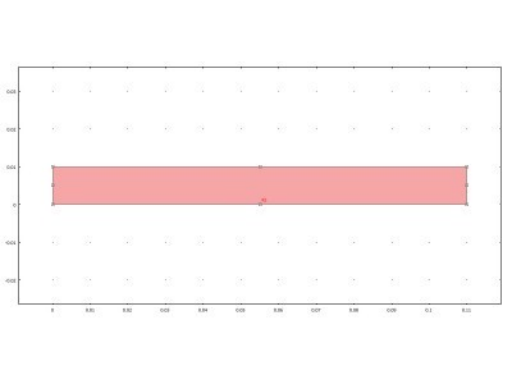
Figure 1: A horizontal bar chart showing the distribution of data across categories. The x-axis represents the magnitude of the data, and the y-axis represents the categories. The bars are colored according to a scale from blue (low) to red (high).

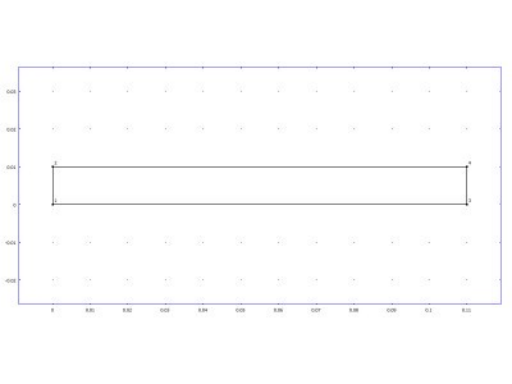


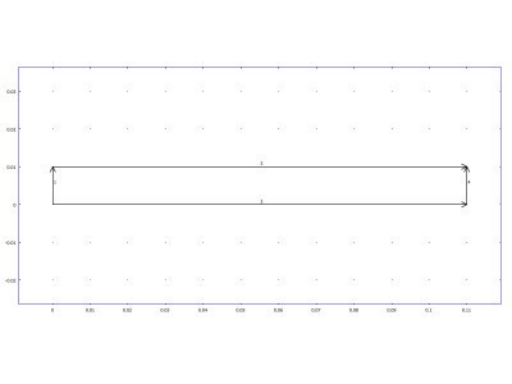
Time=270 Surface var 1488 (mag [Pa]) Subdomain deformation displacement [m] Boundary information: DRG, 11/08/12

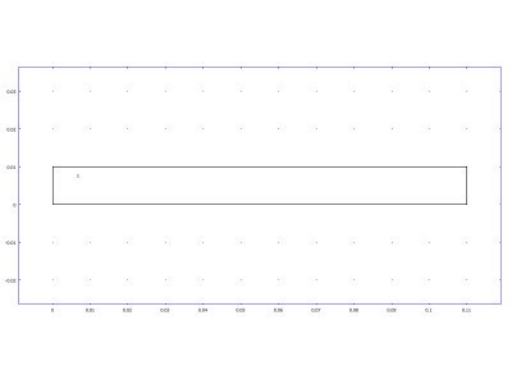












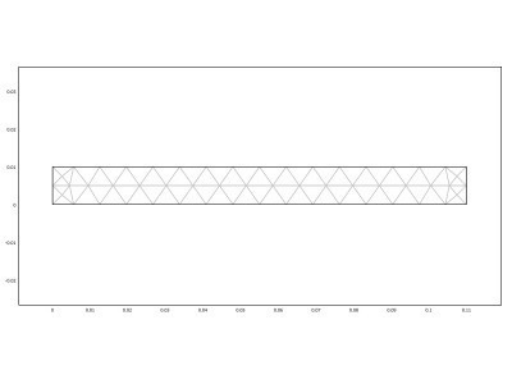


Figure 1: A horizontal bar chart showing the distribution of data across categories. The x-axis represents the magnitude of the data, and the y-axis represents the categories. The bars are colored according to a scale from blue (low) to red (high).



Time=270 Surface var 1448 (mag [Pa]) Subdomain deformation displacement [m] Boundary information: DRG, 11/08/12

